The University of Nottingham

UNITED KINGDOM · CHINA · MALAYSIA

Characterisation of discontinuous carbon fibre preforms for automotive applications

by

Giridharan Kirupanantham
MEng. (Hons.)

Thesis submitted to the University of Nottingham for the degree of Doctor of Philosophy

December 2013

Abstract

The high cost of raw materials, high labour costs and lengthy cycle times have limited the use of conventional ply-based composites in the automotive industry. This thesis seeks to identify the potential of using low cost discontinuous fibre composites (DFCs) for structural applications. Properties of DFCs are governed by the degree of homogeneity of the reinforcement and discontinuities at the fibre ends, which cause stress concentrations; thereby limiting the mechanical performance of the material. This work focuses on material characterisation of laminates moulded from discontinuous carbon fibre preforms manufactured by a robotic spray process. Through the culmination of this work, a suitable design methodology for automotive applications has been identified. Design procedures for aerospace have also been considered.

An analytical model has been developed to determine the tensile stiffness and strength of a discontinuous carbon fibre preform composite. The model can be used within automotive and aerospace design methodologies to define material properties, but a number of other factors must be considered. Areal mass of the preform has been identified as the governing factor in achieving target compaction levels. Poor homogeneity in thin parts prevents the ability to achieve high volume fractions, which determines mechanical performance. It has been demonstrated that the matrix has a greater influence on the properties of DFCs when compared to continuous fibre composites. Toughened resins were particularly effective in improving tensile strength of DFCs that exhibited poor homogeneity. Damage tolerance of DFCs has been evaluated through open-hole and compression after impact testing. Higher property retention was observed compared to continuous fibre equivalents. Greater damage tolerance of DFCs could lead to increased weight-saving in structural applications. However, current safety factors based on conventional laminates may be too conservative and could lead to over-engineering thus limiting the potential of the material.

For Mum,

who will always be the true doctor of the family

Acknowledgements

Nomenclature

Abbreviations

AML	Aston Martin Lagonda
ASMC	Advanced sheet moulding compound
ASP	Advanced structural preforming (project name)
BMC	Bulk moulding compound
CAI	Compression after impact
CFC	Continuous fibre composite
DCFP	Directed carbon fibre preforming
DFC	Discontinuous fibre composites
DFP	Directed fibre preforming
FE	Finite element
NCF	Non-crimp fabric
OHC	Open-hole compression
OHT	Open-hole tension
P4	Programmable Powdered Preforming Process
phr	Parts per hundred parts of resin
pph	Parts per hundred
RFPM	Resin film pressure moulding
ROM	Rule of mixtures
RTM	Resin transfer moulding
SMC	Sheet moulding compound
SSR	Sum of squared residuals
UoN	University of Nottingham
UTS	Ultimate tensile strength
VARTM	Vacuum-assisted resin transfer moulding
VI	Vacuum infusion

Symbols

A	Area [m^2]
C_{b0}	Initial fibre bulk compressibility
C_s	Fibre bulk compressibility
l	Fibre length
l_c	Critical fibre length
E	Young's modulus [GPa]
G_m	Shear modulus [GPa]
P	Pressure [MPa]
P_0	Latent pressure [MPa]
r	Fibre radius
R	Fibre packing factor (shear-lag model)
s_0	Latent/initial fibre volume fraction (at atmospheric pressure)
s_f	Maximum achievable volume fraction
t	Thickness (mm)
v	Volume [m^3]
v_0	Initial (uncompacted) volume [m^3]
V_m	Matrix volume fraction [%]
V_f	Fibre volume fraction [%]
α	1st shape parameter (for a two-parameter beta distribution)
β	2nd shape parameter (for a two-parameter beta distribution)
ε	Strain
ε_{fb}	Fibre breaking strain
σ	Stress [MPa]
σ_f	Fibre strength [MPa]
σ_{tow}	Tow strength [MPa]
ϱ	Density (kg/m^3)
θ	Fibre angle/orientation (radians)
η_l	Length correction factor (shear-lag model)
η_o	Krenchel orientation factor
τ	Shear strength (MPa)
ν	Poisson's ratio

Contents

1 Introduction

1.1 Market forces – the future of the automotive industry

The automotive industry faces intensifying pressure to reduce carbon emissions. The Climate Change Act 2008 legally commits the UK to a 34% reduction in greenhouse gases by 2020 and 80% by 2050 [1]. The Act was the first of its kind to legally oblige a country to its emission standards. Guidelines and legislation continue to change; each merely gives an indication of the status quo. The latest milestones emphasise the intensifying intentions of the UK government, and it is clear that efforts to reduce emissions will not abate. It is generally accepted that industrialised countries need to cut their 1990 emissions by 50-80% by 2050 [2].

The transportation sector currently accounts for 30% of CO_2 emissions in those industrialised countries and 20% worldwide [3]. The sector will play a critical role in delivering the CO_2 emissions cuts need needed to meet the aforementioned targets. Over the last 20 years, the UK has seen a reduction in total domestic carbon emissions. However, those attributed to the transport sector are approximately the same [4]. There continues to be an increase in the number of cars on the road and this trend is magnified on the global scale. By 2050 it is estimated that there will be another 2.3 billion cars in the world [5]. Car growth in industrialised countries is slowing, but global economic growth in the automotive sector will be driven by emerging markets, particularly China and India. Emerging economies may present the most significant obstacle to achieving emissions goals.

Opportunities in the automotive industry

As legislation is tightening and targets become more ambitious, opportunities exist for the research and development of new technologies. Even producers of supercars are having to offer low carbon alternatives to lower their average fleet emissions to comply with legislation. It is essential that emissions are reduced through the advancement of technology. Manufacturers will only be able to capitalise on long

term markets through economies of scale by optimising processes with increased use of automation [6].

It is clear that opportunities also exist in the expanding markets. Many of these markets don't currently adhere to any legally binding commitments to reducing emissions, but companies face more than just a moral obligation to research more energy efficient technology. Rising fuel prices are driving the market towards smaller, more efficient vehicles. The reliance of the automotive industry on finite fossil fuel reserves means that advances in technology are not only desirable to reduce greenhouse gases, but are paramount to the profitability of the sector. The industry is expanding to incorporate emerging technologies that may be able to offer solutions. The broad lines of activities that R&D is targeting can be summarised by the following subject areas:

- engine efficiency
- alternative fuels
- alternative methods of transport
- powertrain efficiency
- advanced materials

From the '80s to late '90s, average fuel economy showed little improvement. Advances in engine efficiency were offset by the implementation of technologies, e.g., power steering and air conditioning, and tighter safety standards [7]. By contrast, the last decade has seen a substantial improvement in fuel economy. As engine efficiency has edged closer to a plateau, weight reduction has become the major focus for many OEMs [8]. In addition to better fuel economy, a reduction in weight can facilitate the growth of hybrid and electric cars.

1.2 Advanced composite materials

As OEMs try to achieve drastic weight reductions in cars, their ability to do so has been hindered by increasingly more stringent crash legislation. There is a need to use materials that exhibit low density and high specific properties. Carbon fibre composites have become the dominant advanced composite material for automotive, aerospace, sporting goods and other applications. They are able to offer greater stiffness and strength per unit weight than conventional materials, easier formability, less corrosion susceptibility, the ability to tailor properties to specific load requirements, and enhanced noise and vibration damping [5, 9].

Composites don't just offer a solution to tightening emission standards; they provide an opportunity for high performance applications. In the past decade in Europe, about half of efficiency improvements have shown up as vehicle fuel consumption reductions with the other half used for enhancing performance [10]. Most high performance applications facilitate the development or generation of materials due to competition in a market driven by customer demand for innovative products. Therefore, it is often this portion of the industry that showcases technologies that may help OEMs to meet their own ambitions. High cost of raw materials, high labour costs and lengthy cycle times have historically limited the use of carbon fibre composites to the most expensive niche vehicles. Manufacturers are intensifying efforts to introduce more composites into commercial vehicles; the dissemination of knowledge gained from high performance applications is crucial for this.

1.3   Discontinuous fibre composites
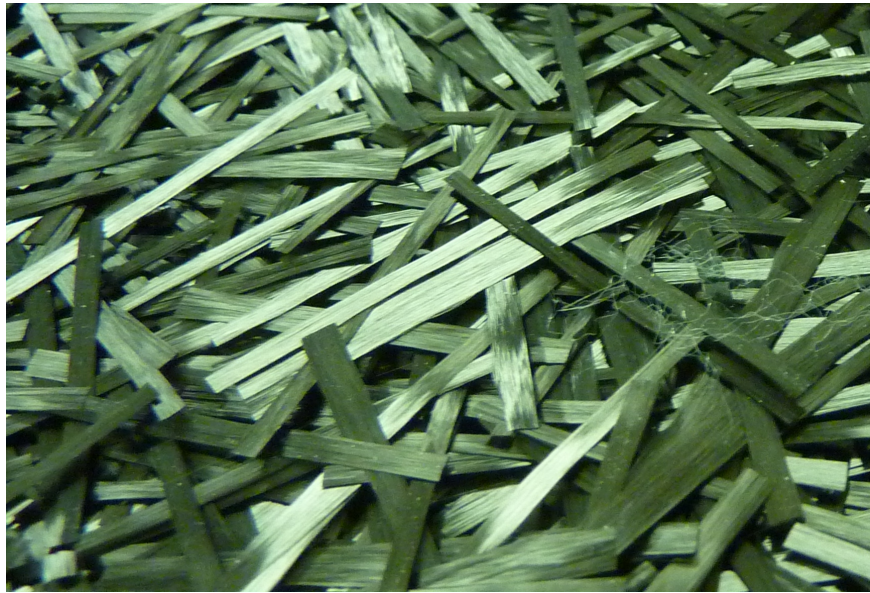
Figure 1. Chopped 3k (3,000 filaments) carbon fibre at a length of 30 mm.

Composites reinforced with fibres that do not traverse the length of the part are referred to as discontinuous fibre composites (DFCs). Discontinuous fibres can vary greatly in length, form and scale. Fibres can be chopped from continuous fibre or manufactured separately. Fibres are usually randomly distributed in two or three planes (Figure 2). This thesis will focus on meso-scale DFCs: those incorporating reinforcing fibres of an intermediate size (relating to lengths of approximately 10 mm – 100 mm) in large bundles (500 filaments or more). These are typically randomly oriented in two dimensions (Figure 1).
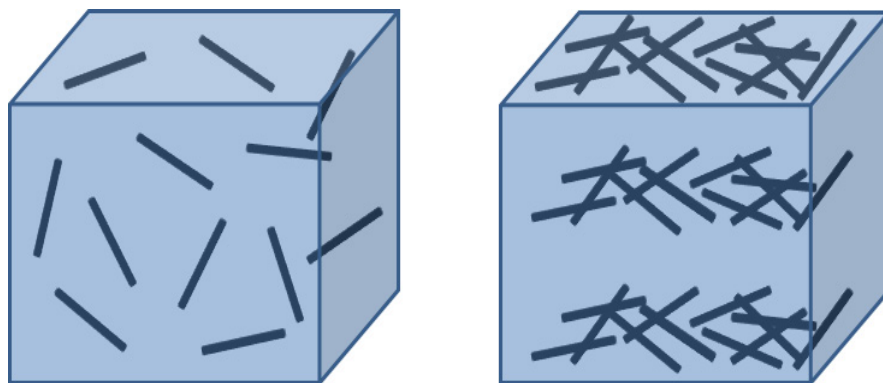
Figure 2. Discontinuous fibres composites in three (left) and two (right) dimensional orientations.

DFCs allow the carbon fibre to be processed in its raw form whilst providing the opportunity to employ rapid automated manufacturing methods. This offers the potential for considerable reductions in cost and cycle time by progressing beyond labour-intensive part production associated with high-performance composites. Despite showing great promise, the adoption of DFC technology by manufacturers in automotive applications has remained somewhat cautious. Until recently its use has largely been restricted to cosmetic, non-structural parts often made with glass fibre. Carbon DFCs are able to provide greater stiffness and strength characteristics, required for structural components, at a smaller thickness and mass. Like their continuous counterparts, they have many of the same needs with respect to the design methodology with a desire to have greater mechanical behaviour understanding.

1.4 Application of DFCs

Many of the first applications of composites in the automotive industry utilised DFCs. Injection moulded parts were used as low cost manufacturing processes for low performance parts [11]. Materials used in injection moulding processes, e.g. bulk moulding compounds (BMCs), typically consisted of individual fibres dispersed in a matrix and were discontinuous at the micro-scopic scale. Compression moulded sheet moulding compounds (SMCs) were an alternative that offered higher volume fractions and better properties. SMC consisted of a layer of chopped glass fibres sandwiched between two layers of resin [12]. Fibres were longer than those used in BMC but the resulting architecture was discontinuous at the same scale. Since the 1970s the automotive industry has strongly supported the advancement of SMCs, which has been significant in the development of mass production applications of composites [13]. SMCs have often been used in body panels for applications where a high quality finish is required [14]. True structural application of DFCs had been limited as there was concern over damage assessment; there were difficulties in determining whether internal damage was caused by an impact [15].

More recently, structural grade SMCs have been identified that are relatively insensitive to damage when compared with CFCs. These materials are produced by compression moulding preforms manufactured from random bundles of slit carbon prepreg and are therefore discontinuous at the macro-scale. The first use of carbon fibre SMC in the Dodge Viper was said to represent a significant milestone for the automotive composite technology as the industry began to explore higher volume applications [16]. Commercial offerings such as HexMC and Quantum Composites are currently available. These materials are often being used to replace complex metallic structures forged from metal with composites that offer the low unit cost of compression moulding [17]. The Lamborghini Aventador and Sesto Elemento incorporate the technology in a carbon fibre monocoque chasis design to produce a complex structure not possible with traditional pre-preg materials [18]. Opportunities to increase automation have also attracted interest in the aerospace sector where there is also growing demand in developing out-of-autoclave methods.

Directed fibre preforming processes produce DFCs that closely resemble the meso-scale fibre architecture of advanced SMCs. Traditionally in directed fibre preforming processes, fibres are chopped and sprayed with a powdered binder onto a perforated screen [19]. Chopped fibre processes are suitable for preforming processes that offer opportunities to facilitate the widespread use of carbon composites through potential production rates above 10,000 parts per annum [9]. The application of directed fibre preforming has been demonstrated through several iterations of the technology. The first widely recognised, Programmable Powdered Preforming Process (P4) utilised glass fibre that was chopped and sprayed via a robotic arm. The equipment and techniques were originally demonstrated by Owens Corning Composite Solutions and Aplicator System AB. Ford's refinement of the original process was labelled the Ford Programmable Preform Process (F3P), which was used to produce parts for the Aston Martin Vanquish and was necessary to meet peak production demand as production grew [20]. The process was implemented by Sotira Composites for the production of class-A finish boot lids and framing for the Aston Martin DB9 at volumes of 15,000 p.p.a. [14].

1.5   Directed Carbon Fibre Preforming

The Directed Carbon Fibre Preforming (DCFP) process utilises high levels of robot based automation to produce low cost, low scrap, low cycle time preforms for liquid moulding [21]. By using chopped fibres in a moulding process there is far more flexibility in producing components with complex geometries while retaining many of the advantages of continuous fibre composites such as high specific stiffness and strength, as well as resistance to creep, corrosion, and fatigue. The process is currently in use for automotive structures where the performance exceeds that of sheet moulding compounds and is suitable for lower production volumes e.g. <10,000 parts per annum.

Figure 3. Carbon fibre tows, containing several thousand filaments of carbon (left – 24k, right – 3k), wound around bobbins.

Fibre is drawn directly from the bobbin (Figure 3) and passed through a chopper gun mounted onto a robot. Net shape preforms are produced by spraying a stream of chopped fibres and binder onto a perforated tool face. Suction on the underside of the tool keeps the deposited fibres in place [22]. Once the fibre has been deposited, a matched perforated tool is lowered to compact the preform. Hot air is

passed through the perforations in the tool to consolidate the binder. Ambient air is used to cool the preform which, can then be removed from the mould [23]. Moulding of the preforms is typically carried out using resin transfer moulding (RTM) or other liquid moulding processes. The process consists of injecting epoxy resin at pressure into a mould cavity containing the preform. A vacuum is used at the outlet to remove air within the mould tool. The resin cures within the tool which can be heated to reduce de-mould time. Material cost of DCFP is significantly lower than comparable pre-preg and semi-preg materials as intermediary treatments such as pre-impregnation are not required. Fully automated robotic operation provides excellent repeatability in addition to ease of manufacturing variation. Preforming cycle times are often under five minutes and fibre wastage is low (<3%) [24].

Conventional ply-based laminates are designed by consideration of the ply angle, stacking sequence and total thickness based on library data for the ply. As all plies perform similarly, laminate theory can describe the performance of the laminate. Unlike conventional laminates the DCFP meso-structure has variation – the locations of the fibre bundles are not known *a priori* and the resulting structure is highly heterogeneous. Several factors, such as tow size and fibre length, can be seen to alter the performance of the resulting composite. With the large number of variables governing the performance of the DCFP fibre architecture and the interaction of those variables it can be seen that there are a large number of combinations which may give similar mechanical performance.

The primary aim of this work is to determine how DCFP can be designed through consideration of tow size, fibre length, laminate thickness, fibre volume fraction and matrix properties. Rigorous modelling approaches give predictions of material properties that agree well with experimental values, but for design purposes it is more useful to have procedures for estimating laminate properties than more exact intractable solutions [25]. This research has focussed on gaining an understanding of the complex behaviour of DCFP in order to develop analytical models and outline a design methodology integrating the idiosyncrasies of the material.

1.6   Theme of work

The research presented here has been carried out as part of the Advanced Structural Preforming (ASP) project – an industrially driven research programme in collaboration with the automotive OEM, Aston Martin Lagonda (AML). The project involved the development of DCFP technologies for greater integration in new vehicles. Work at the University supported the vehicle programme by improving understanding of the process and characterising the performance of DCFP materials. The work presented here was primarily concerned with the development of design procedures for DCFP fibre architectures, which involved static characterisation of trial materials along with the development of models to describe the performance of different aspects of the process.

An analytical model (Chapter 2) has been developed to predict tensile stiffness and strength for a given preform fibre architecture, with a static characterisation study used to validate results. The findings identified the influence of tow size, fibre length and thickness on tensile properties. Compaction behaviour of dry preforms was studied (Chapter 3) to determine the effect of these parameters on the ability to attain high volume fractions using RTM. The influence of matrix properties was considered in a toughness study (Chapter 4) where the aim was to determine the degree to which resin modifications alter material properties of DFCs. Feasibility for high performance applications was evaluated through the type of testing typically required for classification of aerospace-grade materials (Chapter 5). The culmination of the work in this thesis helped to shape design methodology (Chapter 6) and formed the basis of the development of an Aston Martin Engineering Specification (AMES) for DCFP structural mouldings for a vehicle platform. The findings will add to the current knowledge needed to accelerate the use of DFCs in the automotive industry while seeking to determine its potential in others.

2 Mesoscopic homogeneity – modelling mechanical properties

2.1 Introduction

Properties of discontinuous fibre composites are strongly determined by homogeneity in the mesoscopic fibre architecture. A number of factors can influence the degree of homogeneity at this level. Manufacturers using the DCFP process are easily able to change three of these: tow size, fibre length, and areal mass. The latter directly determines the volume fraction and thickness of the laminate. The effect of volume fraction is well understood, and the linear trends seen in continuous fibre composites have previously been shown to be applicable for DFCs [26, 27].

The effects of the other parameters are less clear. Unlike conventional composites, properties vary with thickness as fibre coverage is heterogeneous and considerably poorer in thin parts. The composition of the tow is also known to significantly affect material properties. Bundles containing fewer filaments typically result in better tensile properties as a greater proportion of the filament surface is exposed, while longer fibres lead to a larger build-up of stress, which can also improve these properties. Conventional length effects based on stress transfer across the fibre may be applicable but probabilistic factors also have to be considered as shorter fibres lead to more homogeneous coverage.

Consequently, mechanical properties can be achieved using several preform architectures – each incorporating a different combination of the three variables. Any degradation of properties associated with a change in one of these parameters can be offset by another. This has significant implications on the design of preform architectures for three dimensional parts. A manufacturer may, for instance, wish to utilise shorter fibres in an area of a component with complex geometry. A reduction in properties could be counteracted with a local increase in areal mass. By gaining clearer understanding of the relationship between the preform architecture and laminate properties, greater optimisation of DFC structures can be achieved.

2.2   Objectives

This work seeks to determine the effect of three macro-structural parameters on the mechanical performance of two-dimensional DCFP laminates. The influence of tow size, fibre length and laminate thickness has been investigated. Analysis of existing models in the literature was used to develop an analytical model while a finite element (FE) model developed by Harper [28] was used to provide initial comparative results. An experimental study was carried out to validate the analytical model and substantiate trends between variables in the preform architecture and tensile properties in the laminate.

The information gained from the study was used to identify two benchmark DFCP fibre architectures that are able to provide suitable stiffness and strength characteristics for semi-structural automotive applications. Flexural, compressive, shear and Charpy impact testing have also been undertaken on these benchmark architectures. Mechanical properties of DCFP have been compared with other discontinuous fibre composites (DFCs) and conventional continuous fibre laminates.

2.3   Literature Review

This review focuses on the factors affecting macro-scale DFCs where four variables are critical in defining homogeneity: tow size, fibre length, thickness, and volume fraction. Effects of each factor on the properties of the laminate are identified. Existing analytical models, used to determine the tensile properties, of composites are also evaluated. Of particular interest is the exploration of the applicability of these models to tow-based DFCs, in order to establish how existing rules may be applied to the DCFP meso-architecture.

2.3.1   Tow size

Exact costs of carbon fibre are often hard to define as costs fluctuate greatly with variations in the market. A common trend used to exist with larger tows [>12k] costing approximately half that of smaller [<12k] tow-size fibre [29]. For this reason, recent studies have often focused on the evaluation of larger, cheaper tow sizes to understand property degradation compared to employment of smaller tows. As carbon fibre costs have decreased in recent years, so has the cost variation between small and large tow sizes. With material costs being a small proportion of total manufacturing costs, a new paradigm may be required where less emphasis is placed on the cost benefits of using larger tows.

Many authors recognise the benefits of using smaller tow sizes. Fibre distribution is improved so that there is a lower level of variability [30]. Following an experimental study, Dahl et al. [31] go as far as stating that they are more favourable in every respect. In their study, carbon fibre preforms were manufactured using the P4 process with several variations in tow size that were all overall equivalent to 36k (0.5k x 72, 1k x 36 etc.). All other processing variables were identical, and laminates were moulded at a thickness of 2 mm. Smaller tow sizes resulted in improved fibre distribution, increased mechanical properties, and lower variability in properties. By fixing certain processing variables they were easily able to determine the effect of tow size. However, it is also important to investigate whether the reductions in

tensile stiffness and strength are as significant with increased thickness or different fibre lengths.

The advantages of using smaller tow sizes have been accepted and validated by several other authors [11, 32], but a clear understanding of the underlying reasons is needed. Are mechanical properties determined predominantly by fibre coverage, or are there other significant factors? The negative effects of large tows have been linked to larger stress concentrations at the fibre ends. Rondeau et al. [11] explain that groupings of fibre filaments result in stress concentrations at the ends of the tows greatly reducing the strength of the composite while slightly reducing the stiffness. They postulate that the tow itself acts as a large-diameter fibre and hence may need to be longer to achieve the best performance. This would suggest that larger fibre bundles exhibit a longer optimal length. In reality, the prediction of tow properties is much more complex and other factors need to be considered. Variations in fibre strength mean that the breaking stress of a bundle is different from that of its constituent fibres. This variation in fibre properties has a secondary effect as broken fibres result in a change in stress distribution. A broken fibre can again build up stress and break into even shorter segments, affecting the properties of the material [33]. While this more rigorous analysis is beyond the scope of this thesis, the idea of modelling the tow as a single fibre may offer a simple approach for use in analytical models and to help in understanding property trends.

The utilisation of smaller tow sizes would prove beneficial in the preforming of multifaceted three-dimensional parts. Using a smaller tow size provides the opportunity to achieve target properties using a shorter fibre length, something that would be desirable when the preform has to comply with steep draft angles or complex geometry. While smaller tow sizes result in improvements in final part properties, there is an issue regarding manufacture. Carley et al. [34] found that coarser fibre strands produce a more porous, open preform which will allow resin an easier flow path, especially with large parts. Two types of resin flow are regularly seen in RTM processes: in-plane and through-thickness. Smaller tow sizes

result in more nesting which prohibits in-plane flow, and as preform homogeneity improves through-thickness flow is impaired by the reduction of gaps in the fibre architecture.

A degree of tow fragmentation occurs as fibres are processed and break up into smaller bundles. Filamentisation has previously been employed as a method for intentionally fragmenting large tows to reduce average filament count and improve preform coverage in DCFP parts. Increases in tensile stiffness (13%) and strength (55%) were observed in a study when induced filamentisation was maximised for a 24k tow [23]. Highly filamentised fibre architectures are also more porous but exhibit a significantly greater degree of preform loft. This may be problematic if high volume fractions (>30%) are required.

2.3.2 Fibre length

Short fibres result in better surface finish, greater fibre placement precision and improved definition of part dimensions [22]. Hence, there is an interest in understanding the effect of fibre length on material properties. The idea of an optimal length, pertaining to the ultimate realisable performance of fibres in a composite, is postulated by many authors [35-38]. A critical fibre length has also been defined as the minimum fibre length which will allow tensile failure of the fibre rather than shear failure of the interface [27]. Failure in composites where fibres are sub-critical is initiated by matrix failure rather than the fibre failure.

In determining an optimal length, a number of factors should be considered as different properties have varying dependencies on fibre length. Tensile stiffness and strength are the focal interest in this thesis, but other properties, such as impact energy absorption, have been studied by other authors. It has been suggested that the net effect of reducing fibre length in DCFP parts is clear; shorter fibre lengths significantly improve composite performance down to the critical length due to fewer critical flaws, improved preform coverage and natural fragmentation resulting in lower filament counts [35]. If tensile properties are considered, this

optimal length for stiffness and strength are different. The optimal length for modulus has been shown to be relatively short, but the length at which a plateau in strength occurs may be up to ten times longer and within the range of fibre lengths currently utilised by manufacturers [28, 39].

Jacob et al. [40] reported lower tensile strengths and stiffnesses as fibre length was reduced (from 50 mm to 25 mm) and suggest that this is possibly due to increased concentration of stress raisers with shorter fibres. Their study was carried out on composite plates manufactured from chopped carbon tows compression moulded with an epoxy system. They also considered the impact of fibre length on specific energy absorption (SEA) desirable for crashworthy structures. SEA decreased with longer fibre lengths, highlighting different optimal lengths for different properties. Indeed, Hitchen et al. [41] confirm that maximum toughness and stiffness cannot be obtained simultaneously. In a study of a random two-dimensional carbon DFC, they found that reducing the fibre length (from 15 mm to 1 mm) increased fracture toughness whilst decreasing Young's modulus. Fracture toughness was measured using single-edge notched specimens with crack lengths of 1-11 mm. Below the critical length where fibres do not break, it is necessary for the fibres to pull out of the matrix for the crack to extend [42]. It has been suggested that maximum toughness is achieved just below this critical length when failure occurs exclusively through fibre pull-out [43]. Near the critical length it may be possible to limit reductions to Young's modulus and toughness. However, the increase in toughness is made at a greater expense of composite strength [44].

2.3.3   Thickness

In contrast to laminar materials, DFC parts show variation in properties as thickness is changed. Mechanical properties are reduced in thin parts due to poor fibre coverage leading to unreinforced areas [22]. Increasing part thickness improves stiffness and strength as a consequence of improved homogeneity. Whether this trend remains true for all thicknesses would influence the design process for structural components. There is limited data in the literature demonstrating

variation in tensile properties, with thickness, of tow-based DFCs. A performance plateau is likely to exist where tensile properties no longer increase with thickness. This may arise as preform homogeneity approaches an optimum level.

2.3.4   Volume fraction

Structural performance of a meso-scale DFC component is governed largely by the volume fraction of fibres. It is commonly known that increasing volume fraction in composites results in enhanced mechanical performance. However, it is theorised that this trend is only observed up to a point. Reduction in material strength of continuous fibre composites, with increased volume fraction, has been associated with material porosity [45]. This could also be applied to randomly orientated DFCs. In results published from the first part of a study on the influence of fibre length and volume fraction, Thomason & Vlug [46] suggest that reduced modulus at high volume fractions could be related to fibre packing problems resulting in increased void content. Higher volume fractions may also require variations in the manufacturing process, e.g. increased injection pressure, which may have a significant effect on the properties of the final part [26]. Greater injection pressures can lead to movement of fibres within the mould. It should also be noted that, by adding fibres to the matrix, the composite may exhibit lower ultimate tensile strength than that of the matrix [47]. This is typically only seen at low volume fractions, where the addition of discontinuous fibres introduces stress concentrations at the ends.

2.3.5 Analytical models for determining mechanical properties in DFCs

Stiffness

The rule of mixtures is, perhaps, the most well-known and commonly used method for estimating longitudinal stiffness in composites. It is derived by assuming that both the fibres and matrix experience equal strain, a theory first proposed by Voigt [48]. The material is treated as if it were composed of parallel slabs of the two constituents bonded together [49]. This is illustrated in Figure 4. The solution for a continuous fibre composite is given by [50]:

$$E_c = V_f E_f + V_m E_m \, ,$$ Eq. 1

where E and V are the Young's modulus and volume fraction; and the subscripts c, f, and m refer to the composite, fibres, and matrix. Stiffness in discontinuous fibre composites is dependent on fibre aspect ratio, volume fraction, fibre-to-matrix modulus ratio, and fibre orientation distribution [51].
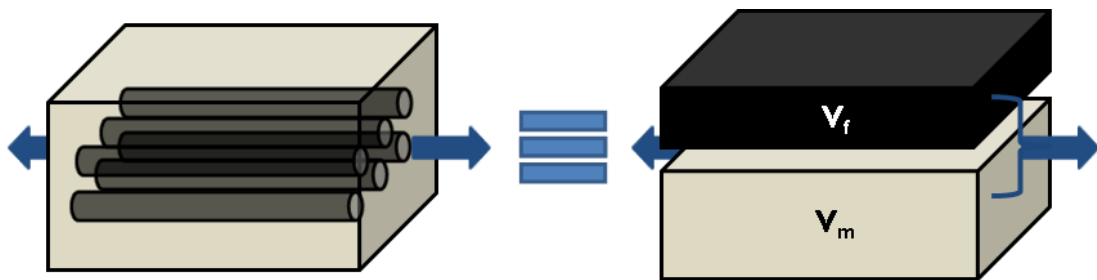
Figure 4. Representation of Voigt's slab model. Both fibre and matrix are assumed to be strained by the same amount in the direction of the applied load. The fibres and matrix are therefore under different stresses as they exhibit dissimilar stiffnesses. The rule of mixtures works on the assumption that the stress in the composite can be determined by the overall contribution of these separate phases.

Many modern analytical methods for determining stiffness in composites are based on the shear lag model, originally proposed by Cox [52], which accounts for the fibre aspect ratio. When the model is applied to resin-bonded fibrous materials each fibre is considered to be embedded in a continuous solid medium of resin. Tensile stress transfer between the fibre and the matrix is assumed to take place through interfacial shear of the two components. The build-up of tensile stress in the fibre is determined by the distribution of the shear stress along its length [49]. The fibre

axial stress is highest at the centre diminishing towards zero at the fibre ends, whereas the interfacial shear strength is maximum (negatively) at the fibre ends and falls to zero in the centre [53]. Consequently, the stiffness is related to the length and radius of the fibre,

$$E = \eta_l V_f E_f + (1 - V_f)E_m \, , \qquad\qquad \text{Eq. 2}$$

$$\eta_l = \frac{1 - tanh\left(\frac{\varphi l}{2}\right)}{\left(\frac{\varphi l}{2}\right)} \, , \qquad\qquad \text{Eq. 3}$$

$$\varphi = \sqrt{\frac{2G_m}{E_f \ln\left(\frac{R}{r}\right)}} \, . \qquad\qquad \text{Eq. 4}$$

It can be seen from the first of these equations that the rule of mixtures has been extended to account for the length of fibres using a length correction factor η_l. This is calculated using the length (l) and radius (r) of the fibre, the shear modulus of the matrix (G_m), and the fibre-packing factor (R). This model was extended by Krenchel [54] to account for the effect of fibre orientation. The Krenchel orientation factor is given by:

$$\eta_o = \Sigma \alpha_i \cos^4 \theta_i \, , \qquad\qquad \text{Eq. 5}$$

where α_i is the proportion of fibres directed in the orientation θ_i. For a two-dimensional random orientation of fibres, where an equal proportion of fibres are assumed to be directed in each orientation, the orientation factor evaluates to exactly 0.375.

Criticisms of shear-lag analysis have been related to how stress is transferred within a composite. Although the greatest shear stresses are located at the ends of the fibres, stress transfer across the fibre ends are neglected. Several authors have modified the shear-lag model to account for stress transfer across the fibre ends. Clyne [55] postulates that the fibre end stress σ_e is equal to the average of the peak fibre stress (neglecting fibre end stresses) and the remote matrix stress values predicted by the standard shear lag model:

$$\sigma_e = \frac{\varepsilon\left[E_f(1 - \text{sech}(\varphi s)) + E_m\right]}{2} = \varepsilon E_m'. \qquad\qquad \text{Eq. 6}$$

At the position x along the fibre, where 0 is the centre and $\pm\frac{1}{2}l$ are the fibre ends, the axial stress is given by

$$\sigma_f = \varepsilon\left[E_f - \left(E_f - E_m'\right)\cosh\left(\frac{\varphi x}{r}\right)\text{sech}(\varphi s)\right]. \qquad\qquad \text{Eq. 7}$$

Using this equation, the estimated axial stress along a carbon fibre has been plotted in Figure 5. It can be seen that for small aspect ratios (≤10), the fibre end stress may be relatively large. The influence of axial stress across the fibre ends becomes very small as aspect ratio increases and the proportion of the fibre bearing the peak axial load becomes larger.
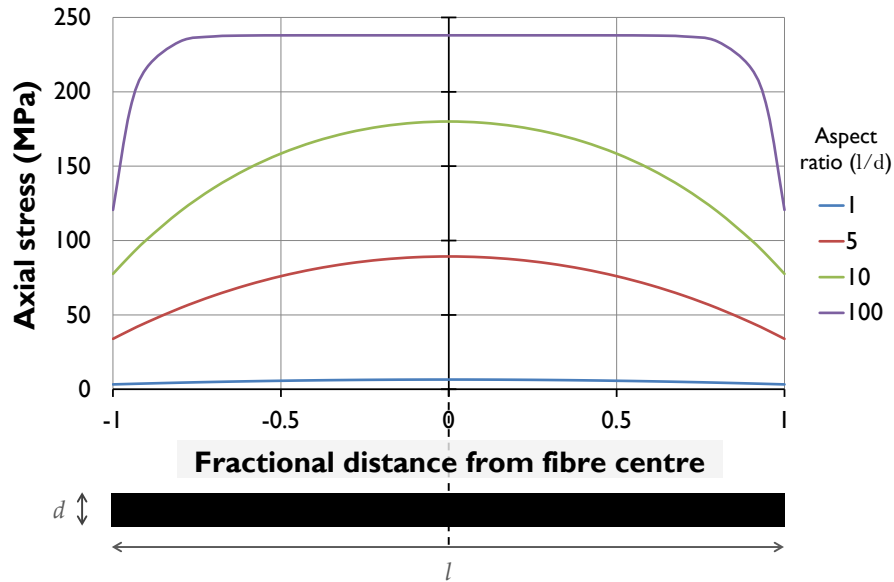
Figure 5. Estimated variation of axial stress along the length of a carbon fibre for four different aspect ratios. Results are for a strain of 0.001 and fibre volume fraction of 30%.

The effect of the modified model on predicted stiffness values are shown in Figure 6. A greater proportional difference is seen between the standard shear-lag model at small aspect ratios as fibre end stresses have a greater influence. Also included is a modified model proposed by Starink and Syngellakis [56], who suggested a similar approach to Clyne but by considering the presence of fibre end stresses in the expression for peak fibre stress. Consequently, larger axial stresses are estimated at the fibre ends resulting in larger predictions for Young's modulus. Both models

follow the form of the shear-lag model in Eq. 2, but the length correction factor has been modified to give

$$\eta_{l\,(Clyne)} = 1 - \frac{\left(E_f - E'_m\right)\tanh(\varphi s)}{E_f \varphi s}, \qquad \text{Eq. 8}$$

$$\eta_{l\,(Starink)} = 1 - \left(\frac{1 - E_m/E_f}{2 - \text{sech}(\varphi s)}\right)\left(\frac{\tanh(\varphi s)}{\varphi s}\right). \qquad \text{Eq. 9}$$
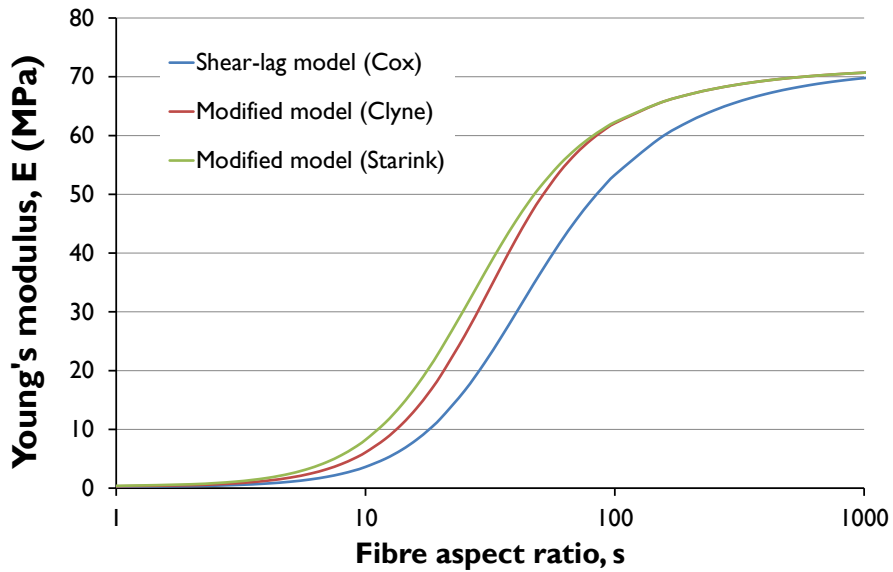
Figure 6. Predictions for the Young's modulus of a carbon-epoxy composite using the standard shear-lag model (Cox) and versions modified (Clyne and Starink) to account for axial stress across the fibre ends. Estimates are for a V_f of 30%.

The modifications by Clyne and Starink are mainly used for discontinuous composites where the fibre/matrix modulus ratio is small. The modified model by Starink was used to estimate properties of Al-SiC composites, which have an E_f/E_m ratio of approximately 6; the carbon-epoxy ratio for DCFP is much larger, around 75. It should also be noted that as there is no scope within the shear lag framework for description of stresses beyond the fibre end [49], both modified methods are based on conjecture. It is reasonable to assume that they should only be considered if the standard shear lag model underestimates Young's modulus of meso-scale DFCs.

In the standard shear-lag model, there is also no consideration of stress transfer between touching fibres. The validity of the shear-lag model for random fibre networks has been examined by Räisänen et al. [57], who ask whether the model applies to such networks. They argue that the dominant loading mode is the transfer of axial stress directly from one fibre to another at fibre crossovers. They also point out another common criticism of the shear lag model – the assumption that transverse stiffness is the same as that of matrix.

Despite these concerns, the shear lag approach continues to form the basis of many analytical models. The methods take the general Cox-Krenchel form where

$$E = \eta_l \eta_o V_f E_f + \left(1 - V_f\right) E_m.$$

Eq. 10

This above model was defined by Curtis et al. [38], but a number of variations have been proposed by authors due to the simplicity and relative accuracy of the method. Taha and Abdin [58] introduce an "agglomeration efficiency factor" η_a which, to an extent, takes into account randomness of many factors that influence properties in DFCs. They also state that modification of the orientation factor is crucial for more accurate property prediction and suggest it is dependent on:

- processing methods
- volume fraction, where lower fibre content yields to lower orientation efficiency (i.e. lower load-bearing efficiency based on low orientation)
- fibre packing

This work highlights the need to attribute a level of uncertainty, which comes as a result of the random nature, to DFCs. Instead of assuming a perfectly random distribution of fibres (and integrating modulus over a 180° range), Sk and Chakraborty [59] used an approach that took into account the statistical variation of the factors that influence stiffness e.g. fibre-fibre distance. The method involved many thousands of simulations and is not appropriate for a simple analytical model. However, their suggestion that probabilistic analysis is essential to study property behaviour of SFRC is applicable to tow-based DFCs. A degree of uncertainty comes as a result of the random nature of DFCs. Sk and Chakroborty point out that many

current methods for determining properties of DFCs are typically deterministic in nature. The orientation correction factor in the rule of mixtures is based on an equal proportion of fibres in each direction. This assumption is more likely to be correct in highly homogeneous fibre architectures but much less likely in heterogeneous architectures that contain fewer fibre bundles. A function to determine the probability of a uniform fibre distribution existing could be appropriate for determining strength and stiffness.

Other models have also received much attention in the literature. A theory proposed by Eshelby [60] applies to a single ellipsoidal inclusion in an infinite matrix but the method was extended to by Mori and Tanaka [61] to composites containing practically useful reinforcement volume fractions [62]. However, the approach is only applicable for low volume fractions and under-predicts properties for larger volume fractions (i.e.>30%) [37] making it unsuitable for meso-scale DFCs where high volume fractions are desired.

Also prominent in the literature are the Halpin-Tsai [63] equations. These form a set of empirical relationships that enable composite properties to be expressed in terms of the values from the equivalent fibre and matrix properties [64],

$$E = E_m \left(\frac{1 + \xi \eta_1 V_f}{1 - \eta_1 V_f} \right) \qquad \text{Eq. 11}$$

$$\eta_1 = \frac{\left(\frac{E_f}{E_m} \right) - 1}{\left(\frac{E_f}{E_m} \right) + 2(\frac{l}{d})} \qquad \text{Eq. 12}$$

The factor ξ is determined by the shape and the distribution of the reinforcement, representing the significance of the fibre arrangement. The equation becomes equivalent to the rule of mixtures when ξ approaches infinity. Good predictions have been found for SFRC if $\xi=2(l/d)$ [65].

Results from the most commonly used models described above are shown in Figure 7. The rule of mixtures (ROM) for a continuous fibre composite (Eq. 1) provides an

upper bound for estimated performance. The Cox (Eq. 2) and Cox-Krenchel (Eq. 10) models produce decreased estimations due to consideration of fibre length in the former as well as orientation in the latter. The Cox-Krenchel model approaches the random ROM ($E = \eta_o E_f V_f + E_m V_m$) for large aspect ratios. Results from a previous study [24] suggest that DCFP performance will be similarly bound albeit with more uncertainty due to homogeneity effects. Similar results could also be achieved using the Halpin-Tsai (Eq. 11) equation if a lower value for ξ is used.
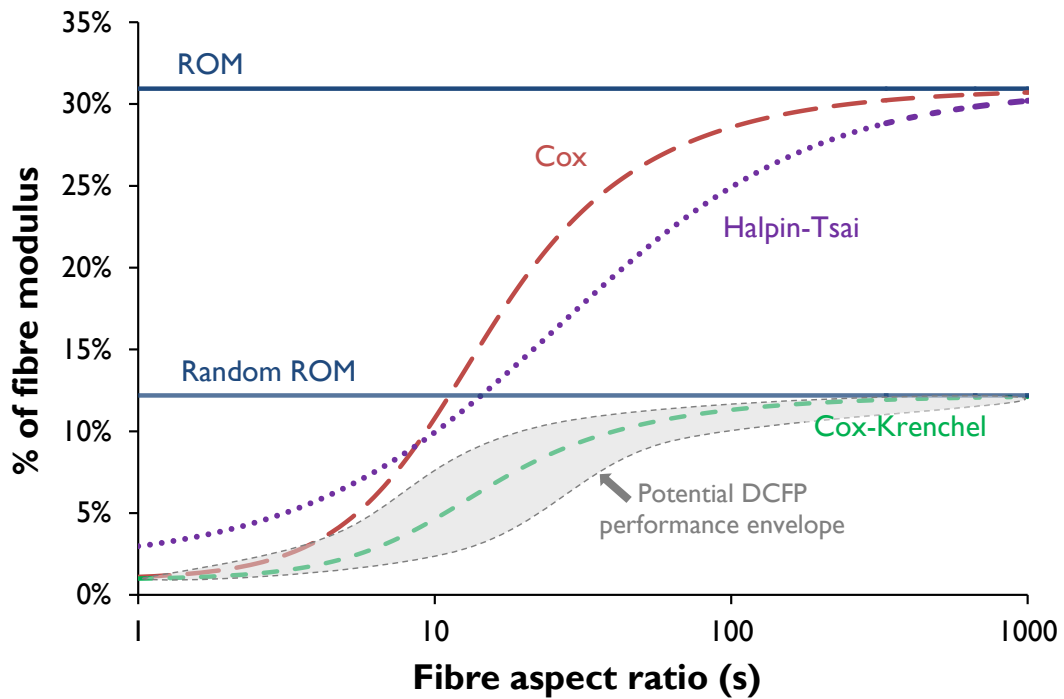
Figure 7. Comparison of analytical models commonly used for predicting Young's modulus in composites. Results were calculated for a V_f of 30%. Halpin-Tsai results were obtained using values equalling $2(l/d)$ for the constant ξ. An estimate of DCFP properties is based on previous experimental results for random architectures.

Strength

Prediction of the tensile strength for DFCs is more difficult, as the ultimate strength is determined by the onset of fracture and not via a yielding mechanism [66]. Rule of mixtures estimates for strength are similar to those for stiffness. For a unidirectional composite, strained to a value ε_{fb} where the fibres break, the stress transmitted by the composite is [47, 49]

$$\sigma_b = \varepsilon_{fb} E_1 = V_f \sigma_{fb} + (1 - V_m) \sigma_m^*. \qquad \text{Eq. 13}$$

Here, σ^*_m is the stress in the matrix which is given by $\varepsilon_{fb}E_m$. The effect of fibre length was evaluated by Kelly and Tyson [67] who developed a modified rule of mixtures using the shear lag model. They proposed a length efficiency factor for short fibre composites based on the concept of critical fibre length,

$$\eta_l = \frac{1}{V_f}\left[\sum_i \left(\frac{l_i V_i}{2l_c}\right) + \sum_j \left(1 - \frac{l_j V_j}{2l_c}\right)\right],$$ Eq. 14

$$l_c = \frac{\sigma_f d}{2\tau}.$$ Eq. 15

Assuming that both the matrix and fibres behave linearly elastically, the stress builds up from zero at the fibre ends to the maximum stress (σ_f) the fibre can be loaded to at the centre [68]. The critical fibre length l_c is the minimum required to build up sufficient stress to fracture the fibre. A proportion of a fibre longer than the critical length will be strained to the same extent as the matrix [69]. As with stiffness, Kelly and Tyson propose using a fibre orientation factor which takes the value of 0.375 for random in-plane fibre composites. Again, this assumes a perfectly random distribution of fibres.

The Weibull distribution is frequently used to describe variability of tensile strength in composites [70] and other brittle materials. Properties are related to the presence of critical size flaws where failure originates. Mortenson [62] describes that for an assembly of N elements arranged as a chain (such as a fibre), the probability that the applied uniform stress (σ) causes the failure of a least one element in the arrangement, causing the chain to break, is given by:

$$P_f(\sigma) = [1 - F(\sigma)]^N.$$ Eq. 16

This implies that failure is caused by the weakest link in the system. If the elements are very small so that N becomes large, the statistical distribution can be described by the Weibull distribution [71]:

$$P_f(\sigma) = 1 - exp\left[-\left(\frac{\sigma}{\sigma_0}\right)^m\right],$$ Eq. 17

where the scaling parameter σ_0 is the characteristic strength and m is the Weibull modulus, which is a measure of the variability of strength of the material [72]. The distribution is skewed to weak specimens with a rapid fall off in the probability of strong specimens. The physical interpretation is that failure occurs when a flaw is present that can propagate under the applied stress [73].

The applicability of the Weibull distribution to DCFP fibre architectures is investigated in Chapter 5 but is introduced here to provide background for a model proposed by Epaarachchi and Gohel [74], who use a unique approach when incorporating the Weibull distribution. Assuming that the strength of a random short-fibre composite can be described by a Weibull distribution, they propose that the fibres aligned in the load carrying direction also follow a Weibull distribution as the aligned fibres are directly proportional to the strength. The volume fraction of aligned fibres in the loading direction is therefore given by:

$$f(V_f) = \beta(1 - V_f)^{\beta-1} e^{-(1-V_f)\beta}, \qquad \text{Eq. 18}$$

where β is a shape parameter. The strength is then calculated using

$$\sigma_C = \left[\left(V_f\left(\frac{\sigma_m}{\sigma_f}\right)\right)^2 \sigma_f + \left[1 - \left(V_f\left(\frac{\sigma_m}{\sigma_f}\right)\right)^2\right]\sigma_m\right]\left(\beta(1 - V_f)^{\beta-1} e^{-(1-V_f)\beta}\right). \qquad \text{Eq. 19}$$

An unusual feature of this method is that the Weibull function is used to model orientation of fibres rather than describing a weak link theory. Due to the nature of the model, composite strength will rarely increase above the matrix strength. Application to DFCs is therefore limited to those dominated by matrix properties e.g. diluted SFRC. The use of a probabilistic function for orientation of fibres could however be applied to other DFCs.

Summary of reviewed literature

Work on defining analytical models for DFCs has typically focussed on fibres randomly dispersed in a matrix. Properties of DCFP fibre architectures are based on random tows rather than individual fibres, so many of these models are unsuitable unless adapted to account for the significantly larger geometry of the fibre bundles. Of particular importance will be the implications on the critical fibre length. As this

is typically defined by filament diameter, a link to tow diameter may exist. The other significant problem with previous models is that they are deterministic; often assuming an idealised case. A degree of probability needs to be incorporated into the analytical model to address uncertainty that arises due to the inherently random nature of DFCs.

2.4 Experimental methodology

2.4.1 Preforming

Rectangular preforms, measuring 400 mm x 600 mm, were produced for each test shown in the study. Carbon fibre was drawn directly from the bobbin and passed through a chopper gun mounted onto a Fanuc 6-axis industrial robot. Fibre lengths were determined by the number of blades used in the chop roller (circumference: 115 mm) of the chopper gun shown in Figure 8. Fibre lengths of 12 mm, 29 mm & 58 mm were chosen to cover the typical operating range of the gun. Preforms were made using tows containing 3,000 (3k) – 24,000 (24k) filaments (details of the fibres can be found in Appendix B).
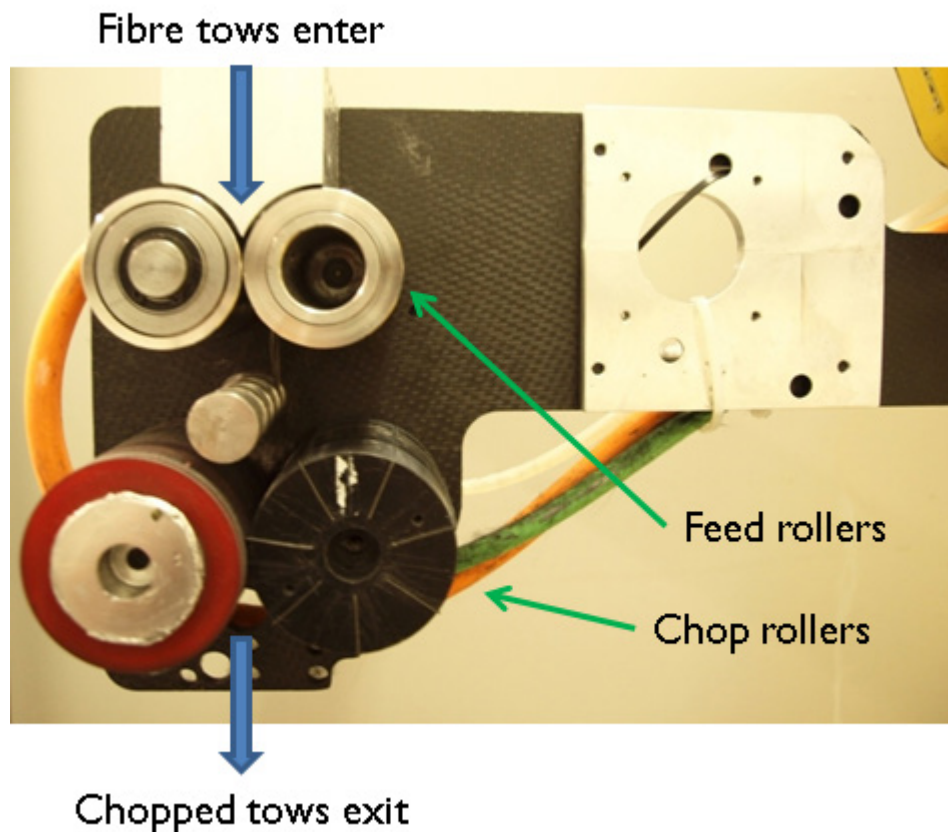
Figure 8. DCFP chopper gun used to manufacture preforms at the University of Nottingham. With smaller bundle sizes (3k and 6k), multiple tows were simultaneously processed through the chopper gun in order to meet the deposition of 269 g/m^2 per layer without having to significantly increase the chopper speed.

The chopped fibre was deposited along with Pretex 110, a powdered epoxy binder (10% wt.). Each single sprayed layer of fibre consisted of an east/west pass followed by a north/south pass of the robot with each sweep offset by 50 mm. Fibre was deposited at a rate of 269 g/m² per layer. Three target areal masses of 538 g/m², 1614 g/m² and 5380 g/m² were achieved by spraying 2, 6 and 20 layers at a deposition rate of 269 g/m² . These masses provided a target fibre volume fraction of 30 % at 1 mm, 3 mm & 10 mm. Each preform was consolidated in a Mackey Bowley heated press at 120°C for 5 minutes. Two preforms were compacted simultaneously at a pressure of 2 bar by applying a load of 10 tonnes i.e.

$$\text{pressure (bar)} = \frac{\text{force } (N)}{\text{area } (m^2)} = \frac{mg}{A}$$
$$= \frac{10000 \times 9.81}{2 \times 0.24} = 204375 \, {N}/{m^2} = 2.0 \, bar.$$

Benchmark laminates were produced from 8 layers of uni-directional 12k T700s non-crimp fabric. Both uni-directional (UD) and quasi-isotropic (QI) preforms were manufactured by sprinkling binder (5% wt.) between layers and consolidating at 2 bar at a temperature of 120°C for 10 minutes. Subsequent moulding and testing was carried out in accordance with the same methods that will be described for DCFP laminates.

2.4.2   Resin transfer moulding

Preforms were stamped into two smaller 400 mm x 300 mm preforms; one for moulding and the other for use in the compaction study (Chapter 3). Preforms were then moulded by resin transfer moulding (RTM). Each preform was weighed and trimmed before being loaded into a steel tool. Rectangular picture frames, with thicknesses equal to the three target thicknesses, were used to control the final thickness of the part. Preforms were trimmed in order to ensure a tight fit within the frame, which prevented race-tracking – a problem that can occur when there is an easy flow path for resin around a preform, resulting in poor part wet-out. Vacuum sealant tape was used to block any flow paths around the preforms. A matched steel tool was lowered onto the installed preform and secured with 4 x M12 bolts. A load

of 100 tonnes force was applied to the closed tool to ensure there were no leaks in the mould tool.

Figure 9. CIJect One™ Resin Injection Machine.

The epoxy resin, Prime20 LV, was injected into the mould cavity using the CIject One™ Resin Injection Machine (Figure 9). Prior to injection, the base and hardener were stored in separate containers. Air was removed from the epoxy system by circulating each component through separate heated hoses. The epoxy base was stored in a tank heated to 70°C. As described by Darcy's law, lower viscosities (achieved through heating) result in higher flow rates meaning lower injection pressures can be used.

$$Q = \frac{-k}{\mu} \nabla P, \qquad\qquad \text{Eq. 20}$$

This helped to alleviate some of the problems occasionally associated with RTM. Fibre washing can occur in the tool cavity when fibres are moved due to the flow of the resin. It can be particularly problematic in parts with a low fibre volume fraction as the fibres and tows are allowed a greater degree of movement within the tool. In parts where there is a high fibre volume fraction, poorer permeability can lead to a build-up of resin at the inlet and cause the entire preform to be pushed along the

cavity. This can result in tow distortion which can be detrimental to properties due to inefficient stress transfer across the fibres. Decreased viscosity permits reduced injection pressures for a given flow rate, reducing the likelihood of both problems. In order to maintain low resin viscosity throughout the process, the tool was preheated to 50°C. A vacuum was used to evacuate air prior to injection. This vacuum remained active throughout injection to aid flow and reduce void content in the final part; a method often used in the manufacture of high performance components.
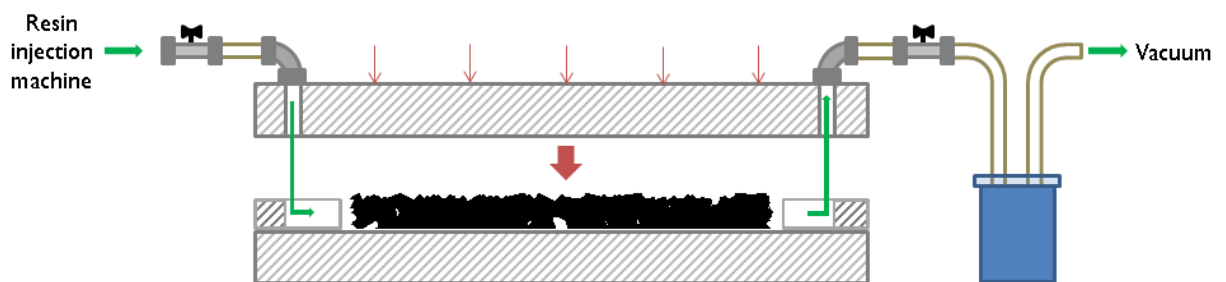
Figure 10. RTM method used to mould preforms in the characterisation study.

The moulding method is depicted in Figure 10. Resin was injected through an inlet, which remained closed until injection, situated at one end of the preform. Upon injection, the hardener was combined with the base, at a volumetric ratio of 31.4%, in a static mix-head. Flow rate and injection pressure were controlled by the system and could be increased or decreased in-process. Initially, injection pressure was set at 1 bar. To ensure continuous flow, injection pressure was increased up to a maximum of 9.5 bar, if required. An alarm was initiated if flow fell below a nominal rate – 0.1 litres in two minutes. Immediately after resin flow was observed at the outlet, the tap was closed with the injection machine still running. Air was evacuated from the tool periodically and flow was monitored to ensure that the alarm wasn't activated. As well as preventing voids, this also worked to promote full wet-out of the preforms. Once injection was complete, both the inlet and outlet were closed, and the injection was stopped at the machine. The injection machine was flushed by passing acetone followed by compressed air through the mix-head and injection hose. Meanwhile, the temperature of the tool was increased to 120°C

for one hour to ensure the part was fully cured. De-moulding was carried out after the tool was cooled to 40°C.

2.4.3   Tensile testing

Each moulded plaque was cut into 10 [0°] and 5 [90°] 25 mm x 220 mm specimens using a circular diamond cut off machine. A spherical micrometer was used to measure the thickness of each specimen, while the width was measured using a vernier caliper. Testing was carried out on an Instron 5581 50 kN loading frame at 1 mm/min, in accordance with BS EN ISO 527-4: 1997 and ASTM D3039. Figure 11 shows a typical test being carried out. Strain was measured over a gauge length of 50 mm using an extensometer. Load values were taken directly from the Instron load cell. Modulus was determined between the strains of 0.0005 and 0.0025, and ultimate tensile strength (UTS) was calculated from the maximum load measured for each specimen (Figure 12).

Figure 11. Tensile test. The specimen is loaded into the jaws of an Instron 5581 frame. Two thin layers of masking tape can be seen and were used to prevent slippage of the extensometer.
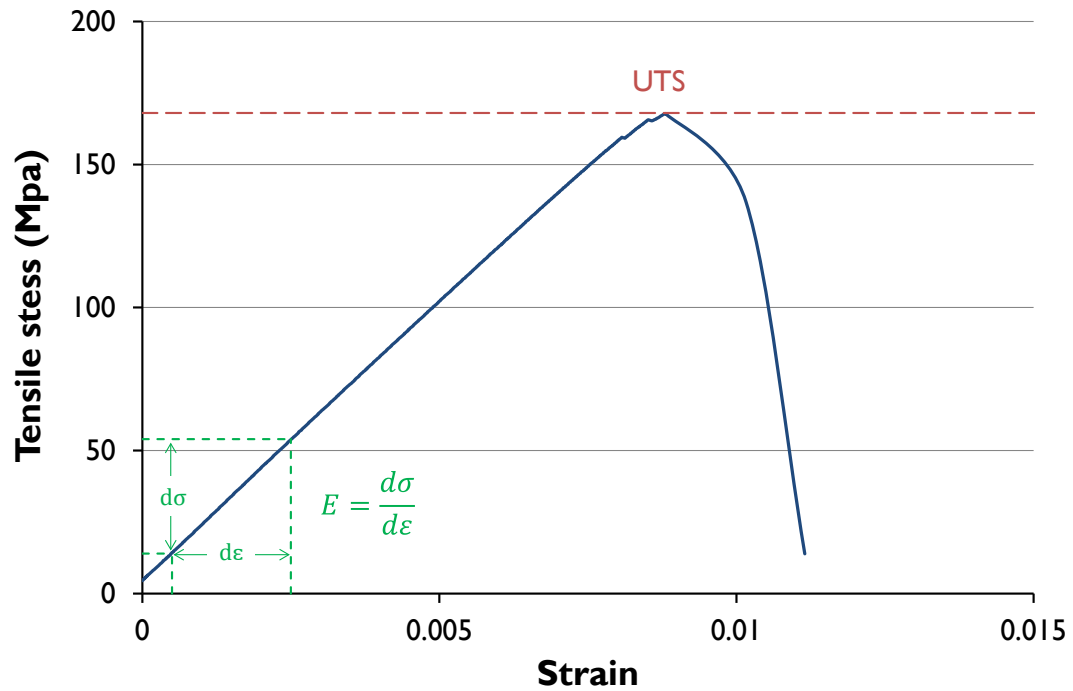
Figure 12. Typical tensile stress-strain curve indicating the UTS at peak load and strain values used to calculate the Young's modulus. Strain to failure was also defined by the peak load.

2.4.4 Further mechanical testing

Further mechanical testing was carried out on two benchmark DCFP architectures. Flexural, compression, shear (v-notched rail) and Charpy impact tests were carried out in accordance with the relevant test methods (shown in Table 1). Each laminate was water-jet cut to provide the necessary geometry of test specimens required for all five test methods.

Table 1. Test methods used for DCFP benchmarks.

Test method	Test standard	Specimen size (mm)	Size of batch
Tension	BS EN ISO 527-4:1997	25 x 220	8
Compression	ASTM D3410 - 03	12.5 x 140	7
Flexural	BS EN ISO 14125:1998	10 x 80	6
Shear (v-notched rail)	ASTM D7078 - 05	56 x 76	5
Charpy impact	BS EN ISO 179–1/1fUc:2001	10 x 80	5

Three-point bend tests were carried out using a Hounsfield testing machine to determine flexural properties. Compression and shear test specimens were loaded into appropriate rigs that were loaded using the Instron 5581 frame. Impact testing

was carried out using a shielded Avery Denison Charpy impact test machine (Figure 13). Specimens were un-notched and tested by flatwise impact.

Figure 13. Avery Denison Charpy impact test machine.

2.5 Analytical model for mechanical property prediction

Finite element analysis provides accurate estimations of component properties but processing times can be lengthy – approximately 4 hours for a 3k tensile specimen (dimensions: 3 mm x 25 mm x 250 mm). As the size of the part increases and approaches the proportions of large automotive components, processing times become significantly longer with powerful processing hardware becoming a necessity. There is interest in cutting down these processing times within the design process. If discretised regions within a component were assigned specific material properties, FE times could be reduced significantly.

Work has being carried out to develop an analytical model for predicting tensile properties within DCFP fibre architectures. The following sections (2.5.1 and 2.5.2) describe the approach that was used and propose new methods for predicting Young's modulus and UTS. A list of material properties used in the analytical model is shown in Table 2. Results of the analytical model have been compared to data obtained from fibre architectures investigated with finite element (FE) analysis using a model developed by Harper [28]. The FE modelling strategy randomly distributes (based on preform input variables) and simulates each tow as a 1D beam element in ABAQUS, with each beam assumed to have a circular cross-section determined by filament count and volume fraction of the tow. Results from the FE model were also used to establish basic trends for the development of the analytical model. Experimental data was used to further evaluate the analytical model in 2.7.

Table 2. List of properties used for prediction of tensile properties. Properties are taken from manufacturer data sheet values unless stated.

Material	Property	Symbol	Value
Fibre	Tensile modulus	E_f	238 GPa
	Tensile strength	σ_f	4265 MPa
	Fibre diameter	d	7 μm
	Tow volume fraction	$V_{f\,tow}$	60%*
Matrix	Tensile modulus	E_m	3.2 GPa
	Poisson's ratio	ν	0.4**
Interface	Interfacial shear strength	τ	40 MPa**

*[75], **[76]

2.5.1 Modulus

Homogeneity

The homogeneity of a material can be defined in numerous ways. Here it is considered at the meso-scale and is defined as the degree of similarity between constituent regions of the fibre architecture, in terms of tow distribution and orientation. A homogeneous structure will have a uniform structure and consequently, properties do not vary. Whilst the random nature of the fibre architecture makes this impossible in meso-scale DFCs, some architectures typically exhibit a higher degree of homogeneity than others. As shown in Figure 14 for example, the distribution of tows is more homogeneous in a preform containing 6k tows than one containing longer 24k tows. Improved preform homogeneity typically also corresponds to a greater number of fibre crossovers
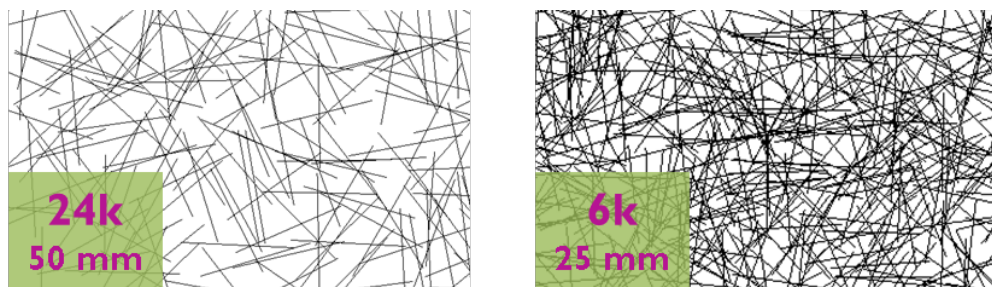
Figure 14. Illustration of the different distribution of tows in a preform containing (a) 24k, 50 mm and (b) 6k, 25 mm tows at a V_f of 10% and thickness of 2 mm. Beams are representative of the length, location and orientation of each tow but tow widths are not to scale.

While many existing analytical models provide the simplicity required predicting properties of meso-scale DFCs, they assume an idealised case. Consider the existing Voigt and Reuss rule of mixtures models. These work well for material systems that exhibit a high degree of homogeneity, which can be described by a repeating unit. The Voigt model is analogous with springs in parallel while the Reuss model (for transverse stiffness) is akin to springs in series (Figure 15).
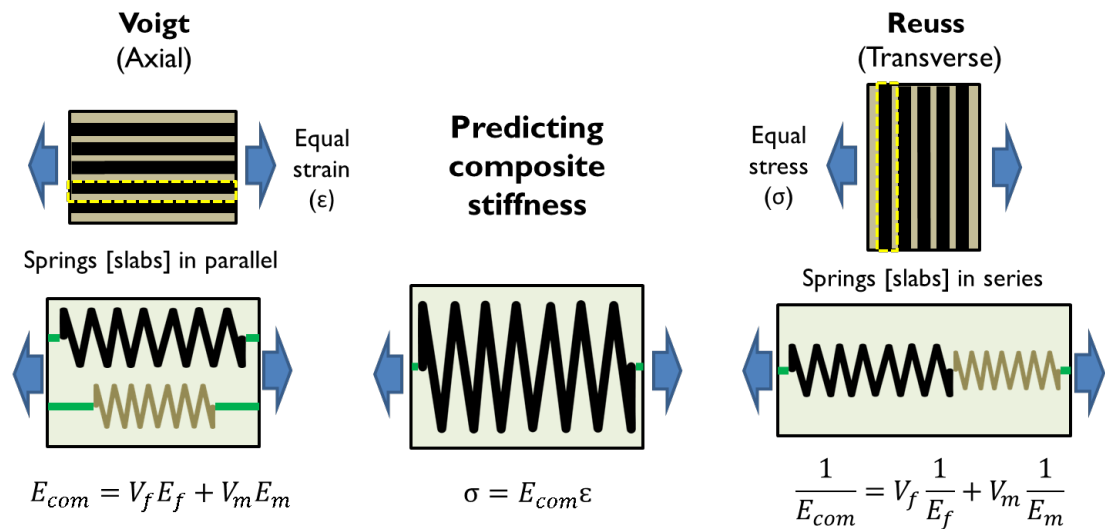
Figure 15. Illustration of springs analogy. Composites are often represented by a repeating unit cell (highlighted in the above). Voigt's method for determining stiffness in a composite follows the same form as determining stiffness in a system containing springs in parallel. Reuss' method for transverse stiffness follows the same form as a system with springs in series.

Direct application of these methods to meso-scale DFCs is limited. There is no easily identifiable repeating unit cell so one needs to be defined that is representative of the material. To an extent, length and orientation factors are already used to do this. Properties can be appropriately reduced to account for stress distributions across short fibres and a random orientation factor is typically applied to DFCs. However, there are also limitations to these methods. Properties are typically based on those of the individual fibres but performance of fibre bundles needs to be considered. Furthermore, a perfectly even distribution of fibre in all directions is assumed for randomly oriented composites, which only becomes likely when a high degree of homogeneity is seen in the preform architecture. The following model works on the principle of defining a representative unit for meso-scale DFCs. This will be defined by the properties of the fibre tow and the distribution of tow orientation based on a probability function for preform homogeneity.

Tow properties

This model considers the reinforcing fibres at the mesoscopic level. Properties of each tow are assumed to take the form of a large individual fibre embedded in a cylindrical matrix (Figure 16). Shear lag analysis is used to predict the stiffness of the tow within a laminate whilst considering the effect of fibre length,

$$E_{tow} = V_f E_f \left(1 - \frac{\tanh(\varphi s)}{(\varphi s)}\right) + (1 - V_f)E_m,$$ Eq. 21

in which the constant η for concentric cylinders where

$$\frac{R}{r} = \frac{1}{V_f}$$

is given by

$$\varphi = \sqrt{\frac{2E_m}{E_f(1 + \upsilon_m)\ln\left(\frac{1}{V_f}\right)}}.$$ Eq. 22
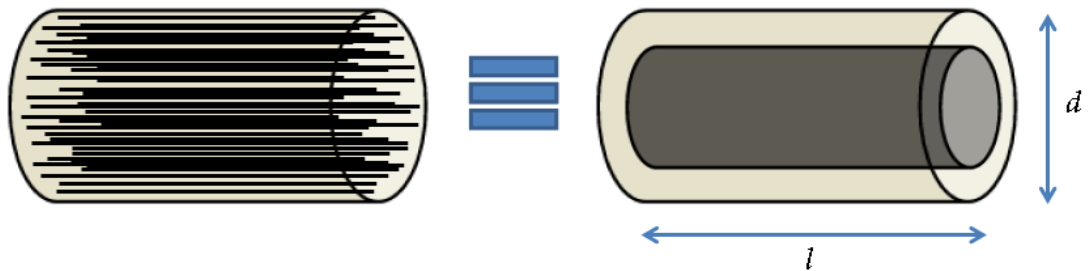
Figure 16. Tow properties modelled as a large individual fibre embedded in a cylindrical matrix.

The fibre aspect ratio *s* is determined by the tow length (*l*) and the diameter of the fibre bundle (*d*). The latter is calculated from the total cross sectional area of filaments in each tow,

$$d_{tow} = 2\sqrt{\frac{A}{n\pi}},$$ Eq. 23

where *n* is the number of filaments in the tow, and from which the aspect ratio is calculated as

$$s = \frac{l}{d_{tow}}.$$

<div align="right">Eq. 24</div>

The length efficiency factor for different fibre lengths for four tow sizes are shown in Figure 17. The figure illustrates that the estimated length at which a plateau in stiffness occurs is much larger for bigger fibre bundles.
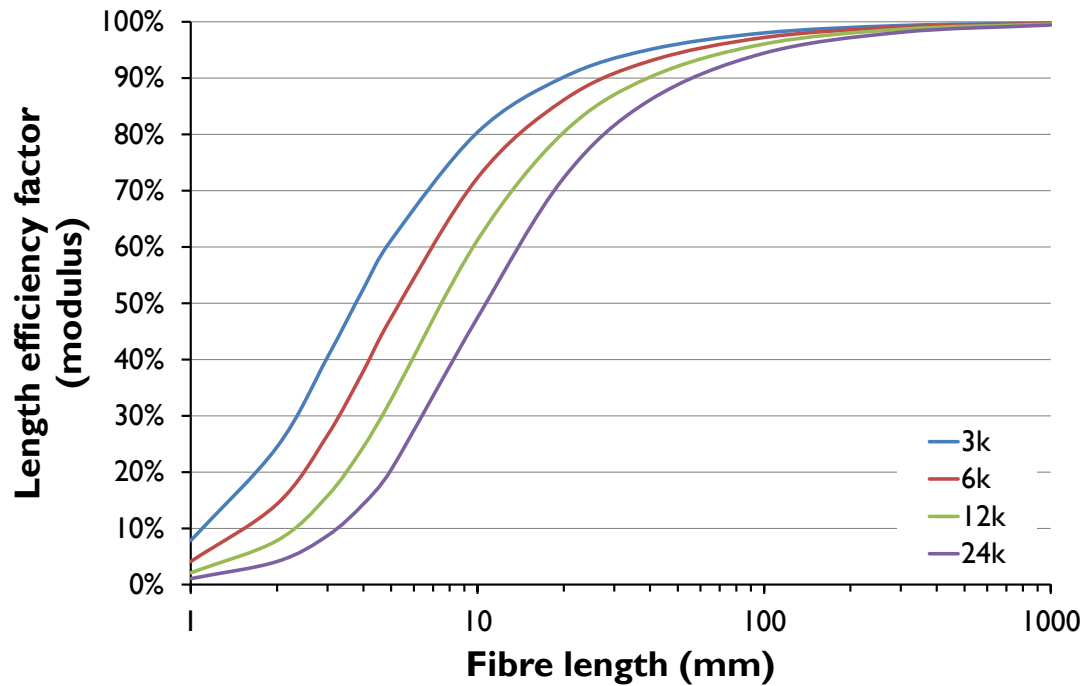
Figure 17. Length efficiency factor for the stiffness of tows with aspect ratios between ≈1 (24k, 1 mm fibres) and ≈2500 (3k, 1000 mm fibres).

Composite properties

Successful property prediction of tow-based discontinuous fibre architectures has been hindered by a lack of analytical models that consider the effect of mesoscopic homogeneity. Properties need to be related to fibre coverage and the random nature of the material. The rule of mixtures already accounts for volume fraction and takes into account length effects if a length efficiency factor is used; it doesn't however consider coverage effects. A modified rule of mixtures is proposed here which considers the effects of meso-scale homogeneity by including a homogeneity efficiency factor:

$$E = \eta_h \eta_o E_f V_f + E_m \left(1 - V_f\right). \qquad \text{Eq. 25}$$

An intermediate fibre volume fraction is used as the properties of each tow have already been determined. The tows are therefore assumed to occupy a volume that is equal to

$$V_f = \frac{tow \; V_f}{composite \; V_f}. \qquad \text{Eq. 26}$$

The theoretical orientation factor for random composites is typically calculated using

$$\eta_o = \Sigma \alpha_i \cos^4 \theta_i, \qquad \text{Eq. 27}$$

where α_i is the proportion of fibres directed in the orientation θ_i. For a random fibre composite where fibres are assumed to be equally distributed in all directions, $\eta_o = 0.375$. In reality, it is unlikely that this will be achieved with DFCs [77]. It is postulated that mechanical property prediction of meso-scale DFCs should incorporate probability effects to account for variability in the preform architecture. The homogeneity factor η_h has been introduced to define the probability that a perfectly random distribution exists that fulfils the above notion. The homogeneity factor η_h is calculated from the cumulative beta probability distribution function [78]:

$$\eta_h = p(x) = \frac{x^{\alpha-1}(1-x)^{\beta-1}}{B(\alpha,\beta)}, \qquad \text{Eq. 28}$$

where the beta function is described by

$$B(\alpha, \beta) = \int_0^1 t^{\alpha-1}(1-t)^{\beta-1}\, dt. \qquad\qquad \text{Eq. 29}$$
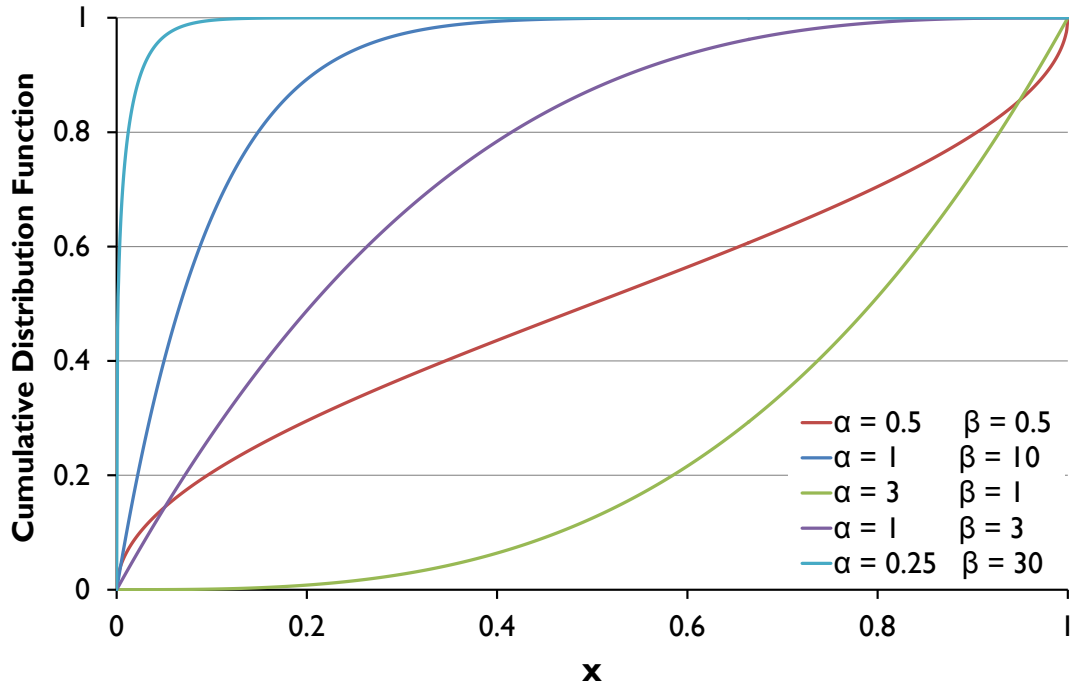
Figure 18. Cumulative beta distribution for different shape parameters.

The variable x is used to quantify the mesoscopic homogeneity of the fibre architecture, and α and β are shape functions. While homogeneity is influenced by thickness, tow size and fibre length; the inclusion of fibre length in the quantification of x results in errors in the trends predicted by the analytical model. The effect of fibre length has already been established in determining tow properties, which may sufficiently account for its influence as improved homogeneity (with shorter lengths) is cancelled out by reductions in stiffness. Inclusion of fibre length in this variable is therefore likely to be superfluous, so x is calculated from the tow size and thickness of the fibre architecture

$$x = \frac{thickness\ (m)}{tow\ size\ (k)} \times 100 \qquad\qquad \text{Eq. 30}$$

Shape functions for DCFP were estimated using FE data for multiple fibre architectures. Data was compared by evaluating the sum of squared residuals (SSR), and good correlation was seen with values of 0.25 and 30 for α and β, respectively. Although slightly lower SSR results were obtained using other values, the chosen values were deemed to characterise materials trends most appropriately.

The beta distribution is commonly used to represent data with natural upper and lower bounds. The standard beta distribution is shown in Eq. 28 (illustrated in Figure 18) and is bound by 0 and 1. At the lower limit this corresponds to no stiffness provided by fibre component in the composite. As preform thickness increases (for a fixed volume fraction), the number of fibre bundles within the laminate also increases. The distribution of tow orientations approaches uniformity, and the probability of the rule of mixtures being correct approaches 1. The same effect is seen by decreasing tow size as there are a greater number of bundles for a fixed mass of fibre. As previously mentioned, fibre length isn't considered (in η_h) as the effect is characterised by the influence of two factors where the increase in properties through improved homogeneity is cancelled out by reductions in stiffness with shorter lengths. Results from the model have been compared with FE data in Figure 19.
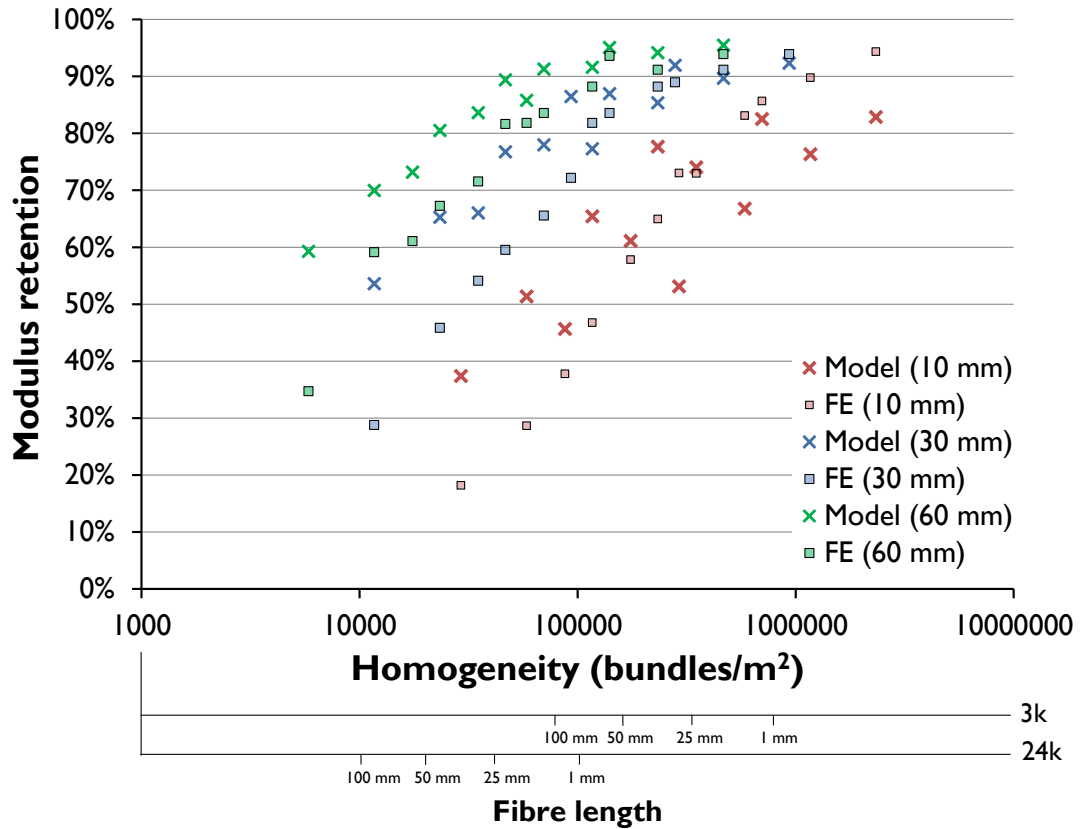
Figure 19. Predicted modulus retention of DCFP fibre architectures based on bundles per unit area. The analytical model with α and β shape parameters 0.25 and 30 was deemed to describe properties most appropriately through FE and experimental validation. Here it is compared with FE data. Results are shown for 36 fibre architectures with varying thickness, tow size and fibre length. Modulus retention was normalised with the value obtained using the rule of mixtures without length and homogeneity efficiency factors – 29 GPa for a V_f of 30%. The number of fibre bundles per m² was determined by dividing the areal mass of the preform by the estimated mass of each fibre tow.

2.5.2 Strength

Application of the model has been extended to predict the tensile strength of discontinuous mesoscopic fibre architectures.

Tow properties

The tow is again treated as a single fibre surrounded by a cylindrical matrix, but different length efficiency factors need to be defined as strength is determined by the onset of fracture. Properties of the tow are calculated using the fibre length efficiency factor proposed by Kelly and Tyson [79]:

$$\gamma_l = 1 - \frac{l_c}{2l}.$$

<div align="right">Eq. 31</div>

The minimum length, i.e. critical fibre length l_c, required to build up sufficient stress to fracture the fibre is calculated using

$$l_c = \frac{\sigma_f d}{2\tau},$$

<div align="right">Eq. 32</div>

where σ_f is the failure stress of the fibre, d is the fibre diameter, and τ is the interfacial shear strength. Length efficiency factors for different tow geometries are shown in Figure 20. Note that the plateau in strength occurs at substantially larger critical lengths compared to those for stiffness in Figure 17. Applying the length efficiency factor to the rule of mixtures leads to:

$$\sigma_{tow} = \gamma_l \sigma_f V_f + \sigma_m (1 - V_f).$$

<div align="right">Eq. 33</div>

It is assumed that the strain in the fibre and matrix are equal. The tow is treated as a continuous fibre composite where failure occurs due to fibre fracture. It follows that failure of the composite is dominated by failure stress of the fibres, so σ_f takes the value of the ultimate strength of the fibres and

$$\varepsilon_f = \frac{\sigma_f}{E_f} = \varepsilon_m = \frac{\sigma_m}{E_m}$$

<div align="right">Eq. 34</div>

The failure stress of the matrix is therefore determined by

$$\sigma_m = \varepsilon_m E_m.$$

<div align="right">Eq. 35</div>
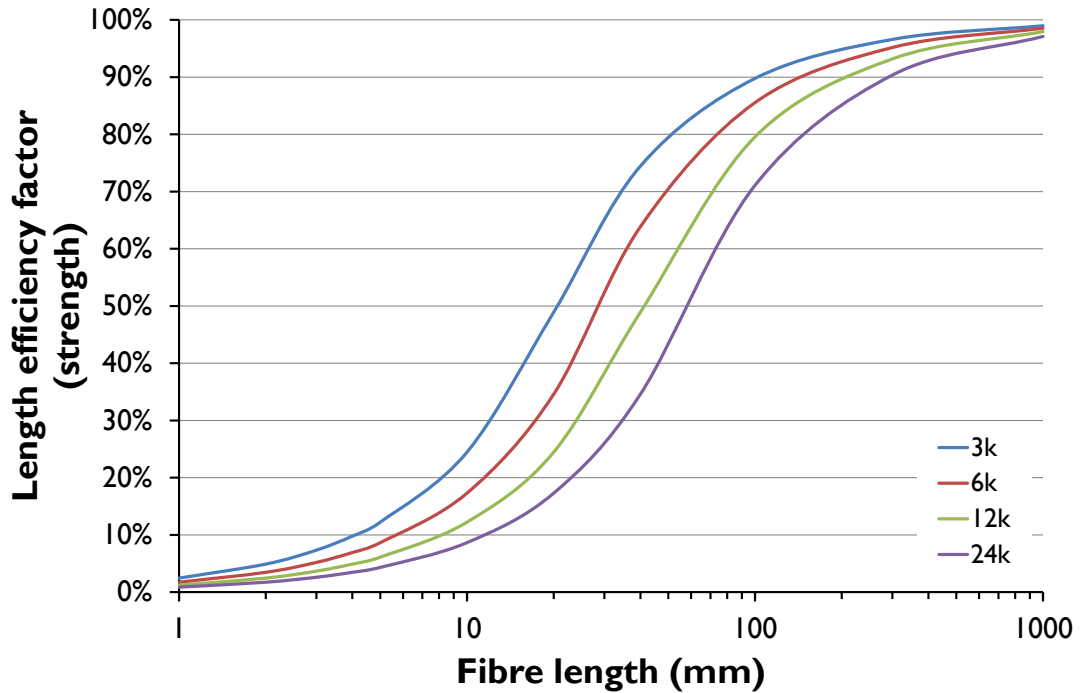
Figure 20. Length efficiency factor for the strength of tows with aspect ratios between ≈1 (24k, 1 mm fibres) and ≈2500 (3k, 1000 mm fibres). Note that the plateau in strength occurs at much larger fibre lengths than for stiffness (Figure 17).

Composite properties

The modified rule of mixtures is used to determine composite properties

$$\sigma = \gamma_h \gamma_o \sigma_f V_f + \sigma_m (1 - V_f). \qquad \text{Eq. 36}$$

Strength is also linked to the amount of fibres in the loading direction. For a quasi-isotropic fibre distribution it has been shown (page 26) that

$$\gamma_o = \eta_o = 0.375. \qquad \text{Eq. 37}$$

The homogeneity factor γ_h is calculated using Eq. 25 with the variable x given by Eq. 30. The intermediate volume fraction is also used again. However, significantly different shape parameters were required to fit the model (by minimising SSR) to FE data. Values of 0.35 and 2 for α and β give the data presented in Figure 21.
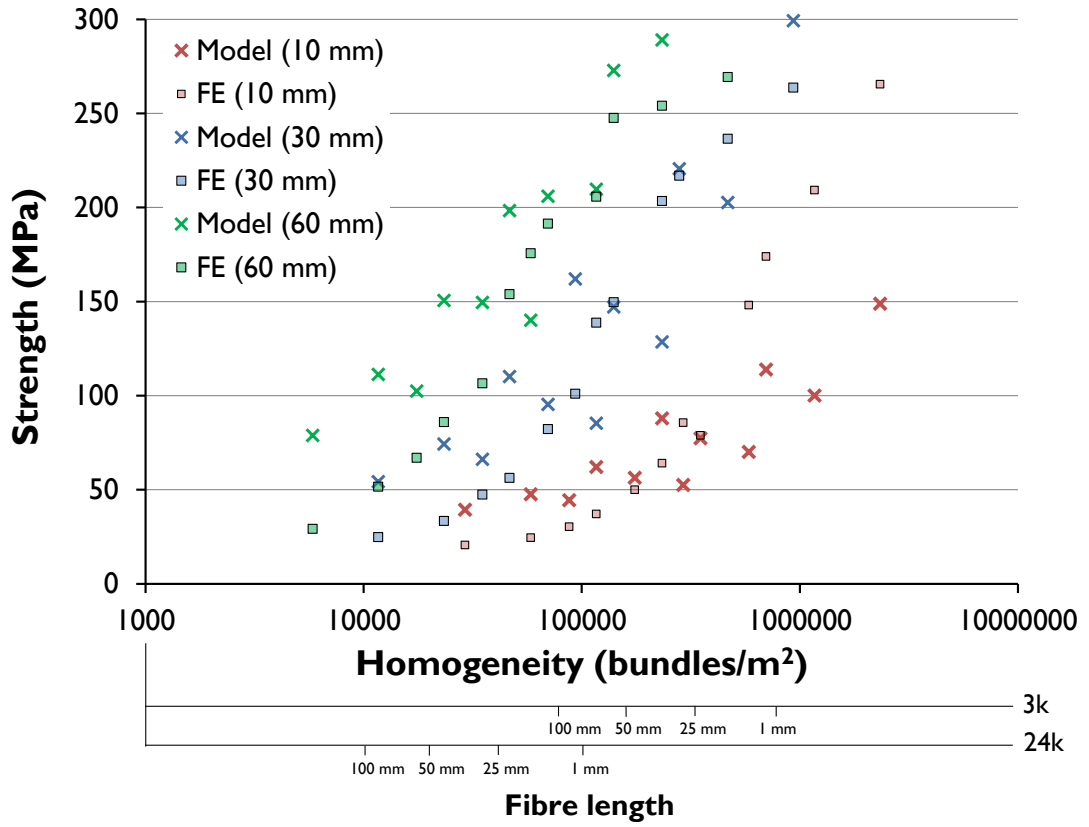
Figure 21. Comparison of the predicted UTS of DCFP fibre architectures using the analytical model and FE analysis. Shape parameters of 0.35 (α) and 2 (β) were used for the proposed model as these were seen to minimise SSR between FE values.

2.6   Design of experiments

The designs of experiments (DOE) for the two core experimental studies are detailed in the tables below. Results were used to validate the analytical model proposed in the previous section (2.5). The first DOE identifies preforms used in a cross-parameter study to characterise the effect of preform homogeneity on tensile properties of the laminate. The second study focussed on determining how such properties changed for a given fibre architecture over a range of thicknesses.

Table 3. Characterisation DOE. Each architecture was moulded at two thicknesses of 1 mm and 3 mm. The thickness and preform make-up are indicated by the designation with the fibre length represented by the nearest integer e.g. HOM010312 represents a 1 mm laminate with a 3k, 11.5 mm fibre architecture.

Designation	Tow size	Fibre Length (mm)	Thickness (mm)
HOM__0312		11.5	
HOM__0329	3k	28.75	
HOM__0358		57.5	
HOM__0612		11.5	
HOM__0629	6k	28.75	
HOM__0658		57.5	
HOM__1212		11.5	1, 3
HOM__1229	12k	28.75	
HOM__1258		57.5	
HOM__2412		11.5	
HOM__2429	24k	28.75	
HOM__2458		57.5	

Table 4. Thickness effects DOE. A DCFP architecture, with a tow size and fibre length of 6k and 60 mm, was selected for further investigation into the effects of laminate thickness. The architecture was moulded at six target thicknesses at a V_f of 50%.

Designation	Tow size	Fibre Length (mm)	Thickness (mm)
ASPTH1mm			1
ASPTH2mm			2
ASPTH3mm	6k	60	3
ASPTH4mm			4
ASPTH5mm			5
ASPTH6mm			6

2.7   Experimental results

2.7.1   Homogeneity effects

Fibre length

Previous work demonstrated that improved tensile properties were seen with shorter fibre lengths as stiffness and strength were primarily influenced by stochastic effects [24, 35]. High filamentisation of large fibre bundles was encouraged to decrease the effective tow size, which reduced coupon to coupon variation. Greater macroscopic homogeneity and filamentisation were observed using short fibres resulting in better performance. The exposure of more filament surface area through filamentisation can improve properties, as there is a greater area for stress transfer to occur, but there are associated problems. Highly filamentised preforms result in greater loft and reduced permeability, which are detrimental to the aim of attaining superior properties with increased volume fractions. Current methods have looked to minimise filamentisation, through low chopper speeds and reduced air pressure, in order to improve processability of manufactured preforms. As such, the same trends were not expected to be seen in this study.

The effect of fibre length is significant in DFCs that incorporate fibre bundles (rather than individual fibres) due to the relatively large diameter of the bundles compared with their length. The effect of the consequently larger aspect ratios was demonstrated by the length efficiency factors calculated for the analytical model in Section 2.5 (Figure 20 and Figure 17), with large increases in strength predicted up to lengths of over 100 mm for 24k tows. The critical length is therefore expected to be much larger than with single fibres.

Results of the experimental study confirm that increases in strength were observed with longer fibre lengths at thicknesses of 1 mm and 3 mm. The trend was most evident in the thicker laminates - results are shown in Figure 22 for 3 mm laminates incorporating tows at three fibre lengths. An average increase in strength of 19%,

across four tow sizes, was observed as fibre lengths were increased from 12 mm to 29 mm; this equated to a 1.1%/mm gain. A smaller increase of 18% (0.6%/mm) was seen by lengthening fibres further (to 58 mm) suggesting that while additional increases are probable, they are expected to be smaller in comparison. The effect of fibre length was more apparent for smaller bundle sizes, for which critical lengths are expected to be shorter due to smaller aspect ratios. It must be noted that, despite efforts to reduce loft, changing the fibre length had an effect on the level of natural fragmentation in preforms; shorter, larger tows were more prone to breaking up. These preforms (12k and 24k) were seen to exhibit high strength values, when compared to that predicted by the analytical model, for short fibre lengths.

The greatest increase in strength was seen between fibre lengths of 12 mm and 29 mm at a thickness of 1 mm (average increase of 62% - 3.6%/mm). A further increase at this thickness was not seen - strength decreased by 1% as fibre length was increased to 58 mm. The results suggest that the optimum fibre length for strength may be smaller for thinner parts. This goes against the expected trend but can be attributed to poorer fibre coverage as a result of tows with a large aspect ratio. It has been discussed that the critical length is determined by stress transfers from the matrix to the tows and the build-up of maximum tensile stress across the fibre length. For DFCs, the effect of stress transfer between separate fibre tows must also be considered. Shorter fibre lengths lead to higher levels of mesoscopic homogeneity due to improved fibre coverage. This consequently leads to more tow crossovers, with each contact point potentially facilitating stress transfer. The results indicate that while properties can be increased with fibre length there is an opposing factor – caused by less efficient stress transfer - that arises due to poorer coverage. It is hypothesised that the effect of this was not obvious in the thicker 3 mm parts as differences in the mesoscopic homogeneity were relatively smaller; so typical shear-lag fibre length effects were the most prominent factor.

The effect of fibre length on Young's modulus was less significant (results are shown in Figure 22). A 4% decrease between fibre lengths of 12 mm and 29 mm (-0.2%/mm) was followed by a 12 % increase between 29 mm and 58 mm (+0.4%/mm). A greater increase was seen between the shortest two lengths at a thickness of 1 mm – modulus increased by an average of 36% between 12 mm and 29 mm (2.1%/mm). No subsequent change was observed between 29 mm and 58 mm. It appears that the optimum length for modulus is also influenced by thickness. The fibre length at which a plateau in stiffness is reached is typically much shorter than the critical length for strength, so in DFCs the effect of fibre length is more likely to be linked to the effect of mesoscopic homogeneity. Consequently, when compared to strength properties, stiffness may be relatively insensitive to fibre length at thicknesses over and including 3 mm.

Fibre length effects

Stiffness
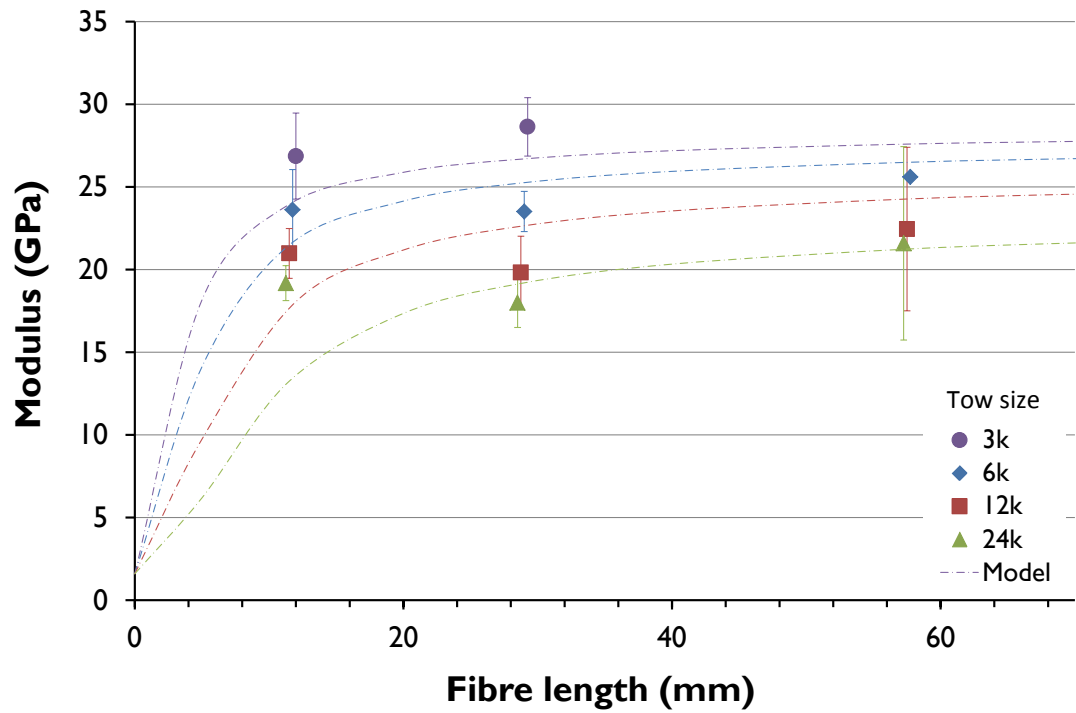
Strength
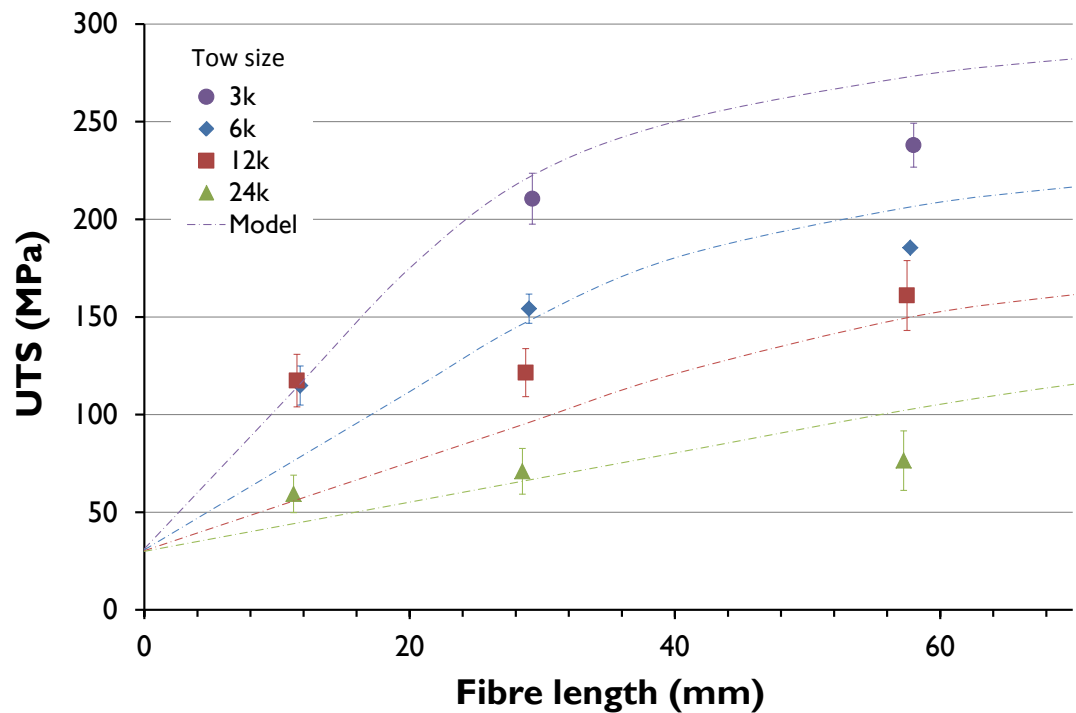
Figure 22: The effect of fibre length on Young's modulus and UTS for laminates at a thickness of 3 mm, with results normalised to 30% V$_f$. Experimental data has been offset (by 0.25 mm) for clarity. Findings are compared with the analytical model.

Tow size

Stiffness and strength were both seen to decrease as tow size was increased. Data is presented in figures Figure 25 and Figure 26. When larger tow sizes are utilised, fibre coverage is worse due to the smaller number of bundles for a fixed areal mass and volume fraction. At a thickness of 1 mm, Young's modulus and UTS decreased by an average of 37% and 74% as the fibre bundle size was increased from 3k to 24k. The effect of this became less significant with thicker parts, and the reductions were seen to decrease to 29% and 67%. A comparison of the property reductions (normalised with 3k) is shown in Figure 23. While reductions becomes less significant with increasing areal mass, it is clear that tow size still has a substantial influence on mechanical properties, particularly strength. Smaller tow sizes, which result in improved homogeneity, increase stress transfer efficiency by producing more interconnected fibre networks through increased surface area (Figure 24). These tows will also exhibit smaller critical lengths due to larger aspect ratios.
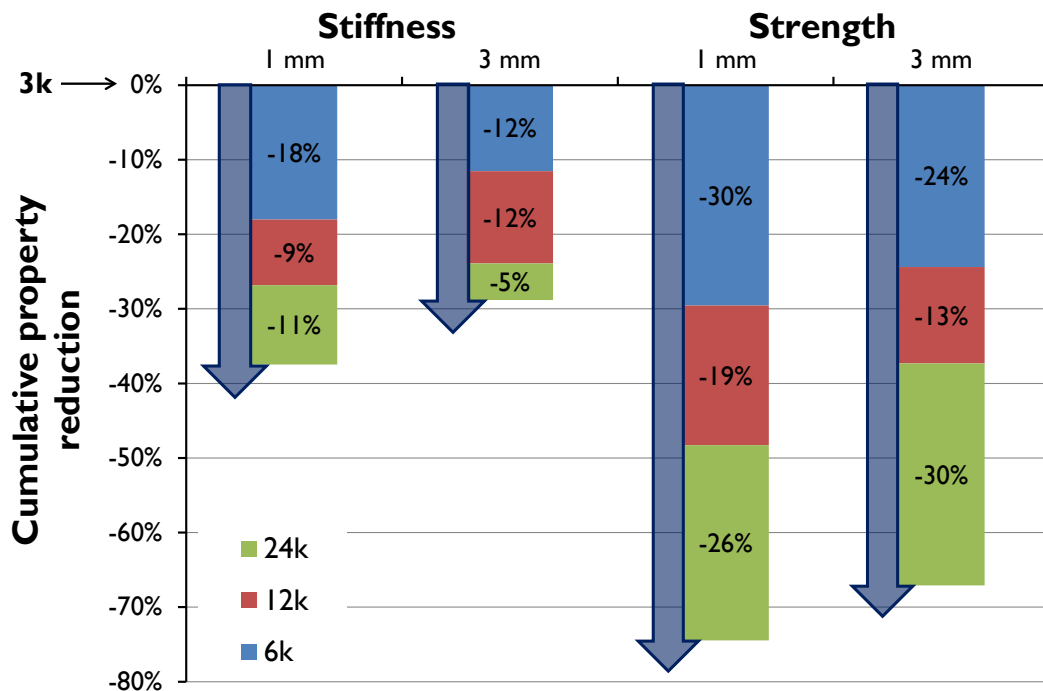
Figure 23. Reductions in tensile properties for increasing tow size. Data was normalised with 3k results which were the highest recorded for stiffness and strength at both thicknesses. The data values represent a contribution to the reduction in properties from each tow. Therefore the property reduction for a tow is the sum of all the values in the bar e.g. stiffness reduction for 12k at 1 mm is 27%.
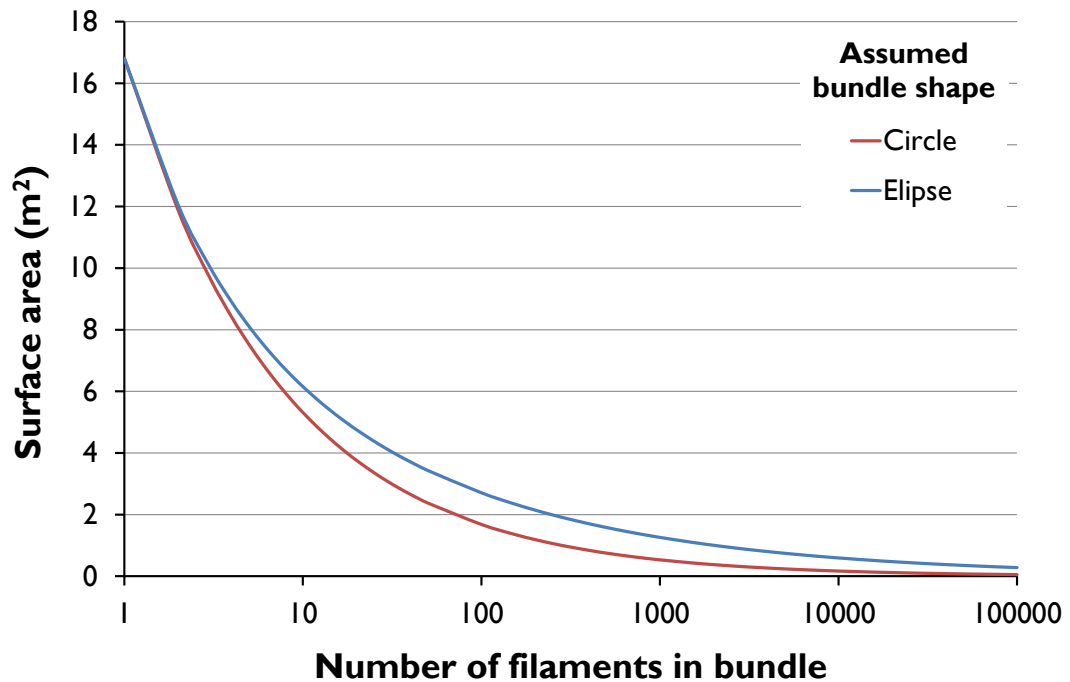
Figure 24. **Decrease in exposed filament surface area as tow size increases. Results are for a V_f and fibre length of 30% and 12 mm. Curves have been presented for data based on the assumption that the cross section of the bundles are either circular or elliptical. The relationship between the tow size and ratio of the ellipse was interpreted through dry fibre tow measurements. It can be seen that the ratio of the ellipse approximates to 1 for small bundle sizes.**

Variability in data was also seen to increase with tow size, as indicated by the larger error bars in Figure 25 and Figure 26. On inspection, 12k and 24k specimens were more likely to exhibit resin rich areas; dry regions were generally uncommon. These laminates also suffered from fibre washing and waviness. Long fibre lengths were most adversely affected, which could have been a minor factor in results that weren't in keeping with the data for shorter fibre lengths. Manufacturing defects such as these lead to inefficient stress loading of the fibre. Whilst some authors believe that this can only affect tensile properties in severe cases [80], others consider it to be more significant; suggesting that the broader the distribution of the fibre misalignment caused by fibre waviness results in smaller tensile strength [81]. The influence on DCFP was seen to be small, when compared to continuous fibre composites due to the inherent degree of fibre misalignment in its heterogeneous meso-structure.

Tow size effects (1 mm)

Stiffness
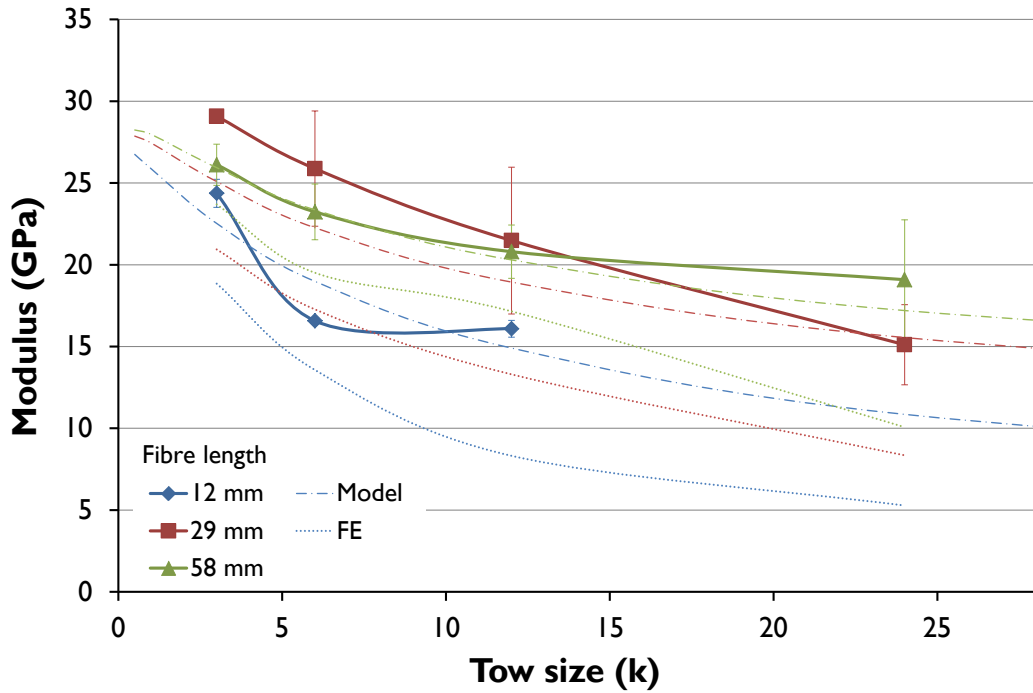
Strength
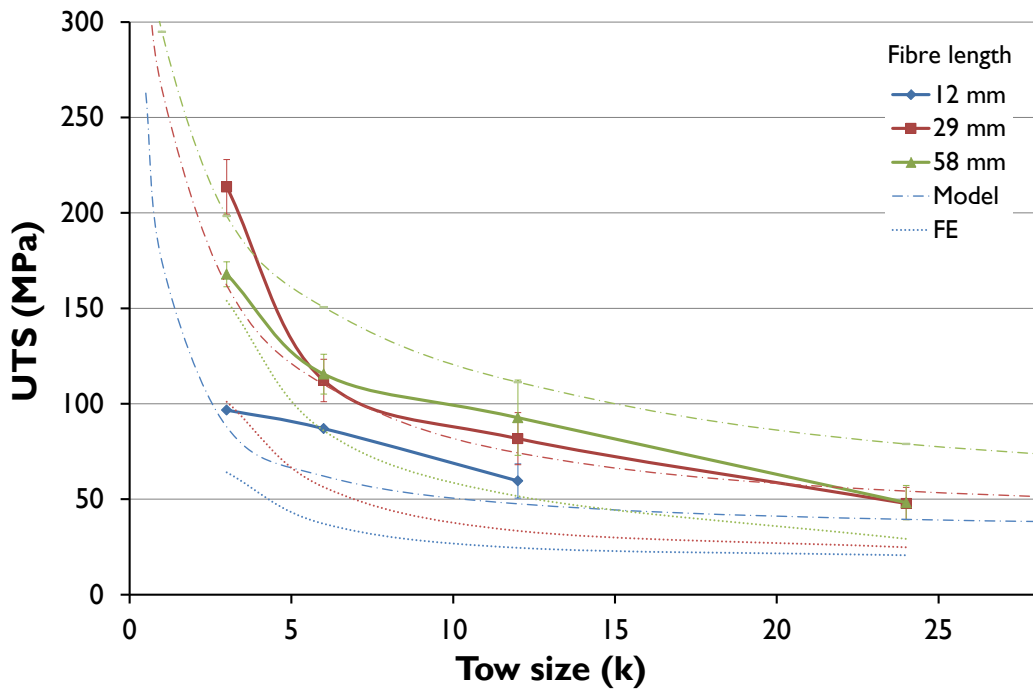
Figure 25: The effect of tow size on the Young's modulus and UTS of 1 mm DCFP laminates. Results are normalised to 30% V$_f$. Results from the analytical model and FE analysis are also shown. Fe results are based on analysis of each architecture in the experimental DOE, while curves for the analytical model were produced from numerous data points.

Tow size effects (3 mm)

Stiffness
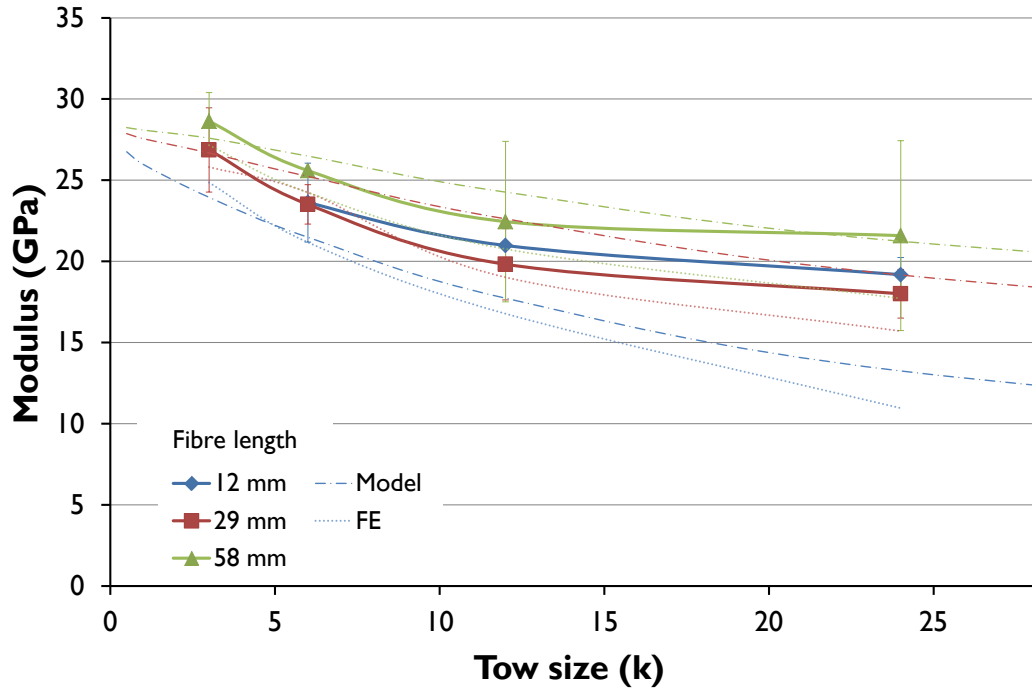
Strength
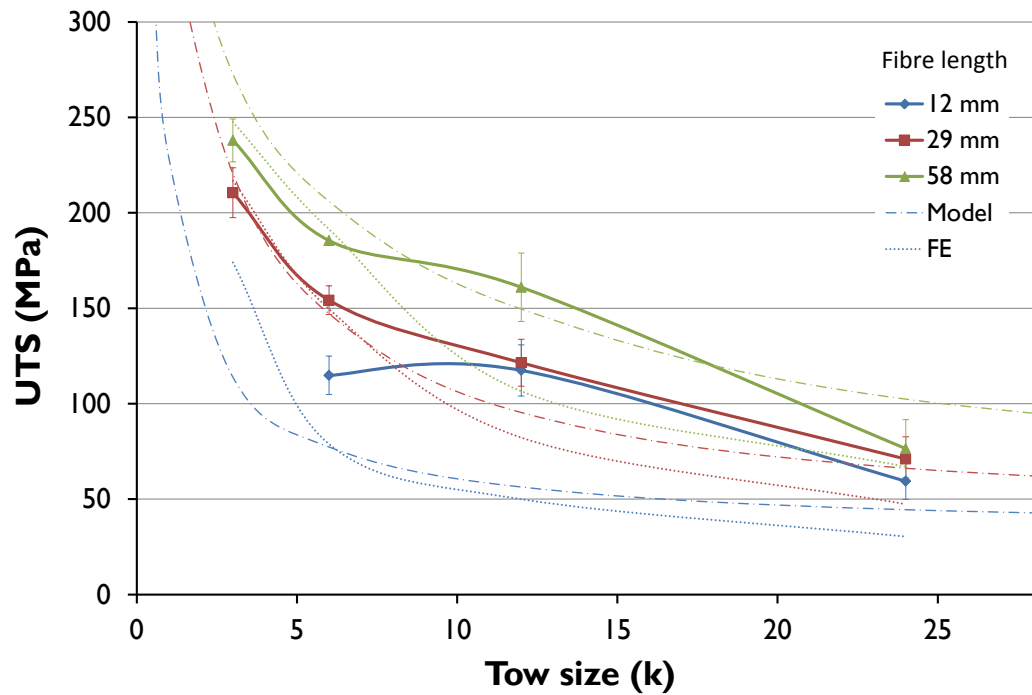
Figure 26: The effect of tow size on Young's modulus and UTS for 3 mm DCFP laminates at three different fibre lengths. Results are normalised to 30% V$_f$. Results are also shown from the developed analytical model and FE analysis.

Thickness

Stiffness and strength were both seen to increase as a function of thickness. Modulus was seen to rise by an average of 11% (for a given fibre architecture) between thicknesses of 1 mm and 3 mm. The effect on strength was greater - an increase of 50% between the same thicknesses. This improvement in properties was also more significant with longer fibre lengths. This is due largely to poorer homogeneity in parts with low areal mass; hence, as thickness increases this effect is seen to diminish.

The DOE (Table 3) originally incorporated fibre architectures moulded at a target thickness of 10 mm, but problems arose in the moulding process: the relatively low volume fraction [30%] used in the study became more problematic with these preforms, as washing and tow waviness were seen to be severe. This was evident in the poor results obtained for the majority of laminates at this thickness. Testing for many of these laminates was not possible, or produced invalid results, due to the poor quality. Results have been included in Figure 27 for two fibre architectures where test results were deemed valid. Both incorporate a fibre length of 29 mm, with tow sizes of 6k and 24k.

A plateau in Young's modulus appears to have been reached before 10 mm for the 6k fibre architecture. This was not the case with the bigger 24k fibre bundles. An increase of 19% between 1 mm - 3 mm was followed by a larger increase of 40% between 3 mm – 10 mm indicating that properties will continue to increase beyond 10 mm. Increases in strength were seen up to the maximum tested thickness for both tow sizes. Between 3 mm and 10 mm, increases of 29% and 88% were measured for 6k and 24k architectures, respectively. This was in contrast to results from the analytical model as increases of 39% and 29% were predicted, highlighting a limitation of the model. Good correlation with experimental results was seen with 6k parts up to 10 mm, but properties were under-predicted for both stiffness and strength of 24k parts at that thickness. This is a result of the homogeneity factor being too small, which is a consequence of the factor being based on only tow size

and thickness. Other factors are also in effect: most significantly, stress transfer between fibre tows, which is likely to be considerable in thick parts.

The more significant impact of thickness on properties of 24k preforms is likely to be a result of poorer homogeneity in the fibre architecture. Stress transfer between fibre tows has previously been discussed as a contributing factor to the properties of parts and is less efficient in parts with low areal mass, or those that incorporate large tows, due to poor fibre coverage. An initially large increase in properties (with thickness) levels off as mesoscopic variability approaches a ceiling where stress transfer is most efficient. Beyond this point, mechanical properties are predominantly determined by properties of the tow so a performance plateau is reached. The results indicate that this hasn't been achieved by 24k preforms as both properties are still rising. A continued increase in UTS for the 6k tows is indicative of a larger dependence of strength properties on mesoscopic homogeneity. This may be a consequence of strength also being determined by weak regions in the fibre architecture. A plateau for tensile strength may also be achieved if a more homogeneous preform is used – something that may be achieved through larger volume fractions. Further analysis was required to determine whether a performance plateau, relating to thickness, can be reached for a given fibre architecture. A more comprehensive study is detailed in Section 2.7.2.

Thickness effects

Stiffness
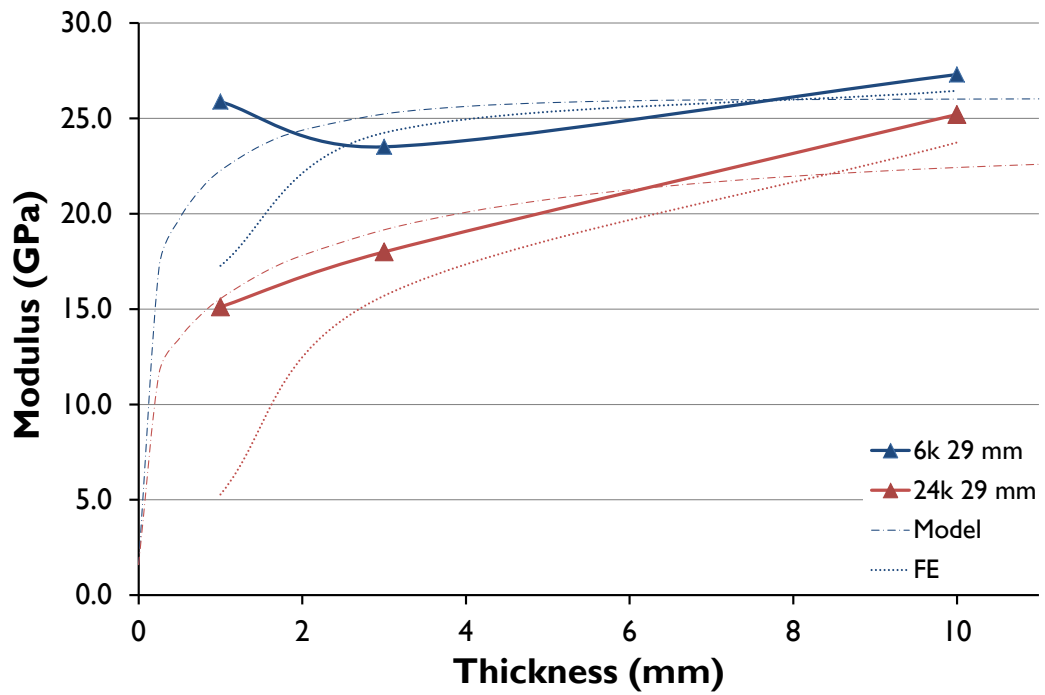
Strength
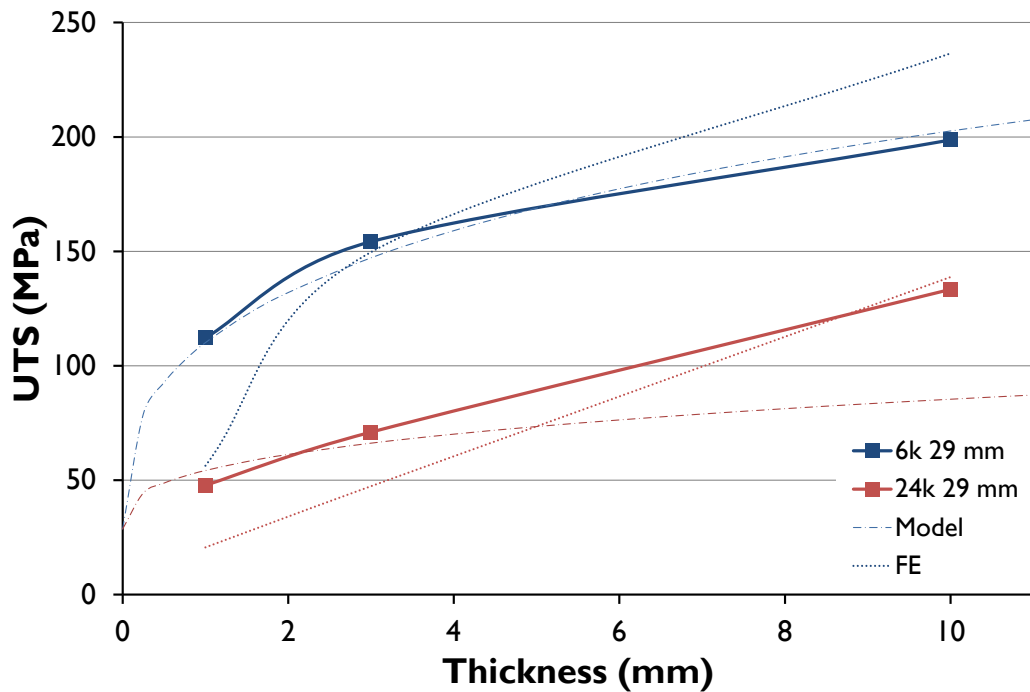
Figure 27. The effect of thickness on the Young's modulus and UTS of two DCFP architectures – 6k and 24k – with a fibre length of 29 mm. Results have been normalised to 30% V$_f$. Data is compared to results from the analytical model and FE analysis.

Volume fraction

Tensile data is presented in Figure 28 and Figure 29 for all 1 mm and 3 mm results from the characterisation study. A linear increase in modulus as a function of volume fraction was observed. Results have also been included for a resin film trial, details of which can be found in Appendix C. Preforms from the aforementioned trial were moulded with a different epoxy system, Gurit ST 70, at a nominal target thickness of 3 mm. Fibre architectures resemble those from this study, incorporating different tow sizes but with a fixed fibre length of 29 mm. A line of best fit has been fitted for all stiffness data at 3 mm. This crosses the y-axis at 3.52 GPa – a value which corresponds with the modulus of the neat resin provided by the manufacturer (3.28 GPa).
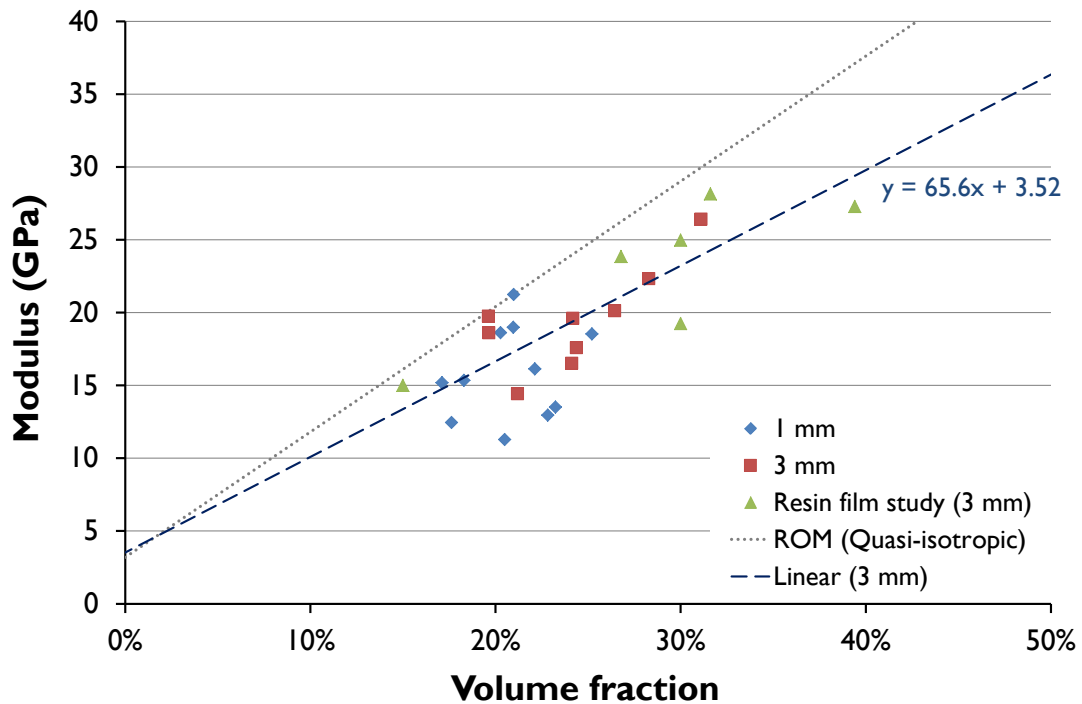
Figure 28: The effect of volume fraction on tensile modulus for fibre architectures in the characterisation study. Results are included for a resin film trial that incorporated the same fibre architectures used in this study at a target thickness of 3 mm. A linear line of best fit (E = 65.6V$_f$ + 3.52) is shown for results from the homogeneity study at 3 mm as a comparison for the expected modulus calculated from the Krenchel-derived rule of mixtures for quasi-isotropic laminates.

Strength was also seen to be an approximately linear function of volume fraction, but greater variability was seen in the spread of strength data (Figure 29). Several laminates exhibited lower UTS values than that of the neat resin (68.6 MPa). These were all preforms with a coarse fibre distribution – with a preform thickness of 1 mm or a tow size of 24k – indicating that in such cases the fibre reinforcement can weaken the composite through the introduction of stress concentrations.
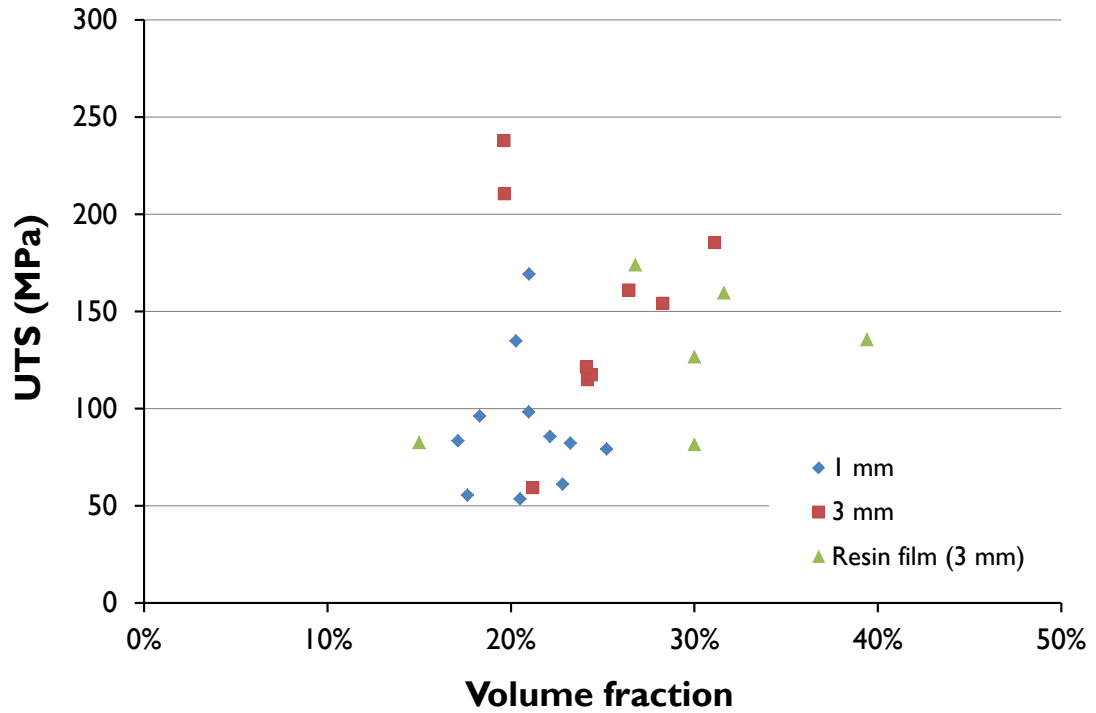
Figure 29: The effect of volume fraction on UTS. Results are included for a resin film trial. A linear line of best fit (UTS = 203V_f + 68.1) is shown for results from this resin film study.

Model evaluation

The conventional rule of mixtures for a randomly oriented composite represents the upper bound of both stiffness and strength models. The model approaches this value as the number of bundles (per unit area) increase and/or fibre length is increased. The lower bound is represented by the stiffness/strength contribution of the matrix. Figure 30 shows results for fibre architectures at various extremes (e.g. short fibres - 5 mm) and demonstrates the range of values estimated by the model.

Performance of large bundle sizes and the shortest fibre length (12 mm) were under-predicted by both the analytical model and FE analysis. This is due, in part, to the effect of fragmentation but assumptions relating to stress transfer in the composite also need to be considered. Small improvements were seen in stiffness prediction by incorporating axial stress transfer at the fibre ends using methods proposed by Clyne (Eq. 8) or Starink (Eq. 9). However, it is thought that stress transfer at the fibre ends is likely to have less of an influence than stress transfer between fibre tows. The significance of stress transfer between fibre tows has been highlighted by the experimental results. Neither model incorporates this effect resulting in poor agreement for shorter fibres where there are likely to be more fibre crossovers.
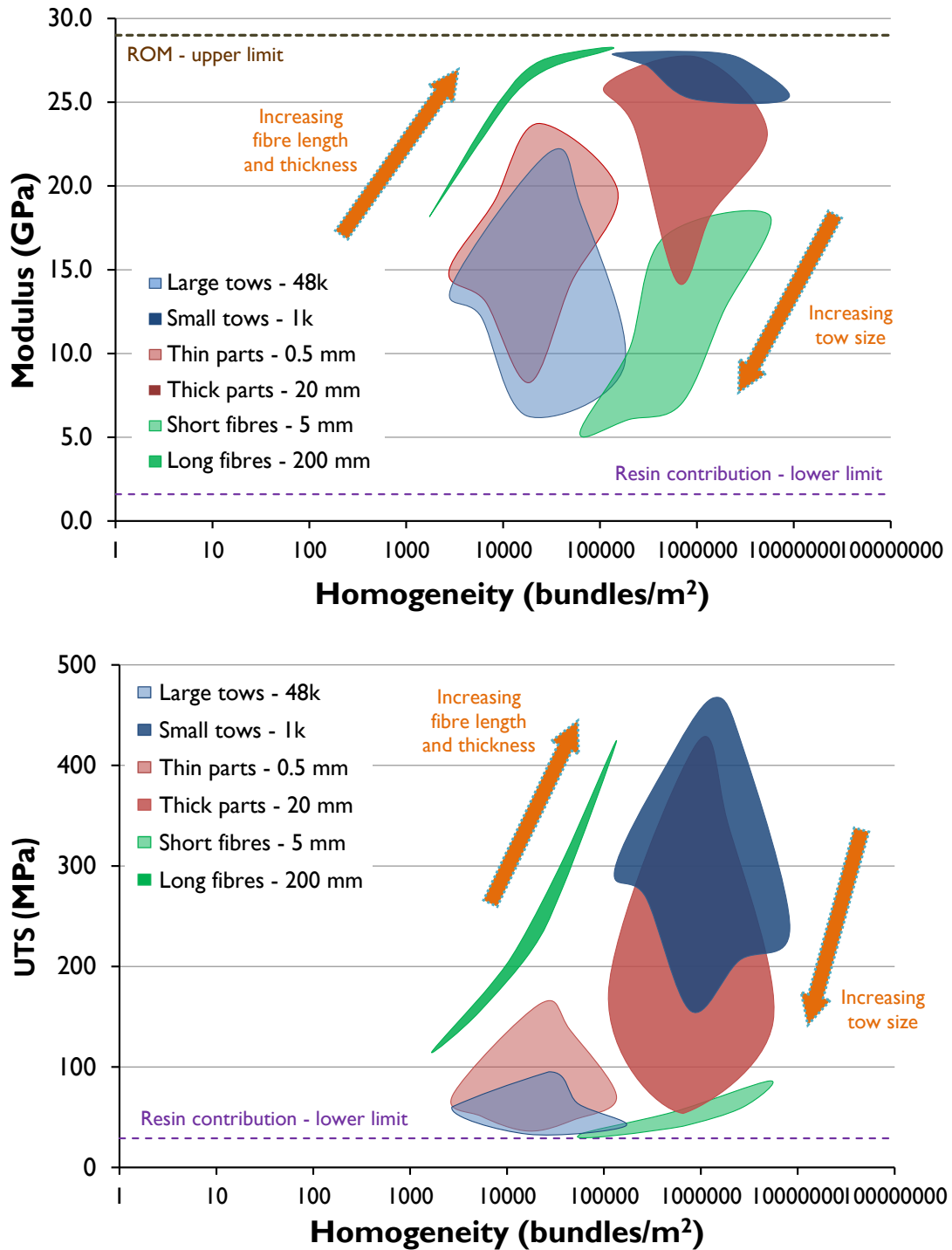
Figure 30. Tensile property results from the analytical model for fibre architectures with extreme values for thickness, tow size and fibre length. The model was run, using a macro, for ranges of values and envelopes were drawn manually around the clusters of points. All results are for a V$_f$ of 30%. Each shape represents the spread of results from the original characterisation DOE (Table 3) but with an extreme value substituted for a particular variable e.g. tow size of 48k. The extreme tow sizes represent the smallest and largest tow sizes typically used in the manufacture of DCFP preforms. The shortest and longest fibre lengths are typical of the limits of a chopper gun, whereas those for thickness are hypothetical limits for the thickness of a laminate.

2.7.2   Thickness effects

Unlike conventional laminates, the tensile properties of DCFP parts have been seen to vary with increasing thickness. Testing was carried out over a range of thicknesses using a fibre architecture known to give good performance (the architecture was also selected for further study detailed in 2.7.3). The laminates tested are detailed in the table below with the results presented in Figure 31 and Figure 32.

Table 5: Summary of laminates tested in the ASP thickness study. Binder mass, at 5% of fibre mass, was assumed to be constant for all preforms when calculating the fibre volume fraction.

Designation	Description	Target fibre mass (g)	Measured preform mass (g)	Moulded mass (g)	Laminate thickness (mm)	Volume Fraction
ASPTH1mm	4 layers of 6k, 60 mm, 0.223 g/m², chopped carbon fibre	107	106	210	1.29	36%
ASPTH2mm	8 layers of 6k, 60 mm, 0.223 g/m², chopped carbon fibre	215	222	429	2.66	37%
ASPTH3mm	12 layers of 6k, 60 mm, 0.223 g/m², chopped carbon fibre	322	328	578	3.40	42%
ASPTH4mm	16 layers of 6k, 60 mm, 0.223 g/m², chopped carbon fibre	430	416	634	3.69	50%
ASPTH5mm	20 layers of 6k, 60 mm, 0.223 g/m², chopped carbon fibre	537	538	921	5.65	42%
ASPTH6mm	24 layers of 6k, 60 mm, 0.223 g/m², chopped carbon fibre	644	632	1036	6.39	46%
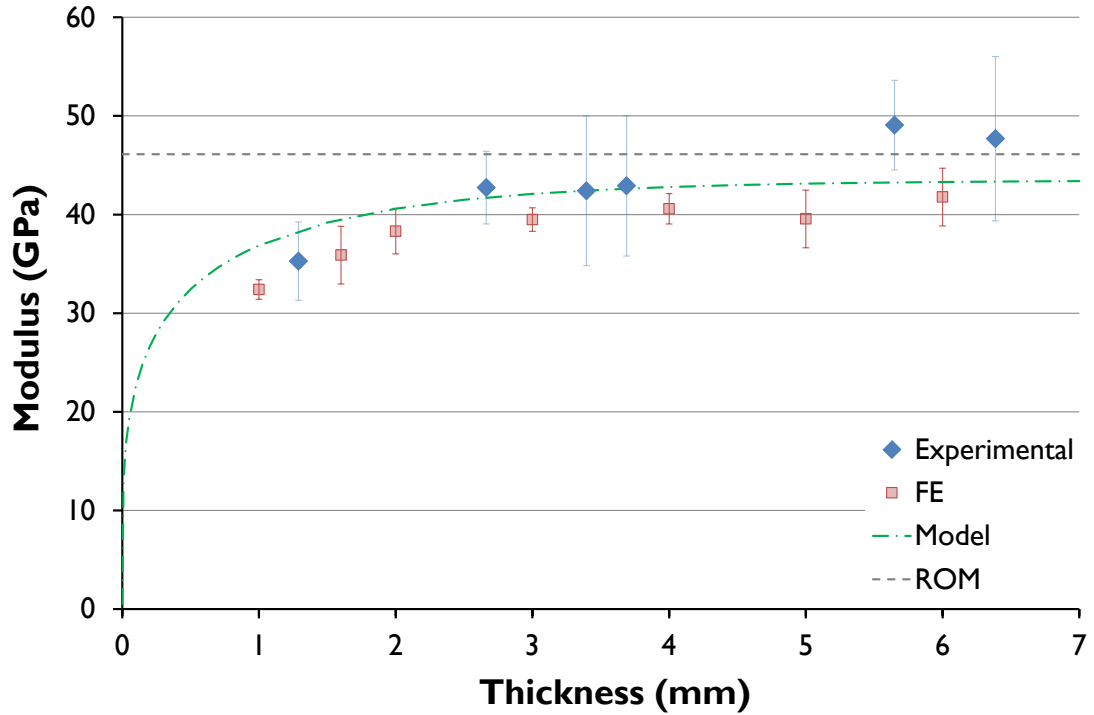
Figure 31: The effect of thickness on the modulus of FA1 laminates. All experimental data has been normalised to 50% V$_f$. Results are compared with FE and ROM results. Error bars on FE results relate to scatter from multiple runs of randomly-generated FE models.
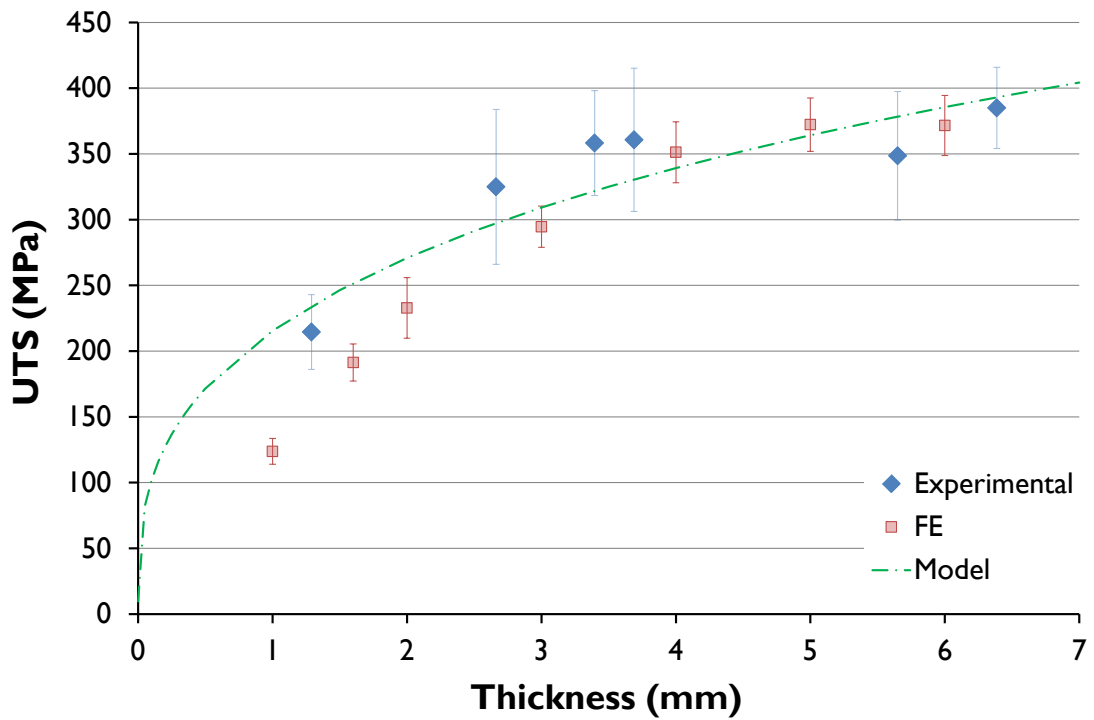
Figure 32: The effect of thickness on the ultimate tensile strength of FA1 laminates. All experimental data has been normalised to 50% V$_f$. Error bars on FE results relate to scatter from multiple runs of randomly-generated FE models.

Results showed an increase in modulus as thickness was increased from 1 mm to 6 mm (Figure 31). A larger increase was seen in thinner parts – 21.1% between 1.3 mm and 2.7 mm compared to an increase of just 0.43% between 2.7 mm and 3.7 mm, albeit over a smaller range. Experimental data showed good agreement with the analytical model and FE analysis up to 4 mm. Results at 5.65 mm and 6.39 mm were considerably higher than expected. Both results were also seen to be more than the estimated value calculated through rule of mixtures. It should be noted that smaller batches, with approximately half the number of specimens, were tested at these thicknesses due to difficulties in moulding. Thicker laminates should typically result in lower variability due to improved preform homogeneity, but results from these smaller batches were more inconsistent. The coefficient of variation was particularly high for the strength of ASPTH6mm and may account for differences in the expected results. A degree of tow alignment was also seen in the preforms and may be another reason that results were higher than predicted. This can be an associated problem when using longer fibre lengths due to the manner in which the tows fall onto the preforming tool [82].
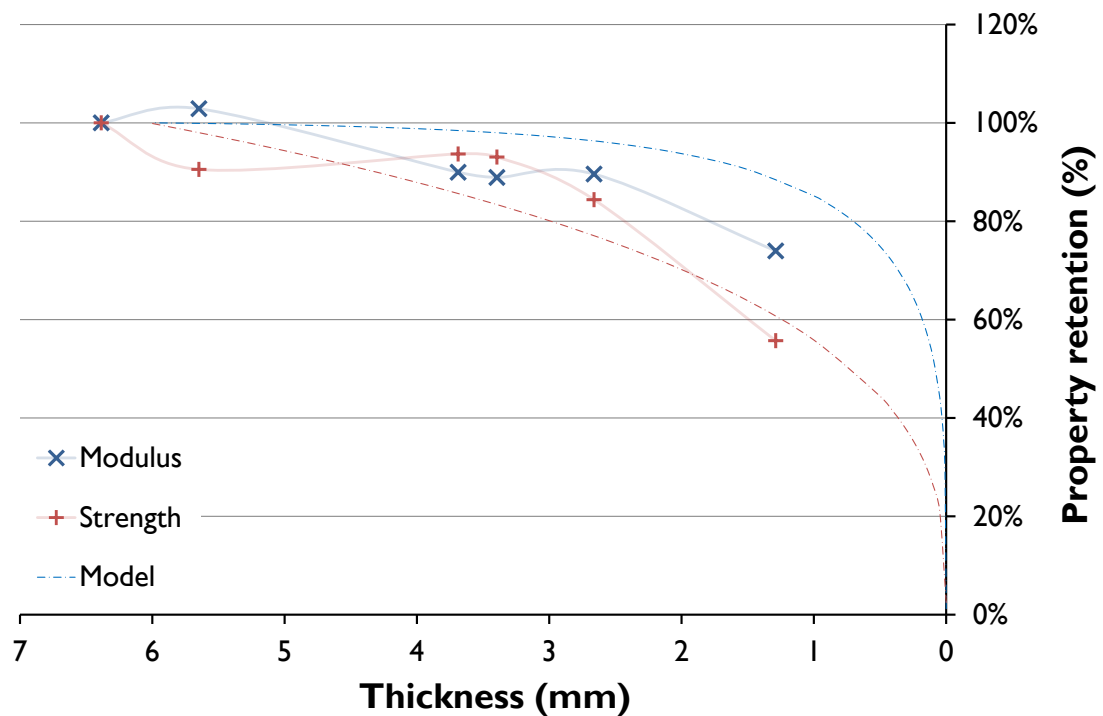
Figure 33: Property retention for FA1 laminates at 50% Vf. Maximum values for stiffness and strength were assumed to be obtained from the thickest laminate tested. Retention values were therefore calculated as a proportion of results from ASPTH6mm, indicated by the starting point (on the far left of the chart) of each experimental curve.

Increases in strength were more significant – 51% (1.3 mm - 2.7 mm) and 11% (2.7 mm - 3.7 mm) – indicating that reductions are a greater for UTS. Property retention at each thickness was estimated by normalising results with data from the thickest preforms in the study. Figure 33 shows the reduction in property retention if 6 mm parts are assumed to be indicative of absolute properties. Experimental results indicate that for a 3 mm specimen, property retention of 93% (97% and 95% based on the analytical model and FE, respectively) is expected. For strength however, the results indicate only an 86%% retention (80% and 79% for the model and FE). Moving to 4 mm parts would yield retention values of 97% and 95% for modulus and strength, respectively. The results have highlighted a need to evaluate current testing parameters. The majority of testing carried out on DCFP specimens has been on parts of a thickness of 3 mm. The analytical model and FE analysis indicate that modulus and UTS may plateau between 4 mm and 5 mm, and such a trend has been confirmed by experimental data. With a good understanding of thickness effects, it may not be necessary to alter standard testing procedures, but in determining property values it will be important to specify achievable properties for increased thickness.

2.7.3 Benchmark materials

Two DCFP fibre architectures have been identified as benchmarks that have the potential to meet the structural requirements required for directed fibre preforms in automotive applications. Testing was carried out on these architectures as well as continuous fibre benchmarks. The findings have been used in Chapter 6 to compare the performance of components made from the different materials.

Fibre architecture 1

The initial characterisation study (2.7.1) determined the tensile properties of a range of fibre architectures at a volume fraction of 30%. While this study helped to identify the effects of fibre length, tow size and thickness; in reality, structural applications would require improved performance. Greater stiffness and strength properties can be achieved by increasing the fibre volume fraction [40]. A 50% fibre volume fraction preform architecture - fibre architecture 1 (FA1) - was chosen for more detailed material characterisation. The architecture was identified at an early stage in the project to give good mechanical performance at reasonable cost. FA1 provides a benchmark throughout the course of this thesis; thickness data was presented in the previous section. This data was obtained in order to characterise the effect of thickness on tensile properties and can be used to determine performance reductions or increases if thicknesses other than 3 mm are used.

FA1 specifications:

Orientation	Random
Volume fraction	50%
Thickness	3 mm
Tow size	6k
Fibre length	60 mm

Further static testing was carried out to determine tensile, flexural, shear and compression properties of FA1. Dynamic testing was also carried out to determine Charpy Impact strength. Results are presented in Table 6; all tests were carried out in accordance with the standards mentioned.

Table 6: FA1 (6k, 60 mm, 3 mm, 46%) material data card. Tensile properties are an average of all laminates produced and tested with the FA1 architecture at the UoN during the ASP project. All other properties are from the initial benchmarking of this preform.

Material property		Test standard	Orientation		
			0°	90°	Average
Tensile	Modulus (GPa)	BS EN ISO 527 -4	42.5 [9%]	44.3 [18%]	**43.4 [14%]**
	Strength (MPa)		317 [12%]	243 [19%]	**280 [16%]**
	Max Load (N)		24716 [14%]	20049 [20%]	**22383 [17%]**
	Rupture Strain		0.81% [3%]	0.71% [25%]	**0.76% [14%]**
Flexural	Modulus (GPa)	BS EN ISO 14125:1998	33.5 [21%]	30.3 [20%]	**31.9 [20%]**
	Strength (MPa)		432 [11%]	452 [19%]	**442 [15%]**
	Strain to Failure		1.68% [19%]	1.87% [12%]	**1.78% [15%]**
Charpy	Impact Strength (kJ/m^2)	BS EN ISO 179–1:2001	86.3 [14%]	83.4 [18%]	**84.9 [16%]**
Shear	Modulus (GPa)	ASTM D7078-D/M5	13.7 [16%]	12.3 [20%]	**13.0 [18%]**
	Strength (MPa)		207 [1%]	210 [9%]	**209 [5%]**
Compression	Modulus (GPa)	ASTM D3410 – 87	*	38.0 [15%]	**38.0 [15%]**
	Strength (MPa)		267 [6%]	249 [4%]	**258 [5%]**

*No acceptable results due to measurement errors

Further to the study of FA1, testing was carried out on an architecture comprising a shorter fibre length – FA1b (results in Table 7). The results provide further insight into the effect of reducing fibre length, which facilitates better coverage and greater formability. Of particular interest was whether reductions previously observed for tensile properties were seen for other material properties.

FA1b Specifications:

Orientation	Random
Volume fraction	50%
Thickness	3 mm
Tow size	6k
Fibre length	30 mm

Table 7: FA1b (6k, 30 mm, 3 mm, 50%) material data card.

Material property		Test standard	Orientation		
			0˚	90˚	Average
Tensile	Modulus (GPa)	BS EN ISO 527 -4	45.9 [24%]	34.8 [10%]	**40.4 [18%]**
	Strength (MPa)		214 [20%]	190 [14%]	**202 [17%]**
	Max Load (N)		18479 [17%]	15492 [14%]	**16985 [16%]**
	Rupture Strain		0.54% [37%]		**0.54% [37%]**
Flexural	Modulus (GPa)	BS EN ISO 14125:1998	28.3 [8%]	34.3 [4%]	**31.3 [6%]**
	Strength (MPa)		408 [12%]	447 [5%]	**427 [8%]**
	Strain to Failure		1.82% [18%]	1.67% [11%]	**1.74% [15%]**
Charpy	Impact Strength (kJ/m^2)	BS EN ISO 179–1:2001	85.7 [0%]	88.4 [10%]	**87.0 [5%]**
Shear	Modulus (GPa)	ASTM D7078-D/M5	13.0 [7%]	11.9 [22%]	**12.5 [14%]**
	Strength (Mpa)		200 [5%]	208 [34%]	**204 [20%]**
Compression	Modulus (GPa)	ASTM D3410 – 87	37.7		**37.7**
	Strength (Mpa)		229 [5%]	267	**248 [4%]**

Properties of FA1b were seen to be lower [than FA1] in most instances. Tensile strength was most sensitive to the change in fibre length, decreasing by 28%. A slight increase (2%) in Charpy impact strength was observed. The results corresponding with the findings of the literature review which suggested that shorter fibres would lead to better energy absorption.

Fibre Architecture 2

The characterisation study has shown that by utilising small tow sizes, improved mechanical properties can be achieved. For this reason there was also interest in evaluating the performance of a second 'high performance' 3k fibre architecture. The second benchmark architecture uses 3k tows at a length of 30 mm. Using a smaller tow size provides the opportunity to achieve target properties with a shorter fibre length. Better preform coverage is seen through a finer distribution of tows and composite performance is improved.

FA2 Specifications:

Orientation	Random
Volume fraction	50%
Thickness	3 mm
Tow size	3k
Fibre length	30 mm

Figure 34: FA2 preform incorporating a distribution of 3k, 30 mm tows.

The fibre length at which a plateau in stiffness occurs has been shown to be relatively short in the literature [36, 37] and experimental results (2.7.1). For tensile strength the critical length is much longer and within the range of fibre lengths currently being utilised in the DCFP process. For instance, to achieve a UTS of 175

MPa with 6k fibres would require an estimated fibre length of approximately 45 mm. To achieve this same target with 3k fibres would require a length of 10 mm. There are additional benefits in manufacture: due to improved fibre distribution, smaller tow sizes result in a lower level of variability and improved homogeneity. Work has indicated that greater levels of compaction are achievable allowing higher volume fractions to be achieved. This will be addressed in Chapter 3. Increased mechanical and thermal properties also allow thinner parts to be used.
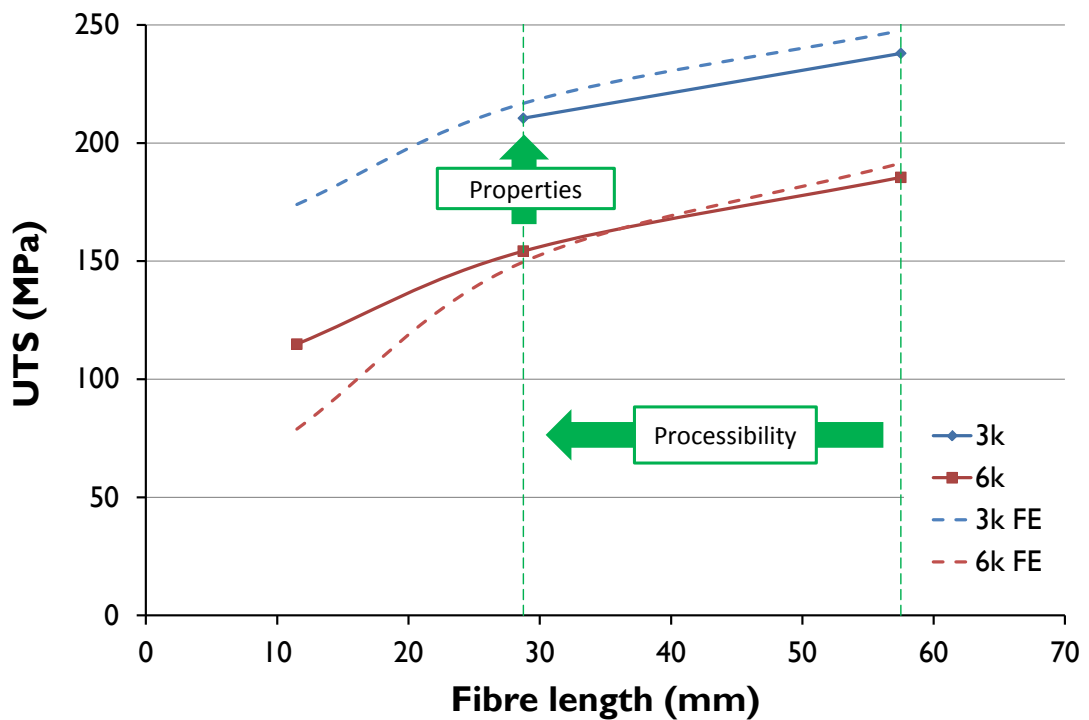
Figure 35: Comparison of tensile strength properties for 3k and 6k fibre architectures at 30% V$_f$. Experimental and FE results from the initial characterisation study are shown. Results are for a 3 mm, 30% fibre architecture at three different fibre lengths. When comparing 3k with 6k; UTS increased by 20% (FE), 37%, and 29% for tow lengths of 11.5 mm, 28.75 mm, and 57.5 mm, respectively. Modulus (not shown) increased by 17%, 13% and 12%.

FA2 performed better than FA1 in the majority of testing. Impact strength, shear strength and flexural modulus all decreased slightly but reductions in properties were always less than 5%. Tensile modulus and strength were seen to rise by 15% and 14%, respectively. Meanwhile, compressive modulus and strength were increased by 15% and 27%. With fibre costs comprising only a small portion of DCFP manufacturing costs, the performance benefits of using 3k fibres arguably outweigh the additional costs. To ensure that deposition levels aren't affected, the

process must be able to incorporate the use of multiple fibre bobbins. 3k preforms were produced by feeding eight fibre tows through the chopper gun simultaneously. To match deposition levels, a 6k preform would require four bobbins to runs simultaneously while a 24k perform would require only one.

Table 8: FA2 (3k, 30 mm, 3 mm 50%) material data card.

Material property		Test standard	Orientation		
			0°	90°	Average
Tensile	Modulus (GPa)	BS EN ISO 527 - 4	40.7 [6%]	36.9 [10%]	**38.8 [8%]**
	Strength (MPa)		342 [11%]	325 [8%]	**333 [10%]**
	Max Load (N)		24465 [11%]	23814 [8%]	**24140 [10%]**
	Rupture Strain		0.91% [11%]	0.99% [7%]	**0.95% [9%]**
Flexural	Modulus (GPa)	BS EN ISO 14125:1998	30.3 [8%]	29.1 [7%]	**29.7 [7%]**
	Strength (MPa)		516 [9%]	470 [9%]	**493 [9%]**
	Strain to Failure		2.20% [7%]	2.10% [15%]	**2.15% [11%]**
Charpy	Impact Strength (kJ/m^2)	BS EN ISO 179–1:2001	85.2 [17%]	80.6 [18%]	**82.9 [17%]**
Shear	Modulus (GPa)	ASTM D7078-D/M5	16.0 [27%]	15.3 [9%]	**15.6 [18%]**
	Strength (Mpa)		209 [15%]	222 [8%]	**216 [12%]**
Compression	Modulus (GPa)	ASTM D3410 – 87	42.5 [6%]	42.2 [20%]	**42.4 [13%]**
	Strength (Mpa)		320 [8%]	307 [6%]	**313 [7%]**

Both FA1 and FA2 have been manufactured on numerous occasions over the course of this thesis and duration of the ASP project. Mechanical test data has been compiled to provide the tensile properties shown in Table 9.

Table 9 Tensile properties of FA1 and FA2 at a thickness of 3mm and 50% V$_f$. Test data has been collated for all laminates utilising the architecture throughout the ASP project.

Material property	FA1			FA2		
	Mean	SD	CV	Mean	SD	CV
Young's Modulus (GPa)	**36.2**	4.5	12%	**41.5**	3.4	8%
Ultimate Tensile Strength (MPa)	**303**	41	14%	**345**	27	8%

Filamentised DCFP

A highly-filamentised DCFP fibre architecture was moulded to determine the effects of filamentisation on material properties. Preforms were produced by the industrial partner Sotira[1] and consisted of randomly chopped 24k tows that were highly filamentised. These preforms were produced using a much larger air pressure than that used at UoN. Fragmentation of the tows is also induced by using a relatively short fibre length of 25 mm.
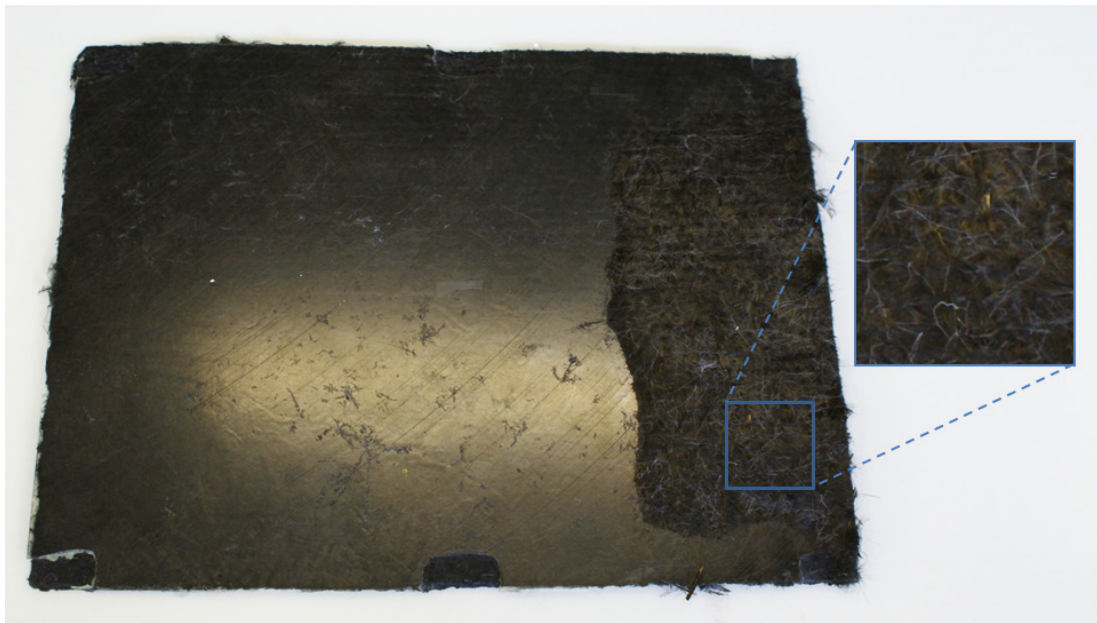
Figure 36. Moulded highly-filamentised DCFP preform with dry regions. The injection point was located on the left. Slow infusion speeds, even at high injection pressures, resulted in only 75% of the preform being infused. This was typical of mouldings carried out on this benchmark.

Properties were shown to be better than the unfilamentised counterpart. However, the improvement in properties comes at the cost of processability. The preforms were more difficult to infuse due to the reduced permeability. An example is shown in Figure 36. Preform loft also resulted in laminates that were significantly larger than the target thickness of 3 mm – the results shown in Table 10 are for a laminate

---

[1] Sotira were an industrial partner in the advanced structural preforming (ASP) project that this work supported. Their plant facilitates production of full-size parts for Aston Martin Lagonda, the primary partner in the project.

at 3.91 mm. Consequently the volume fraction (15%) was much lower than those tested in 2.7.1. The effect of filamentisation on laminate volume fractions is discussed in Chapter 3.

Table 10. Tensile properties of a highly-filamentised DCFP fibre architecture (24k, 25 mm, 3.9 mm, 15%).

Material property		Test standard	Orientation		
			0˚	90˚	Average
Tensile	Modulus (GPa)	BS EN ISO 527 - 4	10.6 [17%]	10.5 [8%]	**10.6 [13]**
	Strength (MPa)		86.9 [11%]	97.2 [8%]	**92.1 [15%]**
	Max Load (N)		8250 [13%]	9317 [18%]	**8784 [16%]**
	Rupture Strain		0.92% [15%]	0.97% [10%]	**0.94% [12%]**

Non-crimp fabric benchmark

Non-crimp fabric (NCF) is a form of reinforcement suitable for high performance structures. Continuous fibre tows are stitched together to produce the virgin fabric. These can be layered, in the required orientations, to produce preforms. These preforms can then be moulded using RTM or similar methods. If preforms are not moulded immediately, they can be stored for future use. NCF preforms provide a suitable benchmark for DCFP as the material utilises carbon fibre in a dry state, and moulding methods are usually similar. Costs of NCF are much lower than that of conventional pre-preg carbon composites but the processing involved in stitching still results in larger material costs to that of DCFP. Results from tensile tests of two layups are shown in Table 11.

Quasi-isotropic plaques share a closer resemblance to randomly orientated DCFP plaques. Uni-directional NCF results are an indication of the maximum achievable performance achievable, using NCF, whilst being a suitable comparison with aligned DCFP, the potential of which is studied in Advances in Discontinuous Composites [77]. While tensile strength of quasi-isotropic NCF was close to double that of DCFP (FA2) specimens, Young's modulus of the benchmark was similar to

that of the DFC. Compression and shear properties of DCFP composites have also previously been shown to be more comparable with continuous fibre laminates.

Table 11: Tensile properties of NCF benchmark.

Orientation	Material property		Test standard	Mean
QI	Tensile	Modulus (GPa)	BS EN ISO 527 - 4	42.1 [9.8%]
		UTS (MPa)		633 [4.0%]
		Max load (kN)		45.1 [3.5%]
		Strain to failure		1.42% [12.7%]
UD	Tensile	Modulus (GPa)	BS EN ISO 527 - 4	121 [7.5%]
		UTS (MPa)		1361 [10.7%]
		Max load (kN)		64.4 [8.8%]
		Strain to failure		1.12% [17.0%]

2.8   Conclusions

Characterisation of the mechanical performance of DCFP fibre architectures was carried out and the effects of four macro-structural parameters have been established. Stiffness and strength increased linearly with volume fraction but the influence of other parameters was more complex. Smaller tow sizes produced better properties as filament surface area increased and preform coverage was seen to improve. As a result of increased coupon-to-coupon heterogeneity, variability in data was seen to be worse with large bundle sizes. Manufacturing defects, such as fibre washing and waviness, were also more common.

The effect of fibre length has two effects. Longer fibres lead to increased stress in the fibres improving performance of the composite up to an optimal length. Shorter fibres promote greater macroscopic homogeneity in the due to more even fibre coverage and increase likelihood of fragmentation, which can both improve mechanical properties. Strength was dominated by the first of these factors, increasing with longer fibre bundles. Stochastic effects were seen to be more significant with stiffness, which is known to have a shorter optimal fibre length. The resultant modulus data was therefore characterised by both factors, with no obvious net effect.

Two DCFP fibre architectures (FA1 - 6k, 60 mm and FA2 - 3k, 30 mm) were selected for further characterisation to provide benchmark data for the project. A non-crimp fibre benchmark was also tested to provide a quasi-isotropic and unidirectional continuous fibre benchmarks. The effect of thickness was studied by carrying out mechanical testing of FA1 at six thicknesses. Modulus and strength were both seen to increase with performance plateauing between 4-5 mm, a factor that must be considered when evaluating most test data, which is typically carried out at 3 mm. Property retention for stiffness and strength at 3 mm were 86%, and 95%, respectively.

An analytical model has been developed to determine the tensile stiffness and strength of a fibre architecture if the tow size, fibre length, thickness and volume fraction are known. This can be used in the design procedure to provide an estimate of material properties or be applied to facets within an FE analysis to reduce computation time. Limitations of the existing FE model and proposed analytical models were seen for architectures that exhibit poor homogeneity. Laminates that were thin (<3 mm) and/or incorporated large bundle sizes were under-predicted.

3 Mesoscopic homogeneity – fibre compaction

3.1 Introduction

The manufacture of composite components using liquid moulding techniques typically requires compaction at two stages. Consolidation of the preform, which is made up of fibres and a binding agent, is carried out by simultaneously applying pressure and temperature. Preforms also undergo compaction in the moulding process where they are placed in a tool that is closed before injection of the resin matrix. This is typical of RTM, but preforms also experience compaction in other moulding processes, some of which have been demonstrated throughout this thesis e.g. vacuum infusion (VI) and resin film pressure moulding (RFPM).

The degree of compaction dictates the fibre volume fraction, which greatly influences the mechanical properties, such as stiffness and strength, in the final part. Preforms that exhibit a high level typically lead to poor, potentially unacceptable, levels of fibre volume fraction. During compaction, preforms exhibit a change in meso-structure that results in an increase in fibre volume fraction. The variation of this volume fraction with increasing load is of interest and can provide important information, regarding the degree of pressure required to achieve target volume fractions, which is essential in attaining target properties. Such information is likely to have consequences on the selection of moulding method, mould design, and equipment specifications. As well as facilitating high volume fraction, significant compaction pressures provide an important restraining force to the preform in the cavity and prevent fibre washing during impregnation [83].

3.2   Objectives

The primary aim of this study was to develop an analytical model to predict the volume response of dry random meso-scale discontinuous preforms for a defined pressure range (i.e. 1-10 bar). Initial experimental data, from the compaction of a benchmark preform (FA1), was used to characterise the compaction behaviour of DCFP and was fitted with existing models that have been highlighted in the literature review. Each model was evaluated by accuracy and practical significance in order to select a model that could be appropriately applied to meso-scale DFCs.

An experimental study was carried out to determine the influence of fibre length, tow size and areal mass on compaction behaviour of DCFP preforms. As well as providing further validation of the model, the results were used to identify the factors that determine the maximum achievable volume fraction. Compaction behaviour of DCFP has been benchmarked against a highly-filamentised variant and non-crimp fabric preforms.

3.3   Literature Review

3.3.1   Factors influencing the compaction behaviour of DFCs

A large number of studies have been carried out on the compaction and compressibility of composite preforms. Work has often been focussed on textile fabrics, with little work seen on the compaction of random meso-scale discontinuous fibre preforms. The general mechanisms for compaction remains the same between aligned and random fibres [84]; DFCs are likely to share many of the contributing factors as for textile fabrics such as fibre bending, twisting, slippage, extension of fibres, and shearing effects.

Processing factors

There are also contributing factors related to processing conditions. Preforms are subject to multiple compactions in the manufacturing process, through consolidation and moulding. A reduction in initial preform thickness has been observed between one compaction and the next [85]. There is still however an increase in thickness due to re-lofting after the compaction load is removed. Consequently it can be deduced that preform thickness is a function of time as well as the number of compaction cycles. Faster compaction speeds have been found to result in reduced permanent deformation due to, what is described by Somasheker et al. [85], as a smaller "settling- in" period. This is associated with the degree of nesting that occurs.

Temperature of the preform may also have an impact on achievable volume fractions. A study was carried out by Aranda [86] to determine the effect of a preheating treatment on the compressibility of dry non-crimp fabric. However, the experimental design does not seem particularly applicable to DCFP manufacture. Preforms were held at elevated temperatures for 24 hours with tests carried out at room temperature, but DFC preforms are unlikely to be stored above room temperature for prolonged periods. Nevertheless, the paper does highlight that the initial thickness of preforms increases with temperature leading to lower volume

fractions for a given pressure. This suggests that preforms should not be preheated in an open mould.

Homogeneity factors

The fibre architecture is known to have a significant effect on the deformation characteristics of a material [87]. Few studies have been seen on tow-based DFCs, but there has been substantial work on random fibre materials. Studies have most often focussed on wool, paper and chopped strand mat. Maximum volume fractions for these materials are typically in the range of 10%-40% [83, 88]. Higher volume fractions have been achieved with meso-scale DFCs - 60% for chopped-prepreg based SMCs [89]. Although there is no literature on the maximum achievable volume fraction for preforms manufactured using DFP processes, comparable values are likely due to similar fibre architectures. Compaction of fibre bundles, rather than individual fibres, may allow for greater volume fractions to be achieved but they bring added complexity when characterising compaction behaviour.

The majority of volume reduction in fabrics results from the compaction of interstitial space [90], which is significant in DFCs due to a high level of mesoscopic variability. Variation in the preform fibre architecture is also likely to result in variability in local pressures. The pressure distribution has been shown to be non-uniform for woven fabrics [91]. Figure 37 shows pressure peaks coinciding with locations where the weft crosses the warp in a plain weave. Preforms with coarser fibre distributions will exhibit more uneven pressure distributions, which will influence local compaction behaviour. As well as affecting the fibre volume fraction, the compaction behaviour of a preform can significantly influence the resin permeability and the geometry of individual tows [92]. This could lead to voidage and poor mechanical properties of the laminate.
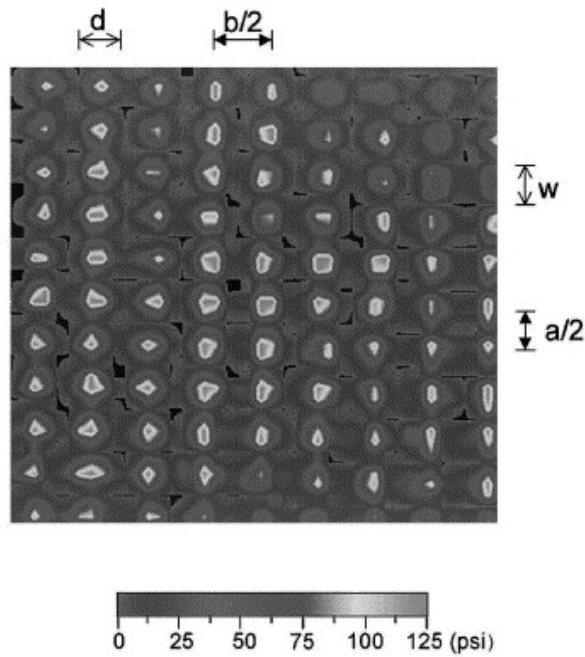
Figure 37. Compaction pressure distribution between adjacent layers of a plain weave woven fabric (reprinted with permission) [91].

Thickness will affect the compaction behaviour of the reinforcement if load is non-uniform throughout the preform [83]. Robitalle et al. [93] state that as the number of layers of random mat increases, the initial fibre volume fraction is increased and the stiffening index decreases. A study by Yang et al. [94] shows that resulting volume fraction increases as the number of layers increases (i.e. it is easier to compact). However, they note a change of less than 2.5% between 10 and 100 layers. No experimental data is given for fewer layers but this suggests that the effect diminishes as thickness increases.

Compaction of the fibre tows themselves must also be considered. Preforms made with tows with lower initial fibre packing contain more room for the tow to be compacted before reaching the maximum fibre packing fraction [95]. Hsiao et al. [96] found that tow shape had a strong correlation with the compaction response of prepregs, with rounder tows showing a better resistance to deformation when pressure is applied. They also state that rounder tows lead to a more open fabric that help to promote nesting. However, this is unlikely to be the case with DFCs. The shape of the tows is typically ellipsoidal with larger tows sizes having a larger width. Consequently, smaller tow sizes will appear to be rounder, but the smaller

aspect ratio means that interstitial space is likely to be smaller. The deformation of individual fibres has been acknowledged in the literature but largely disregarded when describing compaction behaviour. This suggests the effects may be insignificant when describing compaction behaviour at the meso-scale.

The maximum volume fraction achievable within a fibre tow can be determined by considering a hexagonal array (depicted in Figure 38) which is assumed to give the most efficient packing method for cylindrical objects and therefore the largest volume fractions [97].
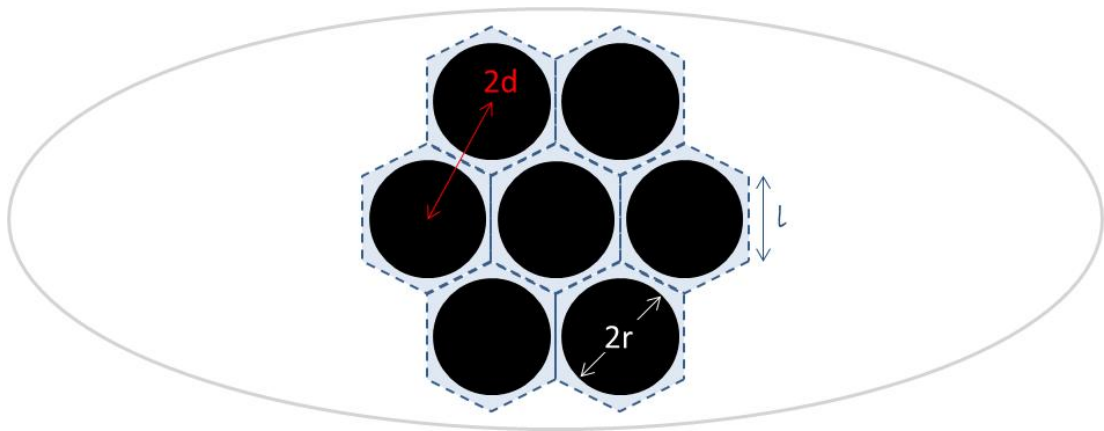
Figure 38. Representation of hexagonal packing within a fibre tow. The fibre volume fraction is approximated by the fibre/hexagon area.

Each filament is assumed to occupy the area of a hexagon; the size of the hexagon is dependent on how closely the fibres are packed. The fibre volume fraction can be calculated by determining the ratio of the cross sectional area of the fibres to the total area occupied by those fibres. Optimal packing occurs as is the distance between the fibres (d) approaches the fibre radius (r). When $r = d$, the fibre volume fraction simplifies to

$$V_f = \frac{\pi}{2\sqrt{3}} = 90.7\%.$$

A number of authors have stated the difficulties in achieving volume fractions greater than 80%. The representation in Figure 38 is clearly an idealised case. Although fibres may be packed optimally in certain regions, it is unlikely that this will be the case throughout the tow Figure 39. Misalignment of fibres, fibre

bunching and sizing effects could all be factors. Lower fibre content is also likely to result in more irregular packing as these factors become more significant [49].
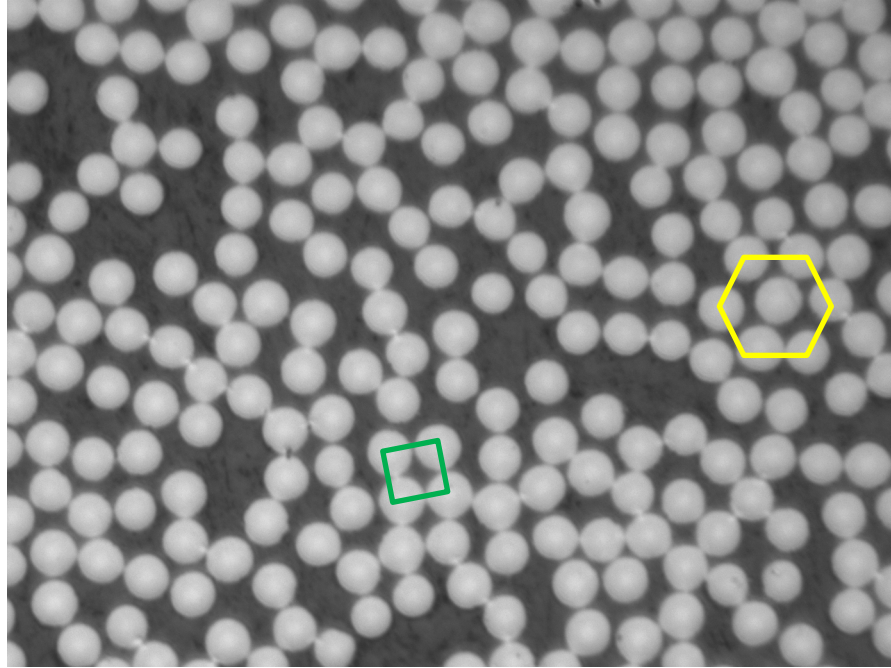
Figure 39. Variability in packing within a fibre bundle of carbon UD NCF compacted to a V_f of approximately 45%. Local hexagonal and square packing arrangements are indicated.

3.3.2 Compaction models

Many relevant fibre compaction models that have been published, have utilised non-linear models for describing compressive deformation behaviour, where volume fraction was assumed to be a function of stress [98]. This section details some of the most well-known methods, whist considering applicability to DFCs.

Eggert

The observation that the volume of dry fibres does not increase linearly with applied stress was first established in work by M. and J. Eggert [99], who suggested the following equation for modelling the compaction pressure behaviour of wool:

$$\left(\frac{v}{v_0}\right)^{\gamma} (P - P_0) = P_0,$$

Eq. 38

where v_0 is the initial volume, P_0 is the latent pressure (of the wool with no applied pressure), and γ is an empirical constant [100]. The equation was formulated empirically and consequently, criticisms of the Eggert model have centred largely

on the lack of a relationship between its coefficients and the characteristics of the fibres. Van Wyk [101] argued that P_0 and γ are too sensitive to experimental errors and depend heavily on the observed value of P_0 – a quantity that is "hardly reproducible". Furthermore, he highlights a growing inaccuracy with higher pressure values, where packing becomes more uniform.

Van Wyk

In order to derive a model that was based on common engineering principles Van Wyk simplified the problem by only considering the bending of fibres. Fibres were modelled as simple rods supported horizontally by a large number of points. Fibre-fibre contacts were introduced to the problem as forces acting on these rods. The mean distance between adjacent contacts was determined as the element length and was accounted for in the empirical constant K. The fibre elements were assumed to be randomly orientated. The observed inverse cubic relationship between the applied pressure and the change in volume is modelled by the equation:

$$P = \frac{KEm^3}{\rho^3}\left(\frac{1}{v^3} - \frac{1}{v_0{}^3}\right),$$
Eq. 39

where m is mass of the fibre. The equation can also be written as [100]

$$P = KE\left(V_f{}^3 - V_{f0}{}^3\right).$$
Eq. 40

The constant K cannot be found theoretically, but can be found experimentally as long as Young's Modulus E is known. Van Wyk noted that, in his experiments, the coefficient K was independent of fibre length for an established range of 4 cm - 20 cm. At shorter fibre lengths the coefficient was seen to drop; a phenomenon that he attributed to the number of free ends. As well as increased fibre ends, shorter fibre lengths in DCFP fibre architectures lead to increased filamentisation, which in turn lead to more lofty preforms. This would result in an even steeper drop in K.

Cai and Gutowski [102] later developed a similar expression, which has received significant attention, but the model is largely limited to describing the compaction of aligned fibres [103]. Van Wyk postulates that the applicability of the equation to fibres other than wool may be determined by the extent of fibre slippage as this is

ignored in the model. An interesting effect in the DCFP fibre architecture, is that fibre slippage is limited by the effect of the binder so this is unlikely to be an issue. Despite this, other problems need to be considered. A number of other factors are ignored in the model including twisting and extension of fibres [84]. The fibres are also assumed to be uniformly packed with no frictional force between them. Such assumptions are unlikely to be upheld when considering DCFP fibre architectures.

Power laws

The power law has often been used to describe experimental data, rather than predict behaviour of materials. Several authors [93, 94] have used models that take the form

$$P = cv^n,$$
<div align="right">Eq. 41</div>

where v is the volume of the material, to describe the compaction behaviour of fibre reinforcements. These models share the same basic form as the Eggert model (Eq. 38), where volume fraction is a fraction of stress alone. The empirical constants c and n vary greatly from one material to another, and several authors have underlined the large dispersion of results obtained for these two parameters [104]. The large number of variables in meso-scale DFCs makes it impractical for manufacturers to test every possible fibre architecture in order to establish the empirical constants, and doing so may be particularly difficult with preforms that exhibit poor homogeneity. Robitaille et al. [93] gathered published experimental data related to the compaction of random mats and woven reinforcements. They defined the coefficients needed to fit their power model to each set of data with values quoted for different compaction speeds, layups, and compaction cycles. By using this approach they were able to compare the compaction behaviour of a range of materials. The basic notion provides good premise for comparing performance of different fibre architectures. However, as the meanings of the constants are widely debated, it may be difficult to establish how trends in these constants are related to physical behaviour of the preform.

Chen et al.

Chen et al. [90] present a conceptual nonlinear constitutive law, for dry glass fibre preforms, with coefficients that are linked to measurable physical parameters:

$$P = \frac{1}{C_b(s)}\left(1 - \frac{s_0}{s}\right),$$

Eq. 42

where $C_b(s)$ is the bulk compressibility which is calculated by

$$C_b(s) = \frac{(1-s)(s_f-s)^k}{(1-s_0)(s_f-s_0)^k}C_{b0} + \left[2 - s - \frac{(1-s)(s_f-s)^k}{(s_f-s_0)^k}\right]C_s.$$

Eq. 43

The compaction behaviour of woven fabric preforms was studied by moulding the fabric at pre-determined compaction level. Observations at the different "regimes" were used to formulate the model above, which is defined by five parameters:

- initial fibre volume fraction (s_0)
- maximum achievable volume fraction (s_f)
- initial fibre bulk compressibility (C_{b0})
- fibre solid compressibility (C_s)
- empirical exponent (k)

Of the parameters, the first four are said to have definitive physical meaning and can be independently measured. There has been some agreement on the value of the other parameter k. In a separate study [105], Chen et al. demonstrate the applicability of the model to carbon preforms with $k = 2$, the same value they found to be valid for glass. Echaabi et al. [104] have also found success in using applying the model, with the same value of k to a carbon twill weave.

3.3.3 Summary

Analytical and empirical models exist that are likely to be suitable for modelling compaction behaviour of DCFP preforms. These models may also provide methods for comparing performance of different fibre architectures and for quantifying preform behaviour data for manufacturers. It is clear that the different stages of compaction need to be defined to determine any differences between conventional fabrics caused by mesoscopic parameters.

3.4   Experimental methodology

Each preform was stamped into six Ø100 mm discs using a die cutter. The stamped discs were trimmed, weighed and placed into a compaction test rig. The Hounsfield testing machine (Figure 40) was used to lower a Ø100 mm flat platen at a speed of 10 mm/min from a datum towards a second flat platen on the machine. The applied force was measured using a 25 kN load cell and the corresponding displacement was measured from the cross-head. The load was limited to 10 kN giving a pressure of approximately 12 bar.

The compaction rig was calibrated in order to account for displacement of the test fixture. Tests were run, before each batch of experiments, with no preform to determine force-displacement data inherent in the rig. Data from these calibration tests were fitted with polynomial curves which were used to estimate (and subsequently subtract) the displacement caused by the rig in each compaction test. In obtaining the calibrated force-displacement data, one can calculate pressure - displacement and ultimately, pressure - volume fraction.
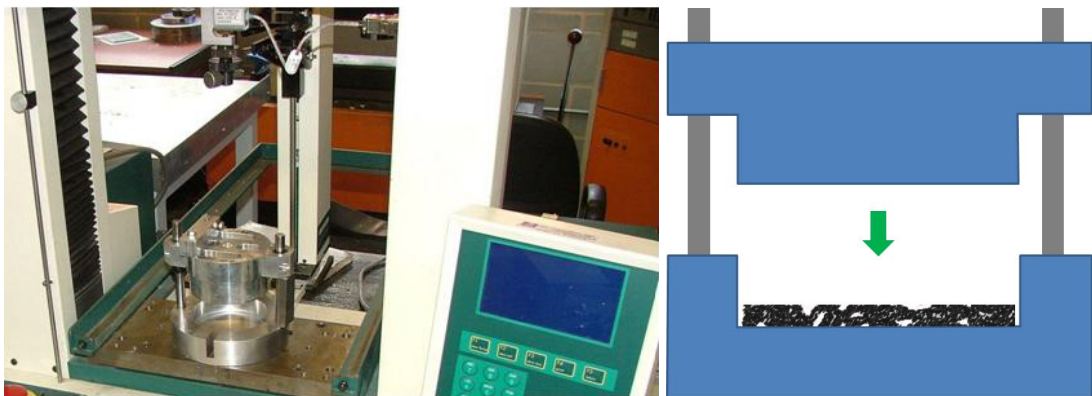
Figure 40. Hounsfield test machine with compaction rig fitted.

Compaction behaviour of individual tows was determined by using a similar test rig. An Instron 5969 was used to lower a Ø50 mm platen at a speed of 1 mm/min towards the second platen flat platen. Strain was measured with two LDVT displacement sensors and results were calibrated in the same way. Experimental measurement of dry fibre tows can be problematic due to disturbance of the geometry of the tow and issues of scale. There is particular difficulty in determining

thickness values as significant deformation of the tows occurs when pressure is applied vertically. Width measurements were less disruptive, so were used to determine thickness values. The free thickness, i.e. without any pressure applied, was calculated by assuming each tow occupied a space that was perfectly elliptical with a fibre volume fraction of 60%. Each individual fibre was assumed to have the same diameter of 7 μm (obtained from the manufacturer's data sheets). By multiplying the area of a single filament by the number within a tow, the cross sectional area of the ellipse can be determined using

$$A = \frac{n \times A_f}{Tow\ V_f}.$$

The initial thickness was then calculated from the equation for the area of an ellipse,

$$A = \pi ab,$$

$$\therefore b = \frac{n \times A_f}{Tow\ V_f \times \pi a}, \qquad\qquad \text{Eq. 44}$$

where b is the radius of the ellipse in the shortest direction and is equal to half the thickness of the fibre tow (Figure 41).
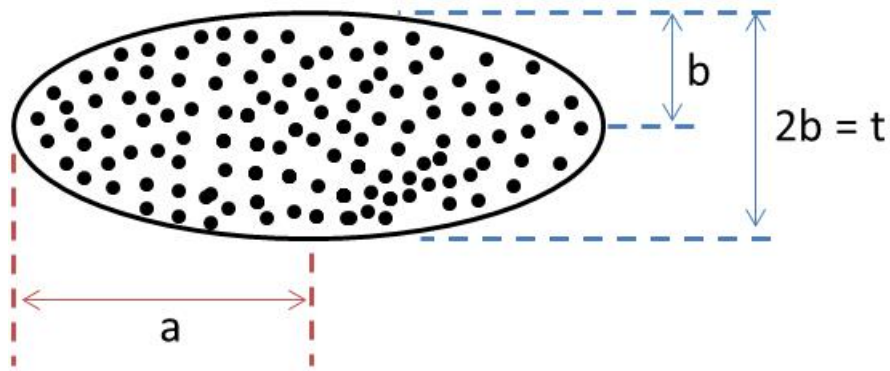
Figure 41. Illustration of the cross sectional area of a single carbon fibre tow assumed to take the shape of an ellipse. The boundary represents the total cross sectional area taken up by the filaments which are denoted by the dots within.

Compaction behaviour of preforms at low pressure (<0.05 bar), before consolidation, was determined by placing weights onto a 600 mm x 400 mm FA2 (6k, 60 mm) preform. The preform was left on the tool after fibre deposition and placed on a set of weighing scales. A matched size aluminium plate and breather were placed on top to distribute the weight evenly over the preform. Gaps between the preform tool

and the aluminium plate were measured at four locations, using a digital vernier caliper, to determine the cavity volume for a specific mass. Measurements were taken for seven different weights with the plate and breather acting as the first.

Continuous fibre preforms, used as benchmarks in the study, were manufactured from Sigmatex 200 gsm/PW-BUD/T700SC 12K 50C/0600 mm unidirectional non-crimp fabric (NCF) for comparison. Unidirectional and 0/90° layups were produced with the same proportional mass of binder used as that for the DCFP preforms. Three unidirectional layups (containing one, two and four layers) and two 0/90° layups (containing two and four layers) were studied.

The final benchmark was the highly filamentised DCFP fibre architecture (tow size - 24k, fibre length - 25 mm) produced by the industrial partner, Sotira. The resulting architecture was significantly more 'woolly' in comparison to preforms produced at UoN; both are shown in Figure 42. As a result, these preforms occupy a much larger volume, while the latent volume fraction (volume at atmospheric pressure) is much smaller. Compaction testing was carried out at UoN in accordance with the methods outlined above.

Figure 42. Comparison of highly filamentised 24k tows used by Sotira (right) with unfilamentised tows of the same original bundle size used at UoN.

3.5 DCFP compaction behaviour

The compaction behaviour of DCFP has been studied at several levels to determine the different phases in the compaction of preforms with a discontinuous meso-architecture. A preform under small loads has been used to simulate performance at low compaction levels. Compaction of individual fibre tows was used to characterise behaviour at higher pressures whilst providing information about the differences between incorporating the four different tow sizes. The compaction of the benchmark fibre architecture FA1 (6k, 60 mm, at a target fibre volume fraction of 30% at 3 mm) was used to determine the compaction response of a preform between these two extremes. The results were used to evaluate four models highlighted in the literature review and determine an appropriate model that could be used for DCFP architectures.

3.5.1 Compaction behaviour of benchmark DCFP architecture

The benchmark architecture FA1 was initially studied to assess the compaction behaviour of DCFP preforms. Of particular interest was the shape and characteristics of the pressure - volume fraction curve. The findings would help to determine the different regimes in the characterisation of a meso-scale discontinuous architecture. Six specimens were tested in accordance with the methods outlined in the experimental methodology. The fibre volume fraction (V_f) of FA1 specimens was calculated using

$$V_f = \frac{Fibre\ volume}{Cavity\ volume},$$

$$\therefore V_f = \frac{m_f}{\rho_f tA}, \qquad\qquad \text{Eq. 45}$$

where m_f is the fibre mass of the preform, ρ_f is the fibre density (1.76 g/cm^3), t is the thickness of the specimen, and A is the area of that specimen. Low pressure evaluation of compaction behaviour was also carried out on an unconsolidated preform with results shown in Figure 43.
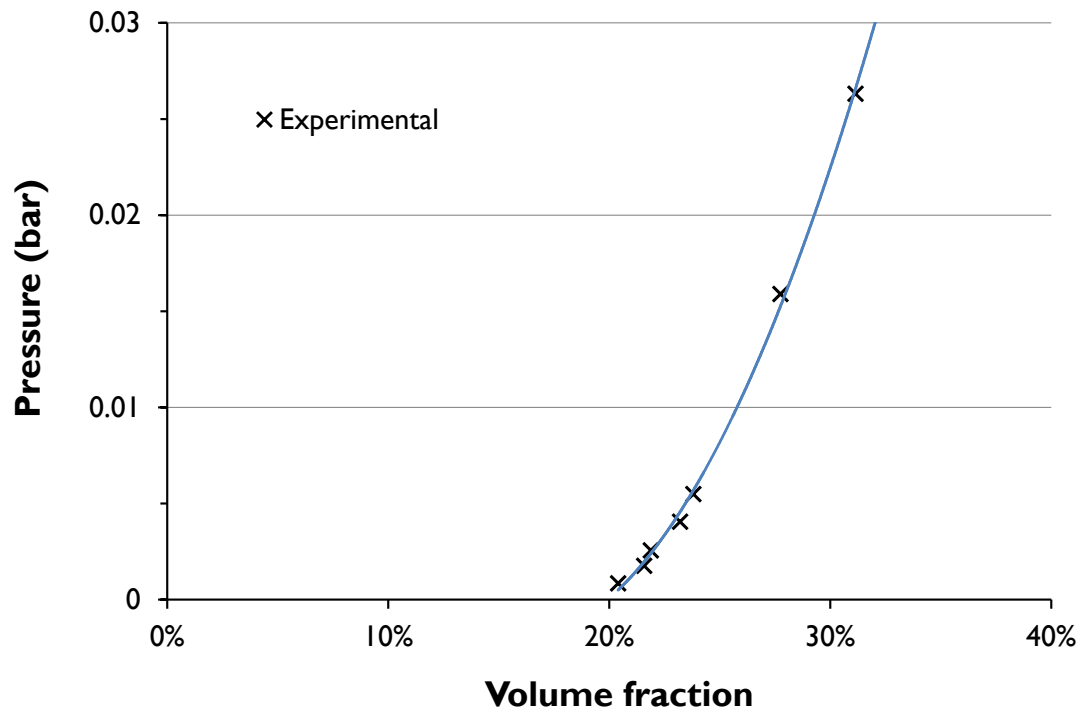
Figure 43. Compaction behaviour of an unconsolidated FA1 preform at low pressure (< 0.03 bar). The preform underwent compaction on the preform tool, immediately after deposition, using seven different weights represented by the points on the graph. The observed thickness response was used to determine the volume fraction of the preform at each pressure. The experimental data has been fitted with a third order polynomial.

Testing of DCFP at low pressures gave clear indication of a latent volume - the volume occupied by the fibres, in an uncompacted state, at atmospheric pressure. The points at which the experimental data deviated from the x-axis on the fibre volume fraction – pressure curve can be used to determine these values but it must be noted that scale effects do exist. Consequently, the latent volume fraction is likely to be a function of measurement resolution as well as material behaviour.

Typical compaction curves for FA1 at larger pressures are shown in Figure 44. Deviations were evaluated at the lowest pressure where a compaction response was observed - 0.05 bar (27 N). By doing this with the data in Figure 44, the latent volume fraction was seen to rise from 28% to 38% and then 39% for repeat compactions indicating that the preform did not relax to its original (pre-compacted) state between tests. This is strongly indicative of nesting of fibre tows between adjacent layers.
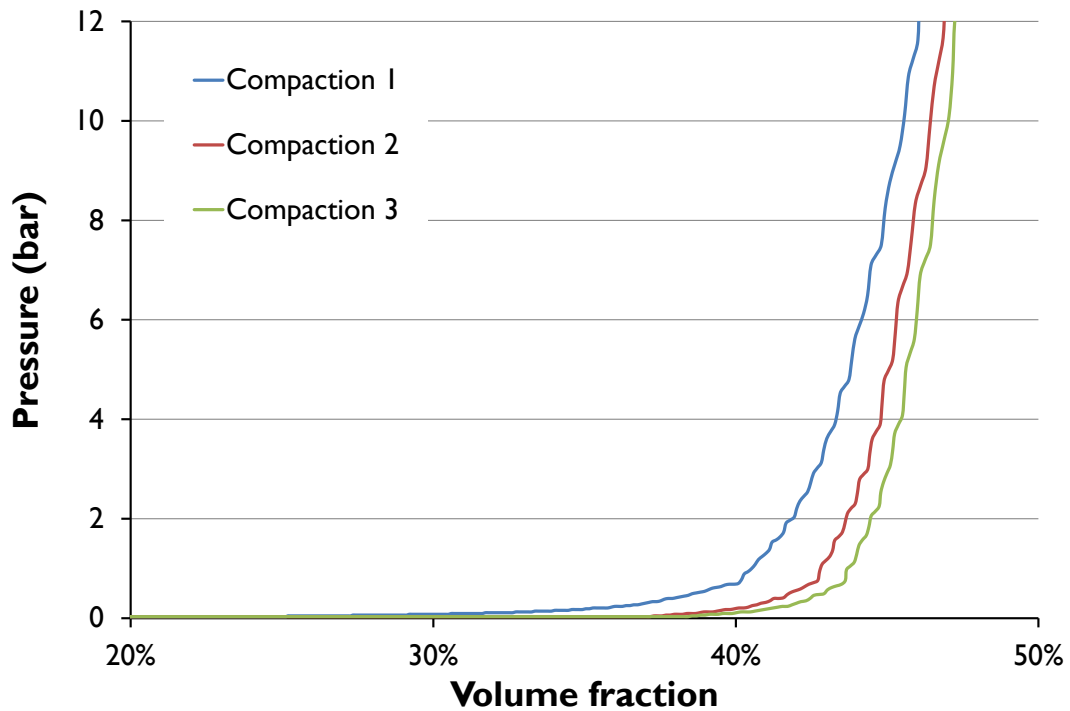
Figure 44. Typical compaction behaviour of the FA1 (6k, 60 mm) fibre architecture under increasing pressure. Specimens were compacted three times up to a maximum load of 10 kN resulting in a pressure of 12.7 bar. Six specimens were studied with the curves above representing data that most closely matched the averages. The average coefficient of variation for the three curves was 1.70%, 1.47%, and 1.38%.

A large change in volume fraction was seen up to a pressure of 2 bar with the decreasing at increased pressures. The highest volume fraction seen in the tests was 48%. The shape of the curve suggests that volume fractions higher than this are achievable, but there appears to be convergence towards a maximum achievable value.

Variation between tested specimens was seen to be small with the coefficient of variation for the 1st, 2nd and 3rd compactions at 10 bar equalling 1.6%, 1.8% and 1.7%. Further compactions are likely to exhibit similar variability; these values appear to represent intrinsic mass variability in the DCFP fibre architecture. The greatest degree of variation was observed during the 1st compaction at low pressures. For instance, at 0.05 bar the CV was 2.9%, but this had reduced to 2.0% by 0.1 bar. From 0.2 bar the CV remained below 1.7% for all remaining test data (including 2nd and 3rd compactions) suggesting an equilibrium had been reached.

The data indicates that results are repeatable for this particular architecture and that specimens exhibit similar compaction characteristics at pressures above 0.1 bar.

3.5.2 Single tow compaction

An investigation into the compaction of individual fibre tows was carried out in order to determine the thickness response, of four bundle sizes, to applied pressure. The work was also used to characterise the final phase of compaction in a DCFP preform and determine the differences associated with using different tow sizes. The effect of pressure on the thickness and displacement of the four tow sizes are shown in Figure 45 and Figure 46. Thickness values were determined by subtracting the downward displacement of the tow from the calculated free thicknesses (method described in experimental methodology). A more significant change in thickness was seen for larger tow sizes with 3k tows seeing a 15% reduction compared to a 40% reduction with 24k tows. The standard deviation was also seen to rise significantly, from 9% to 22%, demonstrating the larger variability in results observed for bigger bundle sizes.
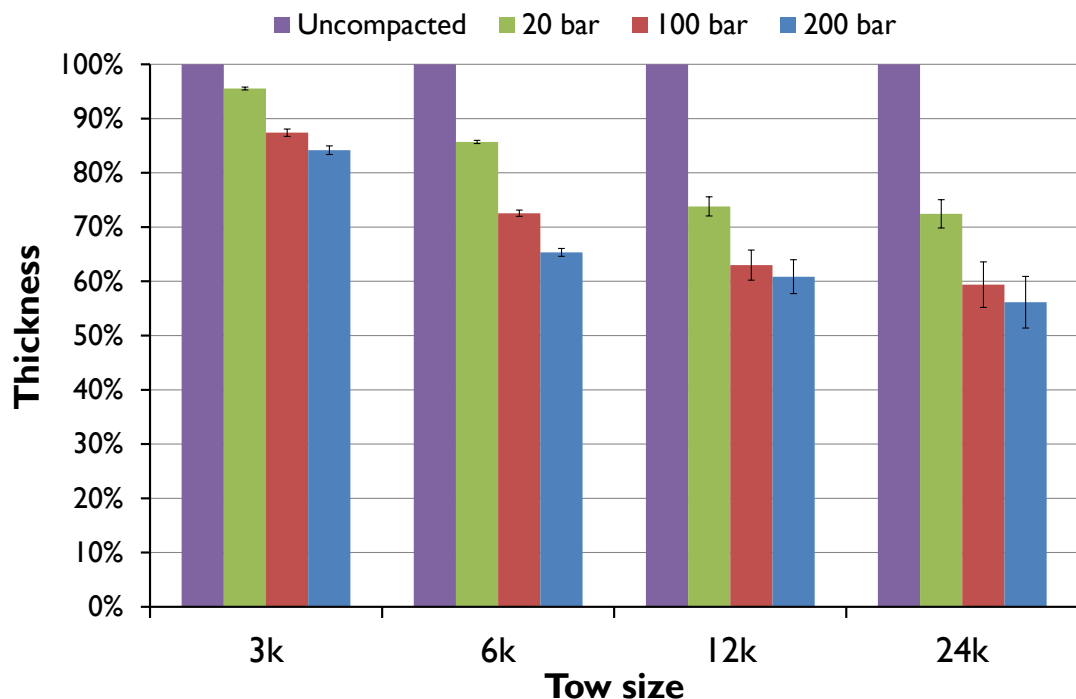
Figure 45. Change in thickness under three different compaction pressures for four tow sizes. Thickness values were normalised with the uncompacted thickness of each fibre tow.

The volume fraction of a compacted fibre tow is directly proportional to its compacted thickness if the width of the fibre tow is assumed to remain constant. However, the compacted volume fractions calculated for larger tows indicate that there was considerable horizontal deformation of the fibre bundles. Indeed, 12k and 24k results were greater than the maximum theoretical fraction (91%) calculated for a hexagonal array in 3.3.1. Nesting of fibres will occur under low loads, and localised nested regions are likely to be a root cause of tow spreading. These congested areas are likely to force fibres away from the centre of the tow as the downward force continues to be increased leading to an increased bundle width. It remains unknown whether significant deformation of the individual filaments occurred. The study does however highlight the idiosyncrasies of different tow sizes under compaction. A trend exists whereby larger bundle sizes experience a greater change in thickness and associated fibre volume fraction. This is followed by a near-linear portion of the compaction curve that is common to all tow sizes, with a similar gradient observed for each.
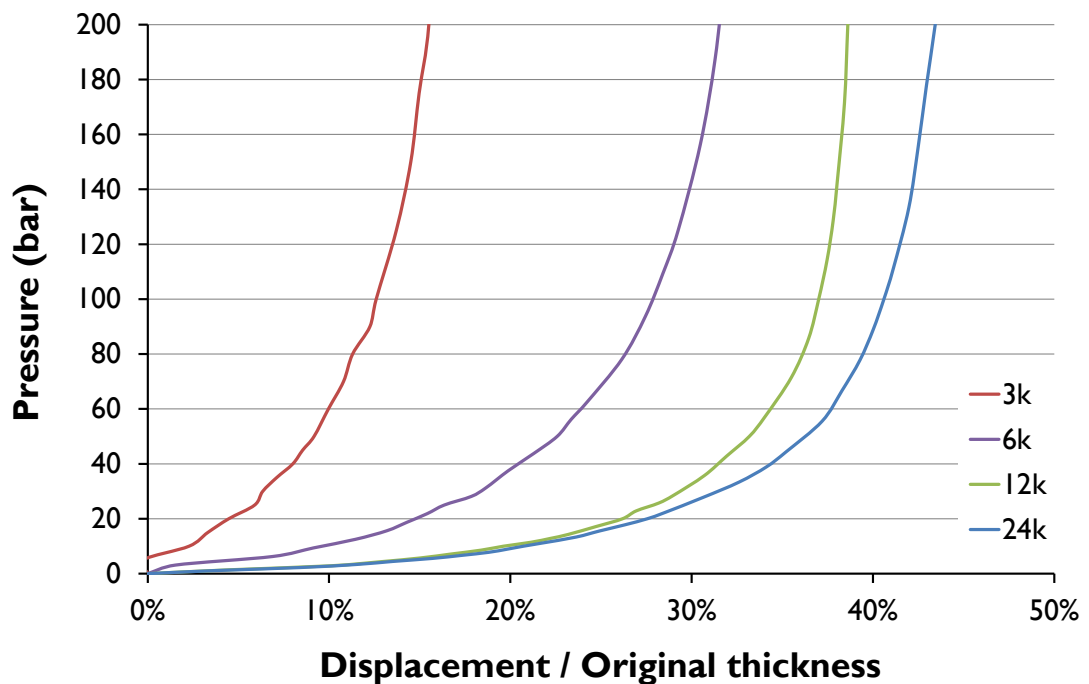
Figure 46. Compaction behaviour of carbon fibre tows at four bundle size levels. Three specimens of the same length (50 mm) were tested for 3k, 6k, 12k, and 24k bundles. The curves represent the average displacement of the specimens normalised by their original thicknesses.

3.5.3   Compaction stages of random meso-scale DFCs

Compaction of DCFP fibre architectures is characterised by compaction in three stages (indicated in Figure 47). These are analogous with other materials and have been confirmed by several authors [91, 106, 107]. Due to heterogeneity in the fibre architecture, different areas of the preform are likely to be in different regimes simultaneously. Chen et al. [90] define an initial state - regime 0 - to describe the uncompacted form of a material. This stage is observed in the manufacture of DCFP preforms if fibres are sprayed without suction being used to hold the fibres in place. This initial state could, for instance, be observed in resin spray applications. In this case, tows could be defined as beams as negligible bending is seen.
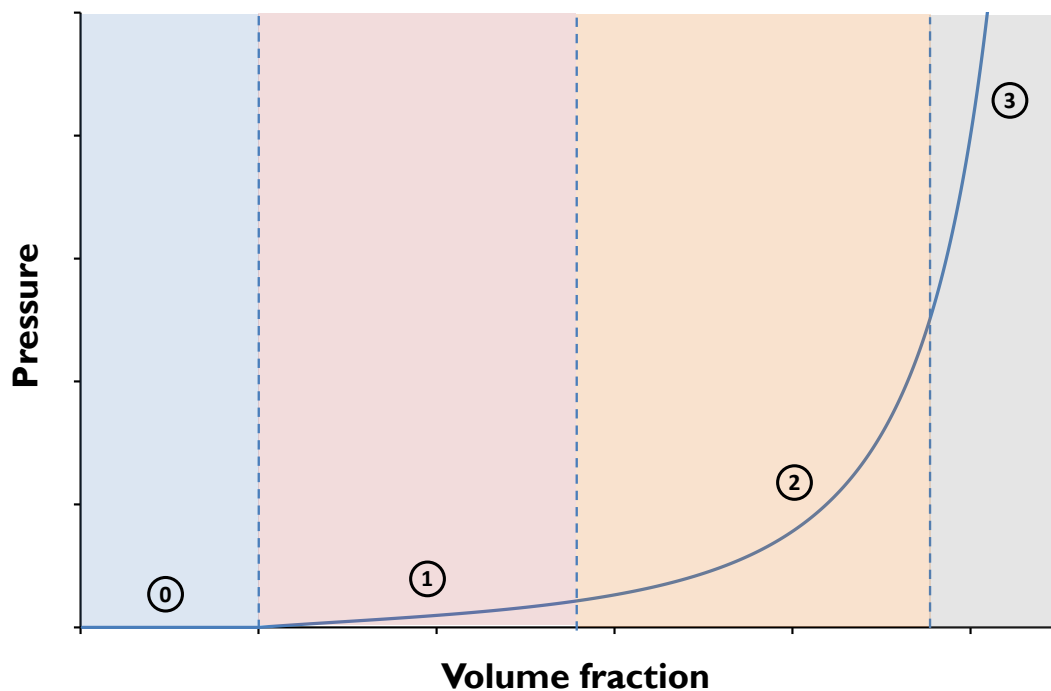
Figure 47. Typical pressure vs. volume fraction curve for a DCFP preform. Each part of the curve is labelled with the theoretical regime which is dominant in defining compaction behaviour at that stage.

Regime 1

In the first stage of compaction the tows bend to fill gaps in the preform architecture. DCFP first enters regime 1 on the preform tool face, where tows experience the downward force of the fan. Compaction behaviour at this level is governed by the flexibility of the tows and the amount of space between the bundles. Figure 43 shows the compaction behaviour of an unconsolidated FA1

preform at low pressure. The first few points on the curve correspond to the transition from regime 0 to regime 1. At this stage the fibre tows bend with very little resistance until all layers are in contact with each other. In highly filamentised fibre architectures this transition would be expected to take place over a larger volume fraction range as there are more spaces between the tows.

Regime 2

This stage is characterised by the non-linear portion of the curve in Figure 47. Many of the larger spaces have been filled. The tows continue to bend to fill the smaller spaces, and compaction of the tows begins. The mesoscopic heterogeneity of DCFP creates an inherently porous structure, so this regime may be larger than it is with continuous fibre preforms. Preforms with larger tows may also remain in regime 2 for a wider pressure range. Preforms initially enter this regime as they undergo consolidation where heat and pressure are applied. As the preform is cooled all deposited layers stay in contact with each other due to the action of the binder. The preform returns to regime 1, but binder inhibits movement of tows in the transverse direction.

Regime 3

Large spaces between tows have been filled. The near-linear function of this regime is characterised by the compaction of fibre bundles as the preform approaches the maximum achievable volume fraction. The single tow compaction study examined the effect of pressure on the thickness response in a fibre bundle. Figure 46 shows the load-displacement curves for four different tow sizes. The initial curved portion of the curve represents regime 3. The tow volume fraction increases as the load increases and the thickness of the tow decreases. The curve becomes steeper as the load continues to increase and the fibres become more closely packed together. As the fibres in the tows reach their maximum level of packing the curve approaches a vertical gradient.

Regime 4?

A further phase may also be considered as the individual filaments within each tow begin to compact. This would be seen when packing within the tows begins to reach its optimal value i.e. when much of the space between filaments is filled. Fibres are likely to deform under sufficiently high pressures and compaction times. Both the pressure range or cycle times used in this study were unlikely to be of the order required for compaction at the filament level to be seen. This theoretical fourth regime has therefore not received any further attention.

3.5.4   Evaluating a model

Compaction curves were fitted with four models: the power law, and models proposed by Eggert, Van Wyk and Chen et al. A comparison is shown in Figure 48. An explanation of each model, and its variables, can be found in the literature review (3.3). The formula for each model is specified in Table 12 below. The power law was adjusted to accounts for the initial latent volume fraction s_0.
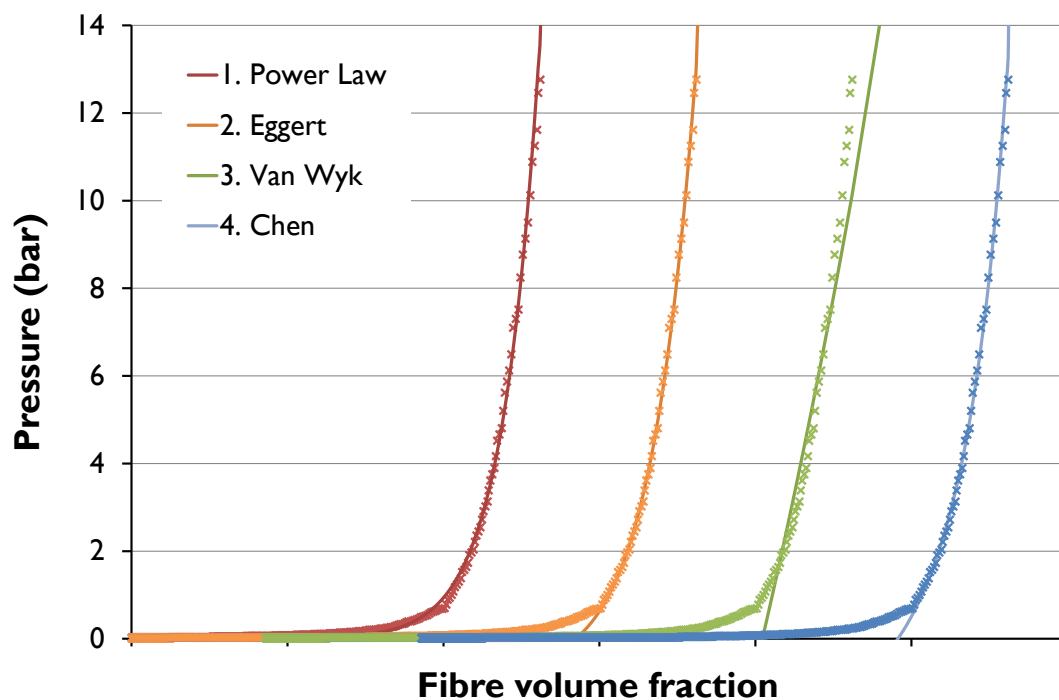
Figure 48. Comparison of four compaction models with experimental data for FA1. The same set of experimental results is fitted with each model. Volume fraction values have been offset for clarity.

The adjusted power law was shown to have the best fit with experimental data (the root mean square error for each model is shown in Table 12). However, the physical meaning of the constants remains unknown. This is also a disadvantage of implementing Eggert or Van Wyk's models. The former showed good correlation with experimental results, but the latent pressure P_0 was difficult to evaluate; this effectively turned it into another empirical constant. Van Wyk's model didn't adequately capture the compaction behaviour of the preform with a near linear model being the best fit for the range being studied.

The model proposed by Chen et al. (Eq. 42) showed good correlation with the experimental data, appropriately modelling each regime. The model is particularly appealing for modelling compaction in DCFP preforms due to the physical significance of each parameter in the calculation of constants; these may show correlation with mesoscopic variables e.g. tow size. Although the model failed to capture the data with the same level of accuracy as the adjusted power law, it captured the general trend well within the data range that represented the greatest change in volume fraction (1 – 10 bar). Deviation from the experimental curve may also be a result of inaccuracies in the experimental procedure or measurement of data.

Table 12. Root mean squared error (RMSE) for four compaction models compared with FA1 experimental data. RMSE, based on absolute error, has been calculated for six data sets. The first includes the full range of volume fraction data, while the next four include data points above volume fractions of 15%, 20%, 25%, and 30%. The final set represents the area of greatest interest and that least likely to be affected by systematic error – results recorded between pressures of 1 and 10 bar.

	Root mean squared error			
	Model			
Range	**1. Power**	**2. Eggert**	**3. Van Wyk**	**4. Chen et al.**
	$P = cs^n$	$P = \dfrac{P_0}{\left(\frac{v}{v_0}\right)^\gamma} - P_0$	$P = c[s - s_0]^n$	$P = \dfrac{1}{C_b(s)}\left(1 - \dfrac{s_0}{s}\right)$
All data	0.08	0.72	18.00	3.49
>15%	0.08	0.49	10.67	1.72
>20%	0.08	0.38	7.15	1.15
>25%	0.08	0.29	4.54	0.78
>30%	0.07	0.21	2.54	0.49
1–10 bar	0.04	0.03	0.12	0.03

For manufacturers, preform deformation will be of most interest in regime 2 where the volume fraction begins to change more drastically with applied pressure. Models are less likely to be required for low pressures, and volume fractions, as the response is close to linear. More significantly, preforms at these volume fractions (e.g. <30%) are unable to provide the properties required for structural applications. When data sets were limited to results between 1-10 bar, the root mean square error was seen to drop markedly from 3.49 to 0.03 (Table 12). The improved accuracy obtained by using the power law or Eggert's model, over that of Chen et al., was also seen to diminish. Results suggest that error reduction may be disproportional to sample reduction. This may be indicative of greater systematic error at low pressures.

Repeat compactions

Hysteresis effects were observed between each of the three compactions. As pressure was removed, the preforms exhibited a degree of relaxation. Preforms soon maintained a steady-state form with a higher volume fraction than that previously (prior to any compaction) exhibited. This was observed largely due to friction between the fibre tows, but binder can also play a significant role. An interesting effect can be seen in the consolidation stage of DCFP manufacture. The thermoplastic binder is activated by heating the preform while it remains under pressure. As the preform is cooled it remains under pressure. Once the pressure is eventually relieved, relaxation is small as the binder has re-solidified, holding the fibre tows in place. Preforms removed from pressure before being cooled have shown a greater degree of relaxation. In this case the binder remains softened until the temperature of the preform falls below the activation temperature, allowing the preform to relax with less restrictive force until the binder re-solidifies.
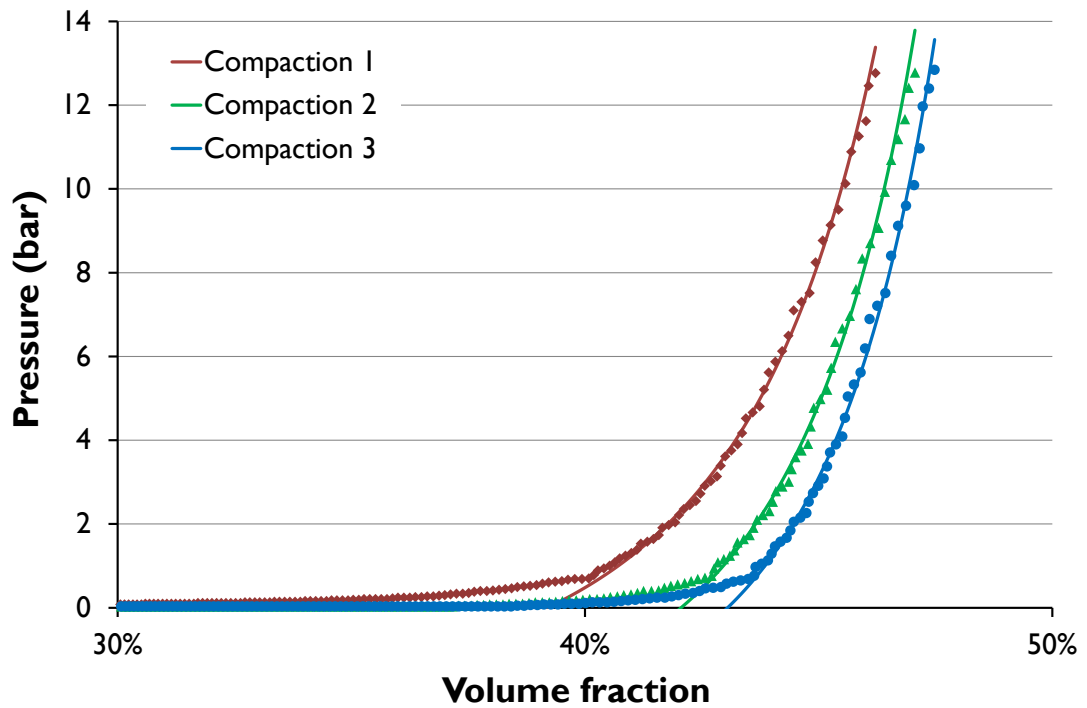
Figure 49. Repeat compactions of the same FA1 preform specimen. Experimental data was fitted with the model by Chen et al. for each test, with the coefficients shown in Table 13. Compaction 1 indicates the initial compaction followed by the two repeat compactions. Data was not recorded as the preform underwent relaxation between compactions.

The model by Chen et al. also showed good correspondence with repeat compactions (Figure 49). The latent volume fraction, s_0, was seen to increase as a result of the hysteresis effects observed. The pressure/V_f gradient was also seen to increase as larger volume fractions were realised with less pressure. To model this there was a decrease in the initial preform bulk compressibility, C_{b0} from 0.475 to 0.258 and 0.215 (Table 13). The maximum volume fraction s_f remained the same at 54%, indicating that repeat compactions are unable to alter this.

The major benefit of repeat compactions is the ability to obtain larger volume fractions for a given load. For instance, at 1 bar the volume fraction during the first compaction was 39%. For the second and third compactions, this was seen to increase to 42% and 43%, respectively. These results do show that the difference between the first and second compaction is far greater than that of the second and third. It can be assumed, *a posteriori,* that subsequent compactions will show even less dissimilarity.

Table 13. Coefficients used in the model for repeat compactions of the FA1 fibre architecture. The parameters *k*, C_{b0} and s_f are used to calculate the bulk compressibility of the preform C_b.

Compaction	Coefficients						
	ν	E	k	C_s	C_{b0}	s_0	s_f
1					0.475	39%	54%
2	0.38	238	2	3.03×10^{-6}	0.258	42%	54%
3					0.215	43%	54%

If a low pressure moulding process is to be used, compaction prior to moulding is likely to have a much larger effect. In high pressure applications the difference at a given pressure between the first compaction and subsequent ones is relatively small. However, these differences become much larger under 1 bar. Manufacturers may wish to "pre-compact" (at high pressure – whether through consolidation or otherwise) their preforms to ensure that they achieve high volume fractions when infused under vacuum. For FA1, volume fraction at 1 bar would increase by a proportion of 8.5%.

3.6 Design of experiments

Fibre architectures nominated in the DOE for the tensile characterisation study (2.6) were also selected for this work and are described in Table 14. The manufacture of preform COM012412 was not possible as the fibre architecture, made up of short bundles with large numbers of filaments, resulted in poor integrity due to systematic gaps between tows. It was consequently omitted from the study. The three benchmark materials are included in the DOE.

Table 14: Compaction DOE. Twelve permutations were repeated for thicknesses of 3 mm and 10 mm. Each sample contained 6 x Ø 100 mm specimens. The designation is denoted by the letters "COM" followed by: target thickness at 30% V_f, tow size and fibre length. A highly filamentised DCFP preform and NCF layups formed benchmarks for the study.

Designation	Tow size	Fibre length (mm)	Thickness (mm)
DCFP			
COM__0312		11.5	
COM__0329	3k	28.75	
COM__0358		57.5	
COM__0612		11.5	
COM__0629	6k	28.75	
COM__0658		57.5	
COM__1212		11.5	1, 3, 10
COM__1229	12k	28.75	
COM__1258		57.5	
COM__2412		11.5	
COM__2429	24k	28.75	
COM__2458		57.5	
COM032410FIL	24k	10	3
NCF			
COMNCF1			1 layer
COMNCF2			2 layers [0]$_2$
COMNCF2QI	24k	Continuous NCF	2 layers [0,90]
COMNCF4			4 layers [0]$_4$
COMNCF4QI			4 layers [0,90]$_2$

3.7 Mesoscopic homogeneity effects

Three features of the mesoscopic architecture were studied to determine their effect on compaction behaviour: tow size, fibre length and target thickness.

3.7.1 Tow size

Larger tow sizes lead to less homogenous fibre coverage throughout the preform. Increased variability, as a result of greater specimen to specimen mass variation, was previously discussed in Chapter 2. Central to this study, this can manifest itself in a greater tendency for tows to cluster and a greater degree of fragmentation resulting in greater preform loft. Localised regions of high fibre coverage influence compaction of dry fibre preforms as they require more pressure in order to be compressed and therefore bear a greater proportion of the load exerted by a flat platen. Consequently, these regions determine the maximum volume fractions achievable within a component. The effects of these localised regions were seen to be more significant in preforms that exhibited high degrees of variability.
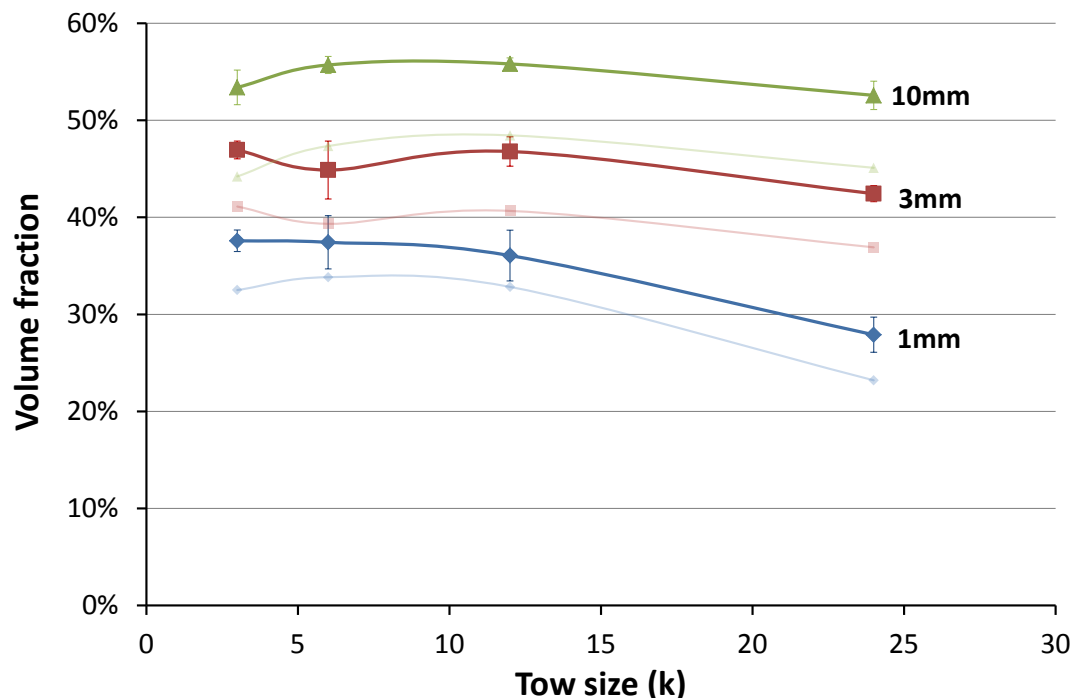
Figure 50. The effect of increasing tow size on fibre volume fractions at a compaction pressure of 10 bar (and 1 bar represented by the lighter curves). Results are shown for a fibre length of 29 mm for three target thicknesses realisable at 30% V_f. Results of the first, of three, compactions are shown.

Figure 50 illustrates the effect of tow size on volume fraction for a given pressure. Larger tow sizes exhibited smaller volume fractions for a given pressure, but this effect was only significant with thinner preforms. At 1 bar, and at thicknesses of 1 mm and 3 mm, 24k preforms exhibited volume fractions that were, on average, 25% and 5% (by proportion) less than those produced with 3k tows. This difference continued to become smaller with increasing target thickness; hence, the effect of tow size was shown to be less significant for increased areal mass. At 10 mm, 3k and 24k preforms were seen to have volume fractions of 44% and 43% at 1 bar – a difference of 2%.At larger pressures, marginal increases were observed in the differences between tow sizes at 3 mm and 10 mm. This was not the case for preforms at 1 mm as results for the achievable volume fraction narrowed at 10 bar, indicating that maximum values were being approached.

3.7.2 Fibre length
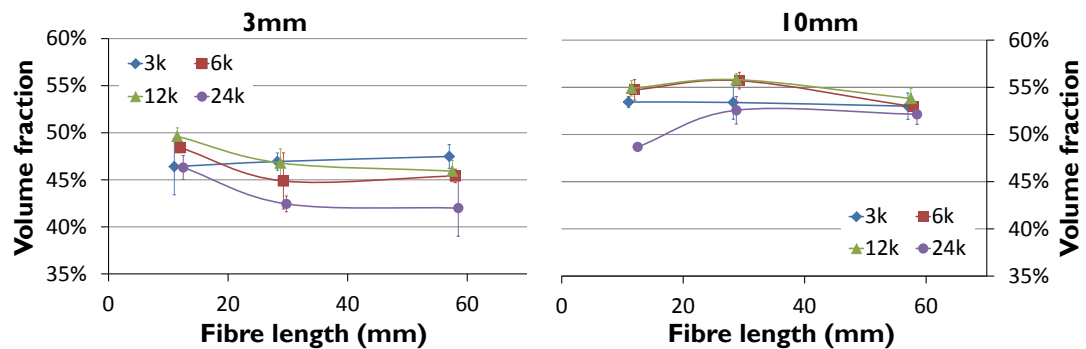
Figure 51: The effect of fibre length on fibre volume fraction at 10 bar for three fibre lengths. Results are shown for two target thicknesses at a volume fraction of 30%: 3 mm and 10 mm. Results have been offset, by 0.5mm in both charts, for clarity.

The effect of fibre length was less significant than that of tow size. Little benefit was seen by reducing fibre length from 58 mm to 29 mm as shown in the 3mm results displayed in Figure 51. By decreasing the chopped length from 29 mm to 12 mm it was shown that the achievable volume fraction could be increased – 11% and 3%, on average, for 1 mm and 3 mm preforms under a pressure of 1 bar. Similar results were observed under increased pressures. Such a trend was not seen with the larger 10 mm preforms with a fibre length of 28 mm yielding the greatest achievable volume fractions.

As noted in the tensile characterisation study (Chapter 2), length effects were not seen in isolation as shorter fibre lengths resulted in a larger degree of fragmentation during the fibre deposition process. The relatively small influence of fibre length on results suggests that improvements in preform homogeneity, by using shorter fibres, have been offset by a greater degree of tow fragmentation. This fragmentation incurred by using shorter fibres is representative of the manufacture of preforms of such architectures and should be considered as a foreseeable outcome of choosing to adopt shorter chop lengths.

3.7.3 Areal mass

Effects of both tow size and fibre length have been shown to become less significant with increasing target thickness. Areal mass was studied in an attempt to understand whether an ultimate trend exists, for achievable volume fractions, regardless of the architecture of the preform. The relationship between areal mass and achievable volume fraction at 10 bar, for all fibre architectures in the study, is shown in Figure 52. A clear trend exists where the volume fraction, observed under a defined pressure, increases with the amount of fibre being compacted. Above an areal mass of 1.5 kg/m^2, achievable volume fractions appear to be dictated less by the preform architecture; similar results were seen regardless of tow size or fibre length. The lowest value recorded at the target thickness of 10 mm was for the 24k 12 mm preform that was shown to be adversely affected by fragmentation. The result is noticeable in Figure 52 as the only heavy preform (i.e. >3kg/m^2) with a volume fraction below 50%. Results indicate that the distribution of achievable volume fractions decreases with increased fibre mass. Despite a greater spread in preform mass, heavy preforms were seen to give more consistent volume fractions for a given pressure with a smaller range of 7% at a target thickness of 10 mm (5.37kg/m^2), compared to 10% at 1 mm (0.537kg/m^2).
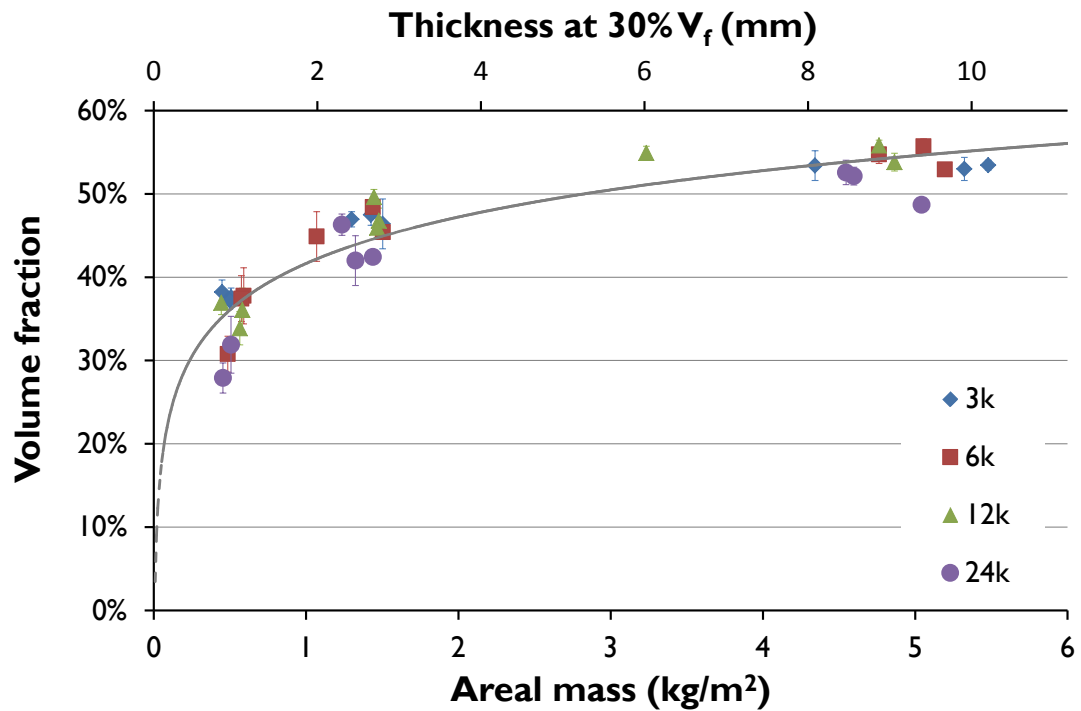
Figure 52. The effect of areal mass on the achievable volume fraction of DCFP fibre architectures at 10 bar. Results are shown for all preforms in the compaction study with the areal mass determined by the average mass of six specimens. The error bars indicate the standard deviation of each sample. A logarithmic line of best fit [y = 0.08ln(x) + 0.42] has been fitted to all data.

3.7.4 Comparison with other materials

Compaction behaviour of the random meso-scale discontinuous preforms were compared with three benchmarks: uni- and bi- directional layups of continuous non-crimp fabric, and a highly filamentised discontinuous fibre architecture produced with 24k tows at a length of 25 mm. Typical compaction curves for the three benchmarks are compared with three DCFP fibre architectures produced at UoN in Figure 53, with the expected volume fractions at 1 bar detailed in Table 15. Samples of similar areal mass were chosen for the comparison. The best and worst cases from the initial compaction DOE (for a target thickness of 3 mm thickness) were included. The third preform from the DOE was that which most closely represented the highly filamentised benchmark in terms of tow size and fibre length.
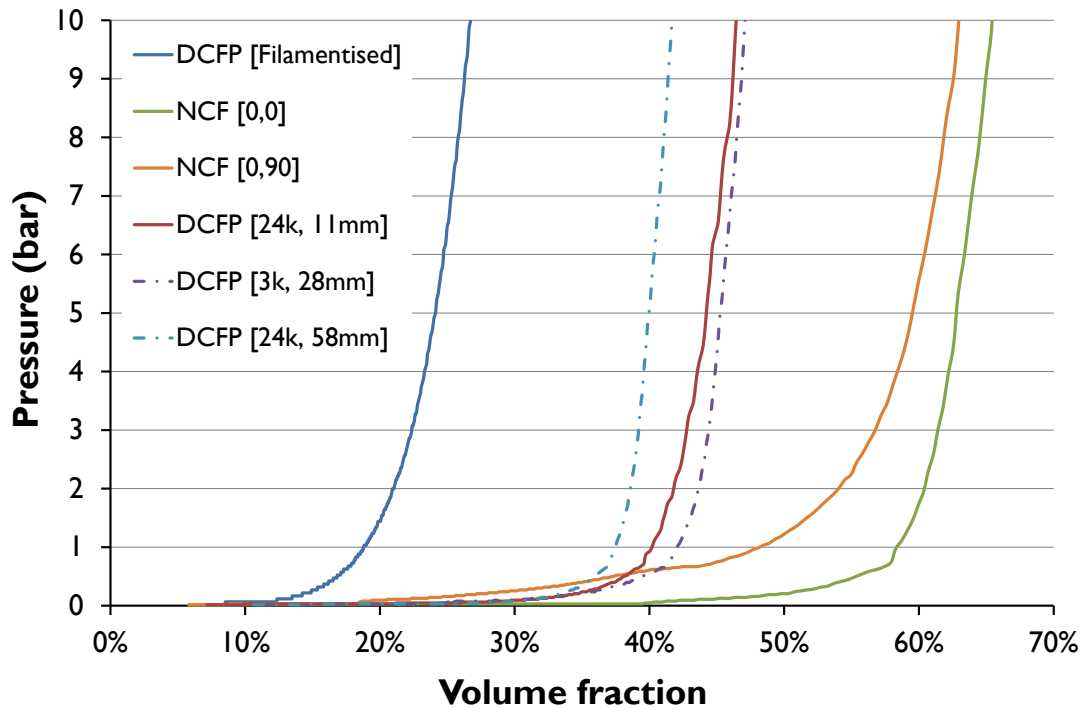
Figure 53. Compaction behaviour of DCFP compared with two NCF layups and a highy filamentised DCFP fibre architecture produced at Sotira. The first UoN DCFP preform incorporates a fibre architecture that most closelt resembles that of the Sotira fibre architecture. The other two curves represent the upper and lower bounds of the results at this areal mass. The volume fraction for each curve has been calibrated to account for displacement caused by the compaction rig.

Table 15. Expected fibre volume fractions at 1 bar under a compaction of by rigid tool.

	Material	Expected V_f at 1 bar
DCFP	Highly filamentised	20%
	3 mm 24k 58 mm	38%
	3mm 24k 12 mm	40%
	3mm 3k 29 mm	42%
NCF	[0/90]	50%
	[0]	60%

All preforms showed a similar response to pressure. In response to applied pressure an initially large increase in volume fraction was followed by a constant, but gradual, increase in volume fraction. Similar slopes were seen for all materials at higher pressures (>5 bar). It can be concluded that this region is dominated by a factor common to all of these fibre architectures; tow compaction was previously identified as the major element of compaction in this region (regime 3).

Natural fragmentation of fibre tows has been shown to be beneficial in some instances. The experimental study has shown that increased volume fractions can be

achieved but has shown that this may only be the case with larger tow sizes at low target thicknesses. In such situations, tow sizes fragment in a relatively well-ordered fashion to produce tows with fewer filaments e.g. 24k splits up into 2 x 3k and 1 x 6k. At large areal masses (i.e. >2 kg/m^2), mesoscopic variability of the fibre architecture decreases so the benefits of fragmentation are seen to diminish. Mesoscopic homogeneity was seen to improve in the highly filamentised preform, but tows broke up in a much more irregular fashion. Misalignment of fibres becomes more of a concern as fragmented tows with extremely low numbers of filaments, i.e. less than 500 filaments, exhibit very low bending stiffness, so waviness is more prominent. Fibre packing becomes highly inefficient and compaction behaviour is seen to be poor in relation to unfilamentised DCFP architectures. It has already been suggested that wavy fibres can reduce performance as they are unable to transfer loads properly, which can be lead to reduced strength. The compaction of NCF preforms was seen to be relatively independent of thickness due to a more even pressure distribution. Results are compared with DCFP architectures in Figure 54.
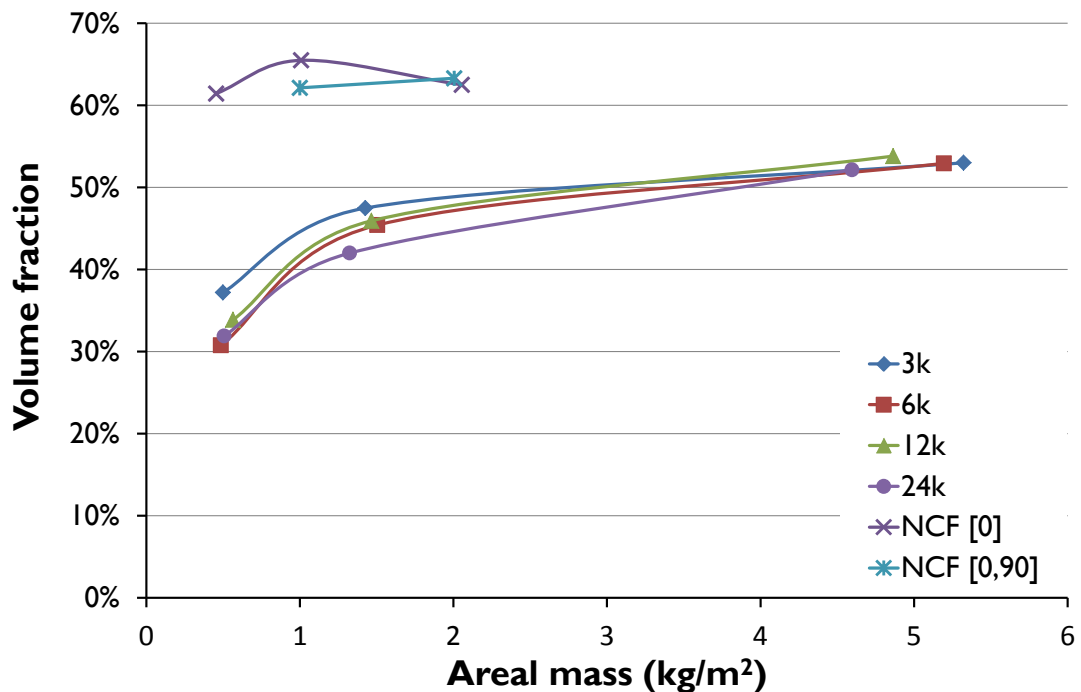
Figure 54. The effect of areal mass on preform fibre volume fraction. Results are shown for the first compaction at a pressure of 10 bar. All data for DCFP architectures are for a fibre length of 58 mm. The three groups of data points correspond to the three target thicknesses of 1 mm, 3 mm and 10 mm at 30% V$_f$. Data is included for uni- and bi-directional stacks of NCF with the points corresponding to 1, 2 and 4 layers.

3.7.5   Modelling compaction behaviour of DCFP Architectures

The appropriateness of the constitutive law proposed by Chen et al. for DCFP architectures was tested by fitting the model to experimental results of all preforms in the compaction study. Difficulties were found in applying the model to preforms of a low areal mass i.e. those with a target thickness of 1 mm. Good correspondence was shown for larger thicknesses with varying degrees of accuracy depending on the makeup of the preform. Only the application of the model to 3 mm and 10 mm preforms will be discussed here. These results have been used to provide further insight into the compaction of meso-scale DFCs.

Specimens were chosen for each preform that most closely represented the mean values and compaction behaviour of the particular architecture. Models were fitted to data from the three compactions using a least squares method to reduce the sum of squared residuals (SSR) between 1-10 bar. This was observed as the region least likely to be affected by systematic error and the one of most interest due to the most significant changes in volume fraction. Difficulties arose in comparing the fit of different thicknesses due to the variation in the number of data points, which was a consequence of using a fixed sampling rate. A larger propagation of uncertainty was seen in thin parts due to less data and proportionally larger systematic error.

Three variables were required in order to implement the model: the initial compressibility C_{b0}; and the latent and maximum volume fractions, S_0 and S_f. The latter were determined by evaluating experimental results across the range of architectures. The latent volume fraction (39%) was likely to have been defined, to some extent, by the consolidation pressure. The maximum volume fraction (61%) provides an indication of the intrinsic limiting volume fraction. The latter S_f was fixed for all compactions while S_0 was fixed for the initial compaction only. The initial compressibility was determined individually for each architecture. The procedure described is summarised by:

1.   Fixed S_0 and S_f of 39% and 61%

2.   Determine C_{b0} for 1st compaction by minimising SSR

3. Vary S_0 and C_{b0} to minimise SSR for 2nd and 3rd compactions

The coefficients for all 3 mm and 10 mm architectures are detailed in Appendix D.

Initial compressibility C_{b0} was seen to decrease in repeat compactions due to reduced compressibility of the preforms. The majority of this reduction was observed between the first and second compactions with an average decrease of 45%, but only minor differences were seen subsequently with values decreasing by 7% between the second and third compactions. All preforms maintained a greater resting volume fraction after the initial compaction resulting in an increase in S_0.

Subtle differences were observed in the compaction curves of different fibre architectures. This manifested itself in the model through variability of C_{b0}, which was affected by thickness, fibre length and tow size. Areal mass, was the most significant factor with C_{b0} averaging 0.604 at 3 mm and 3.912 at 10 mm. This was indicative of the ability to increase the volume fraction of thicker parts with greater ease i.e. smaller pressures. Compressibility was seen to increase with larger bundle sizes up to 12k following a linear trend shown in Figure 56. Preforms incorporating 24k bundles did not follow this trend exhibiting lower compressibility than the smallest bundles size, 3k, used. This could be a result of increased fragmentation observed for these tows.
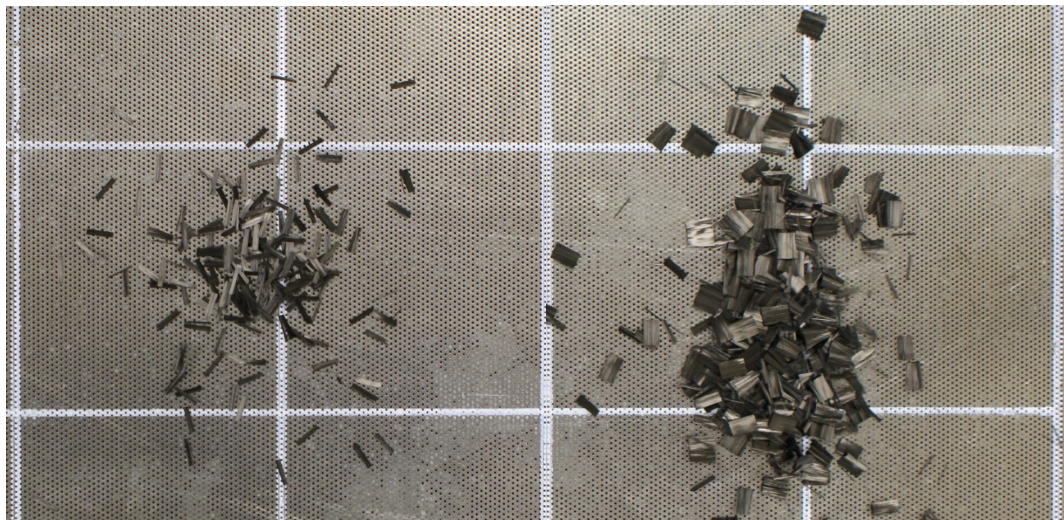
Figure 55. Increased fragmentation observed with 24k tows (right) compared with 3k tows (left). Note that the masses are different as each deposition used 1.8 m of fibre to achieve the same number of chopped tows.

Shorter tows resulted in preforms with the largest values for C_{b0} but the initial compaction saw lower values for 12 mm fibres than with 29 mm. A change was seen in subsequent preforms where C_{b0} was larger for preforms incorporating 12 mm tows over the other two lengths in the study. Increased latent volume fractions S_0 in the second and third compactions were observed for larger thicknesses, tow sizes and fibre lengths.
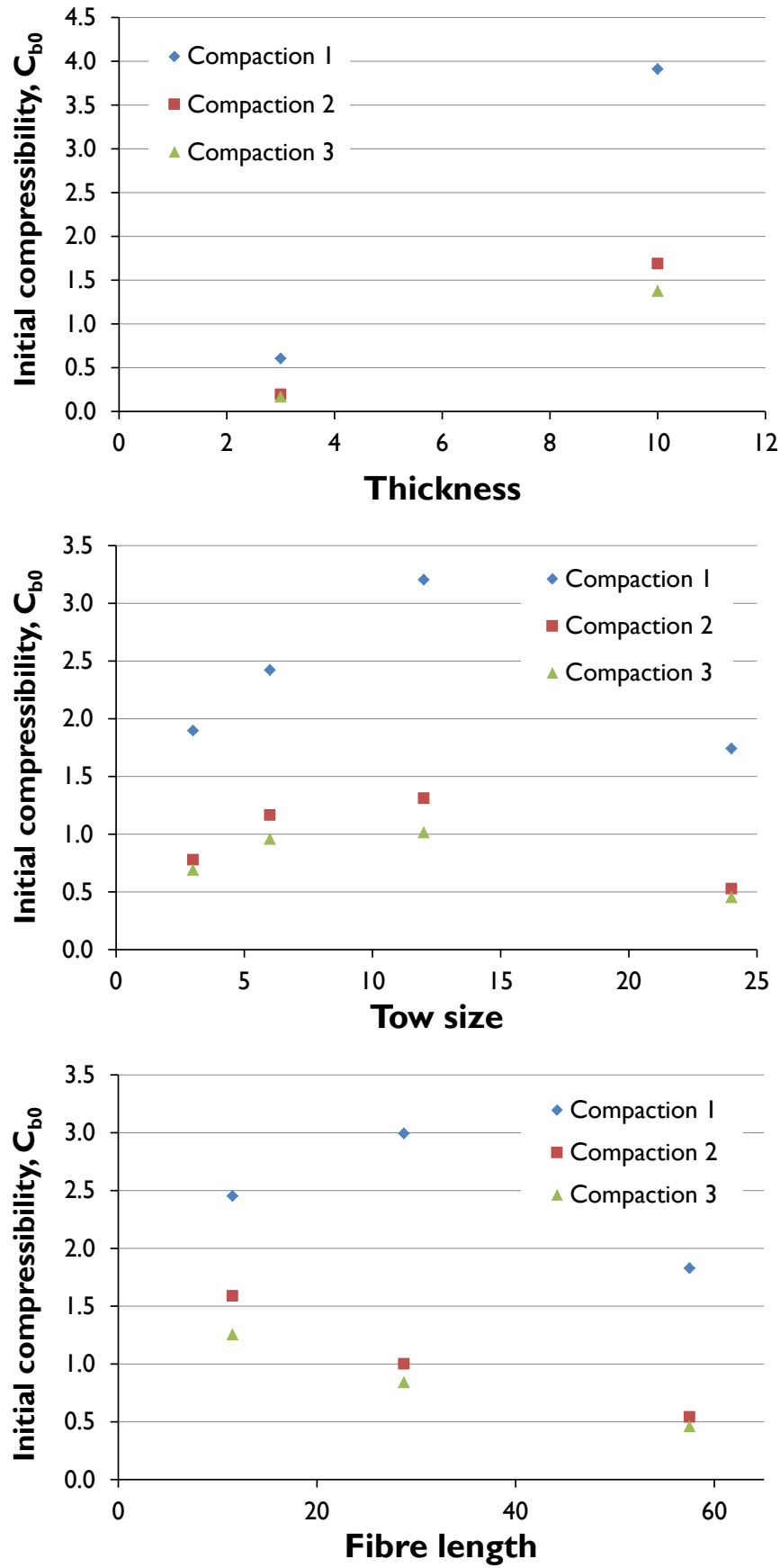
Figure 56. Main effects of thickness, tow size and fibre length on the initial compressibility, C_{b0}, of DCFP architectures.

3.8   Implications for tooling and preform design

The study indicates that homogeneity greatly affects the maximum achievable volume fraction for a given pressure. Improved preform coverage arising from smaller tow sizes, shorter fibre lengths, and increased areal mass reduces the severity of fibre rich areas. These sites are subject to locally high pressures, which lead to regions of high volume fraction that can result in potential problems with impregnation and voidage. It is known *a priori* that this can lead be detrimental to mechanical performance. Difficulties are likely to arise when attempting to mould thin parts with a high target volume fraction. The greater relative mass variability at low areal mass was shown to yield lower volume fractions for a given pressure (Figure 57). Higher volumes can be achieved with fibre architectures known to give good coverage (i.e. 3k, 12mm), but results are still significantly lower than they are with heavier preforms.
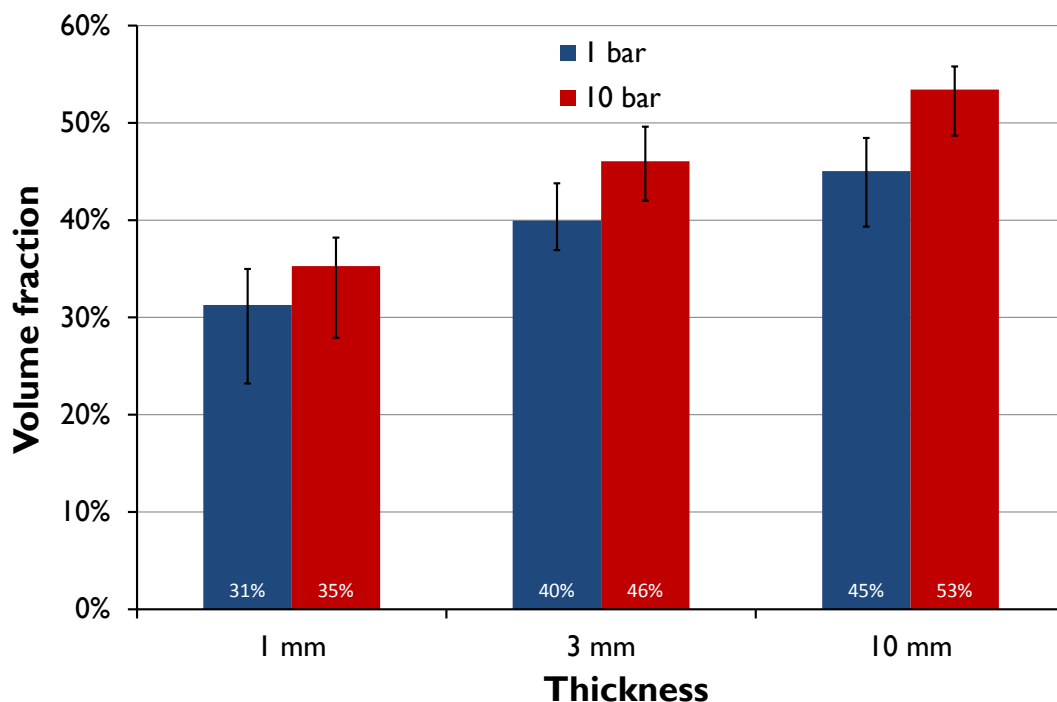
Figure 57. The average volume fractions observed for preforms of three target thickness (achievable at 30 V_f) under two different compaction pressures. The thin bars overlaying the results indicate the range of values at each thickness, with the maximum and minimum at the upper and lower ends.

The reductions in mechanical properties for low thicknesses was discussed in the previous chapter. The findings of this compaction study accentuate the problems associated with thin parts. Poor mesoscopic homogeneity leads to reduction in mechanical performance through high coupon-to-coupon variability; it also hinders the ability to achieve high volume fractions.

The choice of moulding method for random meso-scale discontinuous fibre preforms will have a bearing on the mechanical properties of a component due to the differences in compaction pressures that can be applied. Vacuum infusion, at 1 bar, will produce components of a significantly lower volume fractions then the same preforms moulded under RTM and compression moulding processes. However, flexible tooling is likely to be a significant benefit for fibre architectures that exhibit high degrees of variability as an even pressure distribution is seen over the whole preform. For a rigid tool, mesoscopic variability in the preform architecture can lead to uneven pressure distribution thus increasing the likelihood of locally high volume fractions, which are symptomatic of problems with impregnation and porosity in the final part. Moulding tools and methods should be optimised for target volume fractions, applicable compaction pressures, and mesoscopic homogeneity of the preform architecture.

Application of constitutive model

The model is expected to be applicable for large three-dimensional preforms but fine-tuning of the existing coefficients (determined in the previous section) will be needed. A database of the coefficients for 3 mm and 10 mm DCFP architectures is included in Appendix D and can be used as a guide. The large drop in compressibility between the first and second compaction (compared to a relatively small drop between the second and third) advocates the use of a second compaction if high target volume fractions are required. Preform behaviour under this second compaction is also easier to model, which would lead to better estimations of required tool pressures.

3.9   Conclusions

A study on compaction behaviour of dry discontinuous fibre preforms highlighted areal mass as the most important factor in determining the maximum achievable volume fraction for a preform. Poor mesoscopic homogeneity in thin parts hindered the ability to achieve high volume fractions. As areal mass increased there was initially a large increase in the achievable volume fraction at 10 bar followed by a convergence (from approximately 1.5 kg/m^2) to a volume fraction of between 55%-60%; this was indicative of the value for maximum theoretical volume fraction.

Larger tow sizes were seen to be affected more by areal mass; the use of large tow sizes for thin parts would not be recommended. The effect of fibre length was less significant. A small increase in volume fraction was seen for 12 mm fibres in relation to 29 mm but this was only true for parts of low areal mass. This was not seen in the thicker preforms where fragmentation of short fibres may result in fibre packing issues.

The compaction behaviour of DCFP is characterised by three stages. In response to applied pressure an initially large increase in volume fraction is followed by a transitional phase, which is succeeded by a, but gradual, increase volume fraction. A constitutive model proposed by Chen et al. was selected to model this behaviour in DCFP preforms due to the physical significance of each parameter in the calculation of its constants. The model showed good correlation with experimental data for target thicknesses of 3 mm and 10 mm.

Compaction of UoN DCFP preforms was compared with a NCF benchmark and a highly filamentised DCFP architecture produced by Sotira. Results indicate the advantages of using non-filamentised preforms as the expected V_f at 1 bar was approximately 40% compared with 20% for the highly filamentised equivalent.

4 Increasing toughness in meso-scale discontinuous carbon fibre composites

4.1 Introduction

The highly cross-linked structure of epoxy resin makes it an inherently brittle material with poor fracture properties compared with that of thermoplastic resins. A lack of toughness has prevented its expansion to high performance applications such as aerospace structures [108]. Manufacturers are increasingly developing resin systems to improve properties in composites.

Much work has been carried out to improve the relatively poor fracture properties of epoxy resins [109] and there is a desire to improve damage tolerance in the composites. Properties of components that have been subjected to impact damage depend on resistance to the initial impact event. Resistance to impact damage is primary governed by the matrix and in toughened systems that resistance is made greater by increased energy absorption. Whilst this is desirable for DCFP components, there is an interest in the effect of these toughened systems on tensile properties.

DFCs offer a great deal of flexibility due to the relative ease in which the fibre architecture and matrix can be modified. Unlike continuous fibre composites, external loads are not directly applied to the fibres in DFCs. The load is transferred to the fibres through the matrix via fibre ends and surfaces [74]. Consequently, the properties of the resin may have a more significant effect upon mechanical performance.

4.2   Objectives

This work seeks to determine how the performance of meso-scopic DFCs change with highly plasticised matrices. Candidate modifiers were mixed with an existing epoxy resin system, Prime 20LV, to determine an additive that provided improved strain to failure and fracture toughness. Both flexibilisers and tougheners were initially considered in order to gain understanding of their impact on the existing epoxy system. Suitable addition levels needed to be determined to ensure that high concentrations of the modifier didn't degrade properties.

The modified matrix was used to mould DCFP fibre architectures. Of particular interest was the effect of highly plasticised matrices on architectures that show a high coupon-to-coupon preform mass variability. It was desirable to understand the effects of factors that are known to impact variability, such as tow size, on the effectiveness of toughening. Tensile properties of DCFP architectures were compared to NCF laminates to determine whether toughening had a more significant impact, positive or negative, on DFC architectures that exhibit significantly higher levels of variability.

4.3 Literature review

Achieving improved toughness in composites has followed two distinct strands of study. Resin manufacturers are focussing on the first: working on new resin chemistries that look to reduce cross-link density of the epoxy network to improve toughness of the resin. There has also been a desire to engineer existing composite systems to improve mechanical and dynamic properties. The ability to tailor composites makes them particularly attractive for use in crash components [110]. This review will focus on the latter approach, using modifying agents and methods to improve the properties of existing, commercially available, epoxy systems.

4.3.1 Flexibilisers

The majority of resin modifiers can be categorised as flexibilisers or tougheners. Flexibilising modifiers increase strain to failure in epoxy systems by facilitating increased deformation under stress. Crosslink density is reduced at the expense of glass transition temperature, tensile and shear strength as well as decreases in chemical and heat resistance [111]. Consequently, flexibilisers tend to be added to epoxy resins for adhesive applications [112]. The degree of degradation to other material properties may however be too severe for any progress in the development of flexibilised resins for composite structures. Hitchen et al. [113] found that greater quantities of flexibiliser in short carbon fibre/epoxy composites resulted in poorer material properties. A flexibiliser was added in two quantities - 15 parts per hundred (phr) and 59 phr - to the matrix of randomly dispersed carbon fibres. The larger addition of the flexibiliser resulted in a reduction of Young's modulus (13.5 GPa – 12.7 GPa) and UTS (154 MPa – 138 MPa). Hitchen et al. suggest that this may be a consequence of the larger mismatch in modulus between the fibres and the matrix, which could lead to greater strain magnifications making damage initiation and propagation easier. While the elongation of the resin may be increased by the flexibiliser, the results may not translate to a larger strain in composite properties. A decrease in tensile strain to failure (1.18% - 1.11%) was observed. Fatigue properties were also seen to decrease in specimens produced with the higher concentration of flexibilising agent.

4.3.2   Tougheners

Tougheners have been shown to provide many of the advantages as those provided by flexibilisers without as significant a reduction in Young's modulus. Increased properties are the result of greater absorption energy to offset crack propagation – the primary failure criteria for composites [114]. A number of toughened systems are commonly utilised. A variety of butadiende-acrylonitrile tougheners have been especially successful in both DGEBA and DGEBF types of epoxy resins. Carboxyl terminated butadiene acrylonitrile (CTBN) & amine terminated butadiene acrylonitrile (ATBN) are commonly used in structural epoxy formulations. Molar mass of the resin increases during curing meaning the solubility of the rubber reduces and eventually leads to phase separation and the formation of a distinct second phase in the resin, which is able to absorb greater energy and prevent crack growth [115, 116]. CTBN tends to be the elastomer of choice due to its miscibility in many epoxy resins. By using low levels of these liquid polymers, the fracture energy of cured DGEBA type epoxy resins can be increased by a factor of 15 [111].

Appropriate addition levels need to be established in order to establish optimum improvements in properties. Cech and Kretow [117] have shown that modification up to 10 parts per hundred resin (phr) can maintain the principal thermal and mechanical properties of the resin. Fracture toughness was shown to improve significantly with modification up to 15-20 phr. The concentration of the modifier may also affect processability. The addition of CTBN tougheners typically result in increased resin viscosity, due to the high molecular weight of the modifiers, making impregnation more difficult to achieve using RTM processes [118].

The use of preformed toughened particles, comprising both rigid and rubbery phases, has been investigated by Day et.al. [115]. Three-layered core/shell particles with an outer epoxy functional shell were compared with acrylic toughening particles (ATP) and CTBN. With the exception of Young's modulus the tensile, compressive and impact properties of RTM moulded unidirectional carbon fibre were all improved.

Preforming applications often incorporate toughening mechanisms between layers of reinforcement. Unlike the previous methods, these approaches do not have the aim of improving fracture toughness of the base resin system. Instead the modifier acts as a mechanical toughener by deflecting crack direction to require more energy to be expended per unit length of crack growth [119]. Work by Cano & Dow [120] has found that materials that incorporate a compliant interleaf for added toughness show improved damage tolerance in comparison to those that have not.
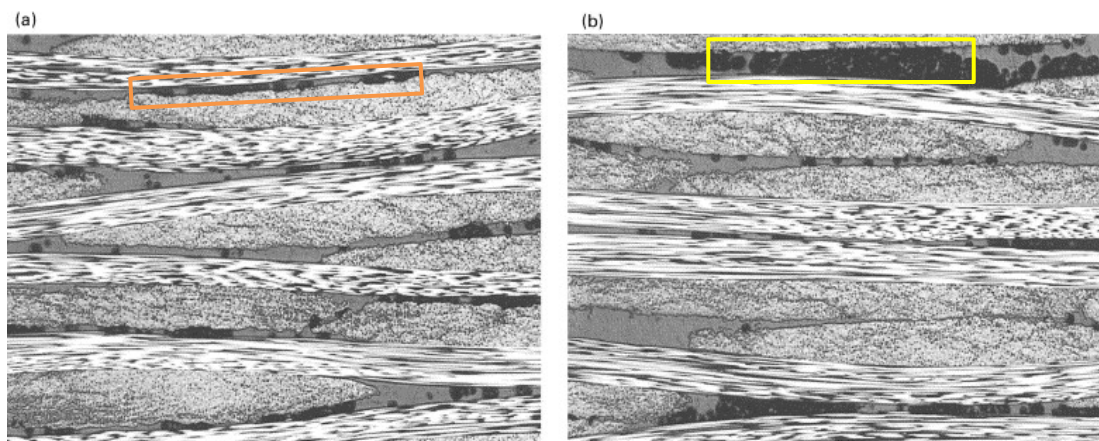
Figure 58. Interlayers in a laminates containing modified powder (a) and spray (b) tackifiers, at 25x magnification. Note the more even distribution in (a) compared with the clusters observed in (b). Reprinted with permission [118].

Hillermeier and Seferis [118] used polyamide particles to modify reactive epoxy powder binder as well as an uncatalysed spray binder. Micrographs of cross sections taken from both laminates are shown in Figure 58. The modified binders were applied between layers of 6k carbon fibre satin ¼ fabric with the spray providing a more uniform interlayer with better test results. A 30% improvement was seen for mode II inter-laminar K_{IC} whilst inter laminar shear strength showed a slight increase. This highlights the need to evaluate the method in which toughening agents are introduced into a system. Bagheri and Pearson [121] found that in almost all concentrations of modifier examined, smaller particles proved to be more effective toughening agents. Kamae et al. [122] suggest that toughness improvement depends on inter-particle distance, reiterating that improvements can be seen with more uniform coverage with smaller particles. The dispersion of particles in discontinuous fibre architectures will be heavily dependent on mesoscopic homogeneity.
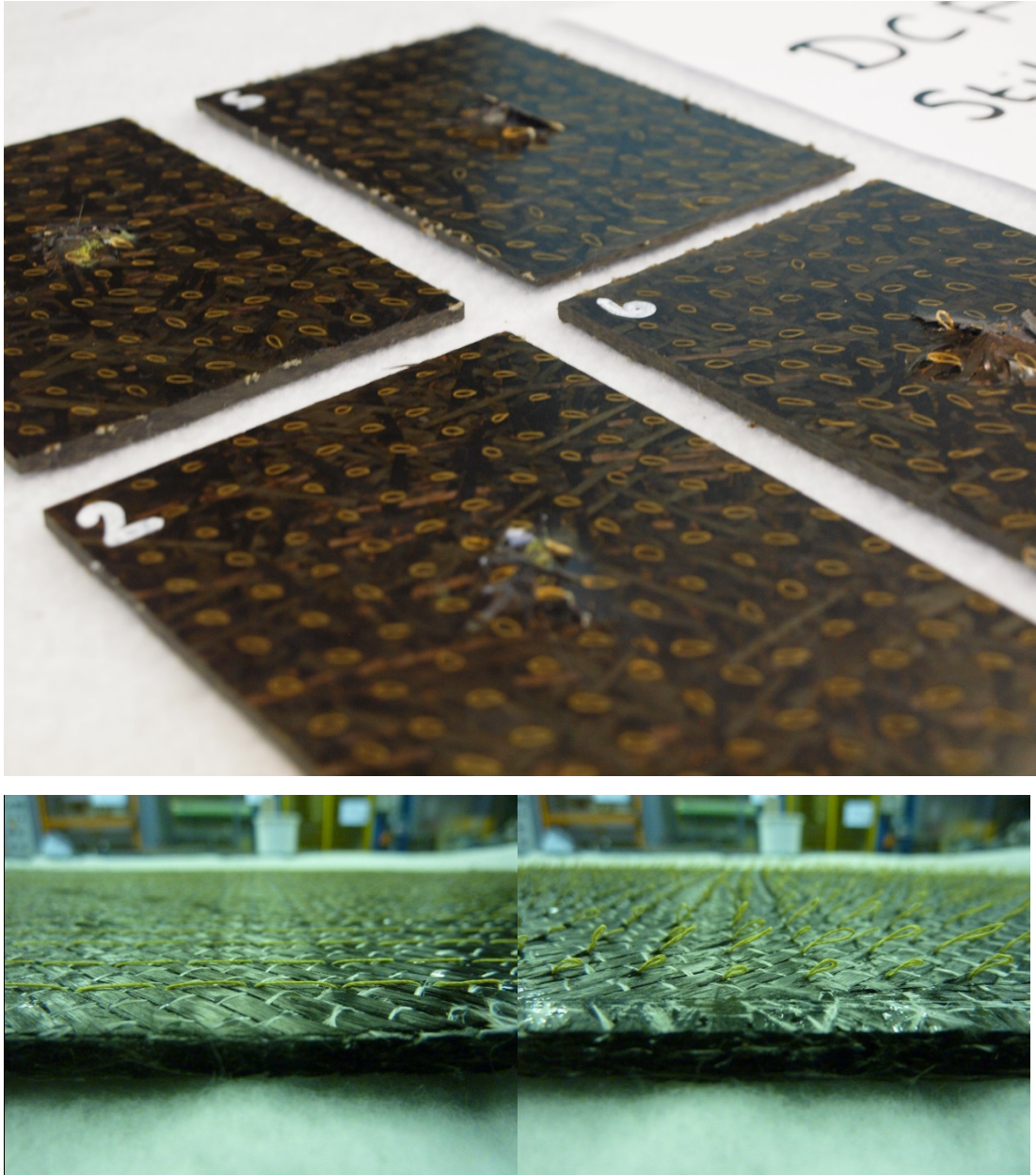
Figure 59. Stitched DFCP specimens (above) and NCF preforms (below) as part of a compression after impact study.

Stitching (Figure 59) provides another toughening mechanism that is suitable for use in preforming applications. Two significant disadvantages are the time required to apply the stitching, as well as reduced in-plane properties [119]. Hogg and Smith [123] used carbon fabric preforms intermingled with nylon fibres to determine the benefits of using thermoplastic fibres as a toughener. Slight decreases in tensile and compressive strengths were seen but other tests provided improved performance. Resistance to impact damage was improved with increased energy absorption, compression after impact properties and mode I and mode II fracture toughness.

Plastic deformation of the nylon fibres allows increased energy absorption without adversely affecting load bearing capabilities. While the study was carried out at low volume fractions, it is assumed that these benefits will also be seen at higher volume fractions. Recent generation of nano-toughening technology has been utilised to toughen epoxies but, due to the very small size of the particles, without compromising ease of processing as a result of increased viscosity [124]. Higher specific surface area of nanoparticles can promote stress transfer, and required concentrations are usually much lower than those of micro-fillers so that intrinsic benefits of the neat resins are retained [125].

4.3.3 Failure modes

Selecting a modifier that produces successfully toughened matrix systems may not always improve properties of the composite. Biswas [126] found that toughening achieved at the matrix level doesn't necessarily translate to improved properties in the composite. He highlights that failure mechanisms are different in a neat resin and a composite. The main objective of a study carried out by Tsotsis et al. [127] was to determine how neat resin properties affect composite properties. Results showed that un-notched tension results were still dominated by fibre bundle properties. However, open-hole tension results show strong correlation with neat-resin fracture toughness (Figure 60). The introduction of a defect clearly makes resin properties more important and suggests that properties of DFCs, which inherently contain many defects in their fibre architecture, are more dependent (than CFCs) on resin properties. The performance of random, discontinuous composites have been shown to be strongly influenced by the mechanical properties of the matrix material [75]. As described in Chapter 4, this is due to transfer of applied loads to the fibre bundles via the matrix.
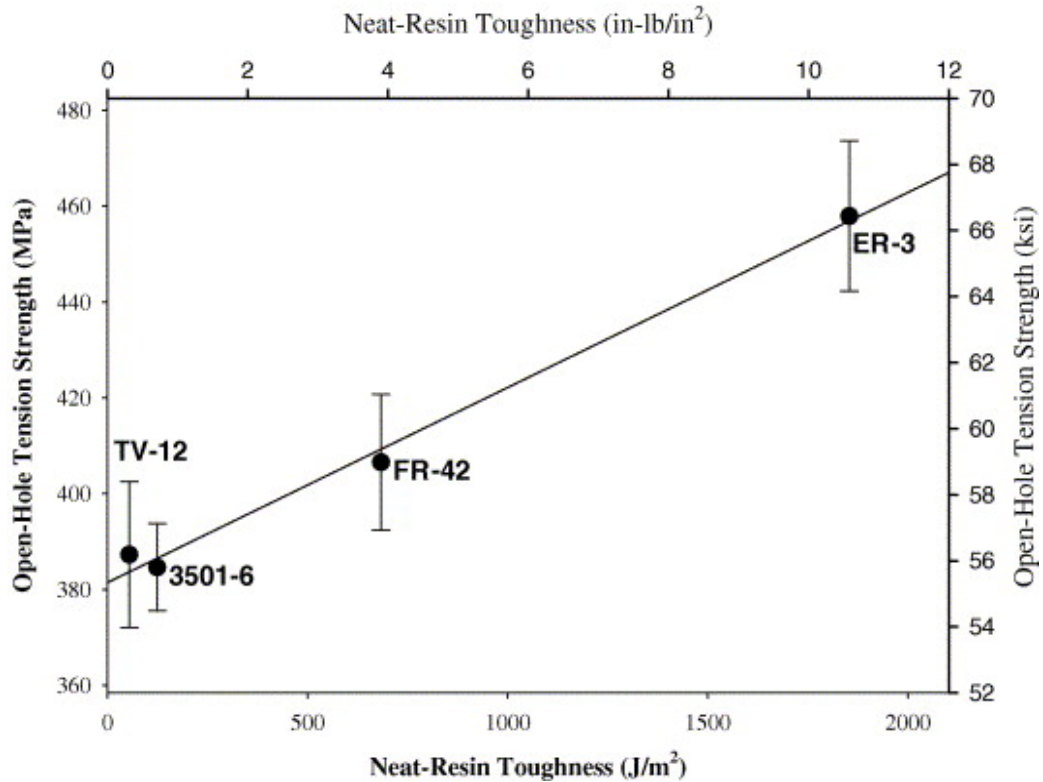
Figure 60. The effect of resin toughness on open-hole tension strength of laminates manufactured with warp-knit carbon fabric preforms (reprinted with permission) [127].

Tsotsis et al. [119] carried out a number mechanical tests and stated that correlations between neat-resting and composite properties ranged from fair to poor. There have been difficulties in establishing relationships between properties of the neat resin and composite. The range of effects for different types of test suggest that the correlation is determined by the failure mode. Jacob et al. [110] propose that a composite fails through a sequence of fracture mechanisms that include:

- fibre fracture
- fibre pull-out
- matrix crazing and cracking
- de-lamination
- inter-ply separation

They go on to suggest that the actual mechanisms and sequence of damage are said to be dependent on geometry of the structure, lamina orientation, and the type of failure.

The importance of the fibre- matrix interface has often been highlighted. Kaynak et al. [128] used a silane coupling agent (SCA) to improve interfacial adhesion between glass fibres and an epoxy matrix. They also premixed modifying agent - hydroxyl terminated polybutadiene (HTPB) – with hardener, for an hour before mixing with the epoxy resin component, to allow possible reactions to occur. Pre-mixing improved flexibility. Rubber molecules might react with hardener fully, leading to strong reaction with the epoxy. Therefore, load transfer from epoxy matrix to rubber particles may happen more easily. Non-treated fibre reinforcement (with SCA) lead to fibre pull-out (Figure 61). When dispersed particle size becomes smaller and more uniform, a greater improvement on flexibility will be seen.
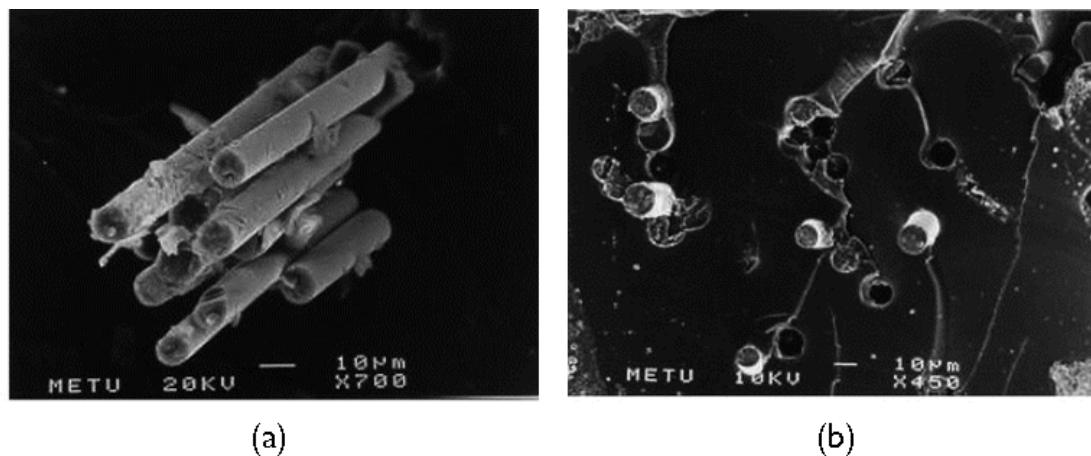
Figure 61. Smooth fibre surfaces due to poor interfacial adhesion (a) and holes due to fibre pull-out (reprinted with permission) [128].

4.3.4   Summary

The literature review has highlighted that the successful implementation of toughening mechanisms can improve properties in composites. The work on nano-toughening is particularly promising. In this study, where the objectives are not to optimise performance, other modifiers e.g. CTBN provide suitable modifying agents at low cost. There is currently a lack of data on the effect of neat resin properties on DFC properties. The degree to which DFC tensile properties change with modified systems needs to be evaluated and there is significant scope for work determining the effect on tensile properties as attention has often focussed on damage resistance.

4.4 Experimental methodology

4.4.1 Neat resin testing

All modifiers were pre-reacted (adducted) to the base component of the epoxy resin. This not only reduced the likelihood of early phase separation but maintained solubility in the uncured resin system. This was important in order to ensure viscosity remained low enough to ensure moulding of laminates wasn't largely affected. Modifiers were added to the resin at quantities of 5 phr, 10 phr, 15 phr and 20 phr. Due to the high viscosity of the additives they were heated to 65°C before mixing.

Each modified component was degassed for thirty minutes. Hardener was added to the base at 26 pph. Epoxy formulations were not adapted for different modification levels as epoxy equivalent weights were not available. All resin formulations were degassed for a further ten minutes before moulding. Neat resin samples, with dimensions of 250 mm x 250 mm, were moulded by pouring each formulation onto a flat aluminium sheet. Release agent was applied to the sheet prior to moulding and a 5 mm wall was constructed using vacuum sealant tape. Resins were heated slowly, at 1°C/min, to prevent significant exothermic reactions. The addition of Hypox DA323 and Hypox RF928 lengthened the standard cure cycle. Consequently each sample was cured at 60°C for a longer duration of two hours in an autoclave under vacuum without elevated pressure. Subsequently, post cure times were also adjusted to 6 hours at 70°C. Exact cure times for each formulation are unknown and would require separate dynamic mechanical analysis (DMA). After undergoing the full cure schedule, samples were surface ground to a thickness of 3 mm, and Test specimens were cut by water-jet. Tensile, flexural and Charpy impact tests were carried out in accordance with the following standards:

- tensile   -   BS EN ISO 527:1996
- flexural   -   BS EN ISO 178:1:2001
- impact   -   BS EN ISO 179:1:2000

4.4.2 Composite manufacture

DCFP and NCF preforms were produced in accordance with those described in Table 17. For each fibre architecture, two 400 mm x 600 mm preforms were manufactured and stamped to produce four 300 mm x 400 mm preforms. Each DCFP preform was manufactured using the same robot programme – a single sprayed layer consisting of an east/west pass followed by a north/south pass with each sweep of the robot offset by 50 mm. In previous tests, preforms were found to be underweight near the edges. A baffle was introduced to reduce wastage and manage mass variability. Fibre was deposited to achieve target preform masses of 193 g and 322 g for nominal volume fractions of 30% and 50%, respectively. Binder was sprayed with the fibre at a ratio of 5% by mass. After spraying, preforms were compacted at a pressure of two bar. Moulding and testing were carried out according to the methods described in Section 2.4. Prior to moulding, the resin modifier was adducted to the part B constituent of prime 20LV. Injection was typically completed in less than ten minutes. Plaques were post cured at 65°C for seven hours as recommended by the manufacturer.

4.5   Neat resin testing

4.5.1   Determining an appropriate modifier

Three candidate modifiers were examined: Hypox RF928, Hypox DA323 and DER736. All are commercial materials - the first two supplied by CVC Thermosets Specialities and the third by The Dow Chemical Company. Hypox RF928 is an adduct of a DGEBA resin and CTBN (Hypro 1300 x13, 20 wt.%). The adduct can be added to a base epoxy resin to provide a toughened system or used as a resin on its own. Hypox DA323 is an adduct of a DGEBA epoxy resin and a dimer fatty acid and can be added to epoxy to provide a flexibilised system. Both adducts are more easily processed than pure CTBN and dimer fatty acid modifiers. DER736 is another low viscosity flexibiliser that can be added to epoxy systems to impart increased elongation and impact resistance. All modifiers were selected based on compatibility with epoxy resins systems.

All formulations were clear but cured to form resin samples that were slightly yellow (DA323 and DER736) or white (RF928) in colour. This was compared to the translucent grey appearance of the unmodified epoxy resin. The most significant change was seen with addition of the toughening adduct. The CTBN rubber particles separate during cure to produce a distinct second phase [116] forming opaque white samples at high concentrations – an example of which is shown in Figure 62. As described in the literature review, modifying agents, particularly tougheners, typically increase the viscosity of the epoxy. Hypox DA323 produced the most viscous adducts followed by Hypox RF928 and then DER736. The high viscosity of Hypox DA323 ensured difficult integration at all addition levels while that of RF928 became problematic at high modification levels (i.e. 20 phr). In some circumstances this may have resulted in improper blending leading to inconsistencies in properties across the resin sample. An increase in the coefficient of variation for tensile strength was seen as the concentration of modifiers was increased. Maximum CV values of 2% and 3% for blends containing RF928 and DER736 were consistent with results with Prime 20LV. CV values of 6% were

observed in blends containing 15 phr and 20 phr of DA323, and were significantly higher than the 2% seen for the unmodified resin, indicating an adverse effect on property variability.
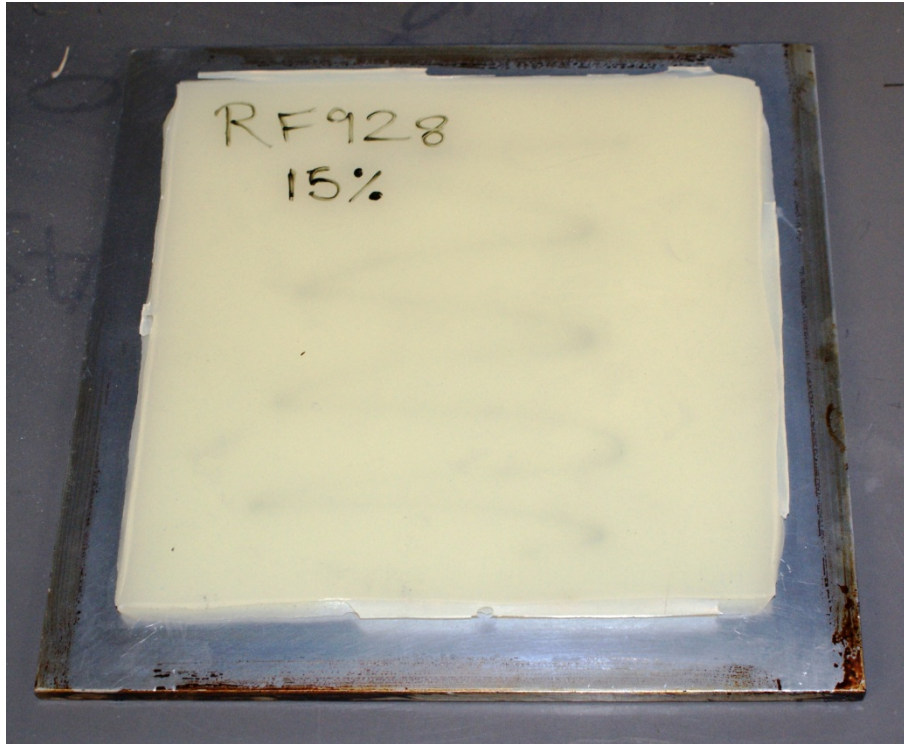
Figure 62. Neat resin sample produced from a blend of Prime 20LV and 15 phr Hypox RF928. The formulation remained clear before moulding, but phase separation of the CTBN rubber occurred during cure to produce a distinctly cloudy appearance in the moulded sample.

Mechanical properties were seen to vary with the concentration and type of modifier used (Figure 63). Reductions in tensile and flexural strength were seen across all resin formulations with the least severe reductions seen with Hypox RF928. Stiffness was also seen to decrease significantly in formulations produced from the two flexibilisers in the study. The toughening modifier, Hypox RF928, again showed the smallest reduction in properties with property reductions only occurring with high concentrations ($\geq$ 15 phr). Young's modulus and UTS of 2.86 GPa and 68.2 MPa were observed at 20 phr – reductions of 6% and 5% compared with the original resin.

Increased strain to failure was the primary goal for the modified system. This property also provided the clearest indication of critical addition levels. The strain

to failure of all formulations in tension and bending are shown in Figure 63. All modifiers proved ineffective at low addition levels (≤ 10 phr) with decreases in tensile strain to failure. As shown in the graph, increases in tensile strain were seen with two modifiers – DER736 and RF928 – when phr was made larger. Lower strain to failure at the highest concentration of DER736 indicates that strain to failure cannot be increased further.
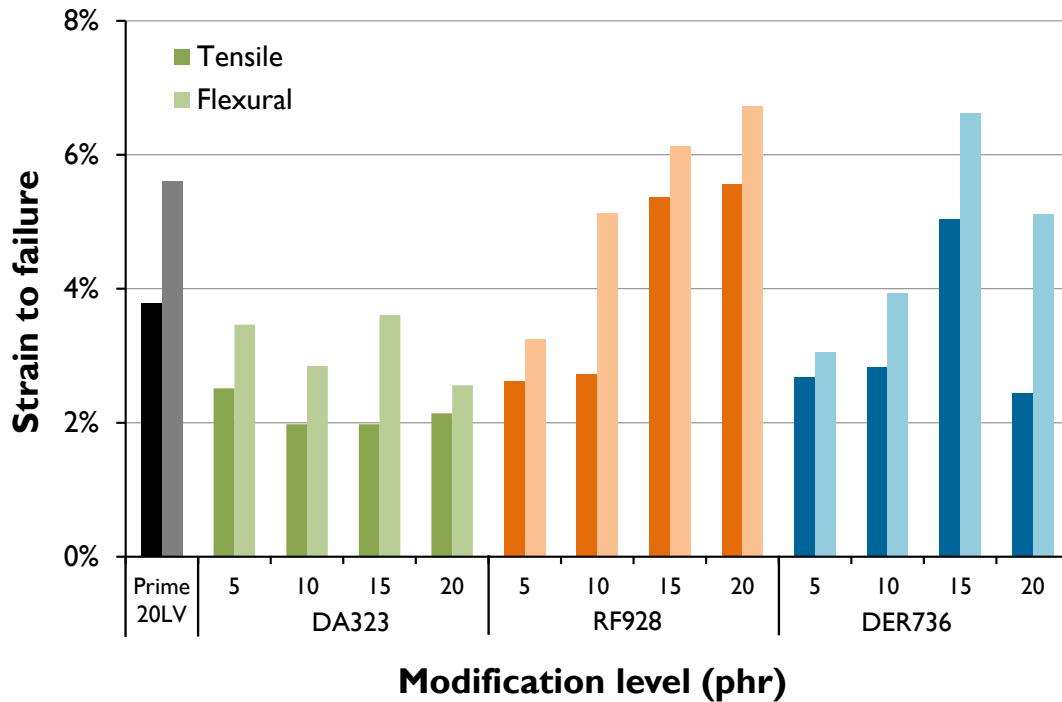
Figure 63. Strain to failure of modified, Prime 20LV, epoxy resin formulations. Results from tensile and flexural (three-point bend) testing are represented by the left and right bars, respectively.

The continual improvement in tensile strain to failure, with larger concentrations, of the toughener was supported by increases in flexural strain at high concentrations. Coupled with the lowest degree of property degradation seen in the study, CTBN and the adduct Hypox RF928 were deemed the most suitable candidates for the highly plasticised matrix to be used for implementation in DCFP architectures. The study highlighted the effect that small modifications can have on the mechanical properties of epoxy resin. The following sections will seek to determine whether these changes in properties affect performance of meso-scale DFCs.

4.5.2 The effect of Hypox RF928 in DCFP fibre architectures

Hypox RF928 was added to two DCFP fibre architectures to examine the effect of incorporating a toughened matrix into a DFC laminate. The two preforms selected for the study were: FA1b (tow size - 6k, fibre length – 30 mm), and a 24k fibre architecture incorporating the same fibre length. Both were moulded at a thickness of 3 mm and a fibre volume fraction of 30%. Hypox RF928 was added to the epoxy at 20 phr prior to infusion with the preforms.
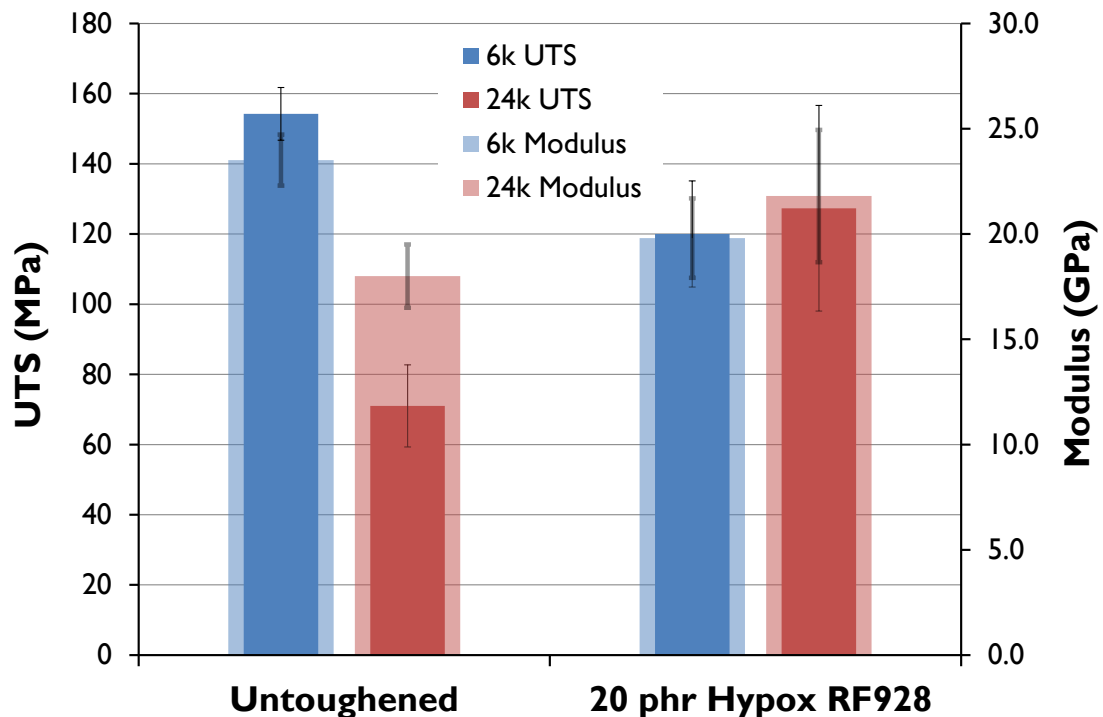
Figure 64: Tensile properties of 6k and 24k DCFP fibre architectures with the untoughened Prime 20LV matrix and a, second, modified matrix consisting of Prime20LV and 20 phr of the CTBN adduct Hypox RF928. Properties were normalised to 30% V_f.

Figure 64 illustrates the variation in properties between laminates produced from the unmodified and toughened resins. Improvements in both modulus (21%) and strength (79%) were seen for the toughened 24k laminate. The increase in modulus is rather surprising as it seems to violate theory – toughened systems typically result in reduced modulus - and might be due to overlapping error bars. Mechanical properties of the 6k architecture were worse than the unmodified laminate - decreasing by 16% and 22%, respectively. Consequently, properties of the toughened 24k laminate were superior to the 6k equivalent.

The study has indicated that benefits can be achieved when a toughened matrix is incorporated into an architecture that typically exhibits high coupon-to-coupon variability. This may provide an opportunity to increase properties in preforms that have previously been shown to exhibit relatively low mechanical properties. Results also demonstrate that modifications to the resin system affect the final properties of, more homogeneous, 6k laminates. Despite an adverse effect in this case, there is still an interest in determining how properties of these architectures change with a highly plasticised matrix and whether any benefits can be achieved.

4.5.3 CTBN formulations for toughened DCFP architectures

The CTBN additive (Hypro 1300 x13) in Hypox RF928 was chosen for further study due to the potential benefits to mechanical properties of DFCs with a toughened resin system demonstrated in the previous section. The purer form of the modifier was used to produce blends that exhibited a greater degree of plasticity. Neat resin testing was carried out to determine appropriate addition levels before examining the effect of the toughened matrices on DCFP architectures.
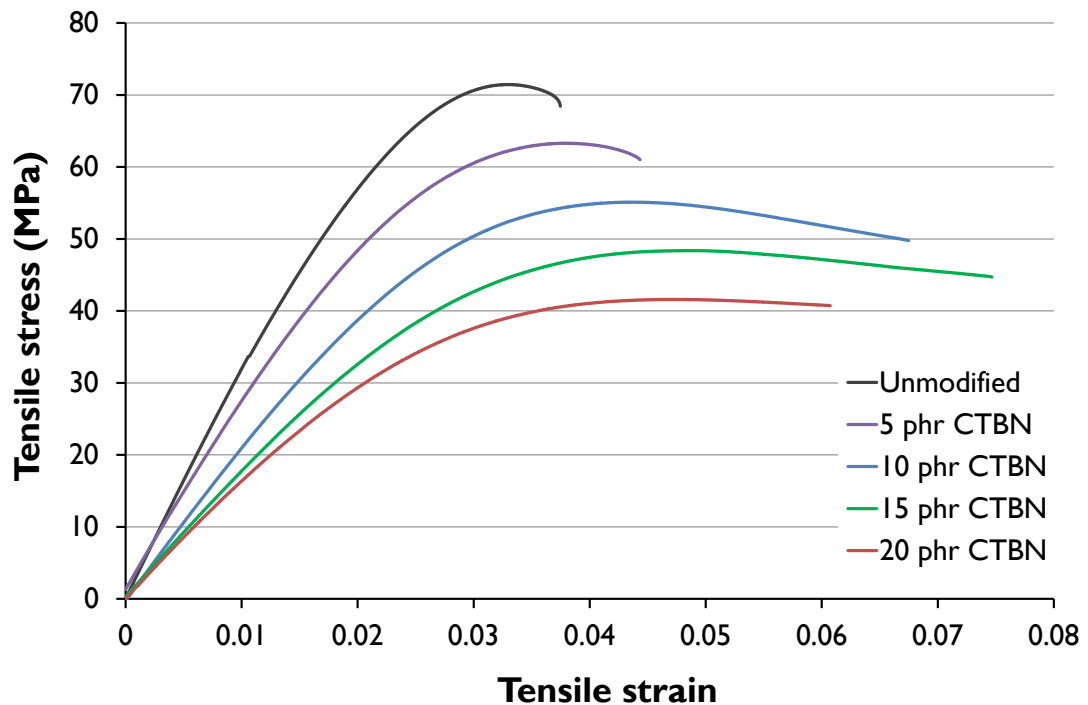
Figure 65. The effect of a CTBN modifier (Hypro 1300 x13) on the tensile properties of Prime 20LV, an epoxy resin system. Hypro 1300x13 was added to the base resin at four addition levels. Five specimens were tested for each modification level. Curves that were indicative of the performance of each sample of data were selected and are shown here.

The addition of CTBN resulted in an increase in the ultimate tensile strain of the resin (as shown in Figure 65) due to increased elongation facilitated by the toughener. This trend was seen up to an addition level of 15 phr. A decrease in the maximum strain was observed as the concentration of CTBN was increased further from 15 to 20 phr, indicating the critical level had been reached. This may have been due to the immiscibility of the toughener with the epoxy at the higher concentration. There is also the possibility that complete cure was not achieved with the blend. For development of a resin for final parts DMA testing would be critical in ensuring that the full cure cycle has been completed.

Table 16. Mechanical properties of Prime20LV with the CTBN additive Hypro1300 x13. Five specimens were tested at each addition level and the best results are shown. Modulus results are shown for two measurement methods – extensometer and digital image correlation (DIC).

CTBN	Modulus (GPa)				UTS (MPa)		Strain to Failure (%)	
	Extensometer	DIC	Average					
Unmodified	3.30	3.08	3.19		71.5		3.78	
5 phr	2.75	2.71	2.73	-14%	63.3	-11%	4.43	17%
10 phr	2.20	2.44	2.32	-27%	55.1	-23%	6.75	79%
15 phr	1.79	2.06	1.93	-40%	48.4	-32%	7.47	98%
20 phr	1.73	1.75	1.74	-45%	41.6	-42%	6.07	61%

Results of the tensile testing are shown in Table 16. A resin formulation containing a concentration of 15 phr of CTBN was shown to increase strain to failure by 98%, but consequently reductions of 40% and 32% were seen for modulus and UTS. Degradation of these properties was seen for all formulations with the most severe at high CTBN concentrations. While the toughener isn't able to improve these properties the CTBN rubber particles, forming a second phase in the resin, are able to absorb greater energy and prevent crack growth [111]. The area under the stress/strain curves for three formulations have been compared in Figure 66. By increasing the concentration of CTBN, work of fracture is improved so energy absorption of the resin is increased.
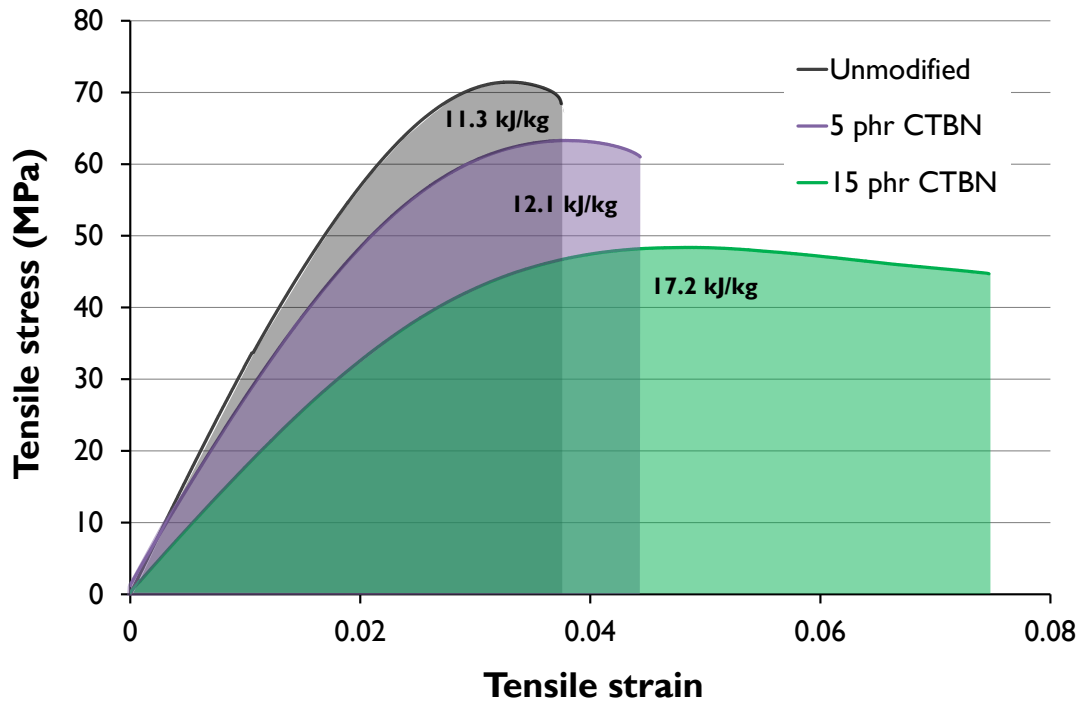
Figure 66. Typical stress-strain curves from tensile tests of toughened Prime 20LV. The curve for the untoughened epoxy is compared with results from the epoxy modified with CTBN at additions levels of 5 phr and 15 phr. Total energy absorbed for each test was approximated by determining the area under the curve using the trapezium rule. Estimates of the specific energy absorption (SEA) for each resin are shown.

4.6 Design of experiments

Performance of toughened meso-scopic DFCs was evaluated by testing preforms moulded with two modified epoxy systems – Prime 20LV plus CTBN additions of 5 phr and 15 phr. Results were compared with fibre architectures moulded with the unmodified epoxy resin. Preforms were studied at two different tow sizes, fibre lengths, and volume fractions. Benchmark fibre architectures FA1a and b (described in 2.7.3) were chosen to represent preforms with a fine distribution of fibres and good coverage. Preforms using 24k tows represent meso-scale DFCs with typically poor coupon-coupon mass variability due to coarser fibre distribution. Benchmarks were produced with quasi-isotropic layups of non-crimp fabric and these provide a continuous fibre composite comparison exhibiting relatively low variability.

Table 17: Description of preforms used for studies on the effect of toughening on DCFP properties. Two tow sizes were studied with two fibre lengths and volume fractions. All plaques were moulded to a target thickness of 3 mm. CTBN was added at two levels (5 phr and 15 phr) following the results of an initial neat resin study.

Designation	Tow Size	Fibre Length (mm)	Volume Fraction	CTBN (phr)	Description
TF06303000				0	8 layers of 0.201 g/m² chopped
TF06303005			30%	5	carbon fibre
TF06303015		30		15	Target fibre mass: 193 g
TF06305000				0	12 layers of 0.223 g/m² chopped
TF06305005			50%	5	carbon fibre
TF06305015	6k			15	Target fibre mass: 322 g
TF06603000				0	8 layers of 0.201 g/m² chopped
TF06603005			30%	5	carbon fibre
TF06603015		60		15	Target fibre mass: 193 g
TF06605000				0	12 layers of 0.223 g/m² chopped
TF06605005			50%	5	carbon fibre
TF06605015				15	Target fibre mass: 322 g
TF24303000				0	8 layers of 0.201 g/m² chopped
TF24303005		30		5	carbon fibre
TF24303015				15	Target fibre mass: 193 g
TF24603000	24k		30%	0	8 layers of 0.201 g/m² chopped
TF24603005		60		5	carbon fibre
TF24603015				15	Target fibre mass: 193 g
TFNCF00				0	8 layers of 0.300 g/m²
TFNCF05	12k NCF	Continuous	44%	5	[0/45/90/-45/-45/90/45/0]
TFNCF20				15	Target fibre mass: 288 g

4.7 Toughened DCFP architectures

Coupon-to-coupon mass variability of each fibre architecture was governed by: tow size, fibre length and volume fraction. Of particular interest was the effect of variability on the change in properties resulting from the toughened resin systems.

4.7.1 Fine fibre distributions - 6k results
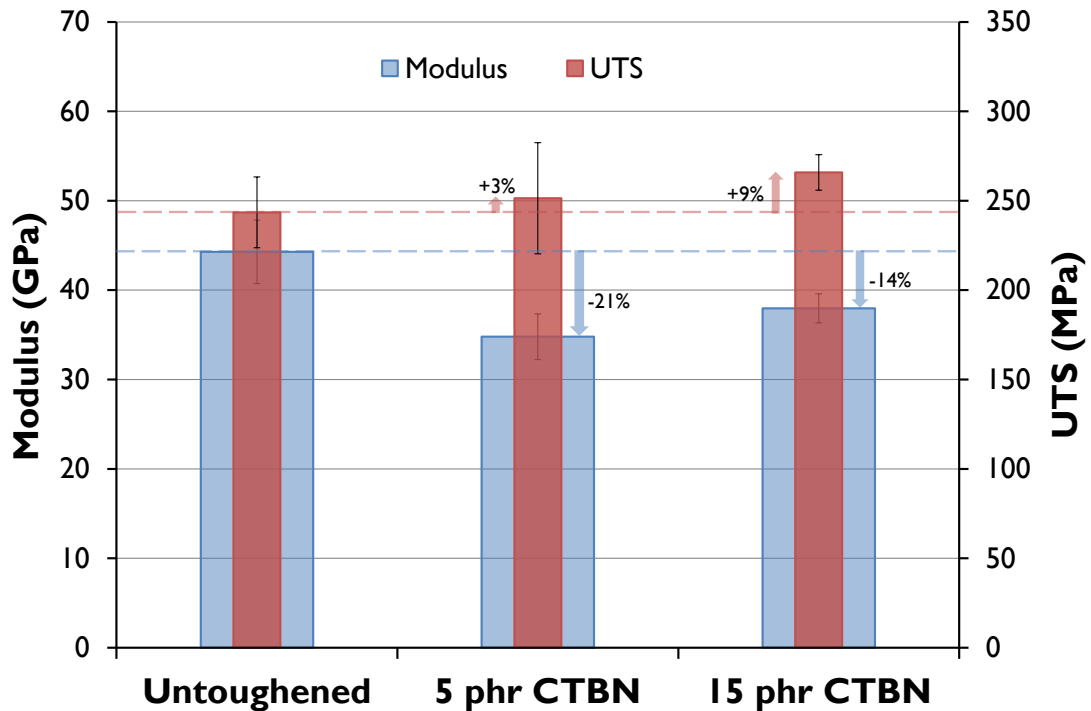
Figure 67. Mechanical properties of 6k, 30 mm, 50% DCFP architecture with three different resin systems: one with an unmodified epoxy resin (TF06305000); two modified with a CTBN toughener (TF06305005 and TF06305015). Properties were assumed to increase linearly with V_f and normalised to a V_f of 50%. Error bars indicate the standard deviation of results within each laminate. Changes in tensile strength and modulus, compared with results from the unmodified resin, are indicated by arrows on the chart.

Mild increases in strength were seen for all 6k preforms moulded with the lower concentration (5 phr) of CTBN, with an average increase in UTS of 5%. Further modification of the resin saw an increase in strength for the 6k, 30 mm, 50% architecture (Figure 67), but this was contrary to the trend. An average reduction in UTS of 7% was seen at this concentration compared with the untoughened equivalent. Findings indicate that the larger modification level of 15 phr CTBN is beyond the optimum point of addition for effective implementation with the 6k fibre architectures in this study.

In the analysis of the CTBN-epoxy formulations (4.5.3), improved strain to failure and toughness were observed for the resin with the higher addition level. Increased strain to failure translated to the composite (29% at 5 phr and 22% at 15 phr). Despite this, difficulties were encountered in the RTM process when the resin was used to mould preforms. Increased viscosity resulted in the need for larger injection pressures to be employed. This was seen to increase fibre waviness, which reduces the load bearing capacity of the composite as a smaller proportion of fibres are aligned with the applied load. Mouldings were more problematic with 6k preforms as these fibre architectures result in less permeable preforms. Degradation of Young's modulus was seen in all toughened 6k architectures with average reductions of 15% and 23% at both addition levels of 5 phr and 15 phr, respectively. This was symptomatic of the reduction in modulus of the neat resin, which was previously seen to be 14% and 40% for the same addition levels.

While the results do not demonstrate any noteworthy benefits of using toughened matrices for 6k fibre architectures, they offer insight into the effects of matrix properties on meso-scopic DFCs. Properties saw a bigger change at a low volume fraction, a direct result of more of the modified resin being incorporated into the composite. Figures Figure 69 and Figure 68 show results from the same 6k, 30 mm fibre architecture at two different fibre volume fractions: 30% and 50%. Changes in properties, from the unmodified resin, can be seen to be much more significant with increased resin content.

The effect of fibre length was less clear. Shorter fibre lengths characteristically result in better homogeneity, but exhibit poorer mechanical properties due to the presence of more fibre ends which are unable to bear any load in tension. Typical increases in strength, with increased fibre length, were seen for fibre architectures moulded with the unmodified resin. However, increases in strength due to the effect of toughened resins were more significant for shorter fibre lengths.
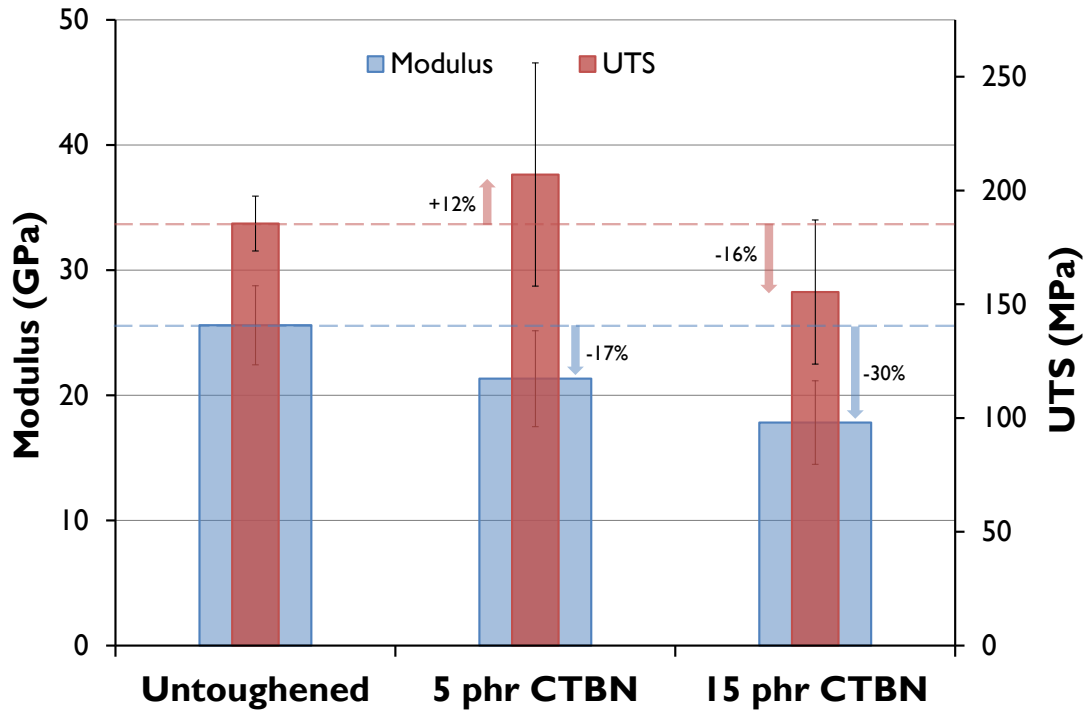
Figure 68: Mechanical properties of toughened 6k, 60 mm, 30% DCFP (TF066030). Properties are normalised to 30% V_f. As indicated by the proportional changes on the charts, a larger change in properties - from the unmodified resin - was observed for this laminate compared with the higher V_f equivalent below.
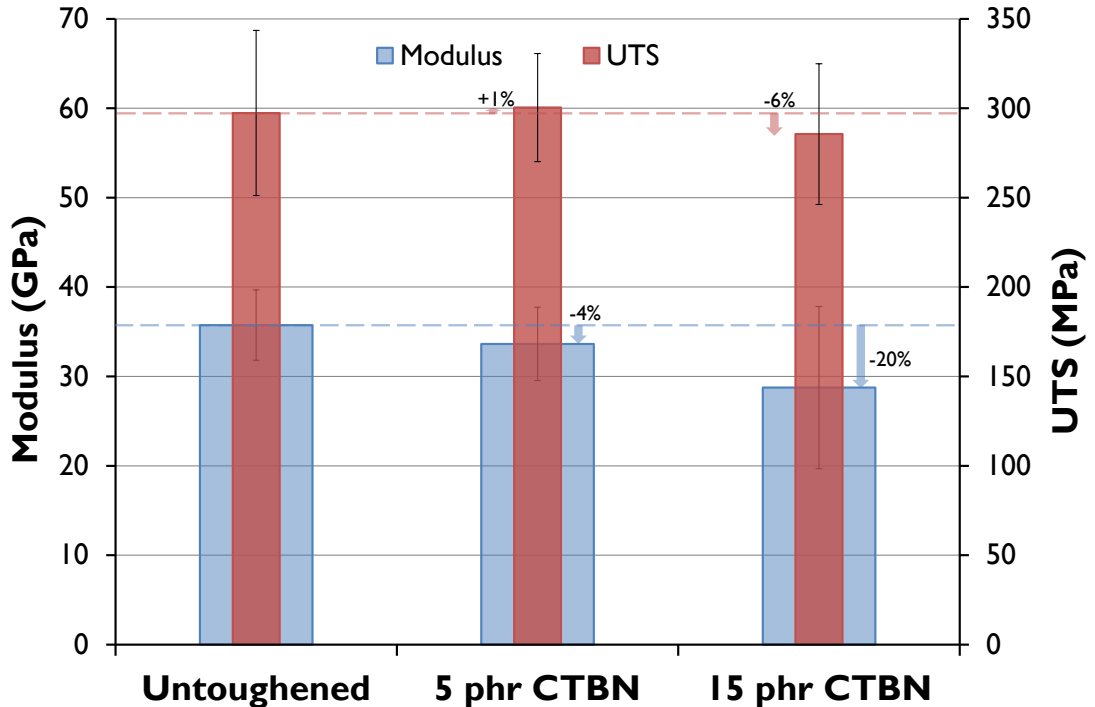
Figure 69: Mechanical properties of toughened 6k, 60 mm, 50% DCFP (TF066050). Properties are normalised to 50%.

4.7.2   Coarse fibre distributions - 24k results

Fibre architectures produced with 24k tows exhibited improved properties with both toughened epoxy formulations. Strength was seen to increase as the concentration of CTBN became larger, while modulus improved in all but one (TF24603015) of the laminates tested. Improvements in strength were greater than those seen for 6k architectures. The largest for the smaller bundle size was seen with TF06605005 which showed a 12% increase in strength. By comparison, a maximum improvement of 33% (TF24303015) was seen from results incorporating the larger tows. This value was indicative of the improvement gained with a higher concentration of CTBN with 24k preforms - an average increase of 31% was seen at 15 phr compared with 18% at 5 phr. Figure 70 compares the changes seen in 6k and 24 k preforms.
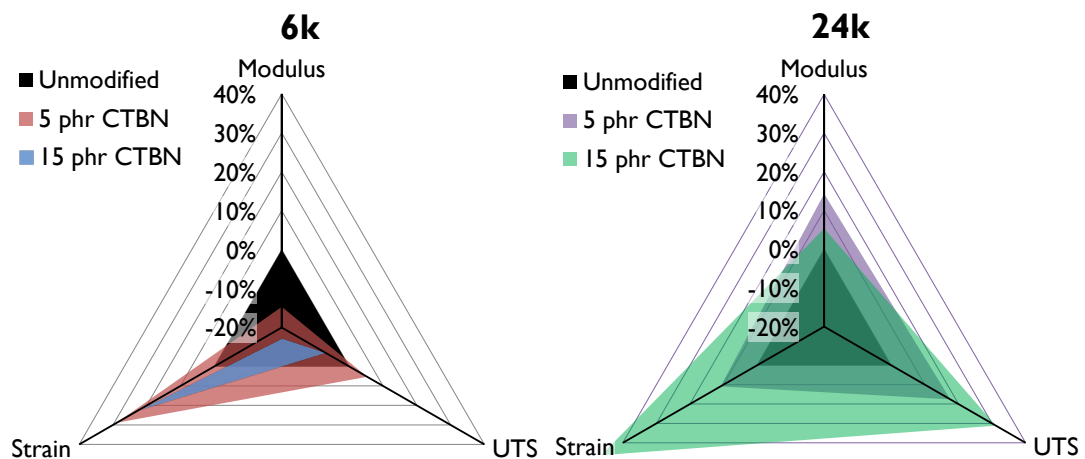
Figure 70. Comparison of average changes in tensile properties of toughened DCFP laminates made with 6k and 24k tows. Results of the unmodified resin are represented by the triangle at the centre of each chart.

The effect on modulus was less clear. The variability of results from toughened 24k laminates was considerably higher, especially with the highest concentration of CTBN. This is likely to account for unexpected increases in Young's modulus (14% at 5 phr CTBN, and 5% at 15 phr CTBN) as it can be seen that the error bars are significantly larger for toughened laminates and indeed overlap with untoughened values. Increased variability in properties may have been caused by improper mixing; specimens would have contained inconsistent levels of CTBN.

Shorter fibre lengths were again shown to result in greater property improvement (Figure 58). By incorporating toughened resins into laminates with the shorter (30 mm) of the two lengths, significant increases in stiffness, strength and strain to failure were achieved. The architecture provides the clearest indication that incorporation of toughening agents into the resin can be used to improve performance of meso-scale DFCs.
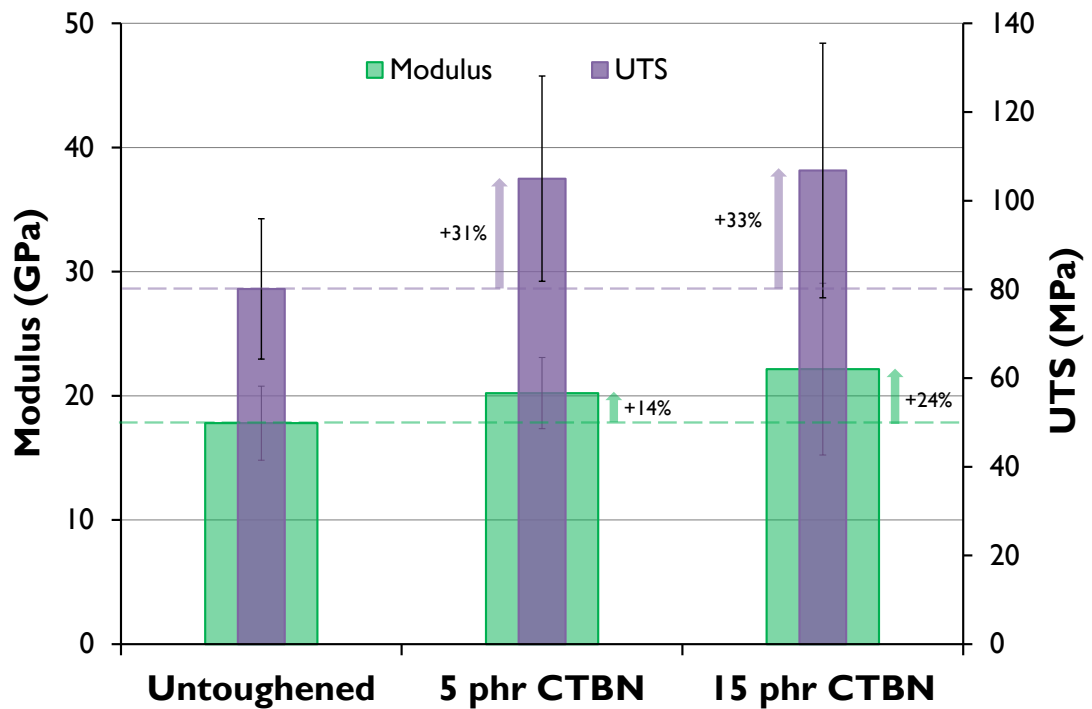
Figure 71: Mechanical properties of toughened 24k, 30 mm, 30% DCFP. Results are normalised to a V$_f$ of 30%.

4.7.3 NCF
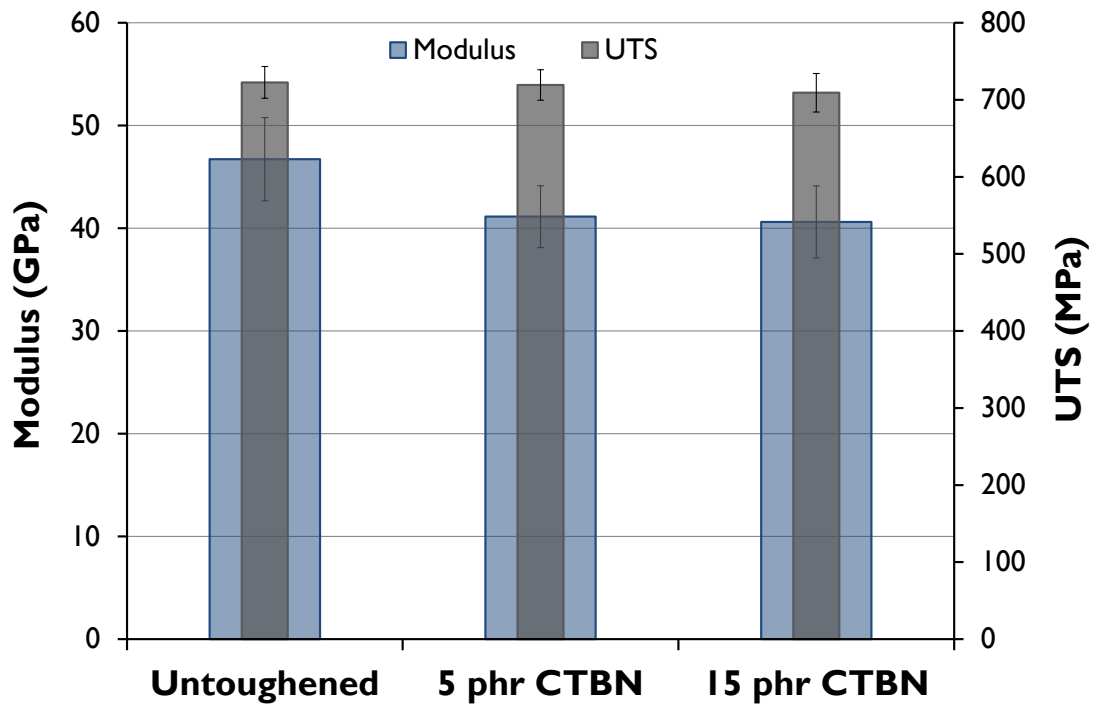
Figure 72: Mechanical properties of untoughened NCF compared with a toughened matrix containing 5 phr CTBN. Results have been scaled to 50% V$_f$.

A smaller effect on material properties was seen for laminates made with non-crimp fabric preforms (Figure 72). With a 5 phr addition of CTBN to the matrix, no change in UTS was observed, while Young's modulus was seen to decrease by 12%. Further addition of CTBN resulted in decreases in tensile strength and stiffness of 2% and 13%, respectively. There was still a significant effect on strain to failure with an increase of 20% and 21% at 5 phr and 15phr.

4.8 Discussion

Tensile properties have previously been shown to vary with thickness, tow size and fibre length. The degree to which these parameters affect tensile properties varies with the level of homogeneity in the fibre architecture. More interconnected fibre networks, in finely distributed architectures, lead to a greater degree of stress transfer via fibre crossovers. In coarser distributions, the matrix is required to transfer more of the applied load to the fibres; the properties of the matrix are considerably more important. The effect of fibre weaknesses due to fibre ends and resin rich areas are also more significant.

Better improvements in UTS, through toughening, have been seen for parts exhibiting greater variability in the preform architecture. The CTBN toughener improves properties by facilitating load absorption in weak areas which can prevent crack growth. For a relatively low increase to material cost, properties may be achievable with a wider range of fibre architectures adding a further degree of flexibility to the design process. The best applications are likely to be in crash structures. Improved effects of toughening on shorter fibres are particularly promising as these are typically better for energy absorption but other properties normally suffer.

Results from finer distributions highlight problems that can occur with modified matrices. High viscosity resin systems can be detrimental to part properties and, according to the literature, have been a significant barrier to application. If a VI process is used the preform may not allow CTBN, or other particulate tougheners, to permeate resulting in uneven distribution of the toughener. The fibre-matrix interface also needs to be considered. A greater mismatch in modulus could lead to changes in the failure mode. For example, fibre pull-out may be more significant due to a poorer fibre-matrix interface. Slight variations in failure modes were observed between toughened and untoughened specimens (Figure 73). Failures in specimens moulded with the unmodified specimens were dominated by fibre fracture. Specimens manufactured with the toughened (15 phr CTBN) showed

mixed failure modes – pull-out of fibre bundles was seen to be more significant, particularly with 6k laminates.
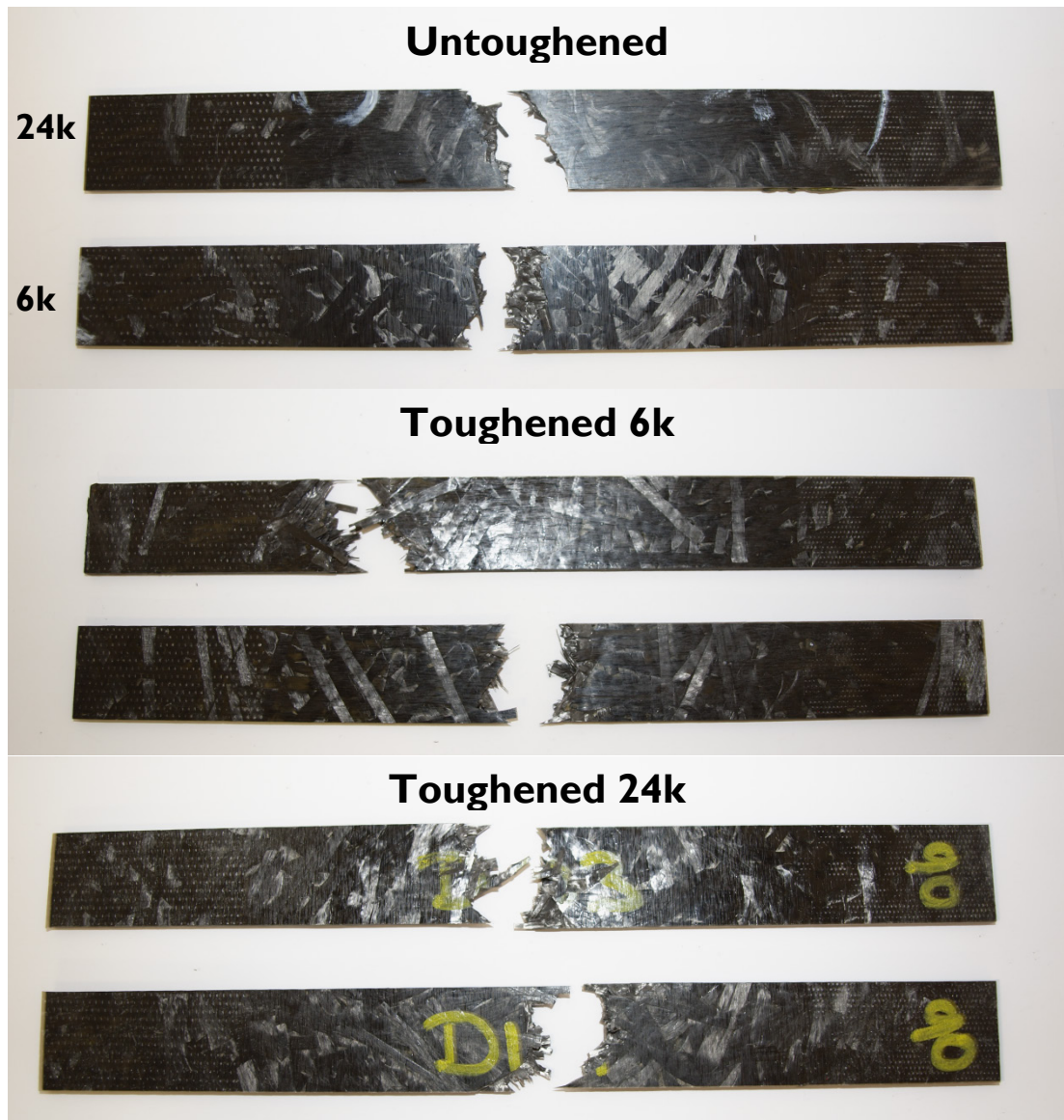
Figure 73. Typical failures for toughened and untoughened DCFP specimens. All toughened specimens contain 15 phr CTBN.

4.9   Conclusions

A CTBN toughener was used to produce plasticised matrices for two DCFP architectures. CTBN (Hypro 1300 x13) was added to the base epoxy at addition levels of 5 phr and 15 phr. Greater strain to failure (increases of 17% and 98%, respectively) and energy absorption of the epoxy were seen through tensile testing of these formulations.

Small improvements were observed in some toughened 6k architectures but generally, properties were worse – 7% and 23% reduction in Young's modulus and UTS for preforms moulded with the matrix containing 15 phr CTBN. The CTBN toughener improves properties by facilitating load absorption in weak areas which can prevent crack growth. In coarser distributions containing more weak regions, the matrix is required to transfer more of the applied load to the fibres so the properties of the matrix are more important. Preforms manufactured with 24k tows, which exhibit a greater level of mass variation from coupon to coupon, exhibited a larger increase in properties. Young's modulus and UTS were increased by 5% and 31% (at 15 phr).

Toughened NCF preforms did not show a substantial change in properties. The results suggest that the benefits of toughening DFCP fibre architectures are more substantial than for continuous fibre composites. Due to large stress concentrations at the bundle ends, a matrix with greater strain characteristics would facilitate a greater level of deformation before fibre-pullout occurs. Incidentally, larger increases in properties are observed for toughened matrices in DFCs.

5   The suitability of DCFP for high performance applications

5.1   Introduction

Conventional composite laminates are able to offer solutions to a wide range of high performance applications, but the high cost of intermediate steps such as weaving and pre-impregnation and the high labour costs associated with touch labour leads to limited applicability and a desire to move towards automation. Existing automated processes (e.g. ATL and AFP) produce high levels of performance and repeatability but are currently only applicable to large planar structures or prismatic sections. The use of discontinuous fibres allows great flexibility in producing components with complex geometries while retaining many of the advantages of continuous fibre composites; particularly in stiffness-driven applications.

Historically, DFCs were used solely in cosmetic and semi-structural parts. Increasingly, higher performance discontinuous carbon fibre based materials are becoming available and there is growing interest in using them for structural parts. The aerospace sector in particular is investigating processes which display greatly reduced hand labour and processing cost and, unlike certain portions of the automotive sector, is willing to tolerate relatively high materials costs. In the automotive sector the raw materials cost is still crucial. Commercial offerings are now available in various product forms. All these materials have a meso-scale fibre architecture where the size of the reinforcing bundles (e.g. 10 mm wide x 50 mm long) is on a similar scale to the size of the composite; this is in contrast to the majority of discontinuous fibre composites (injection moulded thermoplastics, all moulding compounds etc.) which contain single filaments or low tex glass bundles.

Some materials, such as Hexcel's HexMC, are manufactured from slit prepreg whereas others, e.g. Quantum Composites Lytex 4149, are manufactured from 3k carbon tows. Two other related product forms are slit prepregs, e.g. Advanced Composite Group's DForm and stretch broken prepregs. The above materials are often used to overcome lack of formability associated with continuous fibre

prepregs. They are universally moulded by compression moulding almost always employing epoxy resin chemistry. Fibre architectures produced by the DCFP process are very similar to the above materials, however, they are not pre-impregnated and can be moulded by a variety of processes, e.g. resin transfer moulding and resin infusion.

Several barriers to further application of these fibre architectures to high performance parts can be identified. Common aerospace design methods are well defined and provide the necessary vigour for high performance part design, but it is implicit in these methods that the properties of a lamina can be applied to the whole component. With discontinuous fibre architectures the properties can change with thickness, are highly variable from one part to the next and are also dependent upon specimen size. Homogeneity of the reinforcing fibres is critical to the final performance [22] – both in terms of absolute properties and in terms of variability. In addition to these fundamental differences in fibre architecture there is limited certified data available on the potential of these structures – particularly in terms of damage tolerance and more complex load cases.

5.2   Objectives

This work seeks to assess the potential of discontinuous carbon fibre composites for high performance structural applications through mechanical property testing and a review of the relevant design issues. Current design protocol for composites was evaluated by determining whether notched properties and typical statistical interpretation of coupon data applies. A range of damage tolerance tests were carried out to define the knockdown in properties of notched DCFP specimens. The influence of preform thickness and mass variability on mechanical property variation was investigated. The findings will determine whether conventional design rules need be changed to allow more intelligent structural part design using meso-scale discontinuous materials.

5.3 Background

5.3.1 Design protocol

Design for aerospace components is commonly based on the building block approach, where coupon testing provides data for design and is then validated by a scale-up towards a full part – typically through sub-components, components and structural elements [129]. Much of the work is carried out at the coupon level where a large number of tests are used to determine the statistical distribution of the property of interest e.g. tensile strength. A- and B-basis design allowables based on the distribution provide values where the expected percentages of components that do not fail are 99% and 95%, respectively [130]. Knockdown factors are also introduced to account for damage tolerance and environmental effects [131]. This necessitates safety factors to ensure products meet in-service requirements.
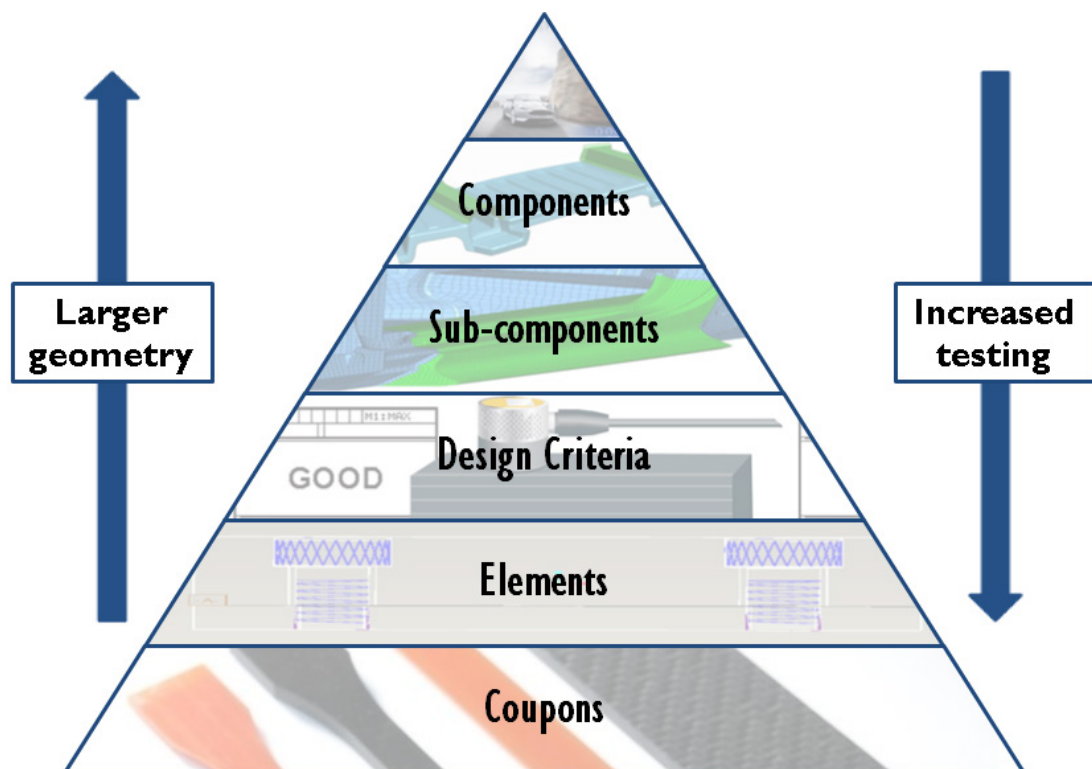
Figure 74. Building block approach to the design of composite parts. Adapted from Figure 11.4 in Long-Term Durability of Polymeric Matrix Composites [132].

The Design and Manufacturing Guideline for Aerospace Composites [133] states the importance of establishing an accurate and reliable material property data base. The

work in this thesis has focussed on defining behaviour and data at the coupon level. Other authors have focussed their attention on a larger scale. Work by Tuttle [134] sought to determine whether nominal properties measured during coupon level tests can be used to predict those at the component level. FE modelling was carried out by modelling each component over a range of moduli reported by Feraboli. Average bending stiffnesses corresponded well while variability was also comparable to coupon tests. However, bucking and failure loads were over-predicted indicating there may be scale effects.

5.3.2   Variability in meso-scale DFCs

Composites are prone to variability in the manufacturing process. This may arise, for example, during the hand lay up of prepreg material or may occur in the form of damage to components when they are being transported. Figure 75 highlights processes that introduce variability into the manufacture of a DCFP laminate. A distinguishing characteristic of the process is the high degree of variability experienced at the preforming stage. One area of debate with short fibre composites is repeatability and the effect of preform variability on a part-to-part basis.
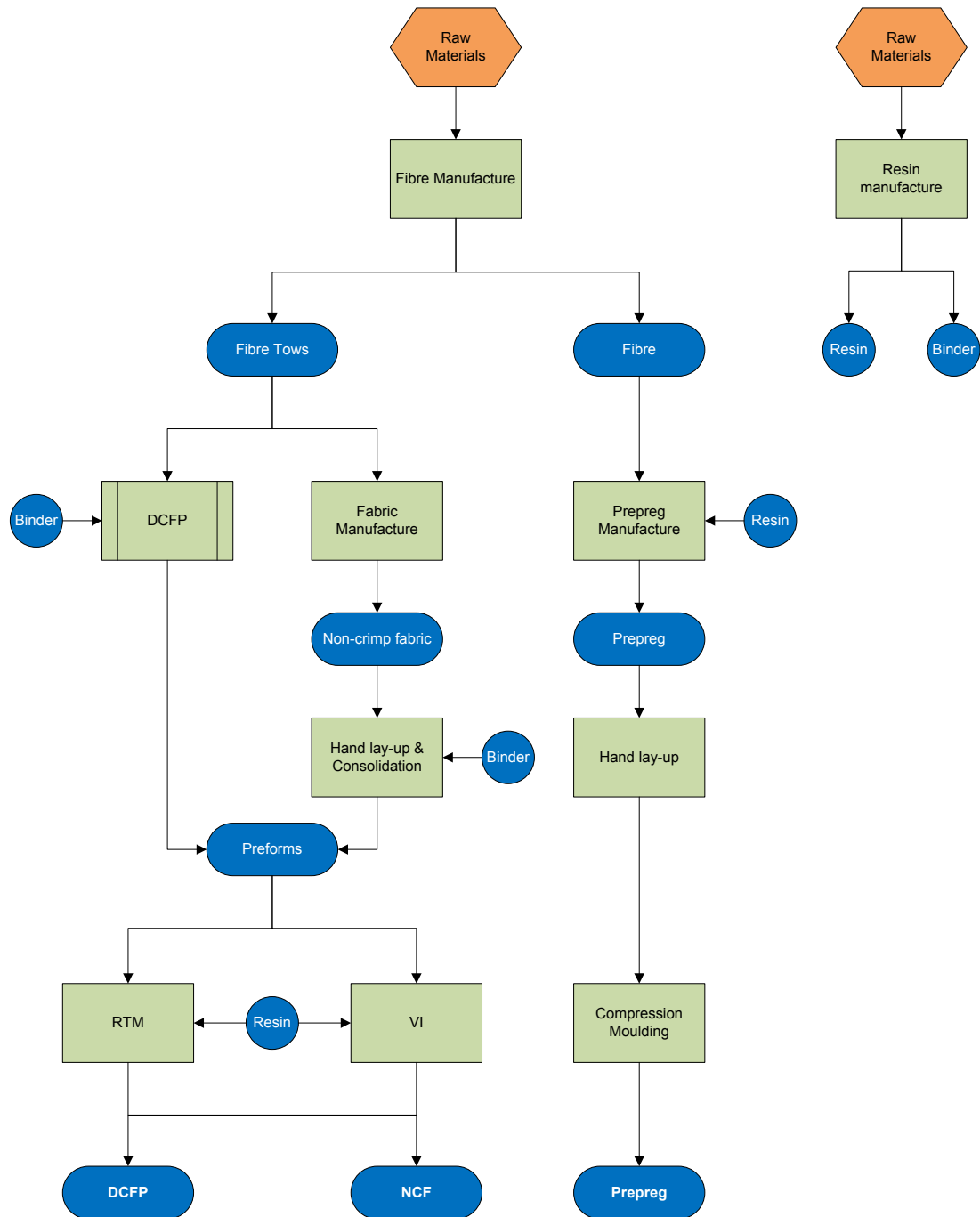
Figure 75. Flow diagram of the manufacturing processes used in this study to produce DCFP and NCF samples. The manufacture of prepreg is also shown to demonstrate the potential for variability in its processing.

Homogeneity of fibre distribution

Mendoza Jasso et al. [135] present a model that studies the effect of spatial variation in fibre volume fraction on location of failure initiation in OHT specimens. Volume fraction was assumed to take a normal distribution and randomly assigned between standard deviations (Figure 76). Results indicate that the dispersion in V_f is one of the causes of probabilistic distribution of failure initiation location in experimentally tested coupons. Many natural defects influence location of failure and the study tries to show that V_f is one of those.
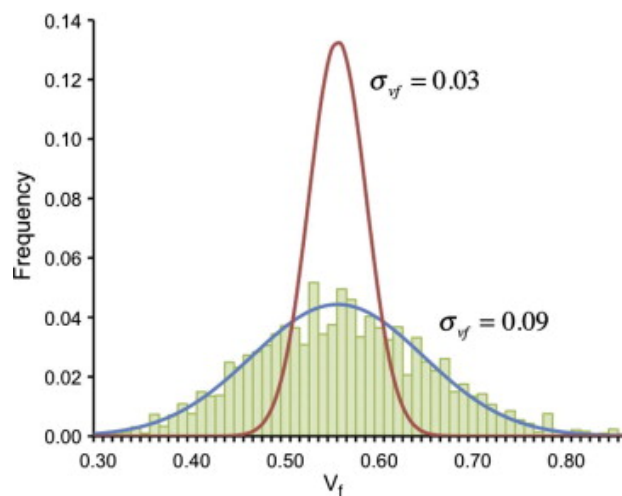
Figure 76. Simulated fibre volume fraction distribution in a CFC (reprinted with permission) [135].

Statistical interpretation of mechanical test data

Anisotropy of composites results in variability of material properties. By reporting mean and standard deviation it is implied that properties follow a normal distribution; often, it is other statistical methods that are used. The three-parameter Weibull distribution is suitable for situations where the minimum material property value cannot take a value less than a predetermined constant [136]. Although this has proved effective for conventional laminates where properties show small deviations, DFCs with large coupon-to-coupon variation can often yield significantly lower than expected properties e.g. in resin rich areas. The two-parameter Weibull function may be more appropriate. Dirikolu et al. [136] used the function to statistically analyse the fracture strength of continuous fibre carbon-epoxy composite plates. Linear regression, based on least squares minimisation, was

used to determine the Weibull parameters, and these were used to estimate percentage failures for a given design strength. The paper only qualitatively assesses the Weibull fit for the data and doesn't make an attempt to remove any anomalous results. Indeed, the data includes a result that appears to be an outlier. While the study questions and rejects the assumption that fracture strength of a composite can be taken as the average, it doesn't consider any other distributions. No statistical evidence is presented that suggests the normal distribution should be rejected.

Despite its wide use, Abernethy [137] points out that the Weibull distribution shouldn't be assumed to be correct. He suggests that if there is engineering evidence supporting other distributions, this should be weighted heavily against the Weibull distribution. He describes the lognormal distribution as the best alternative for some material properties as it is able to characterise accelerating deterioration. The Composites Materials Handbook-MIL 17 [138] provides a set of guidelines that assesses the appropriateness of other statistical distributions. If data doesn't fit the requirements of a Weibull distribution, normal and lognormal distributions are tested.

The Weibull distribution has often been used to model strength, but applicability to other properties is uncertain. Mangalgiri [139] dismiss the notion of basis values (confidence bounds described on page 156), for stiffness saying that this would result in significantly low Young's modulus values being used to estimate buckling loads as it suggests that the buckling load is determined by minimum probable load anywhere in component. Nevertheless, it will still be beneficial to investigate scatter to gain greater understanding of variability in meso-scale DFCs and what sort of distribution Young's modulus follows. The work by Tuttle [134] described in 5.3.1 worked on the basis that moduli took a value over a range that centred around the average.

5.3.3   Design for damage tolerance

Defects in high performance (e.g. aerospace) components can cause stress concentrations which, depending on the size and type, can have a significant impact on compressive strength. Open/filled hole tension and compression tests have commonly been used to simulate situations where defects are intentionally introduced into a component; a drilled hole for example. There is also an interest in uncontrolled defects which can be caused by such events as tool drops and road debris [140]. Low-velocity impacts, such as these, are of particular interest as they can often go undetected. Conventional laminates typically suffer from poor damage tolerance, but previous studies [141-143] indicate that discontinuous fibre composites may not suffer the same knockdowns in properties.

Bibo et al. [144] assess damage in NCF laminates and make a comparison with prepreg laminates. Based on visible extent alone, differences between NCF and UD prepreg are small. Despite lower compression strength, NCF performed marginally better in compression after impact (CAI) tests. The authors suggest that this may be linked to the bridging effect of the through-thickness stitching yarn, inhibiting sub-laminate bucking and delamination. Fibre tows that bridge multiple layers in DFCs may also have an effect on damage growth. This will largely determine by whether DFC acts as separate plies that delaminate.

A database that covers a range of damage scenarios has been suggested by some authors. Razi and Ward [145] suggest that this may allow more cost-effective use of composite structures in commercial aircraft service. It is questionable whether the amount of testing required for certifying materials in this way would be efficient, both in terms of time and labour. A more pertinent problem with mesoscale DFCs is whether damage response at the coupon level is transferable to the subcomponent and component levels. As well as the damage database Razi and Ward propose, they describe another method commonly used for certifying structures and designing for damage tolerance. This method, which may be more appropriate, is designed to show positive margins of safety for: BVID at the coupon and

subcomponent level tested to design ultimate loads, and large damage of subcomponents and component structures tested to design limit loads. This second method seems to be the preferred method amongst researchers and has received significant attention in the literature with a focus on testing at the coupon level. The problems with this second method for mesoscopic DFCs are the assumptions based on scale effects as one moves from the coupon level to the subcomponent through to component.

Razi and Ward state that visible inspection is the most popular method used to detect damage. Recent NDT developments, such as portable phased array ultrasonic systems, may have long superseded this, but there are clear benefits of being able to evaluate composite damage visually. The increasing use of composites in commercial aircraft and quick turnarounds in the airport mean that rapid damage detection and evaluation is vital. Any information regarding damage manifestation in composites will be useful to those working in aircraft maintenance roles, especially those that are not specialised in NDT methods. Differences in failure initiation and the effect of defects in DFCs compared to CFCs have been discussed by Boursier & Lopez [142]. An interesting finding was that random and entangled short fibres in the DFC appear to greatly slow, crack propagation and perhaps even stop it. HexMC, the DFC being studied, was insensitive to "moulded-in" defects, visible damage, and incidental damage which is often classified as barely visible impact damage BVID.

Other forms of measuring damage tolerance have received attention. Rhead et al. [146] have studied the effect of BVID in the form of free edge impacts and found significant reductions in compressive strength of pre-preg by "buckle – driven delamination". Previous studies have indicated that discontinuous fibre architectures may be less susceptible to induced damage [141, 143, 147]. The typical knockdown based design protocol for conventional laminates may not be transferable to DFCs and could lead to a high rate of part rejection and overly conservative design.

5.3.4 Application to high performance structures

Applicability of meso-scale discontinuous fibres (in contrast to e.g. stretch-broken fibres) to primary and secondary aerospace structures is difficult due to the clearly defined limit loads prescribed in design certification e.g. CS 25.301 [148] and the need for high strength. There is a reluctance to use BMC or glass SMC due to the large reduction in properties when compared to a conventional prepreg. Reeve et al. [149] demonstrate the ability to improve stiffness and strength retention, compared with continuous fibre laminate properties, through orientation of fibres. They propose that orientated discontinuous fibre composites are viable candidates for most aerospace structures. It is incorrect however to view oriented discontinuous fibre materials as interchangeable with plies, it is better to introduce a bias to the fibre distribution than to attempt to manufacture a plied layup of aligned layers.

Although discontinuous materials may offer significant cost benefits and higher production rates, strength retention would, in most cases, be unsatisfactory to give a weight save over metallic and simultaneously meet the demands of safety critical primary structures. Well understood methods are also more likely to be used for secondary structures due to greater library data and manufacturing certification. However, there is the possibility for manufacture of low-load bearing components e.g. access/cover panels and cabin components of which there may be many on a typical aircraft. These parts are generally quasi-isotropic, or nearly so, and in such cases randomly orientated fibres may be able to provide the required properties at low cost and high production rates over continuous fibre composites and prepreg systems.

Deo et al. [150] reviewed the application of composite materials in a range of aircraft and highlighted lessons learned from their survey. They state that the integration of multiple parts could reduce fabrication costs. An example from the US Air Force Composites Affordability Initiative [151] is given, while Thuis [152] has demonstrated the benefits of integration in the design of a cargo door for an aircraft (Figure 77). Deo et al. [150] also suggest that fabrication cost can be reduced if

designs are simplified and automation is utilised through the use of preforms and other innovative material forms. They conclude by stating that all aspects of design and manufacturing need to be adapted for composites.
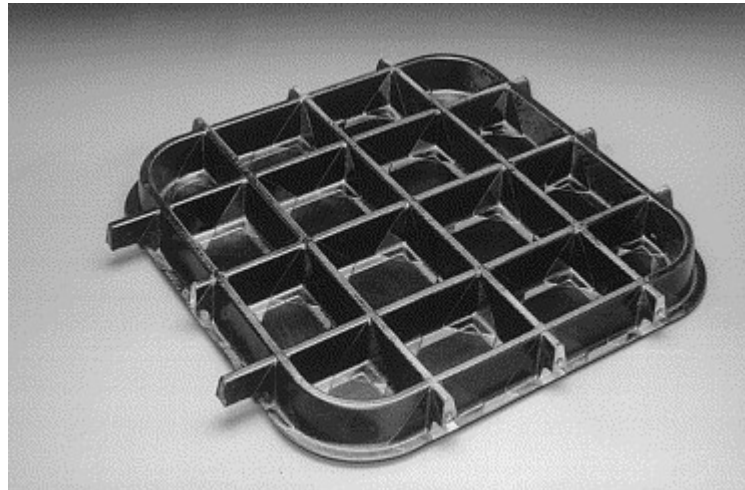
Figure 77. Composite cargo door (reprinted with permission) [152].

5.3.5   Summary

Full benefits of composites are only realised if the design process is specific to the material. Aspects of metallic component design methodology are still being used in some circumstances. The aerospace industry places emphasis on damage tolerant structures exhibiting high stiffness, with design methods dominated by OHC and CAI testing. Conventional composites suffer considerable knockdowns in properties when exposed to damage, which has led to the implementation of knockdown and safety factors that provide the framework for design protocol of high-performance composite structures. Behaviour of DFCs may be different. Previous studies, by Feraboli and at UoN, have shown that DFCs are relatively notch insensitive. Successful design of aerospace components will result in low rejection rates. A database covering a range of damage scenarios may allow for more cost-effective use of composite structures in high-performance applications. Delamination has been highlighted as the failure mode that reduces compressive strength. The inter-laminar shear strength of DCFP is of interest as fibres are typically deposited in layers but these aren't as discrete as fabric or prepreg based layers.

5.4 Experimental methodology

5.4.1 Manufacture of plaques

A DCFP fibre architecture – (FA2 - Figure 78) known to give high performance was selected for this work. 3k were chopped to a 30 mm fibre length and sprayed with a 3% wt. thermoplastic epoxy binder. Target fibre volume fraction was 50% such that the fibre areal mass required was 3580 gsm for a 4 mm thick part. Mouldings for the study of thickness and variability effects were conducted using vacuum infusion at room temperature with Gurit Prime 20LV infusion epoxy (resin A). Some preforms in this study remained unmoulded and were stamped using a sectioned 300 x 400 mm die cutter which was used to chop each preform into 25 mm squares. Each portion was weighed to produce a map of areal mass variability.
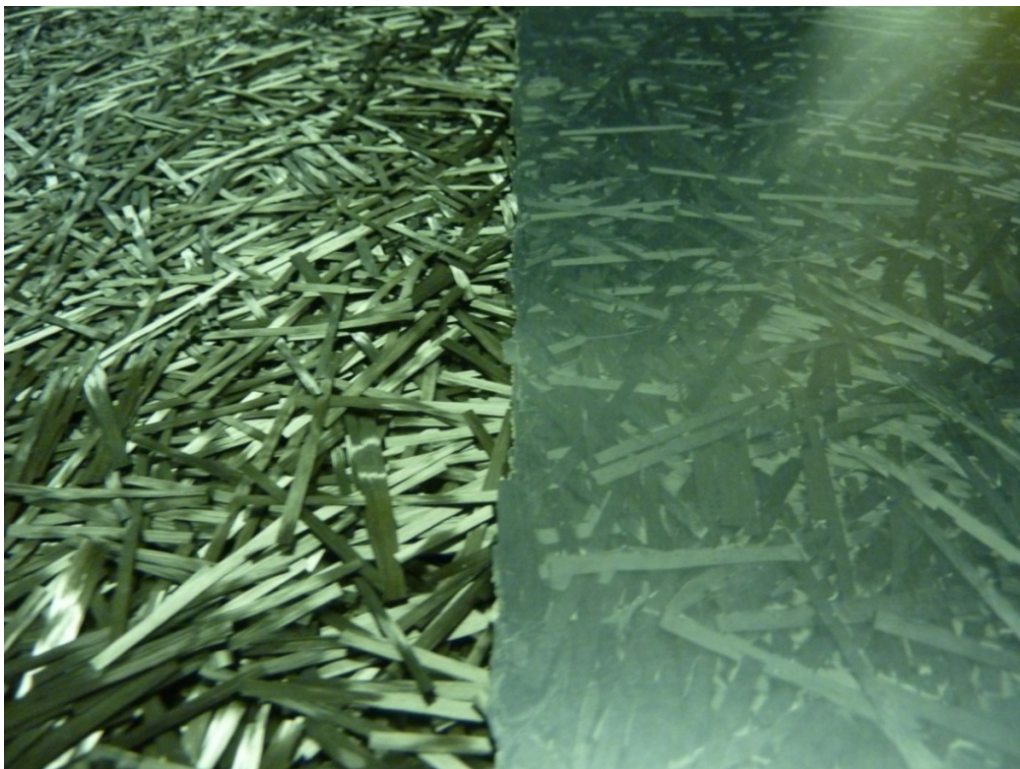
Figure 78. 3k, 30 mm (FA2) DCFP fibre architecture. The preform is shown on the left and the "A-side" of a moulded part is shown on the right.

Mouldings were conducted for final testing using UMECO MVR444 tetrafunctional epoxy (resin B) to provide a matrix widely used for aerospace applications. Resin was degassed for 30 minutes and placed in a heated pot at 70°C. Mouldings were

performed on a ground steel plate with resin ports through the thickness at each end. The plate was heated by two silicone mat heaters. Preforms were debulked for thirty minutes before infusion. Infusion took between thirty minutes and two hours. The tool temperature was 80°C. After infusion, the tool temperature was ramped to 180°C for two hours to complete the cure. Benchmark continuous fibre laminates were manufactured from a quasi-isotropic layup of 20 layers of Sigmatex 200GSM/PW-BUD/T700SC 12K 50C/0600 mm unidirectional NCF for comparison.
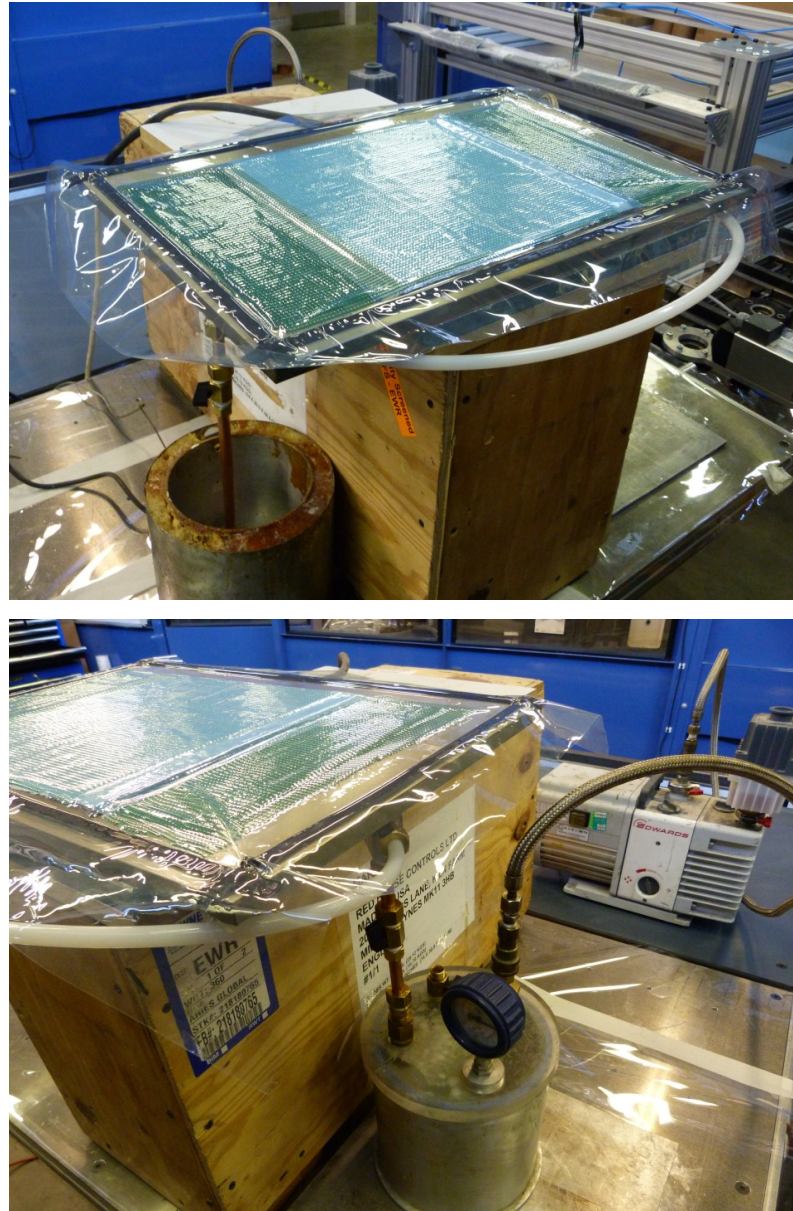
Figure 79. Vacuum infusion set-up. The heated pot is seen on the bottom left. The preform is located at the centre of the tool and covered with peal ply. Flow media is placed over the length of the tool to aid movement of the resin. A curved section of tubing is used to connect the outlet and inlet. This was used to transport excess resin (caused by a build-up at the inlet) directly to the catch-pot positioned on the right of the tool.

5.4.2 Test procedures

Test specimens were ground flat before all procedures except for compression after impact (CAI). Testing indicative of standard aerospace procedures has been employed using an Instron 5581 50 kN universal loading frame with Imetrum video extensometer. Tensile testing has been conducted at various thicknesses at 1.0 mm/min to ASTM D3039. A sample of between 20 and 22 specimens was tested for batches in the variability study with nominal specimen dimensions of 25mm x 200mm. Separate samples, moulded with resin B, were tested to provide un-notched data in the durability study. NCF specimens were tabbed, while DCFP coupons can be successfully tested without any. Open-hole tension was performed on smaller specimens (24 mm x 220 mm) than that specified in ASTM D5766 but the recommended width-to-hole ratio (w/D) of 6, with a hole diameter of 4 mm, were retained.

In-plane compression tests were carried out to BS EN ISO 14126-1999. NCF specimens were tested with and without tabs. CAI performance was assessed by impacting specimens in a Rosand IFW5 instrumented falling weight drop tower using a specimen holding fixture to ASTM D7136. Specimen thickness was measured to determine the drop height required to produce a 6.7 J/mm impact using a 16 mm indenter with a mass of 8.0 kg. Compression strength after impact was determined using a CAI compression fixture to ASTM D7137. A digital image correlation system (Dantec Dynamics Q-400) was used to measure surface strains during testing. Open-hole compression testing was performed according to ASTM D6484 using the rig shown in Figure 82. NCF specimens were tabbed. Inter-laminar shear strength was carried out to BS EN ISO 14130:1998. Ten specimens were tested at 1.0 mm/min.

Figure 80. Open-hole compression test rig. Specimens are loaded into the rig with the hole positioned within the central window.

5.5   Results

5.5.1   Preform thickness and variability effects

A detailed study has been conducted investigating the effects of preform homogeneity as this is known to be a main influencing factor in determining mechanical properties of any meso-scale fibre architecture. Areas of high fibre concentration dictate the ultimate level of compaction the preform can undergo therefore defining the highest achievable volume fraction in RTM and compression moulding processes. Such regions are also prone to poor impregnation in infusion processes due to reduced flow characteristics. Conversely, a low concentration of fibres can lead to areas of high resin content leading to premature failure.

Two forms of variability exist. The spread of test data captures variability due to the processing of the fibres, experimental error and accuracy of measurement. Due to the stochastic nature of the material there is further, intrinsic, variability that is not due to any of these factors, but is a characteristic of the material itself [153]. Manufacturers are normally concerned with inter-plaque variability due to processing. This may still be a concern with the manufacture of DCFP components, but this intrinsic variability in the fibre architecture means that inter-specimen variation is also of interest. The results of this study will quantify preform mass variability and study underlying variability in material. The consequences this has on mechanical properties and how to determine appropriate design values will be evaluated in the next section.

Preforms of three target thicknesses have been studied (Table 18). Maps (Figure 81) depicting the variation of fibre volume fraction across the preforms were produced for the three nominal thicknesses. The areal mass of each 25 mm x 25 mm specimen was converted to give a local volume fractions using the equation:

$$V_f = \frac{m_f}{\rho V},$$
<div align="right">Eq. 46</div>

where m_f is the measured mass multiplied by 0.95 to account for the 5% (wt.) binder. The fibre volume fraction V_f is the volume each sample would occupy in a RTM moulded part, and is equal to 25 mm x 25 mm multiplied by the nominal thickness. Results show that variation from the mean is most significant at the edges of the preform. Figure 81 shows that specimens measured on the northern edge of the preform tended to be overweight whereas those on the southern edge were seen to be underweight. Uneven lay-up is attributable to the movements of the robot. This phenomenon continued to be observed for thicker preforms, but the severity of the over/under-weight sections decreased. A similar trend was seen over the rest of the preform. In particular, the central region was seen to show a significant drop in highly over/under-weight specimens. Variability in this area was less predictable. Some cells were prone to being above or below the average weight of the preform, but the coverage generally appeared to be random.

Table 18. DOE for mechanical property and mass variability in DCFP preforms. Three preforms were produced at each nominal thickness; two were moulded by resin infusion with Gurit Prime20LV (resin A) and surface ground to achieve target thicknesses of 1,2 and 3 mm. The remaining preform was stamped to determine areal mass variation. Nominal thicknesses indicate the thickness of a RTM fabricated plaque with a target volume fraction of 50%.

Description	Fibre architecture	Nominal thickness (mm)	Preform areal mass (g)	Moulded mass (g)	V_f	Ground thickness (mm)
TH1mmA			308	434	55%	1.01
TH1mmB		2.5	308	470	52%	1.01
TH1mmC			306	-	-	-
TH2mmA	DCFP (3k, 30 mm)		410	598	54%	2.02
TH2mmB		3.5	404	594	54%	2.02
TH2mmC			399	-	-	-
TH3mmA			534	770	53%	3.01
TH3mmB		4.5	530	800	51%	3.03
TH3mmC			517	-	-	-

Although it was assumed to be constant it should be noted that variation in binder coverage was also observed. This was not considered in this study as it would have had an insignificant effect on preform mass variability. Nevertheless, more severe consequences may be seen later in the manufacturing process. Short fibres may experience more in regions where binder content is low, for instance.
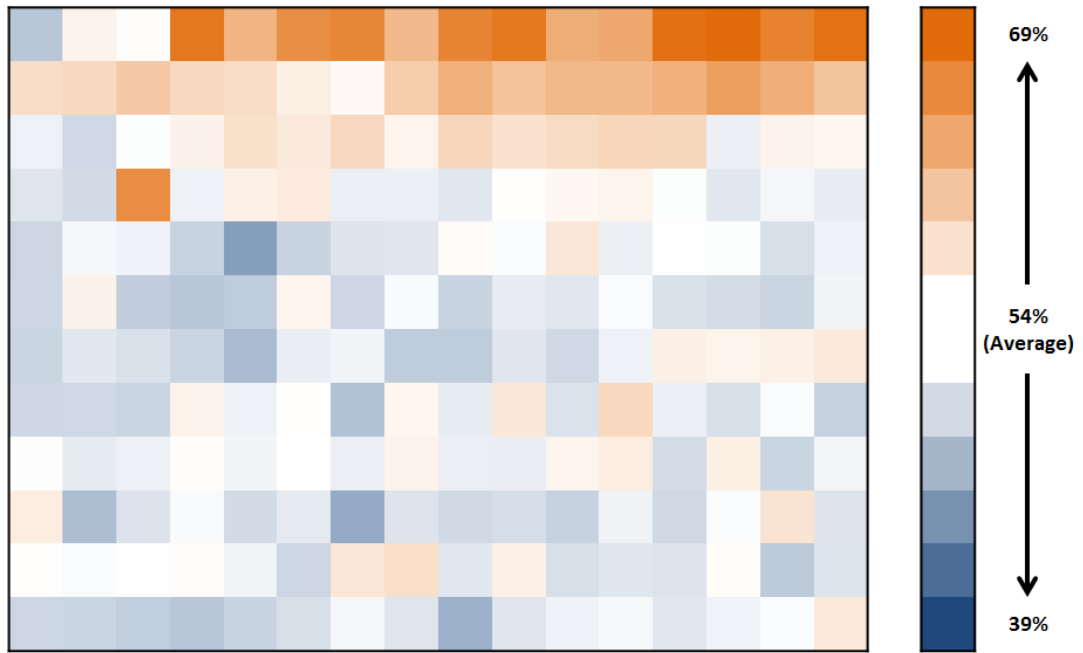
Figure 81a. Mass variability in a DCFP preform with 2.5 mm nominal thickness. Each square represents 25 mm x 25mm of the total area (300 mm x 400 mm) with the colour representing its relative mass. Areas with a volume fraction equal to the average V_f are denoted by a white cell. Overweight regions are represented by orange cells, while underweight regions are represented by blue cells.
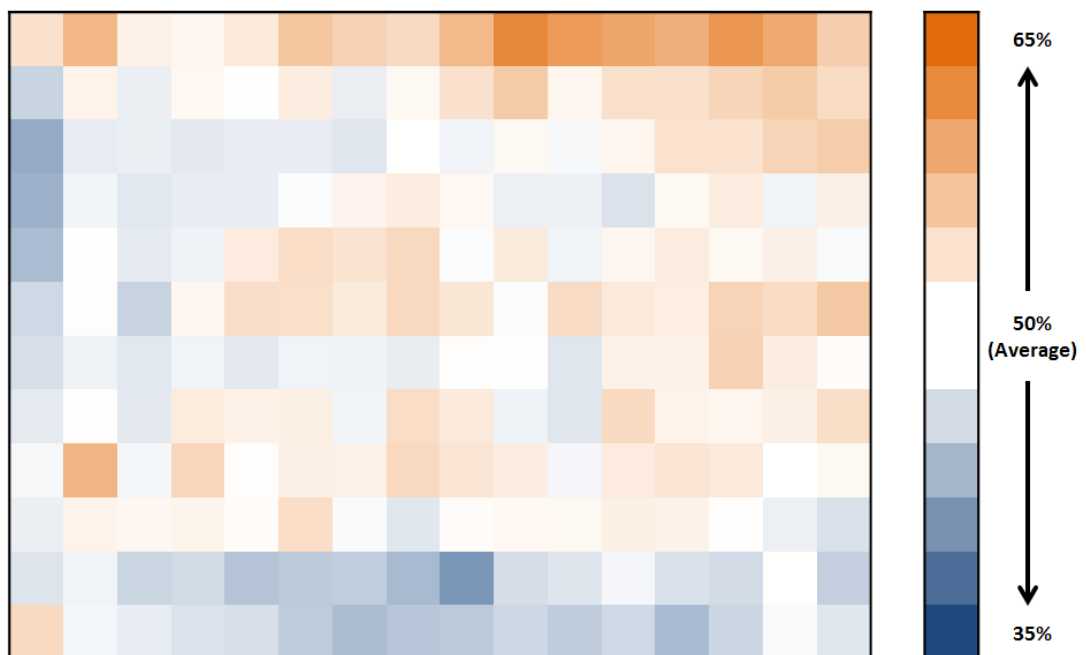
Figure 81b. Mass variability in a DCFP preform with 3.5 mm nominal thickness. Less variability was seen globally. Over/under-weight areas at the upper/lower edges of the preform remain but are less significant than the thinner preform.
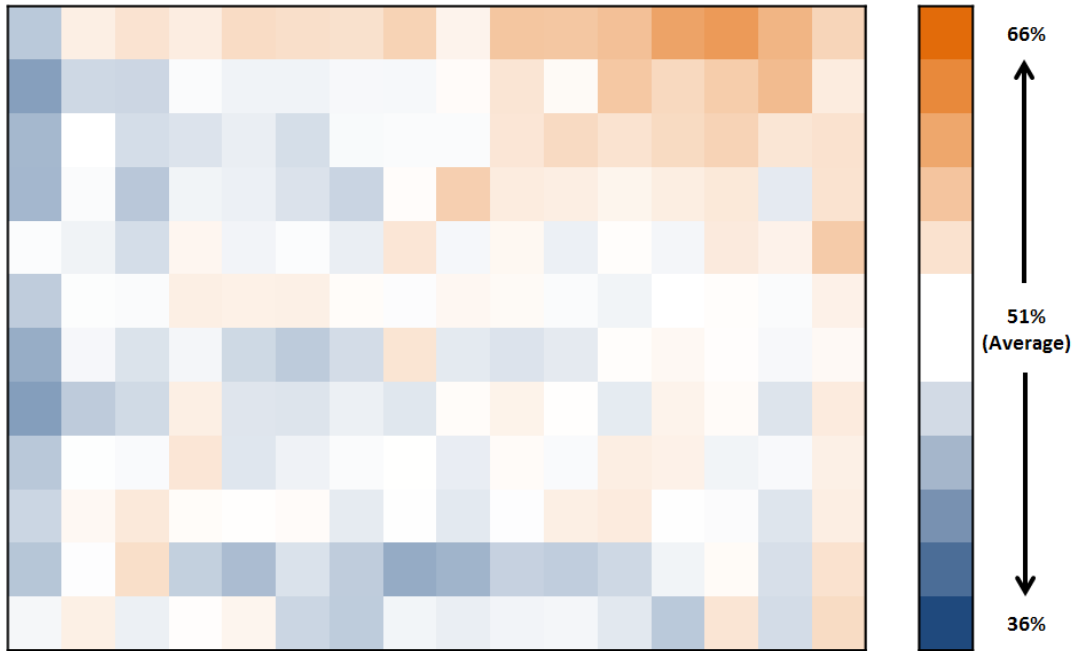
Figure 81c. Mass variability in a DCFP preform with 4.5 mm nominal thickness. Global variability was seen to decrease further, particular in the centre of the preform.

Global areal mass variation was calculated for each preform by determining the average percentage of absolute variation with the mean,

$$\frac{1}{N}\sum_N \left|\frac{m - \bar{m}}{\bar{m}}\right|,$$

Eq. 47

where N is the total number of specimens weighed. Global mass variation can be susceptible to processing conditions (e.g. the overspray of one edge in relation to another). Local variation is more likely to indicate variability that is intrinsic to the material as the smaller region it captures is less likely to be affected by processing of the fibres. Similar to equation Eq. 47 it is calculated by

$$\frac{1}{N}\sum_N \frac{1}{n}\sum_n \left|\frac{m - \bar{m}}{\bar{m}}\right|,$$

Eq. 48

where n is the number of specimens in each local region and is equal to 9 in the values stated in Table 19. This examines variability in a region 75 mm x 75 mm. Global mass variation decreased by 27% and 9% between 1-2 mm and 2-3 mm, respectively. Local mass variation decreased by 21% and 4%. Preforms with a larger areal mass were also seen to exhibit a smaller range in local volume fractions and thicknesses. The difference between the maximum and minimum volume fractions calculated for the thickest preform was 19% compared to 28% for the thinnest. The

distribution of V_f (Figure 82) didn't always follow a normal distribution. Variability was likely to have been influenced by scale effects as standard deviations at the three thicknesses were similar (0.10-0.12 mm). Thicknesses variation was also estimated for each preform moulded using the vacuum infusion method. The range of thicknesses was seen to increase from 1.45 mm to 1.84 mm between 1-3 mm, but as a proportion of the average thickness this was seen to decrease from 51% to 38%.

Table 19. DCFP mass variability for three preform thicknesses. RTM values were calculated by assuming the preform occupies a fixed cavity of a nominal thickness (detailed in Table 18). Vacuum infusion values were calculated by determining the volume occupied by the preform for an assumed fibre volume fraction of 50%.

Preform	RTM based V_f (%)				VI based thickness (mm)				Variability	
	Min	Max	Range	Mean	Min	Max	Range	Mean	Global	Local
TH1mmC	45	73	28	54	2.36	3.82	1.45	2.85	4.29%	5.08%
TH2mmC	40	62	22	50	2.96	4.58	1.61	3.72	3.13%	4.20%
TH3mmC	42	61	19	51	3.97	5.80	1.84	4.81	2.86%	4.02%
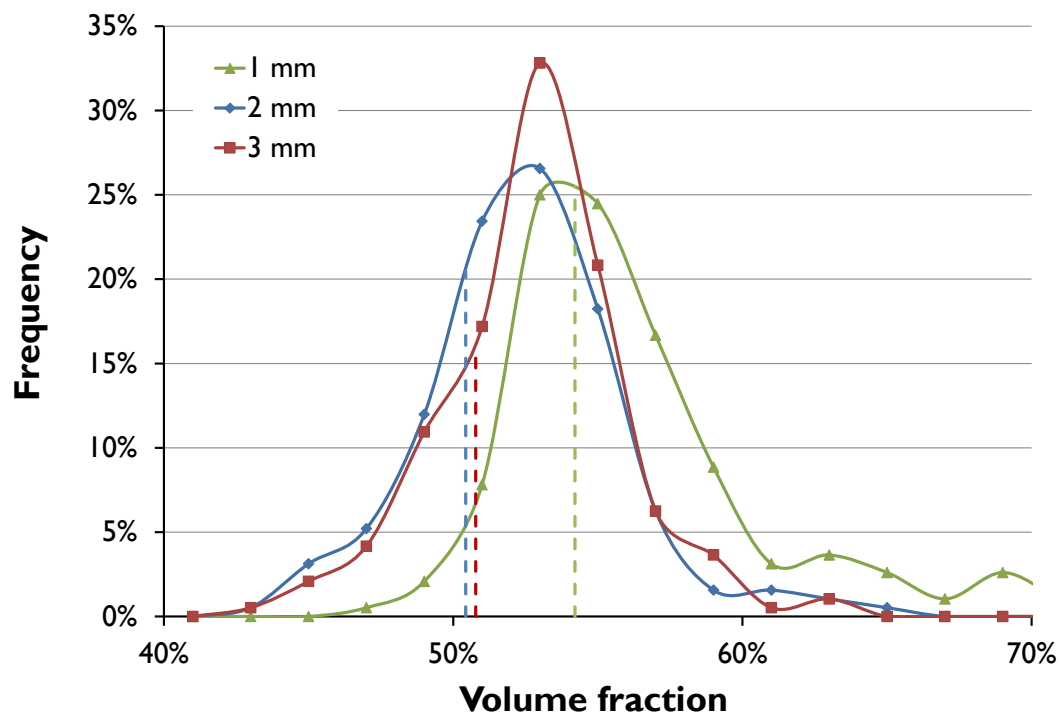
Figure 82. Mass variability of FA2, represented by a frequency distribution, at three thicknesses. Frequencies were determined for a bin size of 2% (absolute). The frequencies are given as a proportion of the 192 (25 mm x 25 mm) samples weighed for each preform. Dashed lines show the mean values at each thickness.

5.5.2 Mechanical property variation

Inter-plaque variability

Across the three thicknesses, modulus was largely unaffected. Young's modulus increased by 8% from 1-2 mm and 3% from 2-3 mm. The spread of results became smaller indicated by the decreasing CV – 19%, 14% and 11% for 1, 2 and 3 mm, respectively. The decrease in mass variability, achieved with larger thicknesses, translated to an increase in UTS. Mean strength increased from 287 MPa to 356 Mpa between 1-2 mm and 367 Mpa at 3 mm, but this increase was less significant than that observed through previous RTM manufactured specimens [22]. The coefficient of variation was seen to decrease from 12% to 6%, increasing slightly to 7% at 3 mm.

Table 20. Tensile properties of 3k, 30 mm DCFP fibre architectures

Plaque	Thickness (mm)	Specimens	Modulus (GPa)		UTS (MPa)			
			Mean	CV	Mean	CV	A-basis	B-basis
TH1mmA	1.01	22	39.7	20%	286	12%	-	-
TH1mmB	1.01	22	36.6	17%	288	12%	-	-
Average	1.01	(44)	38.1	19%	287	12%	207	220
TH2mmA	2.02	20	39.6	16%	349	8%	254	275
TH2mmB	2.02	22	42.4	11%	362	4%	329	344
Average	2.02	(42)	41.0	14%	356	6%	292	310
TH3mmA	3.01	20	44.8	7%	367	7%	-	-
TH3mmB	3.03	22	34.3	16%	368	6%	-	-
Average	3.02	(42)	39.6	11%	367	7%	304	332

Intra-plaque variability

Average variability across the preform is shown in Figure 83. It should be noted that grinding eliminates surface variability and is likely to have reduced the magnitude of the results reported. Other moulding methods may result in greater variability. The highest and lowest stiffness results regularly came from specimens taken from the edge of the preform. These regions were previously seen to be prone to under/over deposition. Underweight areas resulted in low properties, a direct result of locally low fibre volume fractions. At 1 mm, results were up to 33% lower than the mean for that batch. Despite a reduction in overall variability with increased thickness, these poor results (recorded within 75 mm of the preform edge) remained with modulus values 38% and 32% lower than the mean at 2 mm and 3 mm.

Strength results were also influenced by edge effects but the effect was less prominent in thicker plaques. Minimum values 35%, 16% and 21% below the mean were recorded, in order of increasing thickness. Overweight areas didn't necessarily translate to greater performance, but these regions did see a larger range in measured properties. As well as the associated benefits of higher volume fractions, such areas could also be subject to poor impregnation due to reduced permeability in fibre rich zones. In VI processes, preform thickness can also decrease closer to the vacuum source so volume fraction increases [154]. There was no evidence of this in the study. Outer regions are affected by variability that arises through processing/manufacturing (shown in Figure 75), whereas variability at the centre of each plaque is more likely to be due to randomness inherent in the material.

Young's modulus

UTS
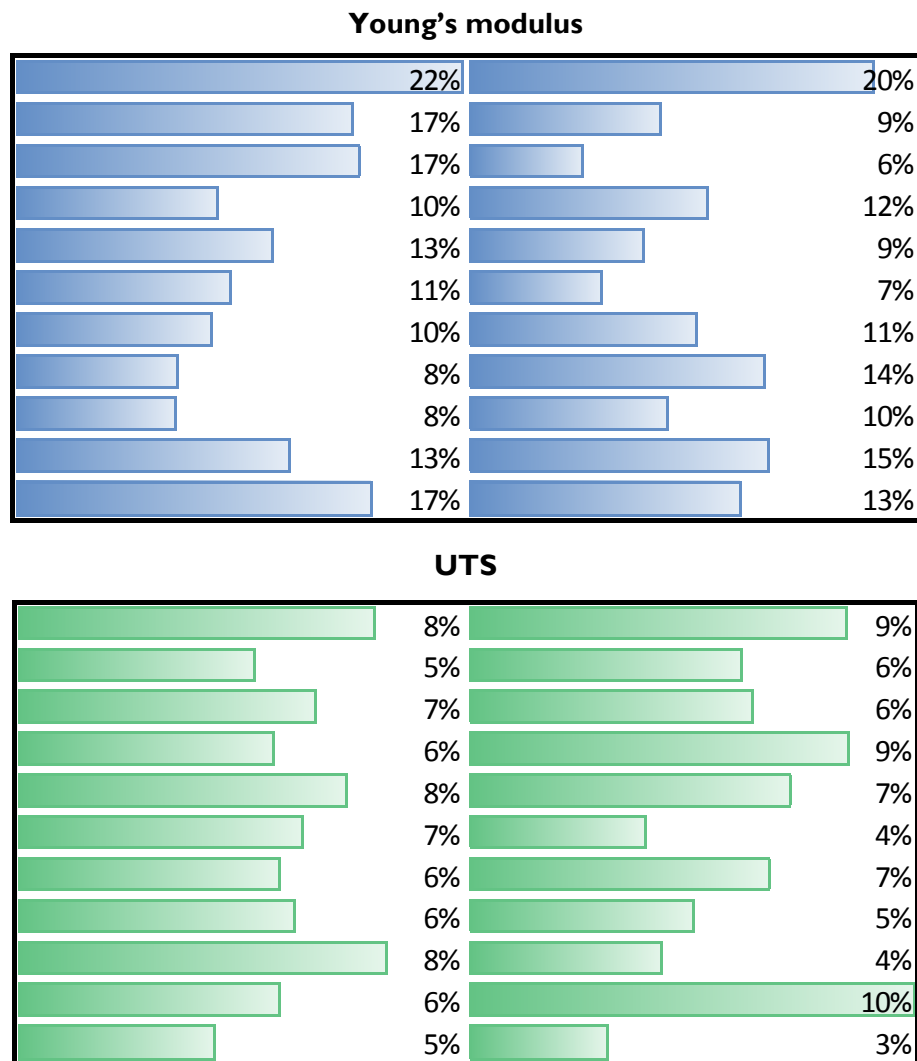
Figure 83. Stiffness and strength variability across a FA2 preform. Deviation from the mean was calculated for each specimen in the sample it was taken from. The average deviation, of the six plaques that were tested, at each location is shown in the figure.

5.5.3 Determination of basis values

Careful statistical analysis is important in understanding the mechanical characterisation of composite materials. Properties often exhibit intrinsic statistical dependence due to inhomogeneity, anistropic characteristics, and the brittleness of fibres and matrices [155]. The Composite Materials Handbook-MIL 17 [138] describes methods used to determine the statistical behaviour of tensile strength in composites and ultimately define A and B basis values based on their distibution.

Each sample of data in this study was analysed using guidelines outlined in the book. Outliers were removed using the Maximum Normal Residual (MNR) method for quantitative screening. It was then determined whether samples of the same thickness could be treated as batches from the same underlying population using the k-sample Anderson Darling method. Combined batches were re-screened for outliers. In order to provide design values based on each batch of data it is first necessary to fit each with an appropriate probablility distribution.

The two-parameter Weibull population is often used to model strength in composites [138]:

$$f(x) = \frac{\beta}{\alpha}\left(\frac{x}{\alpha}\right)^{\beta-1} e^{-\left(\frac{x}{\alpha}\right)^{\beta}}. \qquad \text{Eq. 49}$$

The distribution is typically applied to characterise behaviour when there are multiple opportunities to fail and the interest is in the first failure [156]. It is appropriate for describing strength in composites, especially those with continuous fibre, as failure regularly occurs at the weakest points in the meso-scopic architecure. The strength of the laminate is therefore lower than the arithmetic mean strength of all the specimens taken from it [25], so a normal distribution is only considered once the Weibull hypothesis has been rejected.

To fit the Weibull distribution, estimates of the shape (β) and scale (α) parameters need to be obtained. Three methods were used: rank regression (plotting y on x and vice versa), the maximum likelihood method (MLE) and a nonlinear generalised

reduced gradient (GRG) method. Each estimation was evaluated by calculating an observed significance level (OSL) using a goodness-of-fit test. The parameters giving the highest OSL were carried forward, and if the OSL ≥ 0.05 the hypothesis that the population is Weibull was not rejected. If however the Weibull distribution was not deemed suitable, an OSL for a normal distribution was evaluated.

Statistically determined basis values were calculated using the parameters for the distribution which best fit the measured data. A and B basis parameters provide statistically determined values which take into account the stochastic nature of the strength of composite materials. Correct interpretation of these values can reduce risk of failure in composite structures. The A-basis provides a 95% confidence in a target value above the 1st percentile. The B-basis, once again, provides a 95% confidences but for a value above the 10th percentile [130]. If the unstructured data set is from the population with a normal distribution, the A-basis value is:

$$B = \bar{x} - k_A s, \qquad\qquad \text{Eq. 50}$$

where k_{AS} is the appropriate one-sided tolerance-limit factor from [157]. The corresponding Weibull based design value is calculated using

$$B = \hat{q} e^{\left\{\frac{-V_B}{\hat{\beta}\sqrt{n}}\right\}}, \qquad\qquad \text{Eq. 51}$$

where

$$\hat{q} = \hat{\alpha}(0.10536)^{\frac{1}{\hat{\beta}}}, \qquad\qquad \text{Eq. 52}$$

where V_B is the tolerance factor for a sample size n.

Strength
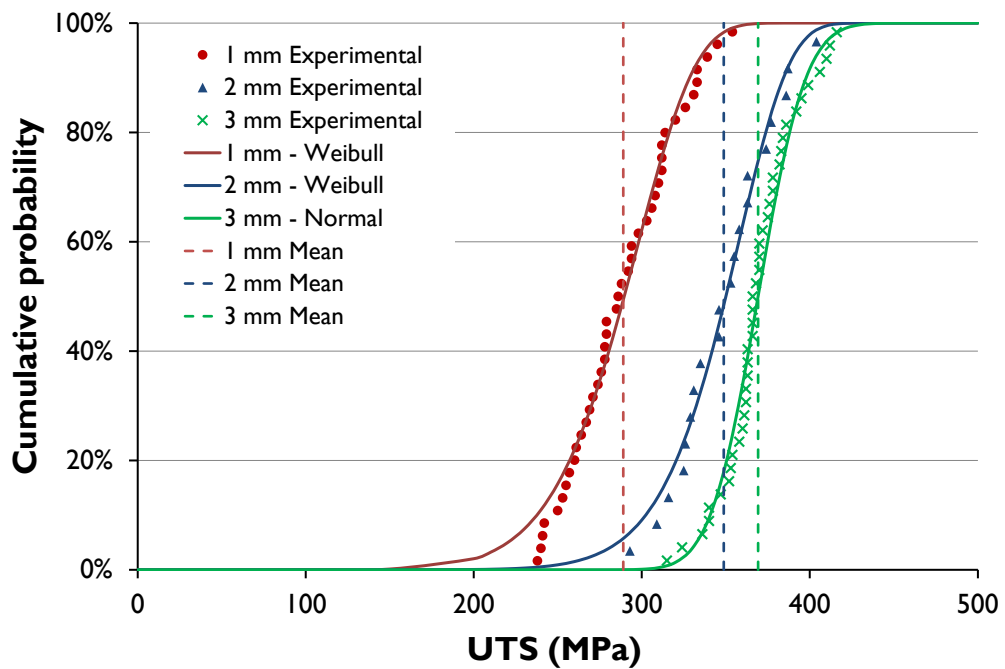
Figure 84. Cumulative frequency distribution - UTS

The MNR method was used to show that both batches at 1 mm were from the same underlying population; they were combined accordingly. An OSL of 0.223 was calculated for a Weibull distribution using α and β values of 301 and 9.52. It was therefore considered approprate for representing this data. Both batches at 3 mm were also shown to be part of the same underlying population. The OSL of 0.011 calculated for the Weibull fit (using α and β values of 380 and 17.5) did not meet the criteria required (>0.05). An OSL value of 0.240 indicated a normal distibution as a suitable fit. Results from 2 mm plaques proved to be significantly different from one another. Th2mmA was fitted with a Weibull distribution (α and β values of 360 and 12.86), while Th2mmB, showed better correlation with a normal distribution.

Larger scale parameters seen with increasing thickness indicate that the data is centred around a higher strength value – a result of improved strength with thickness. The shape parameter, also described as the Weibull modulus, can be used to describe strength variability in brittle materials [71]. This was also shown to increase with thickness. Conventionally this indicates a more even distribution of flaws and is a key component behind the application of Weibull theory to

composites, where laminate failure is seen to be a function of the weakest link. As demonstrated by the results, this is applicable to thin DCFP components with a high level of heterogeneity. As areal mass increases and local mass variation is seen to decrease, stress transfer becomes more efficient through an increased number of crossovers per unit area. These factors ensure that flaws are more evenly distributed and the cluster of minor flaws that have the potential to coalesce into larger ones is reduced. This is shown in the consistency of the results from the Th3mm batch, which gives a narrow (CV = 6%) normal distribution.

Modulus
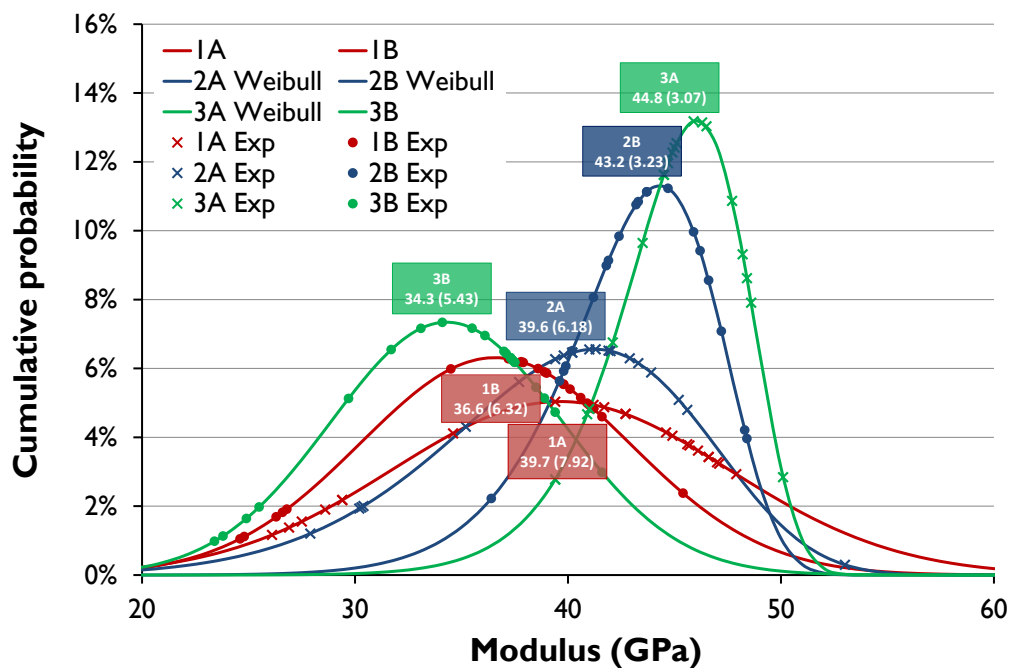
Figure 85. Distribution of modulus data. Experimental data (represented by the individual markers) have been fitted with curves obtained by processing the data in the same way as the strength results using MIL-Handbook 17.

Unlike strength data, the tensile modulus results (Figure 85) were found to be structured and could not be combined according to the k-sample Anderson Darling test for any of the three thicknesses. In such cases other procedures (e.g. ANOVA) should be used to model the distribution of sample data. In the case of Young's modulus, mean values are normally reported [158]. It has been argued that while it is necessary to apply statistically determined basis values to "weakest link" phenomena e.g. tensile strength it is not appropriate for phenomena that are considered to be "total response" [139].

5.5.4 Design for damage tolerance

Damage tolerance of the 3k 30 mm DCFP architecture was compared to 12k NCF laminates Table 21, which were also moulded through infusion of resin B. The tensile strength properties of the resin B based composites were found to be inferior to those based on resin A. Modulus values were similar to those produced with resin A, but strength values were significantly lower – 295 MPa at 3 mm thickness and 50% fibre volume fraction. Higher temperature performance, a requirement for aerospace grade resins, often results in a matrix that is more brittle and less damage tolerant. Brittle resin systems are also susceptible to micro-cracking which could have occurred during the curing cycle or the grinding process [130].
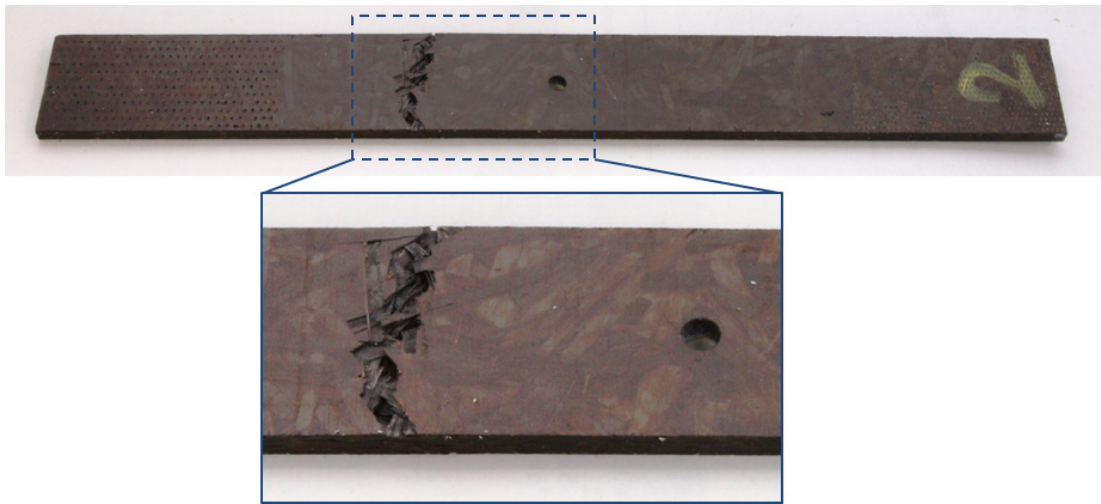
Figure 86. Tested DCFP open-hole tensile specimen showing failure away from the hole.

Open-hole specimens showed no discernible difference, when compared with un-notched counterparts, in gross tensile strength. A change of +/- 1% was seen at 2 mm and 4 mm. In comparison, the notched NCF specimens showed a reduction in strength of 18% at 4 mm. The relative insensitivity of the DCFP architecture to the presence of the hole was highlighted by multiple failures away from it (Figure 86), something that was not observed with the NCF specimens. In accordance with the standard, such failures are not normally accepted. Exceptions must be made for discontinuous fibre architectures where a failure away from the hole is not necessarily the result of poor sample preparation.
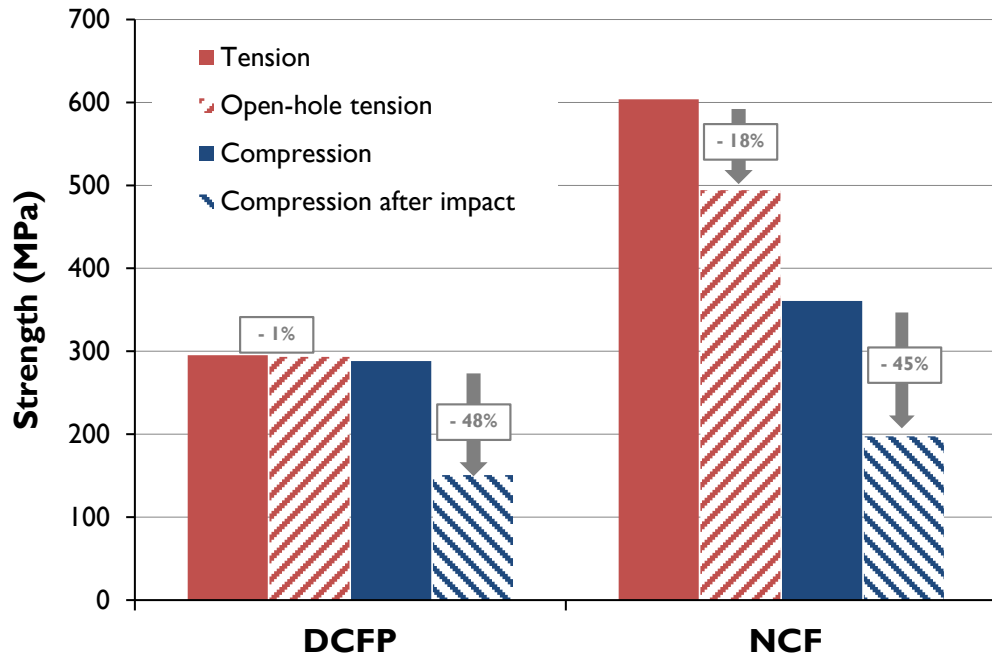
Figure 87. **Tensile and compressive strength properties of un-notched and damaged DCFP and NCF.**

Compression and CAI tests were carried out on specimens cut from the same plaques. Damage on the NCF specimens was seen in the form of small indentations at the point of impact with splitting and delamination on the other side. Visible damage on the DCFP specimens was more significant with large indentations (in some cases to the point of rupture) on the side of impact and substantial protrusion of fibre tows on the opposite (Figure 88). Knockdown, between standard compression and CAI properties, in DCFP was 48% (Figure 87) compared with a 45% reduction seen with NCF and an 81% reduction specified by the manufacturer for a representative uni-directional prepreg.
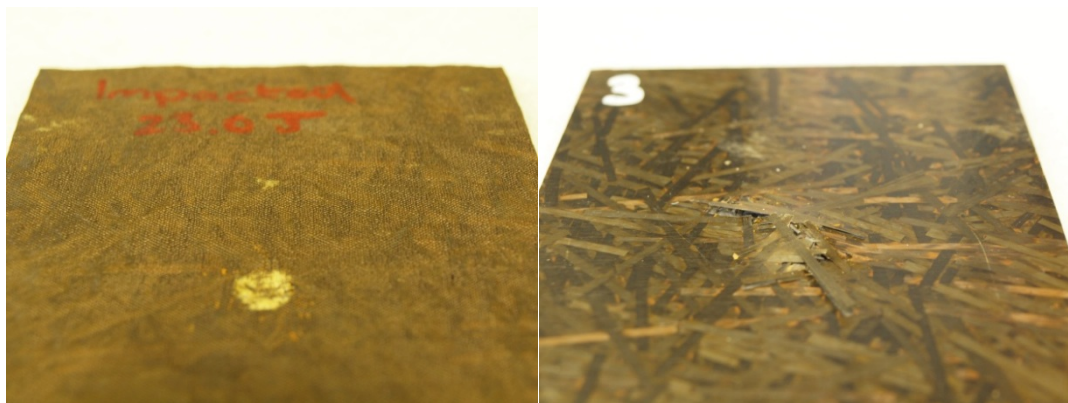
Figure 88. Impacted (6.7 J/mm) DCFP specimen. Impacted side (left) and damage on external surface (right).

Open-hole compression values for DCFP and NCF were similar, 358 Mpa and 359 MPa, respectively. This relatively high value for DCFP compared with un-notched compression results may be due to wider test specimens being used in accordance with the standard for this test method. Typically in brittle continuous fibre composites, larger part volumes result in lower strength values as there is a larger probability of the part containing defects. In meso-scale DFCs this effect may only be seen in thin parts (1-2 mm) when flaws, in the form of resin rich or dry regions, are a result of large areal mass variation.
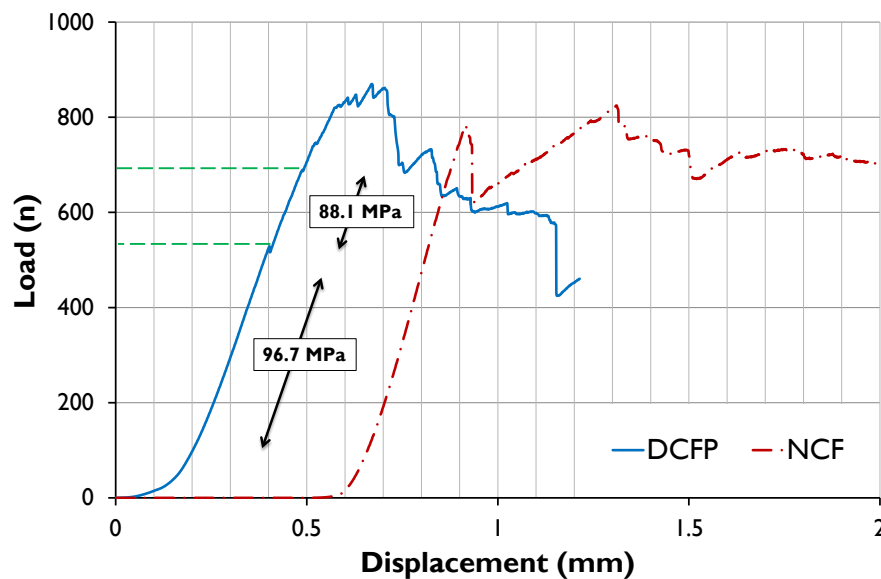
Figure 89. Typical ILSS load-displacement curves and tested DCFP and NCF specimens. Apparent ILSS for the DCFP specimen was taken at the first discontinuity of the curve (528 N), in accordance with BS EN ISO 14130. The specimen was subjected to continued loading with, initially, only a 9% decrease in stiffness. Several further discontinuities occurred before final failure (at 820 N) – a 55% increase on the recorded value.

Apparent inter-laminar shear strength for DCFP at 30.2 MPa was similar to the 31.4 MPa observed for NCF specimens. ILSS is predominately determined by interfacial bonding between the reinforcing fibres and matrix [159]. A relatively poor interface with resin B may explain lower results when compared with HexMC and the quasi-isotropic fabric laminate in Table 21. DFCs typically provide high delamination resistance (relative to continuous fibre composites) [160], but the ILSS test procedure raised questions on the suitability of the test for DCFP composites; or, indeed the suitability of DCFP for ILSS-driven applications, especially with repeated loading close to failure. Strength is determined by the first obvious discontinuity in the load-

displacement curve indicating failure in the first ply. Due to the lack of distinguishable plies in DCFP laminates this first deviation often occurred far in advance of any significant reduction in load-bearing capacity (Figure 89). Also, recent standards have shown an increased emphasis on the failure modes that are accepted as valid, with only inter-laminar failures being accepted. When tested specimens were examined, it was apparent that the majority of DCFP samples failed in tension. Others were seen to exhibit unacceptable failure modes, e.g. plastic deformation, often with no sign of inter-laminar fibre failure.

Table 21. Summary of testing of un-notched and damaged DFCP architectures and a NCF benchmark. Results for Hexcel HexMC [141, 161, 162], an alternative multiaxial fabric laminate and a UD prepreg layup (typical manufacturer data) are included for reference.

Property	Unit	Test	DCFP		NCF		HexMC	QI fabric laminate	UD prepreg
			2 mm [49%]	4 mm [50%]	2 mm [46%]	4 mm [48%]	[55%]	[55%]	[60%]
Ultimate tensile strength	MPa	ASTM D3039	247 [4%]	295 [5%]	-	604 [3%]	325	570	2100
Young's modulus	GPa	ASTM D3039	35.2 [8%]	43.1 [8%]	50.7 [35%]	40.0 [4%]	41	52	130
Open-hole ultimate tensile strength	MPa	ASTM D5766	250 [5%]	293 [7%]	443 [3%]	494 [2%]	228	430	-
Ultimate compression strength	MPa	BS EN ISO 14126	-	288 [11%]	-	361 [5%]	308	580	1300
Compression modulus	GPa	BS EN ISO 14126	-	33.8 [31%]	-	40.6 [8%]	-	-	123
Open-hole ultimate compression strength	MPa	ASTM D6484	-	358 [8%]	-	359 [6%]	243	474	310**
Compression strength after impact	MPa	ASTM D7136/7	-	151 [3%] 23 J	-	197 [4%] 27 J	232	225	260** 32J
Inter-laminar shear strength	MPa	BS EN ISO 14130	30.2* [20%]	-	31.4 [19%]	-	45	45	110

*Unacceptable failure modes
**Values are for a quasi-isotropic layup

5.6 Design implications

Future potential of the material relies on understanding the effect of preform variability on mechanical performance at the component level. Continuous fibre composites are well represented by coupons due to repeating patterns in their architectures. The same is not true for meso-scale DFCs. The difference in results from compression specimens of varying geometries highlighted sizing effects, with samples from larger OHC specimens giving better results than smaller un-notched counterparts. Marissen & Linsen [163] have previously suggested that positive effects may be explained by the size of the defect/flaw relative to the specimen. As well as conventional manufacturing flaws (e.g. voids), meso-scale DFC laminates contain intrinsic defects as a consequence of variability in the random mesoscopic fibre architecture. An indication of this - preform mass variability - was shown to decrease with larger coupons. This effect is likely to be the result of local inconsistencies being smaller in relation to the greater amount of fibre.

Defects are also likely to have less influence on the mechanical properties. Figure 90 shows the range of areal mass and tensile strength values recorded for preforms in this study. The Weibull distribution, typically used to describe weakest link effects in brittle composites, was appropriate for describing tensile strength variability in thin parts where the defects are large relative to the specimen. As thickness of the material was increased, variability was seen to take on a normal distribution – an indication that failure was less dominated by these defects. Consequently, basis values were considerably higher (Figure 90). It is likely that failure is still dominated by weak link effects in thicker parts but that these links are a coalescence of defects. If tensile strength is thereby characterised by the probability that a critical number of defects are in the vicinity of each other, variability will increasingly be more akin to a normal distribution as material volume increases. How this manifests itself in the upper stages of the building block approach, i.e. components and full parts, will ultimately determine whether the methodology is appropriate for meso-scale DFCs.
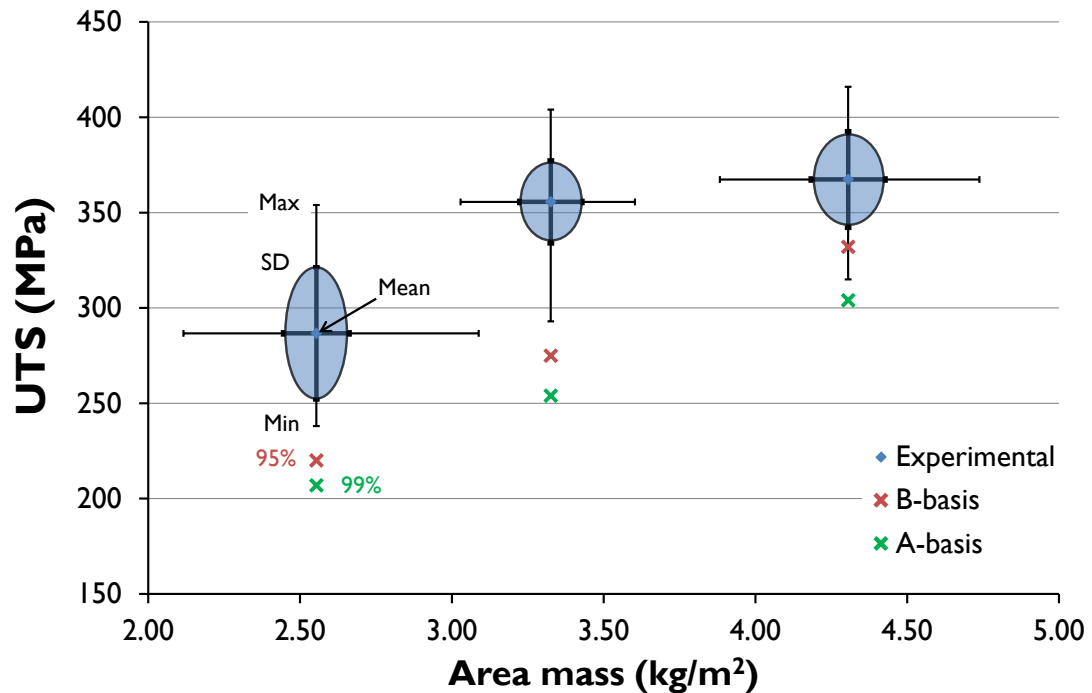
Figure 90. Tensile strength properties of DCFP for increasing areal mass/thickness at a target volume fraction of 50%. The small error bars indicate the standard deviation of the areal mass and UTS. The large error bars indicate the full range of results observed. A and B-basis values are also shown.

Performance of DCFP at the coupon level is promising, but greater benefits (over continuous fibre composites) may be seen at component level, especially in damage tolerance. Open-hole tension and compression results indicate insensitivity to induced damage, and demonstrate a significant advantage of the material over conventional laminates (compared in Table 21) which are known to suffer large knockdowns due to damage caused in manufacturing or in-service. CAI results were inconsistent with this notion and raise questions on the failure modes of impacted specimens. CAI strength of 151 MPa was significantly lower than that expected. Further investigation (e.g. sectioning of impacted/tested specimens) is needed to understand the exact failure mechanisms.

A demonstration of notch insensitivity was also seen in that study, but there are differences in the processing of the material which can have an effect on mechanical properties. The meso-architectures of chopped prepreg laminates are influenced by flow characteristics determined by the geometry of the tool, for instance. As a result, such methods exhibit slight differences in the meso-architecture to DCFP. In-plane

properties have been shown to increase [160] in regions where flow has resulted in fibre alignment (e.g. component edges), but this may also have an adverse effect in areas where alignment is out of plane with applied the load. Problems may arise in larger components where flow is harder to dictate and increasingly difficult to predict.

DCFP offers an alternative to flow-reliant processes providing a greater level of customisation and control over the meso-scopic architecture. The ability to influence tow alignment has been demonstrated [77] and may be able to provide greater properties required for high performance components. Tow size, fibre length and the matrix can all be varied with relative ease and without the associated cost of altering the formulation of a chopped prepreg. The effect of the matrix remains a barrier to further application and its effect on the mesoscopic architecture also needs to be established. Toughened resins are increasingly used in the aerospace sector but have been shown to affect DFCs that show high coupon-to-coupon variability in a different way to conventional continuous fibre composites (Chapter 4).

5.7 Conclusions

The potential of DCFP for high performance structural applications has been assessed through conventional mechanical and damage tolerance tests typically used for aerospace certification. Data has been produced for a 3k fibre architecture known to give good performance.

A strong correlation has been observed between variability of preform mass and mechanical properties for three laminate thicknesses. Greater variability in laminate properties was a direct consequence of variability at the preforming stage. Stiffness was more severely affected than strength, with the latter being dominated by Weibull effects. A- and B- basis design values have been established for the UTS of FA2. While it is necessary to apply design values to weakest link phenomena such as strength it has been established that this is not appropriate for properties that are considered to be total response. Consequently, mean values have been reported for modulus.

Conventional composite design rules, used in the production of damage tolerant structures, must be reconsidered for the manufacture of DCFP components. Results have shown that the discontinuous fibre architectures do not suffer the same knockdown in properties experienced for continuous fibre composites. Open-hole tension testing showed no discernible difference in strength with un-notched batches (247 MPa and 295 MPa), with a change of +/- 1% at 2 (250 MPa) and 4 mm (293 MPa), respectively. CAI properties (151 MPa) did suffer a 48% knockdown in properties compared with specimens tested under the standard un-notched compression method (288 MPa). This was in contrast to open-hole compression results where strength was recorded at 358 MPa. Current safety factors based on conventional laminates may be too conservative and could lead to over-engineering which would limit the potential of material. In many applications randomly orientated fibres may be able to provide the required properties at low cost and high production rates over continuous fibre composites and prepreg systems.

6 Design of DCFP structures

6.1 Introduction

Conventional composite design procedure follows the building block approach, where coupon test results provides data for sub-components to full scale parts. Idiosyncrasies in the DCFP process require a different methodology. One is proposed in Figure 91. The work that follows is a material comparison and a worked example of the design of a DCFP component - a composite seat (for an automotive application) has been used for investigation as a common need exists for the development of new seating systems that are lighter, whilst still being able to fulfil the safety needs of the occupant [164].

6.2 Design
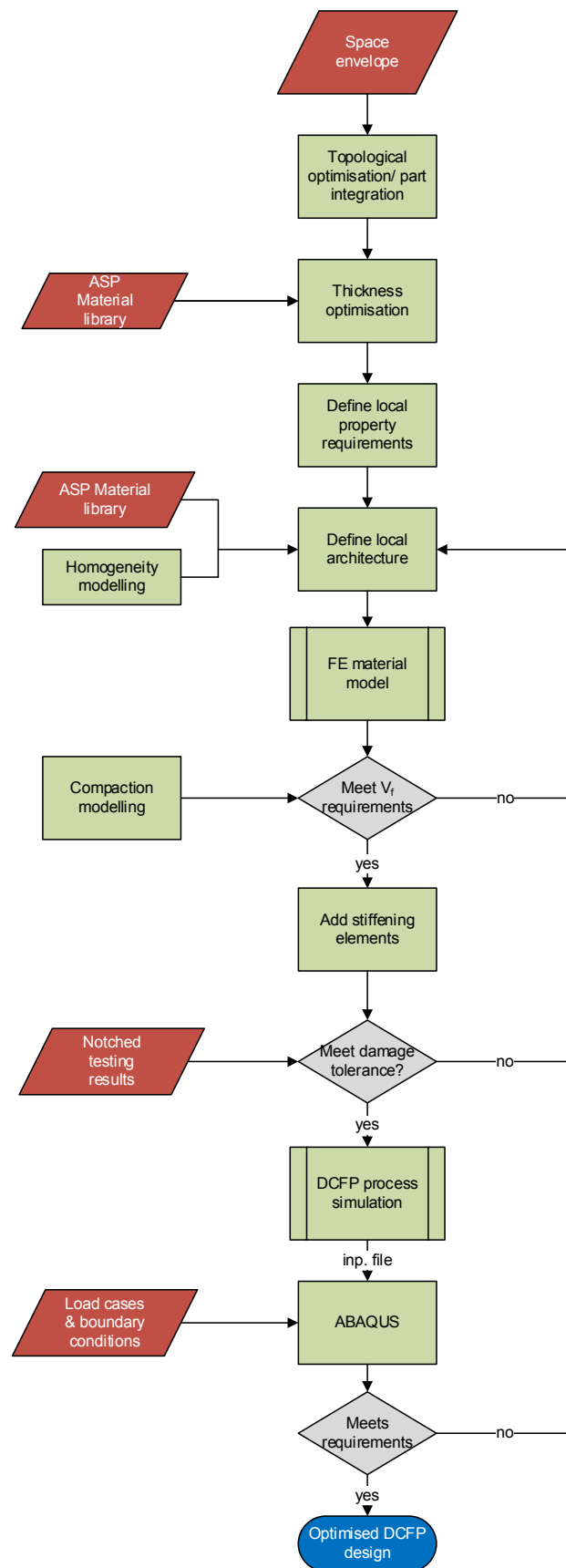
Figure 91: Proposed DCFP design process.

6.2.1   Material properties

Fibre architectures may be determined from existing data from the property library. Alternatively the analytical models may be used to provide the range of preform parameters that meet tensile stiffness and strength requirements. Properties in the worked example have been taken for FA2 at a V_f of 55%.

6.2.2   Finite element material model

The composite model can be discretised into locally homogenised sections (where properties are uniform) to reduce part complexity. Predicted fibre architecture properties can be assigned to each facet of the complete geometry. By taking this approach FE time can be greatly reduced to provide approximate material properties. Thickness can be optimised across the part to give initial estimations for weight savings over aluminium.

6.3   Initial material comparison

Performance of the two benchmark DCFP architectures have been compared with aluminium, comparable conventional (twill weave and NCF) composites, and comparative DFC processes. Thicknesses of each material were normalised to provide a section bending stiffness of 562 Nm – the value calculated for 2 mm, automotive grade (5754) aluminium. The in-plane properties of each material were then calculated using the normalised thicknesses. Results are shown in figures 92 - 94, with weight savings detailed in Table 22.
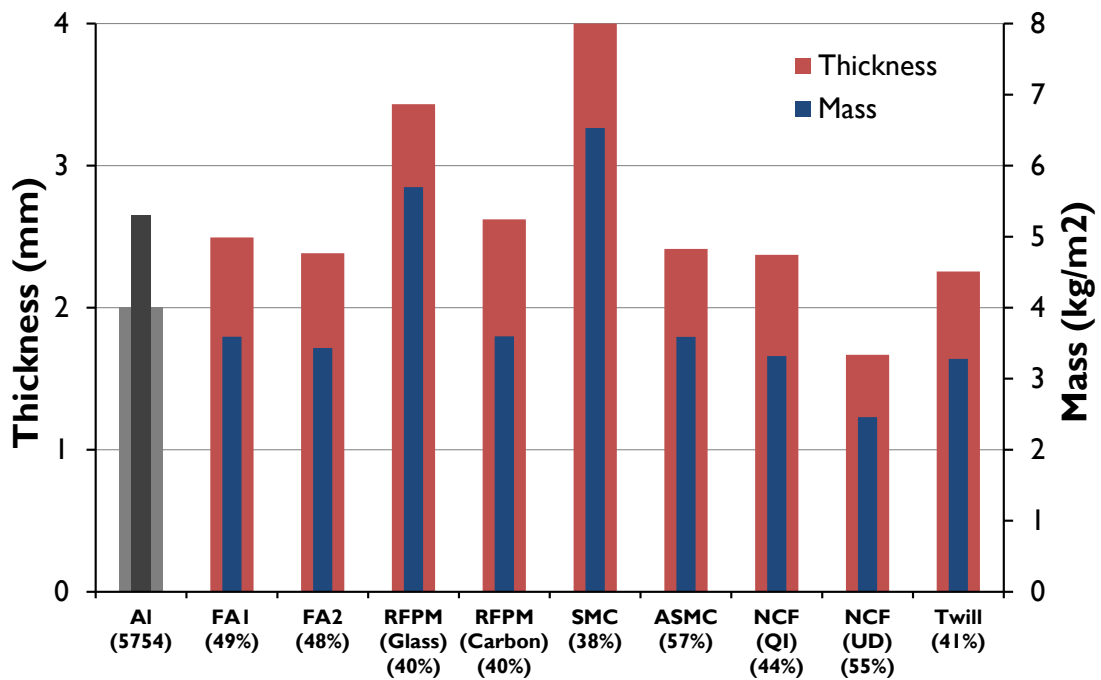
Figure 92. Thickness and mass of DCFP compared with aluminium and composite benchmarks for matched in-plane stiffness.

Table 22. Predicted weight savings over automotive grade aluminium (5754) based on matched bending stiffness.

Material	Weight saving over 2 mm aluminium
DCFP - FA1	32%
DCFP - FA2	35%
RFPM - Glass	-7%
RFPM - Carbon	32%
SMC	-23%
ASMC	32%
NCF (QI)	37%
NCF (UD)	54%
Twill	38%
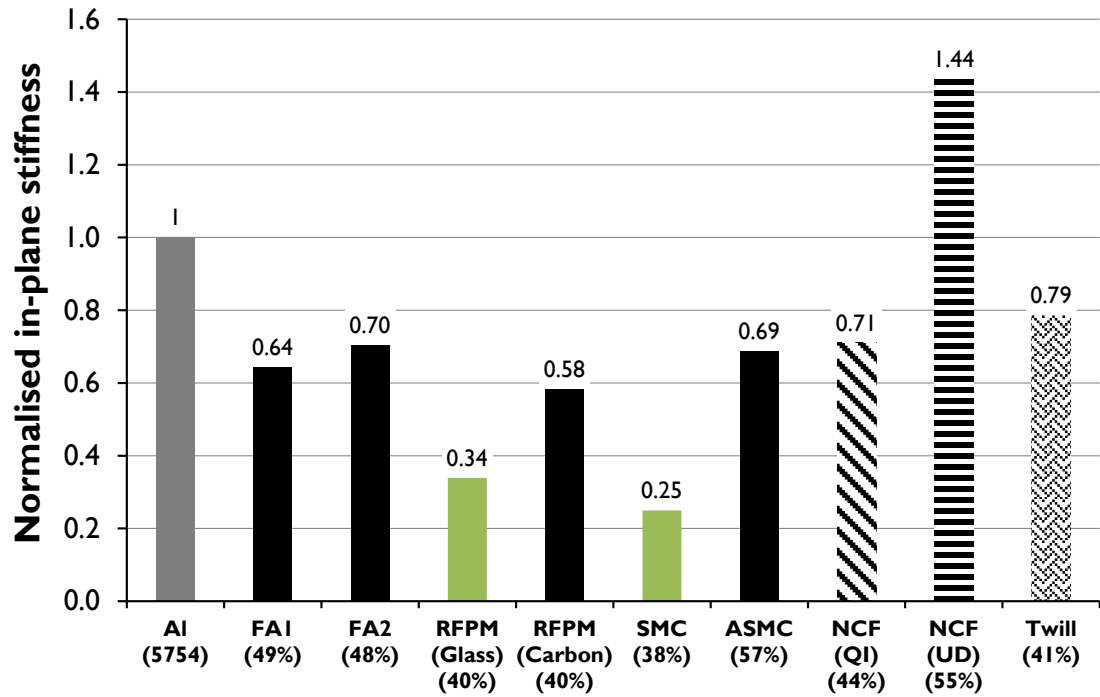
Figure 93. Normalised in-plane stiffness of DCFP compared with benchmarking materials. Section bending stiffness (EI) was matched with 2 mm aluminium and the resultant strengths are shown.
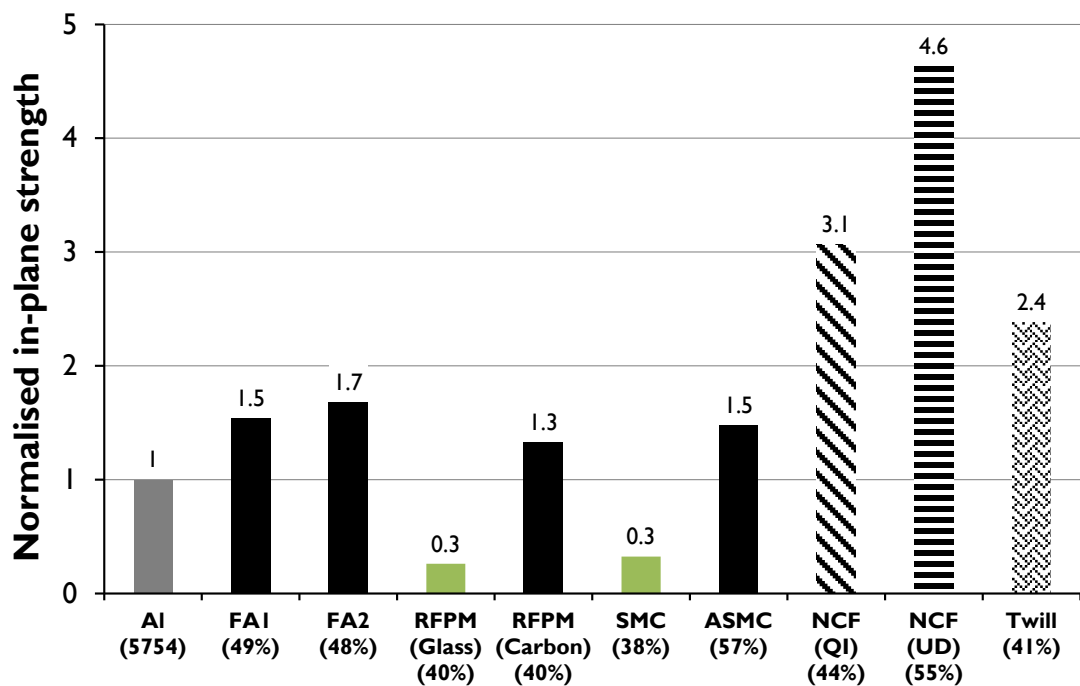
Figure 94. Normalised in-plane strength.

It should be noted that for the UD NCF fabric these properties are only applicable if the load is applied along the same direction as the fibres. Real structures exhibit more complex load cases and exact load paths are often difficult to define. Consequently, it is rarely possible for UD layups to be used throughout a structure but the results are included for reference.

6.4 Worked example – FE based design

This worked example compares performance of DCFP with aluminium and NCF benchmarks. Performance benefits are seen, but the main purpose of this investigation is to demonstrate differences in the design protocol and the increased level of optimisation available by using a fully automated DFC process. In conventional composites, such as NCF, the ability to vary thickness across a part comes at a cost - increased touch labour is required and complex layups often lead to excessive wastage. DCFP allows greater flexibility in part thickness with little influence on cycle times or fibre wastage. This ability will be highlighted through optimisation of a semi-structural automotive part.

The feasibility of spraying the fibre architecture to the desired preform shape and realising the target volume fraction of the laminate should be assessed with the relevant process [82]and compaction models. For the purpose of this investigation it has been assumed that the part can be sprayed, and that the final volume fraction of 55% is achievable through the moulding process.

6.4.1 Benchmark geometry

Loads and boundary conditions have been applied to the composite seat (as shown in Figure 95), and the same mesh (Figure 96) was used for all analysis.
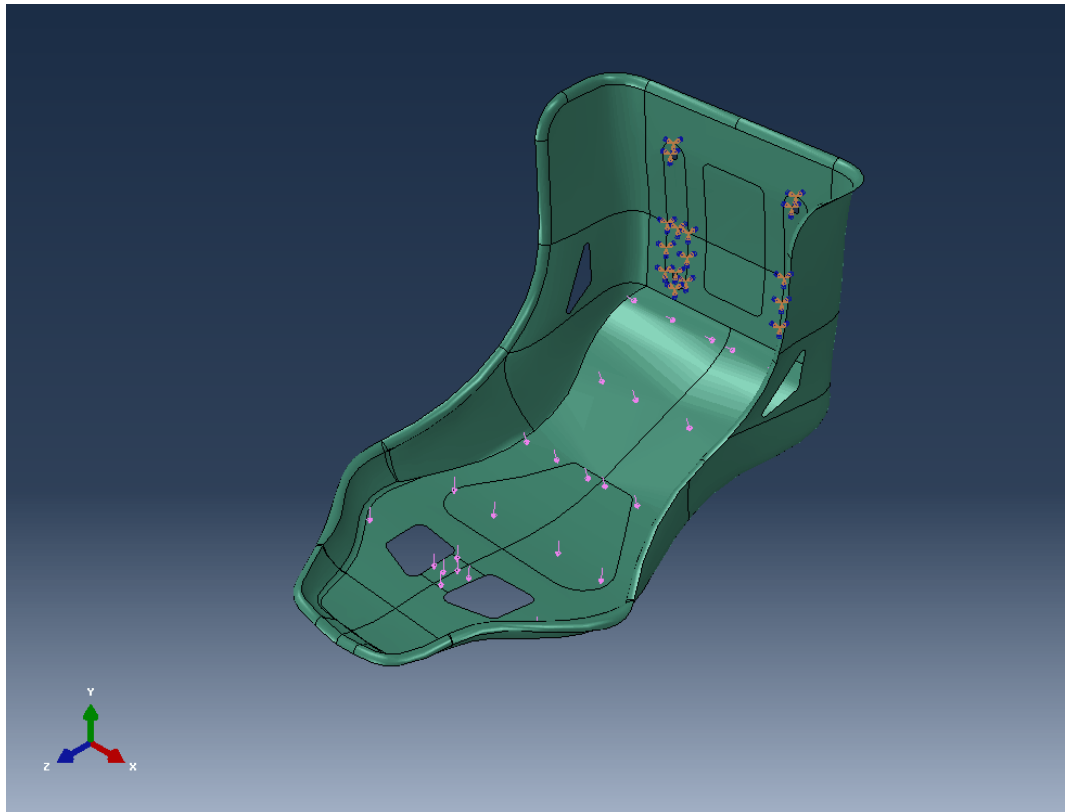
Figure 95. Composite seat with applied loads (0.01 N/mm2) and boundary conditions.
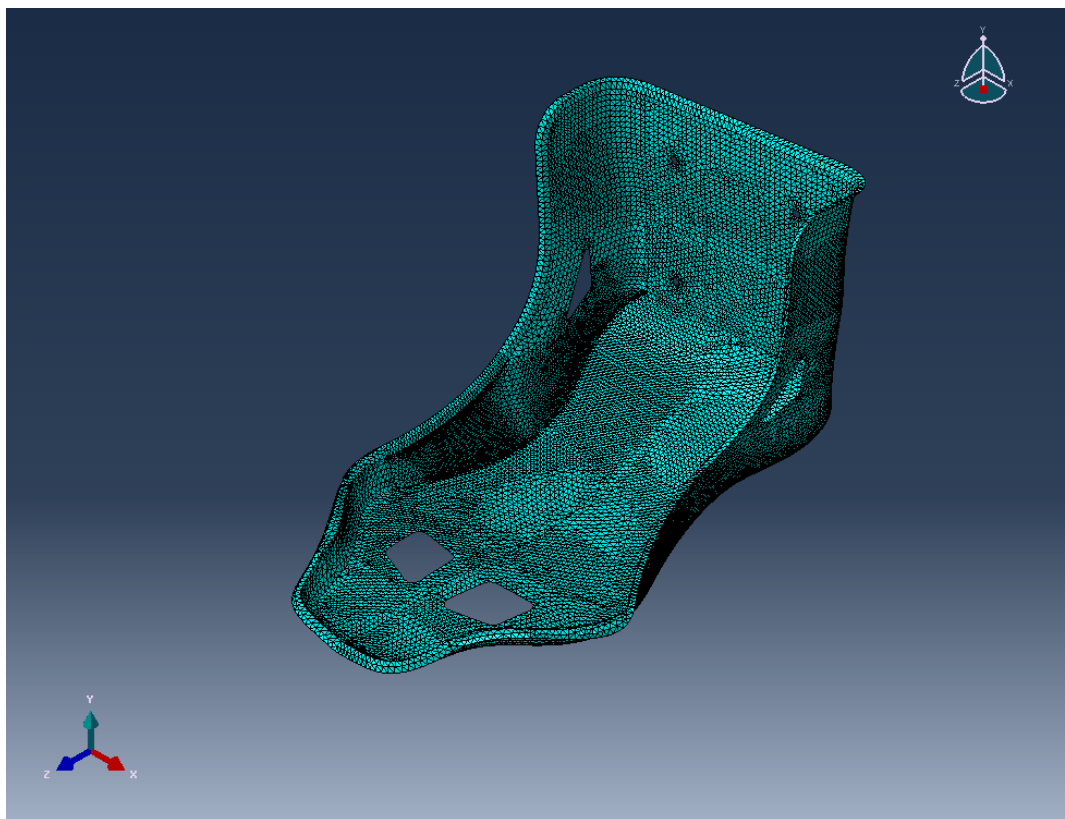
Figure 96. Composite seat meshing. The same mesh was used for analysis carried out in the worked example.

6.4.2 Materials

The following tables contain the data inputs for the three materials in the comparison. Formax FCIM-195 and 226 have been used for triaxial and unidirectional NCF reinforcement, respectively. The cured resin density (1.144 g/cm^3) of ACG MVR444 and Gurit PRIME 20LV has been used for all calculations. Composite behaviour, for NCF and DCFP, is assumed to be perfectly elastic.

Table 23. Properties of aluminium 5251 used in FE material model.

Material property		ABAQUS input	
Mass density		2.77×10^{-9}	
Elastic	Modulus (MPa)	64000	
	Poisson's ratio	0.33	
		Yield stress	Plastic strain
		90	0
		109	0.00118657
		117	0.00337397
		125	0.00801336
		132	0.0128365
		139	0.017647
		153	0.0271839
		163	0.0366885
Plastic		171	0.0461311
		180	0.0554793
		185	0.0647884
		195	0.0759603
		203	0.0884045
		206	0.0948159
		213	0.118911
		220	0.130905
		226	0.144904

Table 24. Properties of NCF used in FE material model.

	Material property	ABAQUS input
	Mass density	1.50×10^{-9}
Elastic	Longitudinal Young's Modulus, E1 (MPa)	132500
	Transverse Young's modulus, E2 (MPa)	10530
	Poisson's ratio	0.26
	Longitudinal shear modulus, G12, G13 (MPa)	4440
	Transverse shear modulus, G23 (MPa)	3790
Failure Stress	Tensile stress in fibre direction (MPa)	2234
	Tensile stress in transverse direction (MPa)	34
	Compressive stress in fibre direction (MPa)	-2234
	Compressive stress in transverse direction (MPa)	-135
	Shear stress (MPa)	68

Table 25. Properties of DCFP used in FE material model. Stated values are for FA2 (3k, 30 mm) at a V_f of 55%.

	Material property	ABAQUS input
	Mass density	1.50×10^{-9}
Elastic	Longitudinal Young's Modulus, E1 (MPa)	42000
	Transverse Young's modulus, E2 (MPa)	42000
	Poisson's ratio	0.33
	Longitudinal shear modulus, G12, G13 (MPa)	15800
	Transverse shear modulus, G23 (MPa)	15800
Failure Stress	Tensile stress in fibre direction (MPa)	295
	Tensile stress in transverse direction (MPa)	295
	Compressive stress in fibre direction (MPa)	-330
	Compressive stress in transverse direction (MPa)	-330
	Shear stress (MPa)	201

Conservative tensile properties have been used to ensure properties are still representative at small thicknesses. The analytical model gives Young's modulus and UTS values of 45.8 GPa and 320 MPa at 2 mm. The model can be used to determine alternative architectures that are able to provide the same properties. For instance, to achieve the same properties as the 3k architecture at 2 mm by instead using 6k would require a fibre length of 85 mm. If this proves to be excessively large for processing, the same properties can be achieved with a 53 mm chop length as long as thickness is equal to at least 3 mm. Alternatively, a toughened matrix could be used to improve properties in the laminate.

A- and B-basis allowables are typically used for aerospace applications but could also be used to reduce risk in automotive structures. The composite seat would only require the use of B-basis values as these are used for structures that are non-critical.

6.4.3 Initial composite design

Aluminium benchmark
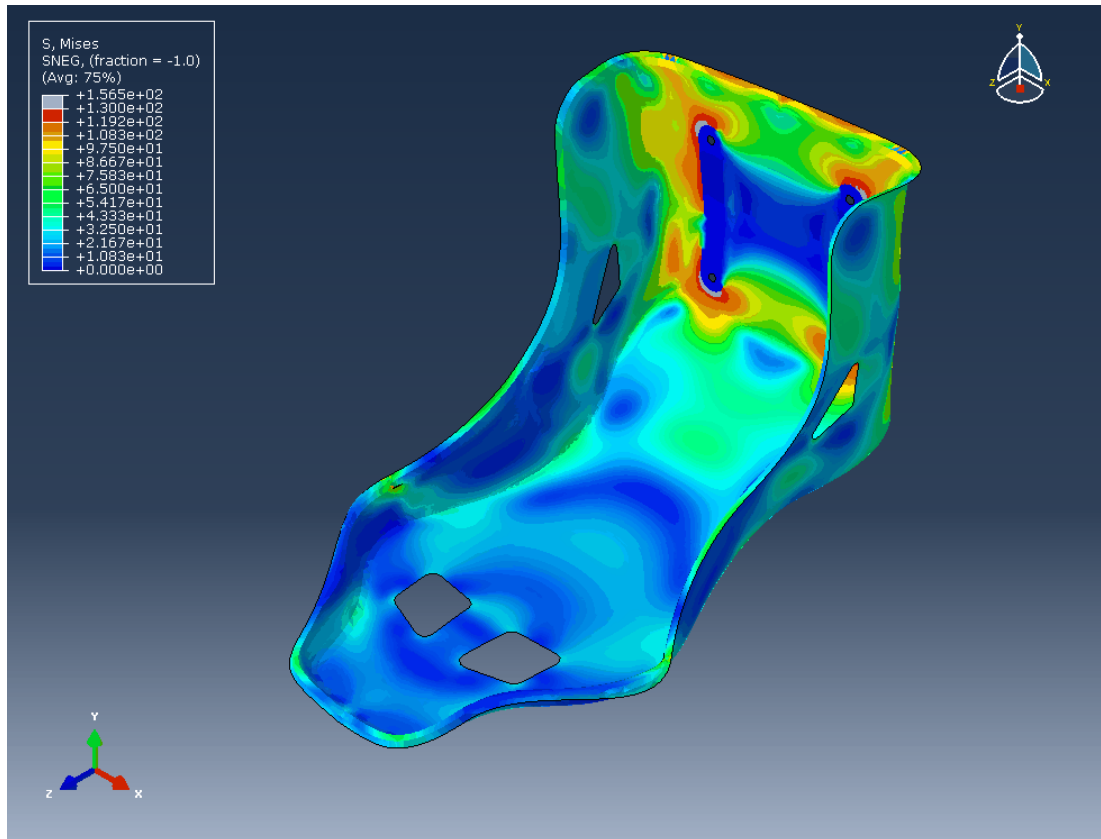
Figure 97. Tsai-Hill failure index of aluminium seat

Table 26. 3 mm Aluminium seat performance.

Material	Thickness (mm)	Mass (kg)	Deflection (mm)	Peak stress (MPa)	Failure index (Tsai-Hill)
Aluminium 5251	3	7.78	61	156	1.18

Analysis of the aluminium seat indicated the onset of plasticity near the boundary conditions (Figure 97). The deflection and failure index (shown in Table 26) will consequently be used as markers for the limit of composite seat performance.

NCF benchmark

		Ply Name	Region	Material	Thickness	CSYS	Rotation Angle	Integration Points
1	✔	ALL TRI 1	(Picked)	NCF_Laminate	0.22	\<Layup\>	0	3
2	✔	ALL TRI 2	(Picked)	NCF_Laminate	0.22	\<Layup\>	45	3
3	✔	ALL TRI 3	(Picked)	NCF_Laminate	0.22	\<Layup\>	-45	3
4	✔	ALL UD 1	(Picked)	NCF_Laminate	0.5	\<Layup\>	0	3
5	✔	ALL TRI 4	(Picked)	NCF_Laminate	0.22	\<Layup\>	0	3
6	✔	ALL TRI 5	(Picked)	NCF_Laminate	0.22	\<Layup\>	45	3
7	✔	ALL TRI 6	(Picked)	NCF_Laminate	0.22	\<Layup\>	-45	3
8	✔	ALL UD 2	(Picked)	NCF_Laminate	0.5	\<Layup\>	0	3
9	✔	ALL TRI 7	(Picked)	NCF_Laminate	0.22	\<Layup\>	0	3
10	✔	ALL TRI 8	(Picked)	NCF_Laminate	0.22	\<Layup\>	45	3
11	✔	ALL TRI 9	(Picked)	NCF_Laminate	0.22	\<Layup\>	-45	3
12	✔	EXTRA UD 1	(Picked)	NCF_Laminate	1	\<Layup\>	90	3
13	✔	EXTRA UD 2	(Picked)	NCF_Laminate	1	\<Layup\>	0	3
14	✔	EXTRA 45	(Picked)	NCF_Laminate	1	\<Layup\>	45	3
15	✔	EXTRA -45	(Picked)	NCF_Laminate	1	\<Layup\>	-45	3

Figure 98. Composites layup of NCF (2) seat. The ply stack for the highlighted region in the bottom-left is shown on the right. The base is reinforced by four extra layers of fabric.

A quasi-isotropic layup (NCF 1) of NCF demonstrated a 43% weight saving over aluminium. A large failure index was improved by adding further reinforcement at the base (NCF 2 - Figure 98) with weight saving reduced to 34%. While it is possible

to optimise the NCF layup further, it comes at the expense of increased layup time and material costs.

Table 27. NCF seat performance.

Material	Nominal thickness (mm)	Mass (kg)	Deflection (mm)	Peak stress (MPa)	Failure index (Tsai-Hill)
NCF 1	2.9	4.56	38.0	445	2.03
NCF 2	2.9	5.07	27.4	313	0.92

6.4.4 Basic DCFP design

Analysis of the DCFP seat was initially carried out by applying a constant thickness to the whole part with results shown in Table 28. The 3 mm (DCFP 1) part showed a 43% weight saving over aluminium, but a high failure index of 1.72. A thickness of 3.5 mm improved properties, albeit with a lower weight saving of 34%. Both iterations show similar weight savings to NCF, but poorer mechanical performance.

Table 28. Performance of initial DCFP seat with constant thickness.

Material	Nominal thickness (mm)	Mass (kg)	Deflection (mm)	Peak stress (MPa)	Failure index (Tsai-Hill)
DCFP 1	3	4.42	58.2	570	1.72
DCFP 2	3.5	5.16	39.7	428	1.30

6.4.5 Optimised DCFP design
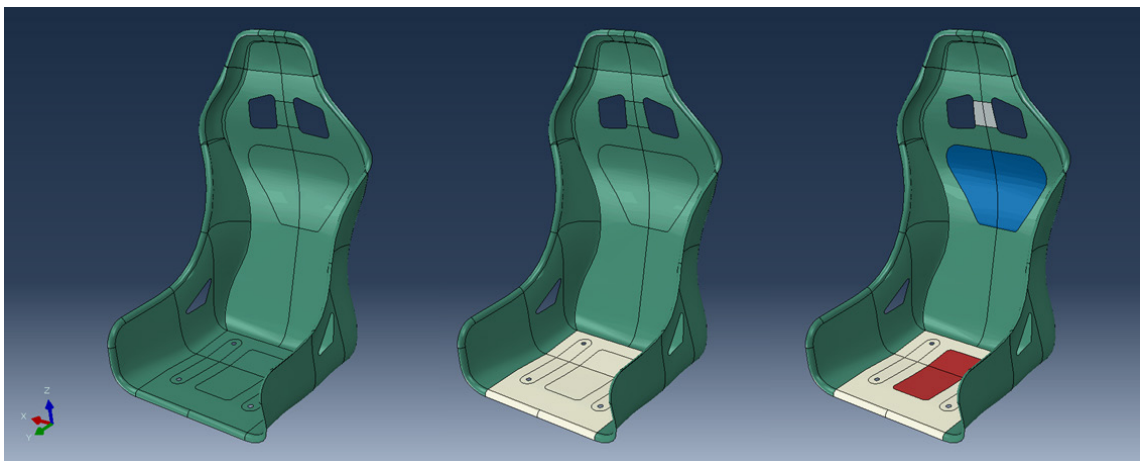
Figure 99. Three stages of DCFP thickness optimisation in the FE material model. The initial stage (DCFP 1 left) incorporates a constant thickness over the whole part. DCFP 2 (middle) reduces overall thickness and adds reinforcement at the base. DCFP 3 (right) reduces thickness in areas that exhibit a low failure index. Further reinforcement is also added at the cervical support.
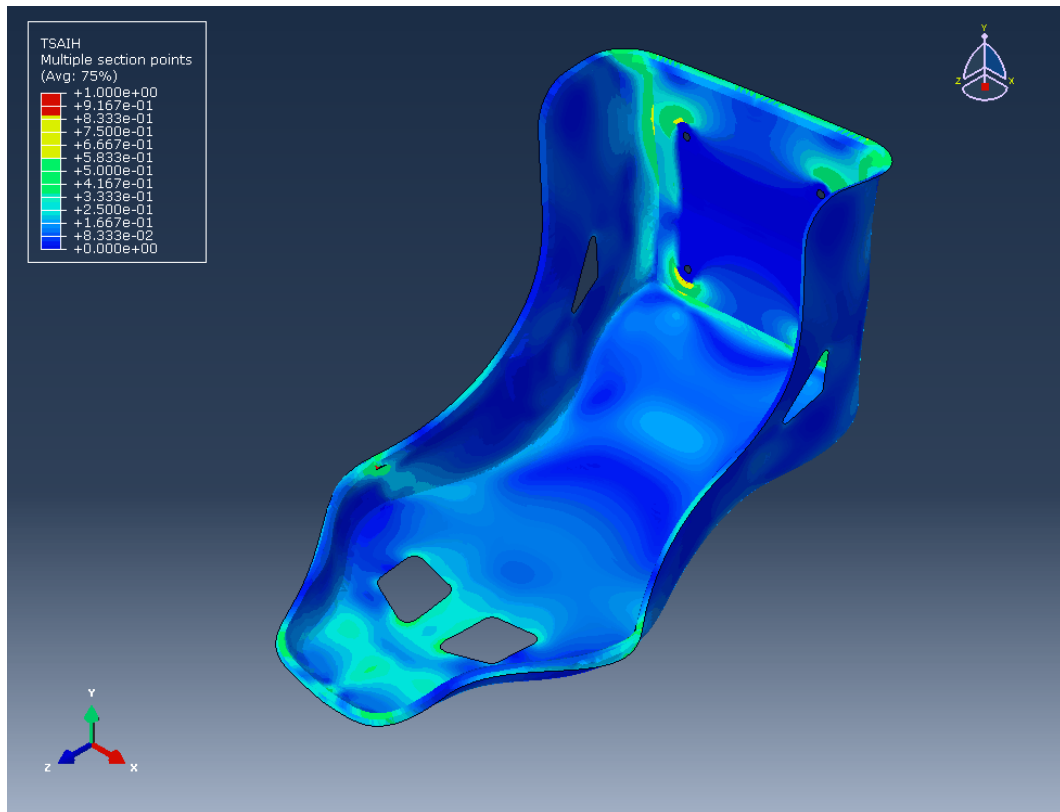
Figure 100. Tsai-Hill failure index for DCFP 3. Low failure indexes are seen in the centre of the base and spine. Further reinforcement is required at the cervical support (left).
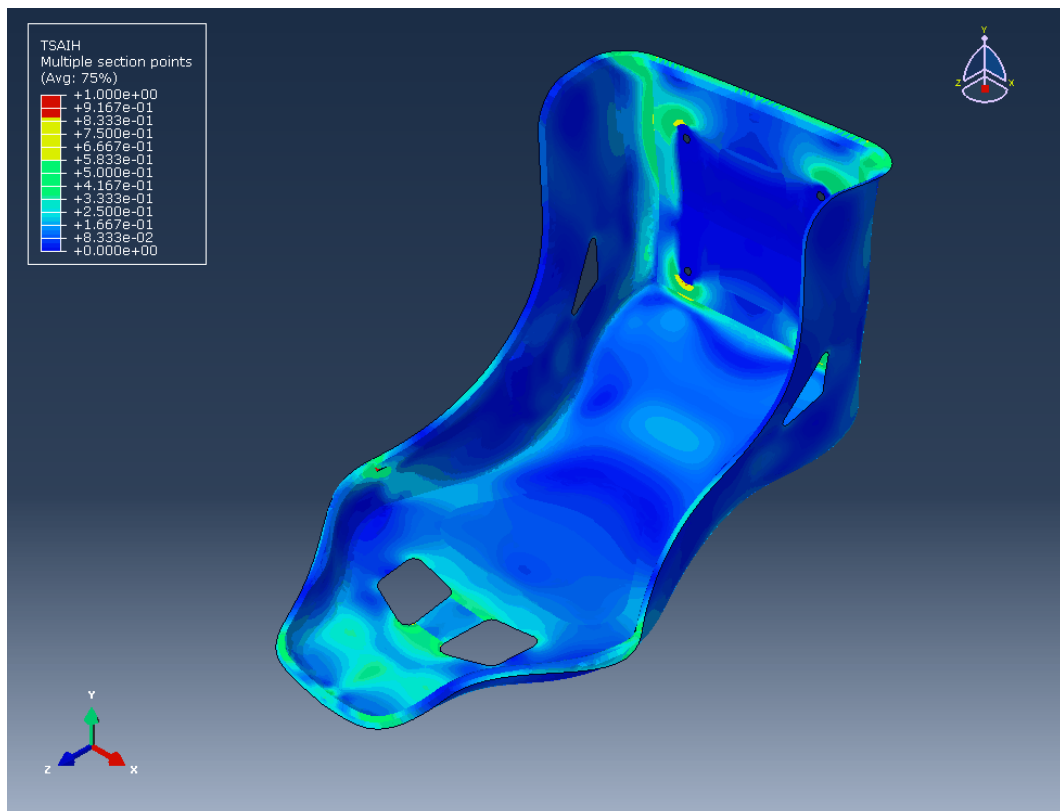
Figure 101. Tsai-Hill failure index across DCFP 4 with reduced thickness at the centre of the base/spine and reinforcement at the cervical support.

Table 29. Performance of optimised DCFP seat.

Material	Nominal thickness (mm)	Mass (kg)	Deflection (mm)	Peak stress (MPa)	Failure index (Tsai-Hill)
DCFP 3	2.25	3.84	61.3	326	0.92
DCFP 4	2.25	3.57	63.1	331	0.92

Initial optimisation (DCFP 3) incorporated a reduction in nominal thickness, over the whole part, to 2.25 mm. A further 2 mm was added to the base (Figure 99 - middle) and a weight saving of 51% was seen. Further optimisation (DCFP4) reduced thickness in areas exhibiting a low failure index – at the centre of the base and thoracic support of the spine. Additional material was used to provide reinforcement between the two holes at the cervical support. Performance was largely unchanged with an increased weight saving of 54%.
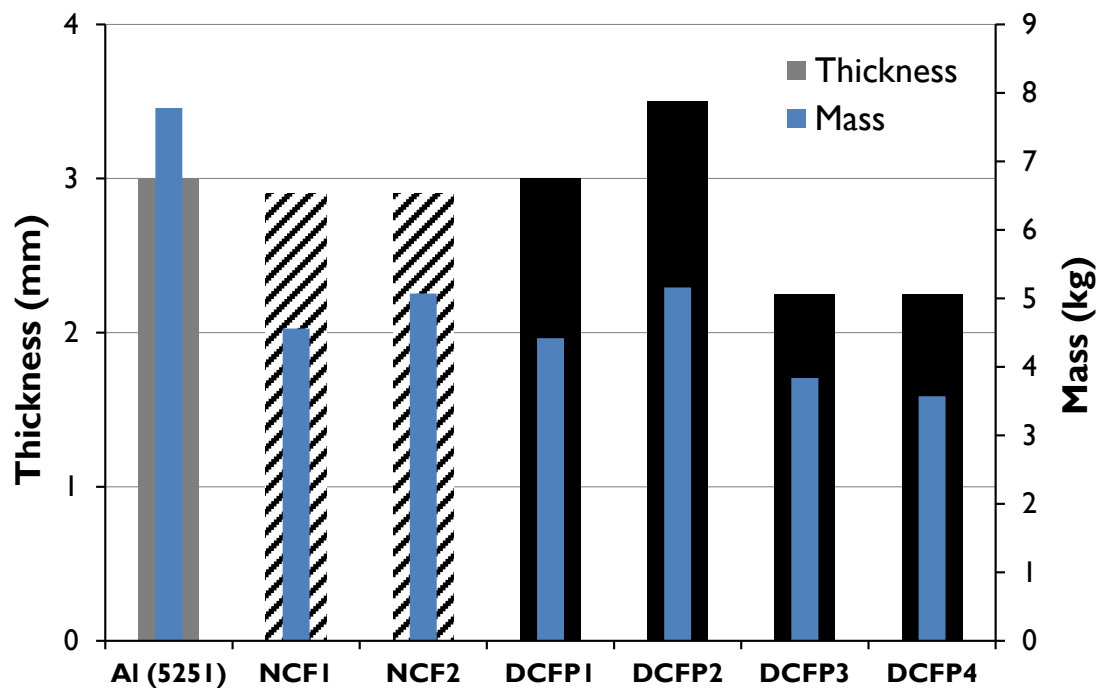
Figure 102. Mass and thickness of a DCFP composite seat compared with aluminium and NCF benchmarks.

Weight savings, over aluminium, of the DCFP seat have been exhibited in Figure 102. A reduction in mass was seen with NCF, but the decrease in thickness is limited by the need to produce a balanced quasi-tropic laminate. Weight/performance of DCFP parts was initially modest, but increased optimisation led to improved

properties. Further optimisation could, not only, lead to a better weight saving, but improve manufacturability of the part.

6.5   Conclusions

The proposed methods for designing a DCFP component have been demonstrated on a semi-structural composite seat geometry. Design methodology has been shaped by findings of the previous four chapters. The composite seat model was discretised into locally homogenised (where properties are uniform) sections to reduce part complexity and significantly reduce FE time to provide approximate material properties. FA2 data was assigned to each facet of the complete geometry but alternative architectures, able to provide similar properties, can be identified using the analytical model. Weight savings over 3 mm aluminium of 54% were estimated for the DCFP seat, compared to 35% using NCF.

7 Conclusions

7.1 Characterisation of tensile properties

The mechanical performance of DCFP has been characterised through tensile testing of a wide variety of fibre architectures. Over the range of architectures tested ($V_f \sim$ 20% - 55%), tensile stiffness and strength increased linearly with fibre volume fraction but the influence of other parameters was more complex. Laminate performance was determined predominantly by the factors that influence mesoscopic homogeneity in the preform fibre architecture: tow size, fibre length and thickness.

7.1.1 Mesoscopic homogeneity

Tow size

Smaller tow sizes produced better properties as the proportion of exposed surface area increased and critical tow length decreased. At a thickness of 1 mm, Young's modulus and UTS decreased by an average of 37% and 74% as the fibre bundle size was increased from 3k to 24k. Smaller reductions were observed for thicker parts (29% and 67% at 3 mm) as the effect of tow size became less significant. The critical aspect ratio for stiffness is relatively small and already within the range of fibre architectures tested. For smaller tow sizes, i.e. 1k and 0.5k, further increases in Young's modulus are likely to reach a limit as results approach the rule of mixtures estimate for a randomly oriented (in-plane) composite. More significant increases would be expected for strength properties as critical aspect ratios are significantly larger. Unlike stiffness properties, the upper bound is likely to be considerably less than the strength that could be achieved with randomly oriented continuous fibre composites. The presence of discontinuities mean there is always a proportion of fibre not loaded to the peak stress.

As a result of increased coupon-to-coupon heterogeneity, variability in data was seen to be worse with large bundle sizes. Manufacturing defects, such as fibre washing and waviness, were also more common. Subsequently, the use of larger

tow sizes (>24k) is not recommend for automotive applications. Properties would continue to fall below those recorded for 24k as the critical length becomes larger and preform coverage becomes poorer.

Fibre length

Up to the critical length, longer fibres lead to improved tensile strength in the composite. An average increase in strength of 19%, across four tow sizes, was observed as fibre lengths were increased from 12 mm to 29 mm; this equated to a 1.1%/mm gain. A smaller increase of 18% (0.6%/mm) was seen by lengthening fibres further (to 58 mm) suggesting that while additional increases are probable, they are expected to be smaller in comparison. These increases are likely to be offset by poorer homogeneity, and if the fibre length is sufficiently large properties will decrease.

Tensile strength was largely dependent on tow size and fibre length, while the effect on modulus was small due to a comparable dependency on the degree of mesoscopic homogeneity in the fibre architecture. Shorter tows with fewer filaments promote improved homogeneity due to more even fibre coverage. Stochastic effects were seen to be more influential on stiffness, which was shown to have a shorter optimal fibre length. The resultant modulus data was therefore characterised by two factors, with no obvious net effect. Shorter fibres also increased the likelihood of fragmentation, which improved mechanical properties through better coverage.

Thickness

The effects of fibre length and tow size were seen to become less significant with increasing thickness. Tensile modulus and strength of a DCFP benchmark (FA1) were both seen to increase with thickness, with performance plateauing between 4-5 mm. Property retention for stiffness and strength at 3 mm were 86%, and 95%, respectively. This is a factor that must be considered when evaluating test data, which is typically carried out at 3 mm.

7.1.2 Matrix properties

Changes to matrix properties were seen to have a significant influence on the tensile strength of meso-scale DFC laminates, while the effect on continuous fibre composites was small (-2%). A CTBN toughener was used to improve the tensile strength of DCFP by facilitating load absorption in weak areas, which prevented crack growth. The most significant improvements were observed with fibre architectures that exhibit poor mesoscopic homogeneity. Some improvements were seen for fine distributions (6k architectures) but generally, properties were worse – a 23% reduction in UTS for preforms moulded with the matrix containing 15 phr CTBN. Coarser distributions (24k) exhibit poorer mesoscopic homogeneity and contain more weak regions. The matrix is required to transfer more of the applied load to the fibres so the properties of the matrix are more important. Increased deformation, enabled by the toughener, promotes failure through fracture in architectures that typically fail through fibre pull-out. Consequently, a larger increase in properties was observed - UTS was increased by 31% (at 15 phr). While tougheners are typically employed to improve properties such as damage tolerance, the findings highlight the potential for improvement of tensile strength properties in meso-scale DFCs. Particular benefits could be seen with shorter fibres that typically provide increased toughness but at the consequence of strength properties.

7.1.3 Prediction of tensile properties

An analytical model has been developed to determine the tensile stiffness and strength of a DCFP fibre architecture if the tow size, fibre length, thickness and volume fraction are known. This can be used in the design procedure to provide an estimate of material properties or be applied to facets within an FE analysis to reduce computation time. Limitations of the existing FE model and proposed analytical models were seen for architectures that exhibit poor homogeneity. Laminates that were thin (<3 mm) and/or incorporated large bundle sizes were under-predicted. Increased tendency for large tows to fragment often results in small improvements in properties and provides explanation for some of the discrepancy. The remaining inconsistencies are likely to be due to two forms of

stress transfer that are neglected in the analytical model: axial stress transfer at the fibre ends and stress transfer between fibre tows. Small improvements were seen in stiffness prediction by incorporating the estimated effect of fibre end stresses (that are most significant for short tows with a high filament count), but it is thought that stress transfer between fibre tows is generally more significant.

7.2 Design considerations for DCFP components

A number of barriers exist to achieving mechanical properties expected from characterisation studies and predicted through the analytical model. Preform compaction is required to attain the target volume fractions in the final laminate, which is known to greatly influence material properties. Damage to components conventionally result in drastic knockdowns in composite properties and remains a major obstacle for use in high performance parts. Consequently, appropriate design methods have to be developed that take these factors into account as well as considering the effects of mechanical performance variability that is intrinsic in composite design procedures. The following sections outline the property reductions that need to be considered when establishing DCFP material properties within automotive and aerospace design methodologies.

7.2.1 Automotive applications

Property reductions of DCFP (FA1 benchmark) that need to be considered for automotive applications are shown in Figure 103. The most significant decrease in properties comes as a consequence of reducing part thickness, which has the knock-on effect of reducing achievable volume fraction for a given compaction level. Increases in properties will arise with thicker parts, while there is also potential for strength improvements through implementation of a compatible highly-toughened matrix.
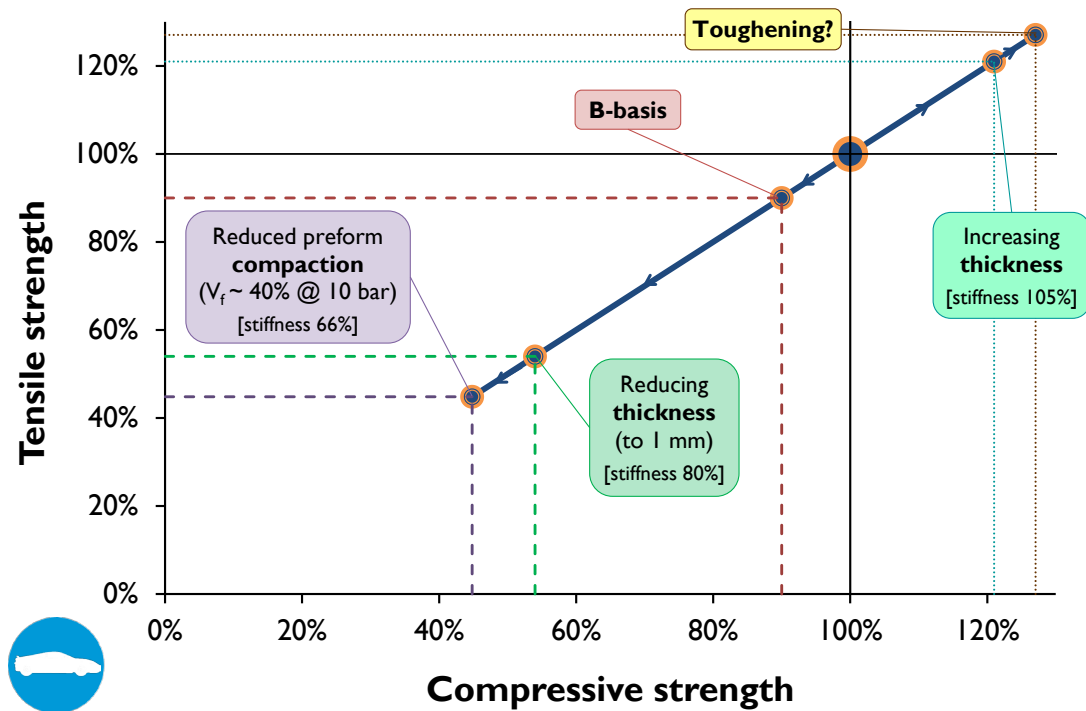
Figure 103. Mechanical property reductions of DCFP to be considered in the design of automotive components. Data is shown for FA1 – 6k, 60 mm fibres at 3 mm thickness and 50% V_f. Baseline values (i.e. 100%) are 250 MPa and 303 MPa for compressive and tensile strength, respectively. Stiffness values are 38 GPa and 36 GPa. Data has been compiled from experimental, FE and analytical model results to determine reductions. Reductions are cumulative, and equivalent reductions for tensile and compressive properties have been assumed.

Compaction

Areal mass has been identified as the most important factor in determining the maximum achievable volume fraction for a preform. As areal mass increased there was initially a large increase in the achievable volume fraction at 10 bar followed by a convergence (from approximately 1.5 kg/m²) to a volume fraction of between 55%-60%; this was indicative of the value for the maximum theoretical volume fraction. As thickness is reduced to 1 mm (0.9 kg/m²) in Figure 103, the achievable volume fraction drops to 40%. Larger tow sizes were seen to be affected more by areal mass; the use of large tow sizes for thin parts would not be recommended.

Poor mesoscopic homogeneity in thin parts hindered the ability to achieve high volume fractions. The effect of fibre length was only seen for these preforms where shorter fibre lengths resulted in a small increase in achievable volume fraction. For a rigid tool, mesoscopic variability in the preform architecture can lead to uneven

pressure distribution thus increasing the likelihood of locally high volume fractions, which are symptomatic of problems with impregnation and voidage in the final part. Results indicate the advantages of using non-filamentised preforms as the expected V_f at 1 bar was approximately 40% compared with 20% for the highly filamentised equivalent.

Weight-savings over conventional materials

DCFP design methodology for automotive applications has been demonstrated on a semi-structural composite seat geometry. The model was discretised into locally homogenised sections (where properties were uniform) to reduce part complexity and significantly reduce FE time to provide approximate material properties. FA2 data was assigned to each facet of the complete geometry but alternative architectures, able to provide similar properties, can be identified using the analytical model. Weight savings over 3 mm aluminium of 54% were estimated for the DCFP seat, compared to 35% using NCF.

7.2.2   Aerospace applications
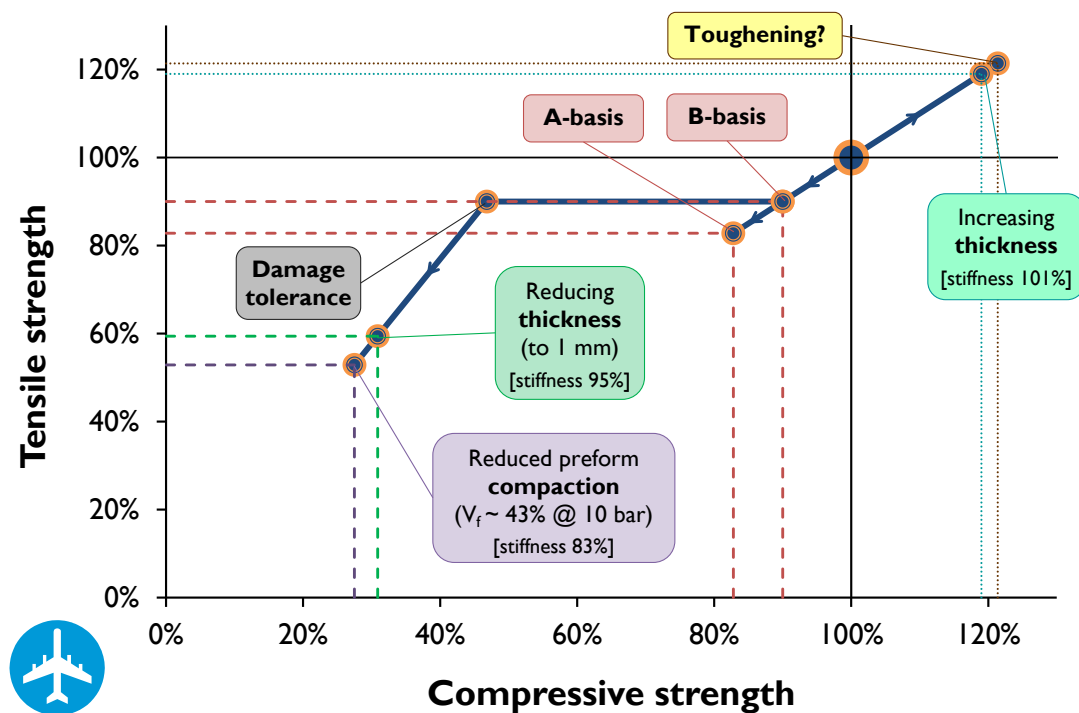
Figure 104. Mechanical property reductions of DCFP to be considered in the design of aerospace components. Data is shown for FA2 – 3k, 30 mm fibres at 3 mm thickness and 50% Vf. Baseline values (i.e. 100%) are 315 MPa and 345 MPa for compressive and tensile strength, respectively. Stiffness values are 42 GPa for both.

Design of aerospace components also requires consideration of damage tolerance and variability in mechanical data. Consequently, design allowables are much more conservative. Property reductions for FA2 are shown in Figure 104.

Damage tolerance

Discontinuous fibre architectures do not suffer the same knockdown in properties observed in continuous fibre composites. Open-hole tension testing showed no discernible difference in strength with un-notched batches (247 MPa and 295 MPa), with a change of +/- 1% at 2 (250 MPa) and 4 mm (293 MPa), respectively. CAI properties (151 MPa) did suffer a 48% knockdown in properties compared with specimens tested under the standard un-notched compression method (288 MPa). This was in contrast to open-hole compression results where strength was recorded at 358 MPa. Current safety factors based on conventional laminates may be too conservative and could lead to over-engineering which would limit the potential of material.

Mechanical property variability

A strong correlation has been observed between variability of preform mass and mechanical properties. Greater variability in laminate properties was a direct consequence of variability at the preforming stage. Stiffness was more severely affected than strength, with the latter being dominated by Weibull effects. A- and B-basis design values have been established for the UTS of FA2 and are displayed in Figure 104. It has been established that mean values should be reported for modulus as it is inappropriate to apply design values, which are used for weakest link phenomena such as strength, to properties that are considered total response.

7.3 Future work

Preform compaction

The compaction work carried out in this thesis is applicable to dry fibre preforms only. The compaction behaviour of wet random meso-scale discontinuous composites may also be of interest. Pre-impregnated random architectures already exist in the form of chopped prepreg SMCs. Developments in the application of resin spray as a binding agent for sprayed tows presents another avenue for research where "semi-preg" preforms are only partially infused. Composites of this nature are typically compression moulded, so there will be an interest in the effect of meso-scale homogeneity on the pressure distribution across a preform. Understanding the effects of lubrication on compressibility will also be desirable in order to model behaviour appropriately.

High performance applications

Potential of the application of meso-scale DFCs in high performance structures relies on the integration of toughened resins. The study on matrix modification carried out in this thesis did not seek to optimise performance. Other methods, such as nano-toughening mechanisms, may offer increased toughness and improve damage tolerance. Considerable work is also needed to characterise the reliability of DCFP composites. Durability and environmental capabilities present further barriers to application and are currently unknown. Testing must also be carried out on sub-components and components in order to determine scale-up factors.

The ease of automation with many meso-scale DFCs presents an opportunity for use in multi-architecture materials. At a basic level, this may involve deposition of different fibre lengths and tow sizes to optimise performance within a single component. More complex structures may integrate continuous fibre interlayers to increase directional properties in localised regions. While performance of the separated constituents may be well known, optimisation of these structures requires further knowledge of the material interfaces and combined properties.

Appendix

A. Publications arising from this thesis

Kirupanantham G., Turner T. A., Warrior N. A.

On the suitability of discontinuous fibre architectures for high performance applications

Awaiting submission

Kirupanantham G., Turner T. A., Warrior N. A.

Mesoscopic homogeneity in discontinuous fibre preforms – fibre compaction

In preparation

B. Materials

B.1 Fibre

Table 30. Summary of fibres used for DCFP reinforcement in work presented in this thesis and throughout the ASP project. Properties taken from manufacturers' data sheets.

Designation	Tensile Strength (MPa)	Tensile Modulus (GPa)	Elongation at break (%)	Linear Density (tex)	Sizing Level (%)	Density (g/ccm)	Filament Diameter (μm)	Studies
6k E HTA 5131	3784	238	1.51	398	1.27	1.76	7	Characterisation, compaction, resin film.
3k E HTA40 E13	4064	238	1.62	201	1.27	1.76	7	
12k E HTS40 F13	4761	240	1.84	799	0.95	1.77	7	6k only - thickness & FA1.
24k E STS 5631	4447	240	1.74	1604	0.94	1.79	7	24k only - toughness
3k HTA40 E13	3825	237	1.53	200	1.27	1.77	7	RFPM, high performance, variability, FA2
6k HTA40 E13	4188	239	1.65	399	1.27	1.76	7	RFPM, Toughness,

B.2 Resin

Table 31. Summary of resins used for as the matrix in for DCFP architectures. Properties taken from manufacturers' data sheets.

Designation	Tensile Strength (MPa)	Tensile Modulus (GPa)	Tensile strain to failure (%)	Cured resin density (g/cc)	Studies
Gurit PRIME 20 LV (fast hardener)	68.6	2.97	4.9	1.089	Characterisation
Gurit PRIME 20 LV (slow hardener)	66.0	3.28	3.2	1.084	Thickness, FA1, FA2, Toughness, High performance
Gurit SPRINT ST70	Not specified by manufacturer	3.00	3.0	1.200	RFPM
ACG MVR444	77.6	3.1	4.0	1.14	High performance

C. Resin film pressure moulding

As part of continued collaborative work with AML, a series of testing was undertaken to determine the feasibility of a new moulding process – resin film pressure moulding (RFPM). Preforms are produced with a string binder that is fed through the fibre chopper gun at the same time as the glass/carbon fibre. Resin film charges are placed on top of the preform at several points. A matched tool is incorporated into a press (heated to 140°C) and lowered to a nominal dwell height for a short time e.g. ten seconds. The drop in resin film viscosity allows the resin to flow across the top of the preform. The press is then closed to apply pressure and stimulate through-thickness flow of the resin. The process has the benefit of very low cycle times – full cure can be achieved in less than five minutes.

C.1 Resin film study

The process incorporates the use of resin film so that the matrix can be added to the reinforcement in solid form. The resin comes in the form of a B-stage prepreg resin. Conventionally, the film is placed on top of preforms in sections or pellets and heated within a vacuum bag to lower viscosity. The resin flows through the thickness and is cured within the vacuum bag. The process offers a low pressure alternative to RTM and allows flexibility in the manufacturing process. There is also scope for the resin to be incorporated into the fibre deposition process – through resin spray for instance. This gives the potential for resin to be used to hold the fibres in place; something that has been considered as an alternative to using a vacuum.

Initial experimental work was carried out to validate the feasibility of the alternative moulding process with DCFP preforms. Four preforms were produced in line with the initial characterisation study – 3k, 6k, 12k and 24k; with fibre lengths of 29mm and a target V_f of 30% at 3mm. Two layers of resin film were situated on top of the 300mm x 400mm preform. The preform was vacuum bagged (layup shown in Figure 105) and heated, and cured, using a heated mat.
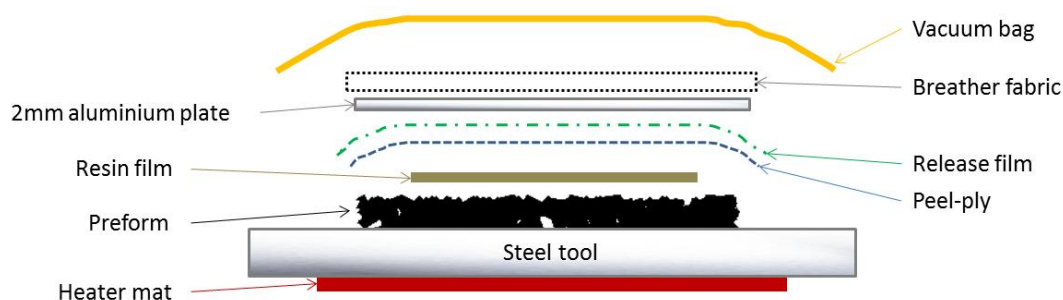
Figure 105. Layup for moulding DCFP laminates using resin film infusion.

Results

Table 32. Resin film DOE showing mechanical properties and part thicknesses. Coefficients of variation (CV) are shown in brackets.

Designation	Tow Size (k)	Fibre Length (mm)	Specimens	Thickness (mm)	V_f	Modulus (GPa)	UTS (MPa)
RFSotira	24	25	15	3.67	15%	15.0 [13%]	83 [17%]
RF3k	3	28.75	11	2.15	27%	23.9 [11%]	174 [10%]
RF6k	6	28.75	10	2.39	32%	28.1 [14%]	160 [11%]
RF12k	12	28.75	14	2.33	30%	25.0 [19%]	127 [12%]
RF24k	24	28.75	14	2.49	30%	19.2 [26%]	81 [27%]

3k results were seen to be poor when compared to laminates manufactured using RTM. The resin film infusion process is governed by through thickness permeability, which is governed by two components: flow through the fibre bundles (perpendicular to the axis) [165] and flow through the gaps caused by heterogeneity in the DCFP fibre architecture. As tow size decreases, and preform coverage improves, the total volume of channels created by gaps in the preform gets smaller. As a result, flow through the tows becomes a larger component and it can be assumed *a priori* that permeability is poorer. The quality of the part is likely to suffer and the mechanical performance would be expected to be decrease.

The problem highlights an inherent drawback of using vacuum infusion (VI) methods. Permeability issues can often be overcome in RTM by increasing injection pressure, albeit with potential washing. VI is limited to a maximum differential pressure of 1 bar. More difficulties are likely to arise when moulding high V_f parts.

Another disadvantage of the process is the lack of control on final part geometry. Part thickness for RTM is determined by the size of the tool cavity, but in VI part thickness is determined by vacuum pressure, preform compressibility and its interaction with the flowing resin [166]. This is evident in the range of thicknesses seen in Table 32. The thickness of the component dictates the fibre volume fraction in the part, which can affect laminates in two ways. The first, permeability, has already been mentioned. As volume fraction increases the preform fibre architecture becomes less porous inhibiting resin flow and potentially reducing laminate properties. In RTM, although increased volume fraction still reduces the in-place permeability of the preform, the benefit is the reduction in the tendency to wash as fibre tows are more tightly constrained. Injection pressure can be increased with little detriment on the final part.

If permeability issues can be overcome there remains an inability to control final part properties as they are directionally proportional to the volume fraction. A study on the compaction of dry DCFP preforms has been carried out and detailed in Chapter 3. Particularly poor compressibility was seen for highly filamentised fibre architectures. The ability to achieve high volume fractions has been questioned for such preforms. Further basis for these concerns is evident in this study, and can be seen in the large thickness measured for the Sotira preform in Table 32. The consequences were seen in poor mechanical properties, but further problems may exist when attempting to meet engineering specifications or space envelopes where part thickness is detailed.
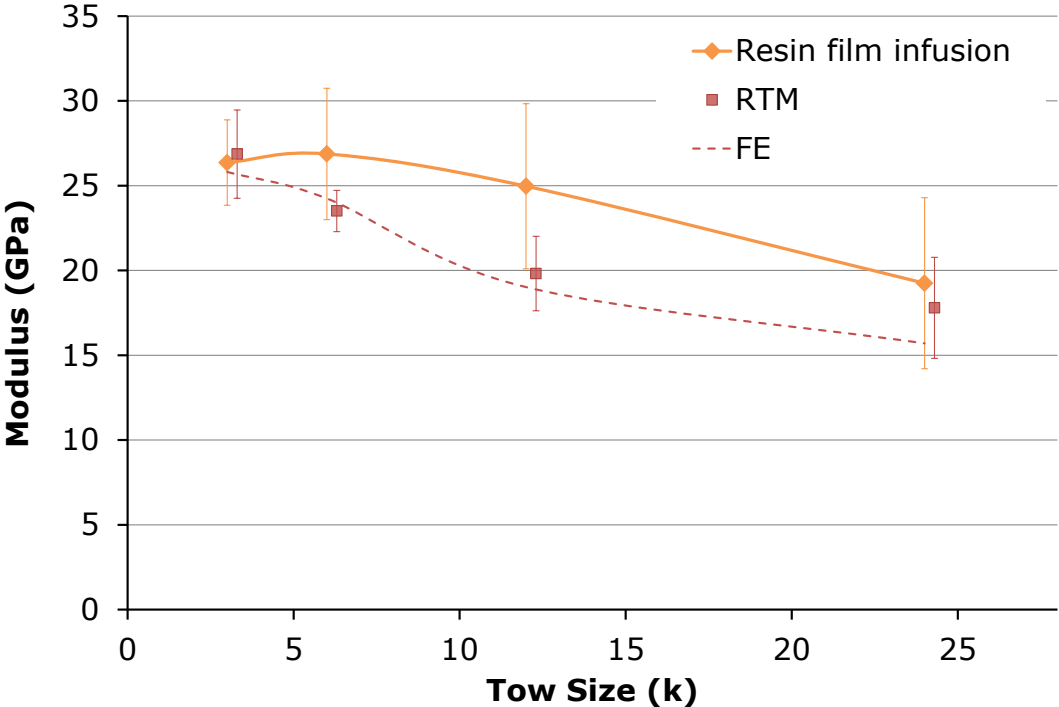
Figure 106. Young's modulus of DCFP moulded through resin film infusion compared with FE and RTM results. RTM results have been offset (+0.3k) for clarity. Results have been normalised to 30% V$_f$.
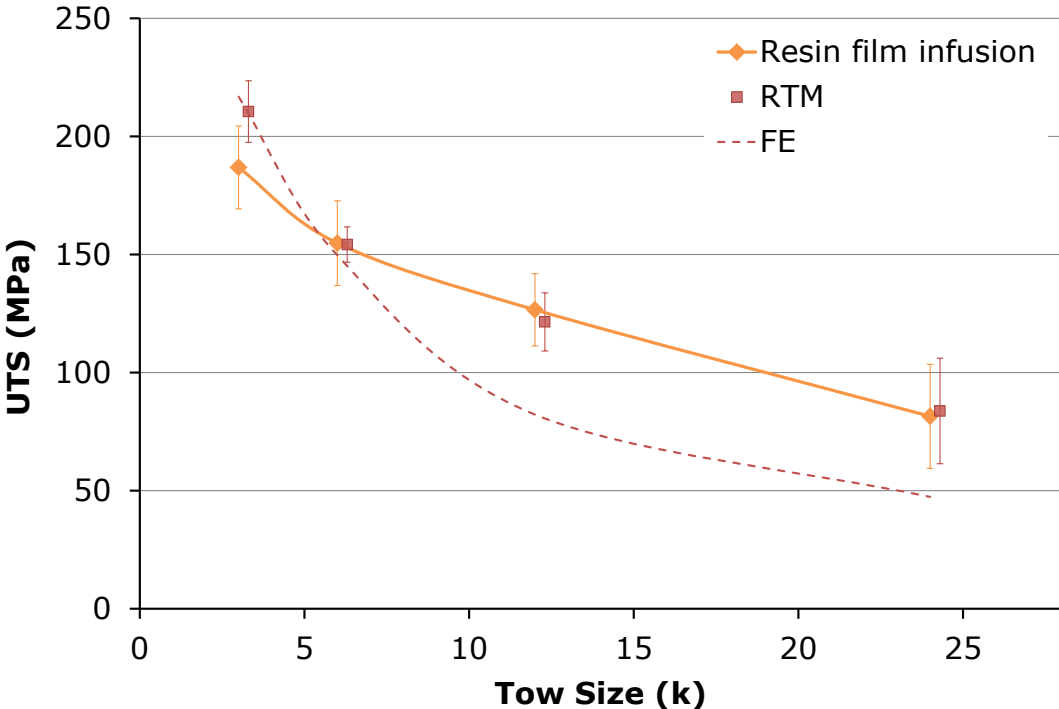
Figure 107. UTS of DCFP with resin film. Results are compared to FE and RTM, with the latter being offset (+0.3k) for clarity. Properties are normalised to 30% V$_f$.

C.2   Discontinuous glass fibre composites

Phase 1

While unable to provide the stiffness characteristics of discontinuous carbon composites, glass fibre has been widely used in non-structural automotive parts. Ford's Programmable Preforming Process (F3P) uses chopped glass fibre to produce preforms in the same manner as DCFP. The process has previously been used to produce door opening ring (DOR) and boot lid surround components [24]. Four DORs, with different nominal volume fractions, were studied to evaluate the feasibility of using F3P with the RFPM process. Mechanical testing and burn off results were used to determine tensile properties and volume fractions.

Figure 108. DOR testing plan.

Samples were taken from three different regions (Figure 108) of the DOR and burnt off at 450°C. **Error! Not a valid bookmark self-reference.** shows the volume fraction results from each region for the four different DORs. Variability is high, with no apparent trends for overweight and underweight areas, highlighting issues associated with variability in the DCFP process. The variation of fibre mass throughout a preform can have great consequences on its moulding and subsequently, its final material properties. Areas of high fibre concentration dictate the ultimate level of compaction the preform can undergo therefore defining the

highest achievable volume fraction. Such regions are also prone to poor impregnation in the RTM process, or other resin infusion methods, due to reduced flow characteristics [26]. Conversely, low fibre concretion can lead to resin rich areas that can be the cause of premature failure in the composite. Two forms of variability exist – that which is intrinsic to the material itself and that which is determined by the processing of the fibre. Much of the variability in **Error! Not a valid bookmark self-reference.** may be overcome by optimisation of the robot programme used to produce the preform.

Table 33. DOR burn off results.

Part designation	Nominal V_f	Specimen number	V_f
RFPMDOR006	25%	1	18.9
		2	24.5
		3	22.2
		Average	21.9
RFPMDOR008	30%	1	27.3
		2	31.9
		3	28.6
		Average	29.3
RFPMDOR0010	35%	1	34.8
		2	30.3
		3	32.0
		Average	32.4
RFPMDOR011	40%	1	40.2
		2	34.3
		3	39.0
		Average	37.8

Table 34. DOR Tensile properties. $*E = \eta_L\eta_o E_F V_F + E_M(1 - V_M)$. **Rule of mixture (ROM) values were calculated using nominal volume fractions.**

Designation	V_f		Tensile modulus (GPa)			Tensile strength (MPa)	
	Nominal	Burn off	Mean	CV	ROM*	Mean	CV
RFPMDOR006	25%	22%	10.7	16%	9.3	140	13%
RFPMDOR008	30%	29%	11.4	21%	10.5	162	29%
RFPMDOR010	35%	32%	13.3	26%	11.8	193	10%
RFPMDOR011	40%	38%	13.9	24%	13.0	203	18%

Tensile properties were close to that predicted by rule of mixtures (Figure 109). The slightly higher than expected performance could be attributed to locally high volume fractions. Fibre coverage across the part was poor. However, tensile specimens were taken from a section that exhibited better coverage.
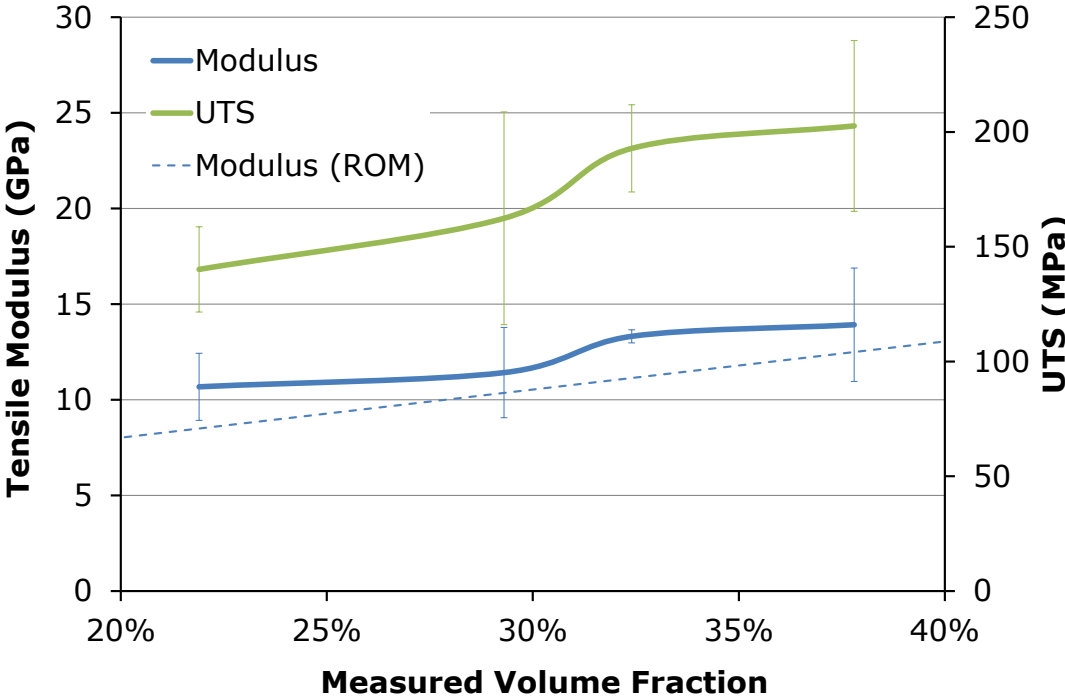
Figure 109. DOR modulus and strength.

C.3   RFPM trials

Phase 2

RFPM was later used to mould 2D carbon fibre preforms. To determine the feasibility of the process with carbon fibre preforms, a succession of trials have been carried out. DCFP and NCF preforms were produced at the University while moulding was done by AML. Testing of all parts was carried out at the UoN. Initial trials, where charges were placed on the top and bottom of the preform, showed poor wet-out (Figure 110). Performance was 20 – 30% lower than UoN moulded preforms and some plaques weren't satisfactory for testing.

Figure 110. Dry RFPM trial specimens. Although top and bottom surfaces of some plaques looked satisfactory a dry region through the centre resulted in specimens that could not be tested. Plaques were cut by a water cooled diamond saw cutter. As specimens were cut dry fibre clung to the blade resulting in filamentisation of any dry fibre tows.

Phase 3

Incorporation of a vacuum and the use of just one charge on the top of the preform improved results. Performance was comparable with plaques produced at UoN.

Phase 4

A study was carried out to determine the effect of a number of processing parameters.

Table 35. Phase 4 DOE and tensile test results. An ejector pressure of 3 bar was used for all tests. Ten samples were tested for each plaque with five in each (0˚ and 90˚) direction.

Part no.	Fibre type	Fibre length (mm)	Chopper height (mm)	Ejector tube	V_f	Modulus (GPa)	UTS (MPa)
100610 -1	6k	50	600	Removed	36%	32.2 [11%]	247 [9%]
100610 -2	6k	50	600	Removed	41%	36.6 [9%]	253 [7%]
100610 -3	6k	50	600	Fitted	43%	33.1 [14%]	271 [9%]
100610 -4	6k	50	400	Removed	43%	35.1 [11%]	257 [11%]
100610 -5	6k	25	400	Removed	45%	37.6 [10%]	283 [7%]
100610 -6	6k	25	600	Fitted	40%	27.7 [19%]	174 [16%]
100610 -7	6k	25	600	Removed	43%	33.2 [10%]	290 [13%]
100610 -8	3k	25	600	Removed	44%	42.7 [13%]	317 [4%]
100610 -9	3k	25	600	Removed	45%	38.0 [13%]	310 [7%]
100610 -10	3k	25	600	Fitted	45%	37.1 [12%]	283 [7%]
100610 -11	3k	25	400	Removed	44%	38.3 [8%]	300 [9%]
100610 -12	3k	50	400	Removed	46%	40.2 [8%]	303 [9%]
100610 -13	3k	50	600	Removed	46%	45.4 [12%]	291 [9%]
100610 -14	3k	50	600	Fitted	44%	37.2 [8%]	306 [4%]

Improved tensile properties were achieved with a decreased chopper height without an ejector tube. As expected, performance of 3k fibre preforms was better than that of 6k. Increases in stiffness and strength were seen for the longer fibre length. Contrary to the characterisation study, the effect was more significant with Young's modulus. Results from part 100610-6 were seen to be particularly low. If this data is rejected a close to linear increase with V_f is seen for UTS and modulus.
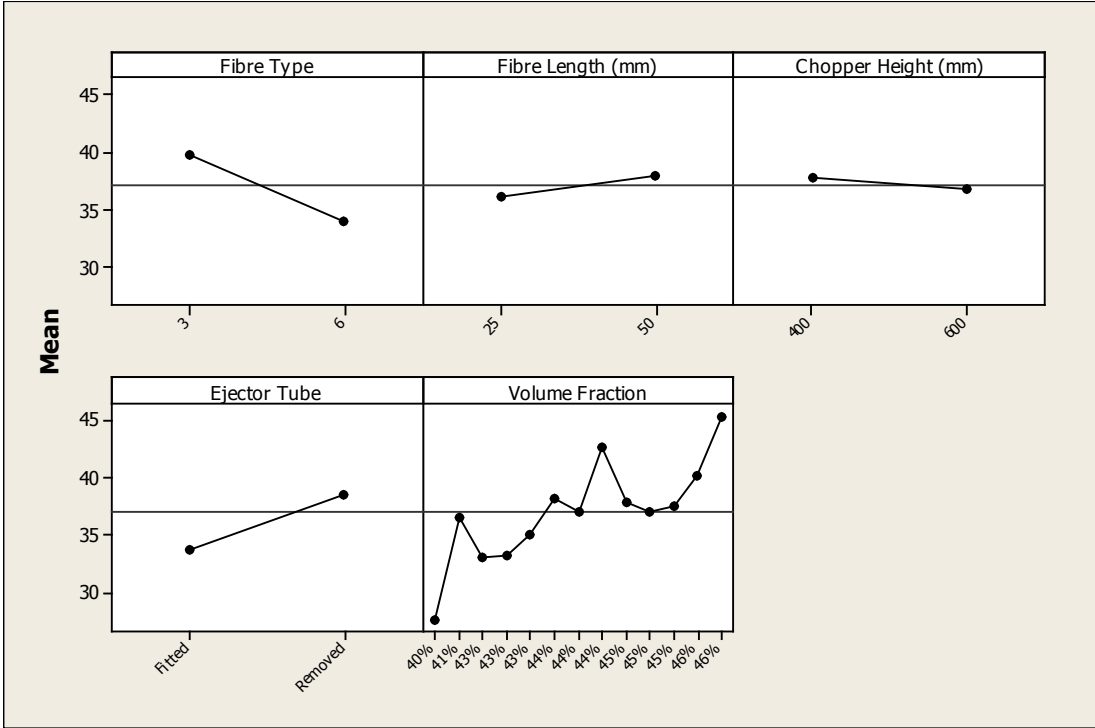
Figure 111. Main effects plot for modulus (GPa) for batches tested in phase 4 of the RFPM development study. Five processing parameters are considered and the mean values are shown for each permutation.
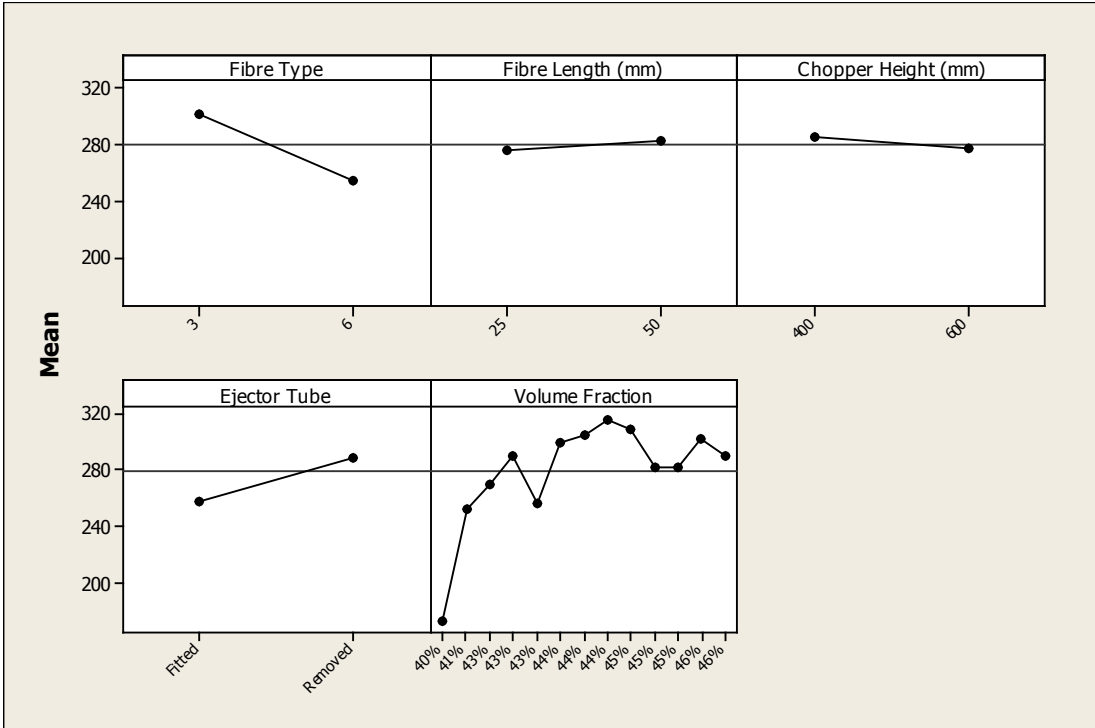

Figure 112. Main effects plot for UTS (MPa) for batches tested in phase 4 of the RFPM development study.

D. Compaction model coefficients

Table 36. Coefficients used to fit the compaction model to experimental results in Chapter 3. The method for determining the coefficients is described in 3.7.5. Good correspondence was seen for all architectures shown apart from those in grey. These results were fitted with a different maximum volume fraction (S_f) to provide a better fit but were omitted from analysis of the effect of preform architecture on initial compressibility (also in 3.7.5)

t (mm)	Tow size (k)	Fibre length (mm)	Compaction								
			1			2			3		
			C_{bo}	S_o	S_f	C_{bo}	S_o	S_f	C_{bo}	S_o	S_f
3	3	11.5	0.328	39%	61%	0.463	40%	61%	0.398	41%	61%
3	3	28.75	0.550	39%	61%	0.144	44%	61%	0.119	45%	61%
3	3	57.5	0.586	39%	61%	0.139	44%	61%	0.117	45%	61%
3	6	11.5	0.804	39%	61%	0.311	44%	61%	0.258	45%	61%
3	6	28.75	0.387	39%	61%	0.207	42%	61%	0.188	43%	61%
3	6	57.5	0.367	39%	61%	0.147	43%	61%	0.124	44%	61%
3	12	11.5	1.397	39%	61%	0.218	46%	61%	0.180	47%	61%
3	12	28.75	0.541	39%	61%	0.231	43%	61%	0.206	43%	61%
3	12	57.5	0.371	39%	61%	0.131	43%	61%	0.108	43%	61%
3	24	11.5	0.437	39%	61%	0.234	42%	61%	0.209	43%	61%
3	24	28.75	0.524	36%	52%	0.353	40%	52%	0.327	41%	52%
3	24	57.5	0.363	35%	54%	0.417	38%	54%	0.395	39%	54%
10	3	11.5	2.629	39%	61%	1.341	44%	61%	1.275	45%	61%
10	3	28.75	3.009	39%	61%	0.693	46%	61%	0.602	47%	61%
10	3	57.5	2.714	39%	61%	1.575	43%	61%	1.340	45%	61%
10	6	11.5	3.956	39%	61%	2.581	43%	61%	2.109	45%	61%
10	6	28.75	6.395	39%	61%	3.096	45%	61%	2.510	46%	61%
10	6	57.5	2.619	39%	61%	0.653	46%	61%	0.557	47%	61%
10	12	11.5	5.491	39%	61%	4.852	42%	61%	3.503	44%	61%
10	12	28.75	7.784	39%	61%	2.007	47%	61%	1.717	48%	61%
10	12	57.5	3.642	39%	61%	0.433	49%	61%	0.377	49%	61%
10	24	11.5	3.379	33%	57%	0.600	41%	57%	0.550	42%	57%
10	24	28.75	2.288	39%	61%	0.632	46%	61%	0.547	47%	61%
10	24	57.5	2.503	39%	61%	0.718	46%	61%	0.600	47%	61%

References

1. *Climate Change Act 2008*. 2008: United Kingdom.
2. Zachariadis, T.I., ed. *Cars and Carbon: Automobiles and European Climate Policy in a Global Context*. 2011, Springer.
3. Weiss, M.A., et al., *On the Road in 2020: A Life-cycle Analysis of New Automobile Technologies*. 2000: Energy Laboratory, Massachusetts Institute of Technology.
4. Department of Energy & Climate Change, *2010 UK Greenhouse gas emissions, final figures*. 2012.
5. Marcos, C., M. Paolo, and O. Yohei, *Mass car ownership in the emerging market giants.* Economic Policy, 2008. **23**(54): p. 243-296.
6. Boszko, C., *Double-dip in Europe and Asia Increases Pressure for Globalization and Consolidation in the Commercial-Vehicle Industry, According to AlixPartners Study*. 2012.
7. Lane, B., *Life Cycle Assessment of Vehicle Fuels and Technologies*. 2006, Ecolane Transport Consultancy: London.
8. Fuhs, A.E., *Hybrid vehicles and the future of personal transportation*. 2008: CRC Press.
9. Norris Jr, R.E., et al., *Advanced High Speed Programmable Preforming*. 2010, Oak Ridge National Laboratory (ORNL).
10. Heywood, J.B., *More Sustainable Transportation: The Role of Energy Efficient Vehicle Technologies*. 2008, Massachusetts Institute of Technology: Cambridge, MA.
11. Rondeau, R., Bond, *The Effects of Tows and Filament Groups on Properties.* 1999.
12. Helps, I.G., *Plastics in European Cars 2000-2008: A Rapra Industry Analysis Report*. 2001: Rapra Technology.
13. Kia, H.G., *Sheet Molding Compounds: Science and Technology*. 1993: Hanser.
14. Vaidya, U., *Composites for Automotive, Truck and Mass Transit: Materials, Design, Manufacturing*. 2011: DEStech Publications.
15. Tucker, N. and K. Lindsey, *An Introduction to Automotive Composites*. 2002: Rapra Technology Limited.
16. Bruderick, M., et al. *Carbon fiber composite body structures for the 2003 Dodge Viper*. in *Proc. 2nd SPE Automotive Composites Conference* 2002. Troy, MI, USA.
17. Gardiner, G., *Forged composites replace complex metal parts*, in *High-Performance Composites*. 2012.
18. Gardiner, G., *Sixth Element: Lamborghini accelerates CFRP*, in *High-Performance Composites*. 2012.
19. Strong, A.B., *Fundamals Of Composites Manufacturing: Materials, Methods and Applications*. 2008: Society of Manufacturing Engineers.
20. Black, S., *High-Volume Preforming for Automotive Application*, in *Composites Technology*. 2008.
21. Brandt, M.R. and S.R. Reeve. *Directed Fibre Preform Case Studies*. in *Composites 2001 convention and trade show*. 2001. Tampa, Florida, USA: Composite Fabricators Association.
22. Harper, L.T., et al., *Characterisation of random carbon fibre composites from a directed fibre preforming process: Analysis of microstructural parameters.* Composites Part A: Applied Science and Manufacturing, 2006. **37**(11): p. 2136-2147.
23. Harper, L.T., et al., *Characterisation of random carbon fibre composites from a directed fibre preforming process: The effect of tow filamentisation.* Composites Part A: Applied Science and Manufacturing, 2007. **38**(3): p. 755-770.
24. Harper, L.T., et al., *Affordable Lightweight Body Structures*. 2006.
25. Harris, B., *Engineering composite materials*. 1999, The Institute of Materials: London.

26. Olivero, K.A., et al., *Effect of Preform Thickness and Volume Fraction on Injection Pressure and Mechanical Properties of Resin Transfer Molded Composites.* Journal of Composite Materials, 2004. **38**(11): p. 937-957.

27. Matthews, F.L. and R.D. Rawlings, *Composite Materials: Engineering and Science*. 1st edition ed. 1999: Woodhead Publishing.

28. Harper, L.T., et al., *Fiber Alignment in Directed Carbon Fiber Preforms - Mechanical Property Prediction.* Journal of Composite Materials, 2010. **44**(8): p. 931-951.

29. Starbuck, J.M. and L.B. Cataquiz, *Evaluation of Large Tow-Size Carbon Fiber for Reducing the Cost of CNG Storage tanks.* 2007, Oak Ridge National Laboratory & US Department of Energy.

30. Dahl, J.S. and T. Hoseck. *Investigation into the light transmission characteristics of random chopped carbon fiber preforms*. in *48th International SAMPE symposium*. 2003. Long Beach (CA).

31. Dahl, J.S., G.L. Smith, and D.Q. Houston, *The Influence of Fiber Tow Size on the Performance of Chopped Carbon Fiber Reinforced Composites*, in *37th ISTC* 2005: Seattle, WA.

32. Dockum, J.F. and P.L. Schell, *Fiber directed preform reinforcement: factors that may influence mechanical properties in liquid composite molding*, in *6th Annual ASM/ESD advanced composites conference*. 1990: ASM International, Detroit (MI).

33. Pan, N., *Prediction of statistical strengths of twisted fibre structures.* Journal of Materials Science, 1993. **28**(22): p. 6107-6114.

34. Carley, E., J. Dockum, and P. Schell, *Preforming for liquid composite molding.* Polymer composites for structural automotive applications, 1990.

35. Harper, L.T., et al., *Characterisation of random carbon fibre composites from a directed fibre preforming process: The effect of fibre length.* Composites Part A: Applied Science and Manufacturing, 2006. **37**(11): p. 1863-1878.

36. Kaverov, A.T., M.E. Kazakov, and V.Y. Varshavsky, *Carbon Fibres*, in *Fibre science and technology*, V.I. Kostikov, Editor. 1995, Springer.

37. Tucker, I.C.L. and E. Liang, *Stiffness predictions for unidirectional short-fiber composites: Review and evaluation.* Composites Science and Technology, 1999. **59**: p. 655-671.

38. Curtis, P.T., M.G. Bader, and J.E. Bailey, *The stiffness and strength of a polyamide thermoplastic reinforced with glass and carbon fibres.* Journal of Materials Science, 1978. **13**(2): p. 377-390.

39. Fu, S.-Y. and B. Lauke, *Effects of fiber length and fiber orientation distributions on the tensile strength of short-fiber-reinforced polymers.* Composites Science and Technology, 1996. **56**(10): p. 1179-1190.

40. Jacob, G.C., et al., *Effect of fiber volume fraction, fiber length and fiber tow size on the energy absorption of chopped carbon fiber-polymer composites.* Polymer Composites, 2005. **26**(3): p. 293-305.

41. Hithcen, S., S. Ogin, and P. Smith, *Mechanical Properties and Notch Sensitivity of Short Carbon Fibre-Epoxy Composites*, in *Developments in the science and technology of composite materials: 6th European Conference on Composite Materials, September 20-24*, B.A. R, K. A, and M. A, Editors. 1993, Woodhead Publishing: Bordeaux, France.

42. Cottrell, A.H., *Strong Solids.* Proceedings of the Royal Society of London. Series A. Mathematical and Physical Sciences, 1964. **282**(1388): p. 2-9.

43. Allred, R.E. and D.M. Schuster, *The impact toughness of discontinuous boron-reinforced epoxy composites.* Journal of Materials Science, 1973. **8**(2): p. 245-250.

44. Salkind, J., *Application of Composite Materials*. 1973: American Society for Testing & Materials.

45. Vasiliev, V.V. and E.V. Morozov, *Mechanics and Analysis of Composite Materials*. 2007, Oxford: Elsevier.

46. Thomason, J.L. and M.A. Vlug, *Influence of fibre length and concentration on the properties of glass fibre-reinforced polypropylene: 1. Tensile and flexural modulus.* Composites Part A: Applied Science and Manufacturing, 1996. **27**(6): p. 477-484.

47. Kaw, A.K., *Mechanics of composite materials.* 2nd edition ed. 2006: CRS Press.

48. Voigt, W., *Theortische student uberdie elasticitats verhalinisse krystalle.* Abh Ges Wiss Goetting, 1887. **34**.

49. Hull, D. and T.W. Clyne, *An Introduction to Composite Materials.* Cambridge Solid State Science Series. 1996: Cambridge University Press.

50. Gay, D.G., *Composite Materials: Design and Applications.* 2003: CRC Press.

51. Kardos, J., *Critical Issues in Achieving Desirable Mechanical Properties for Short Fiber Composites.* Polymer Composites. 28 th Microsymposium on Macromolecules, 1985.

52. Cox, H.L., *The elasticity and strength of paper and other fibrous materials.* British Journal of Applied Physics, 1952(3): p. 72.

53. Kim, J.K. and Y.W. Mai, *Engineered Interfaces in Fiber Reinforced Composites.* 1998: Elsevier Science.

54. Krenchel, H., *Fibre reinforcement: theoretical and practical investigations of the elasticity and strength of fibre-reinforced materials.* 1964: Akademisk forlag.

55. Clyne, T.W., *A simple development of the shear lag theory appropriate for composites with a relatively small modulus mismatch.* Materials Science and Engineering: A, 1989. **122**(2): p. 183-192.

56. Starink, M.J. and S. Syngellakis, *Shear lag models for discontinuous composites: fibre end stresses and weak interface layers.* Materials Science and Engineering: A, 1999. **270**(2): p. 270-277.

57. Räisänen, V., et al., *Does the shear-lag model apply to random fiber networks.* J. Mater. Res, 1997. **12**(10): p. 2725.

58. Taha, I. and Y.F. Abdin, *Modeling of strength and stiffness of short randomly oriented glass-fiber polypropylene composites.* Journal of Composite Materials, 2011.

59. Sk, L. and S. Chakraborty, *Effective Moduli of Random Short Fiber Composite: A Probabilistic Study.* Journal of Reinforced Plastics and Composites, 2004. **23**(7): p. 751-760.

60. Eshelby, J.D., *The Determination of the Elastic Field of an Ellipsoidal Inclusion, and Related Problems.* Proceedings of the Royal Society of London. Series A. Mathematical and Physical Sciences, 1957. **241**(1226): p. 376-396.

61. Mori, T. and K. Tanaka, *Average stress in matrix and average elastic energy of materials with misfitting inclusions.* Acta metallurgica, 1973. **21**(5): p. 571-574.

62. Mortensen, A., *Concise Encyclopedia of Composite Materials.* 2007: Elsevier Science Limited.

63. Ashton, J.E., J.C. Halpin, and P.H. Petit, *Primer on Composite Materials.* 1969, Westport, Connecticut: Technomic Publishing.

64. Mouritz, A.P. and A.G. Gibson, *Fire Properties of Polymer Composite Materials.* 2006: Physica-Verlag.

65. Halpin, J.C. and J.L. Kardos, *The Halpin-Tsai equations: A review.* Polymer Engineering & Science, 1976. **16**(5): p. 344-352.

66. Zak, G., et al., *Mechanical properties of short-fibre layered composites: prediction and experiment.* Rapid Prototyping Journal, 2000. **6**(2): p. 107-118.

67. Kelly, A. and W.R. Tyson, *Tensile properties of fibre-reinforced metals: Copper/tungsten and copper/molybdenum.* Journal of the Mechanics and Physics of Solids, 1965. **13**(6): p. 329-350.

68. O'Gara, J.F., G.E. Novak, and M.G. Wyzgoski, *Predicting the tensile strength of short glass fiber reinforced injection molded plastics.* 2010.

69.   Bader, M.G. and W.H. Bowyer, *The mechanical properties of thermoplastics strengthened by short discontinuous fibres.* Journal of Physics D: Applied Physics, 1972. **5**(12): p. 2215.

70.   Harlow, D.G., *Properties of the Strength Distribution for Composite Materials*, in *Composite Materials: Testing and Design (Fifth Conference)*, S.W. Tsai, Editor. 1979, ASTM International: New Orleans. p. 484-501.

71.   Weibull, W., *A statistical distribution function of wide applicability.* Journal Of Applied Mechanics - ASME, 1951.

72.   Askeland, D.R., P.P. Fulay, and D.K. Bhattacharya, *Essentials of Materials Science and Engineering: SI Edition*. 2009: Nelson Education Limited.

73.   Potter, K., *Introduction to Composite Products: Design, development and manufacture*. 1996: Springer.

74.   Epaarachchi, J., H. Ku, and K. Gohel, *A Simplified Empirical Model for Prediction of Mechanical Properties of Random Short Fiber/Vinylester Composites.* Journal of Composite Materials, 2010. **44**(6): p. 779-788.

75.   Harper, L.T., *Discontinuous Carbon Fibre Composites for Automotive Applications*, in *Polymer Composites Group*. 2006, University of Nottingham: Nottingham.

76.   Palaniappan, J., et al., *Repair efficiency of resin infused scarf repair to marine sandwich structures.*, in *17th International conference on composite materials (ICCM 17)*. 2009: Edinburgh, UK.

77.   Warrior, N.A., C. Patel, and T.A. Turner. *Advances in Discontinuous Composites*. in *SAMPE* 2011. Paris.

78.   Balakrishnan, N. and V.B. Nevzorov, *A Primer on Statistical Distributions*. 2003: Wiley.

79.   Hale, D. and A. Kelly, *Strength of fibrous composite materials.* Annual Review of Materials Science, 1972. **2**(1): p. 405-462.

80.   Mandell, J.F., D.D. Samborsky, and L. Wang, *Effects of fiber waviness on composites for wind turbine blades*, in *SAMPE 2003*. 2003: Long Beach, CA. p. 14.

81.   Sahimi, M., *Heterogeneous Materials: Nonlinear and breakdown properties and atomistic modeling*. Vol. 2. 2003: Springer.

82.   Patel, C., *Development of discontinuous fibre preforming processes*, in *Polymer Composites Group*. 2013, University of Nottingham.

83.   Rudd, C.D., et al., *Compaction and in plane permeability characteristics of quasi unidirectional and continuous random reinforcements.* Materials Science and Technology, 1996. **12**(5): p. 436-444.

84.   Simacek, P. and V.M. Karbhari, *Notes on the Modeling of Preform Compaction: I - Micromechanics at the Fiber Bundle Level.* Journal of Reinforced Plastics and Composites, 1996. **15**(1): p. 86-122.

85.   Somashekar, A.A., S. Bickerton, and D. Bhattacharyya, *Exploring the non-elastic compression deformation of dry glass fibre reinforcements.* Composites Science and Technology, 2007. **67**(2): p. 183-200.

86.   Aranda, S., F. Klunker, and G. Ziegmann. *Compaction response of fibre reinforcements depending on processing temperature*. in *Internation conference on composite materials 17*. 2009. Edinburgh.

87.   Long, A., et al., *Effects of fibre architecture on reinforcement fabric deformation.* Plastics, rubber and composites, 2002. **31**(2): p. 87-97.

88.   Batch, G.L., S. Cumiskey, and C.W. Macosko, *Compaction of fiber reinforcements.* Polymer Composites, 2002. **23**(3): p. 307-318.

89.   Castelli, M.G., J.K. Sutter, and D. Benson, *Thermomechanical Fatigue Durability of T650-35/PMR-15 Sheet Moulding Compound*. 1998, NASA.

90. Chen, B., A.H.D. Cheng, and T.W. Chou, *A nonlinear compaction model for fibrous preforms.* Composites Part A: Applied Science and Manufacturing, 2001. **32**(5): p. 701-707.

91. Chen, B., E.J. Lang, and T.-W. Chou, *Experimental and theoretical studies of fabric compaction behavior in resin transfer molding.* Materials Science and Engineering: A, 2001. **317**(1–2): p. 188-196.

92. Potluri, P. and T.V. Sagar, *Compaction modelling of textile preforms for composite structures.* Composite Structures, 2008. **86**(1-3): p. 177-185.

93. Robitaille, F. and R. Gauvin, *Compaction of textile reinforcements for composites manufacturing. I: Review of experimental results.* Polymer Composites, 1998. **19**(2): p. 198-216.

94. Yang, J., et al., *Compaction Behavior and Part Thickness Variation in Vacuum Infusion Molding Process.* Applied Composite Materials: p. 1-16.

95. Chen, Z.-R., L. Ye, and T. Kruckenberg, *A micromechanical compaction model for woven fabric preforms. Part I: Single layer.* Composites Science and Technology, 2006. **66**(16): p. 3254-3262.

96. Hsiao, H.M., S.M. Lee, and R.A. Buyny, *Core Crush Mechanisms and Solutions in the Manufacturing of Sandwich Structures*, in *Recent Advances in Experimental Mechanics*, E.E. Gdoutos, Editor. 2004, Springer Netherlands. p. 689-700.

97. Powell, P.C., *Engineering with Fibre-Polymer Laminates*. 1993, Springer.

98. Bickerton, S., M.J. Buntain, and A.A. Somashekar, *The viscoelastic compression behavior of liquid composite molding preforms.* Composites Part A: Applied Science and Manufacturing, 2003. **34**(5): p. 431-444.

99. Eggert, M. and J. Eggert, *Beiträge zur Kenntnis der Wolle und ihrer Bearbeitung.* Gebrüder Borntraeger, 1925: p. 69-87.

100. Beil, N.B. and W.W. Roberts Jr, *Modeling and Computer Simulation of the Compressional Behavior of Fiber Assemblies.* Textile Research Journal, 2002. **72**(4): p. 341-351.

101. van Wyk, C.M., *Note on compressibility of wool.* J Text Inst, 1946. **37**: p. T285-T292.

102. Cai, Z. and T. Gutowski, *The 3-D Deformation Behavior of a Lubricated Fiber Bundle.* Journal of Composite Materials, 1992. **26**(8): p. 1207-1237.

103. Samadi, R. and F. Robitaille, *Compaction of aligned fibre assemblies using particulate methods*, in *The 9th International Conference on Flow Processes in Composite Materials*. 2008: Montreal, Canada.

104. Echaabi, J., M. Nziengui, and M. Hattabi, *Compressibility and relaxation models for fibrous reinforcements in Liquid Composites Moulding.* International Journal of Material Forming, 2008. **1**: p. 851-854.

105. Chen, B. and T.W. Chou. *Modeling of nonlinear dry preform compaction in liquid composite moldin processes*. in *European Conference on Composite Materials*. 2000. Brighton, UK.

106. Grujicic, M., K.M. Chittajallu, and S. Walsh, *Effect of shear, compaction and nesting on permeability of the orthogonal plain-weave fabric preforms.* Materials Chemistry and Physics, 2004. **86**(2–3): p. 358-369.

107. Somashekar, A.A., S. Bickerton, and D. Bhattacharyya, *Compression deformation of a biaxial stitched glass fibre reinforcement: Visualisation and image analysis using X-ray micro-CT.* Composites Part A: Applied Science and Manufacturing, 2011. **42**(2): p. 140-150.

108. Hodgkin, J.H., G.P. Simon, and R.J. Varley, *Thermoplastic toughening of epoxy resins: a critical review.* Polymers for Advanced Technologies, 1998. **9**(1): p. 3-10.

109. Zhang, M., *A Review of the Epoxy Resin Toughening*. 2003, Syracuse University: Syracuse.

110. Jacob, G.C., et al., *Energy Absorption in Polymer Composites for Automotive Crashworthiness.* Journal of Composite Materials, 2002. **36**(7): p. 813-850.

111. Petrie, E.M., *Epoxy Adhesive Formulations* 2005: McGraw-Hill Professional.

112. Meister, J.J., *Polymer Modification*. 2000: CRC Press. 936.

113. Hitchen, S.A., S.L. Ogin, and P.A. Smith, *Effect of fibre length on fatigue of short carbon fibre/epoxy composite.* Composites, 1995. **26**(4): p. 303-308.

114. Boyle, M.A., C.J. Martin, and J.D. Neuner, *Epoxy Resins*, in *ASM Handbook Volume 21: Composites*, D.B. Miracle and S.L. Donaldson, Editors. 2001, ASM International. p. 78-89.

115. Day, R.J., P.A. Lovell, and A.A. Wazzan, *Toughened carbon/epoxy composites made by using core/shell particles.* Composites Science and Technology, 2001. **61**(1): p. 41-56.

116. Robinette, E.J., *Toughening Vinyl Ester Matrix Composites by Tailoring Nanoscale and Mesoscale Interfaces*. 2005, Drexel University.

117. Cech, J. and B. Kretow, *The Effectiveness of Toughening Technologies on Multifunctional Epoxy Resin Systems*. CVC Specialty Chemicals.

118. Hillermeier, R.W. and J.C. Seferis, *Interlayer Toughening of Resin Transfer Molding Composites.* Composites Part A: Applied Science and Manufacturing, 2001. **32**(5): p. 721-729.

119. Tsotsis, T.K., *Interlayer toughening of composite materials.* Polymer Composites, 2009. **30**(1): p. 70-86.

120. Cano, R.J. and M.B. Dow, *Properties of Five Toughened Matrix Composite Materials*, in *NASA Technical Paper*. 1992, NASA.

121. Bagheri, R. and R.A. Pearson, *Role of particle cavitation in rubber-toughened epoxies: 1. Microvoid toughening.* Polymer, 1996. **37**(20): p. 4529-4538.

122. Kamae, T. and L.T. Drzal, *Carbon fiber/epoxy composite property enhancement through incorporation of carbon nanotubes at the fiber–matrix interphase – Part I: The development of carbon nanotube coated carbon fibers and the evaluation of their adhesion.* Composites Part A: Applied Science and Manufacturing, 2012. **43**(9): p. 1569-1577.

123. Hogg, P.J. and F.C. Smith, *Novel Toughening Mechanisms for Low Cost Composite Structures*, in *Low Cost Composite Structures*. 2003, NATO/RTO Meeting Proceedings. p. 21-1 - 21-22.

124. Hsieh, T.H., et al., *The mechanisms and mechanics of the toughening of epoxy polymers modified with silica nanoparticles.* Polymer, 2010. **51**(26): p. 6284-6294.

125. Zhang, H., et al., *Property improvements of in situ epoxy nanocomposites with reduced interparticle distance at high nanosilica content.* Acta Materialia, 2006. **54**(7): p. 1833-1842.

126. Biswas, M. and S. Sinha Ray, *New polymerization techniques and synthetic methodologies*. Advances in Polymer Science. Vol. 155. 2001: Springer.

127. Tsotsis, T.K., K.L. Rugg, and B.N. Cox, *Towards rapid screening of new composite matrix resins.* Composites Science and Technology, 2006. **66**(11–12): p. 1651-1670.

128. Kaynak, C., A. Arikan, and T. Tincer, *Flexibility improvement of short glass fiber reinforced epoxy by using a liquid elastomer.* Polymer, 2003. **44**(8): p. 2433-2439.

129. Baker, A., S. Dutton, and D. Kelly, *Composite Materials fof Aircraft Structures*, ed. J.A. Schetz. 2004: American Institute of Aeronautic and Astronautics.

130. Campbell, F.C., *Structural Composite Materials*. 2010, Materials Park, OH, USA: ASM International.

131. Kassapoglou, C., *Design and Analysis of Composite Structures with Applications to Aerospace Structures*. Aerospace Series, ed. P. Belobaba, et al. 2010: John Wiley & Sons.

132. Pochiraju, K.V., G.P. Tandon, and G.A. Schoeppner, *Long-Term Durability of Polymeric Matrix Composites*. 2011: Springer US.

133. NASA Reliability & Maintainability Steering Commitee, *Design and Manufacturing Guidelines for Aerospace Composites*. 1999.

134. Tuttle, M., *Buckling/Crippling of Structural Angle Beams Produced using Discontinuous-Fiber Composites*. 2012, University of Washington.

135. Mendoza Jasso, A.J., et al., *A parametric study of fiber volume fraction distribution on the failure initiation location in open hole off-axis tensile specimen.* Composites Science and Technology, 2011. **71**(16): p. 1819-1825.

136. Dirikolu, M.H., A. Aktas, and B. Birgoren, *Statistical analysis of fracture strength of composite materials using Weibull distribution.* Turkish. J. Eng. Env. Sci., 2002. **26**(1): p. 45-48.

137. Abernethy, R.B., *An Overview of Weibull analysis* in *The new Weibull handbook: reliability & statistical analysis for predicting life, safety, risk, support costs and forecasting warranty claims, substantiation and accelerated testing, usin Weibull, Log Normal, Crow-AMSAA, Probit, and Kaplan-Meier Models.* 2004, Dr. Robert. Abernethy: North Palm Beach, Florida. p. 1.1-1.11.

138. *The Composite Materials Handbook-MIL 17: Guidelines for Characterization of Structural Materials*. Vol. 1. 1999: CRC Press.

139. Mangalgiri, P.D. and V. Seetharaman, *Effect of Scatter in Elastic Modulus on the Buckling Performance of Composite Panels*, in *Computational Structural Mechanics*. 1994, Allied Publishers. p. 501-512.

140. Corum, J.M., R.L. Battiste, and M.B. Ruggles-Wrenn, *Low-energy impact effects on candidate automotive structural composites.* Composites Science and Technology, 2003. **63**(6): p. 755-769.

141. Feraboli, P., et al., *Notched behavior of prepreg-based discontinuous carbon fiber/epoxy systems.* Composites Part A: Applied Science and Manufacturing, 2009. **40**(3): p. 289-299.

142. Boursier, B. and A. Lopez, *Failure Initiation And Effect Of Defects In Structural Discontinuous Fiber Composites*, in *42nd ISTC*. 2010: Salt Lake City, UT. p. 16.

143. Qian, C., et al., *Notched behaviour of discontinuous carbon fibre composites: Comparison with quasi-isotropic non-crimp fabric.* Composites Part A: Applied Science and Manufacturing, 2011. **42**(3): p. 293-302.

144. Bibo, G.A., et al., *Carbon-fibre non-crimp fabric laminates for cost-effective damage-tolerant structures.* Composites Science and Technology, 1998. **58**(1): p. 129-143.

145. Razi, H. and S. Ward, *Principles for achieving damage tolerant primary composite aircraft structures*, in *11th DoD/FAA/NASA Conference on Fibrous Composites in Structural Design*. 1996: Fort Worth, TX.

146. Rhead, A.T., D. Marchant, and R. Butler, *Compressive strength of composite laminates following free edge impact.* Composites Part A: Applied Science and Manufacturing. **41**(9): p. 1056-1065.

147. Bond, M., et al., *Full-field strain measurement of notched discontinuous carbon fibre composites*, in *ICCM 17*. 2009: Edinburgh.

148. European Aviation Safety Agency, *Certification Specifications for Large Aeroplanes CS-25*. 2007. p. p 36.

149. Reeve, S., et al., *Mechanical property translation in oriented, discontinuous carbon fiber composites*, in *SAMPE international symposium*. 2000: Los Angeles.

150. Deo, R.B., J.H. Starnes Jnr, and R.C. Holzwarth, *Low-cost composite materials and structures for aircraft applications*, in *Low Cost Composite Structures*. 2001: Loen, Norway.

151. Russel, J.D., *Composites Affordability Initiative: Transitioning Advanced Aerospace Technologies through Cost and Risk Reduction.* AMMTIAC Quarterly, 2009. **1**(3).

152. Thuis, H.G.S.J., *Development of a composite cargo door for an aircraft.* Composite Structures, 1999. **47**(1–4): p. 813-819.

153. Sampson, W.W., *Modelling Stochastic Fibrous Materials with Mathematica.* 2009: springer.

154. Campbell, F.C., *Manfacturing processes for advanced composites.* 2003, NL: Elsevier Science.

155. Barbero, E., J. Fernández-Sáez, and C. Navarro, *Statistical analysis of the mechanical properties of composite materials.* Composites Part B: Engineering, 2000. **31**(5): p. 375-381.

156. Abernethy, R.B., *The New Weibull Handbook, Second Edition.* 1996.

157. Lieberman, G.J., *Tables for one-sided statistical tolerance limits.* 1957, Office of Naval Research: Arlington, VA.

158. Tomblin, J.S., Y.C. Ng, and K.S. Raju, *Material Qualification and Equivalency for Polymer Matrix Composite Material Systems.* 2001, National Institute for Aviation Research.

159. Chamis, C.C., *Mechanics of Load Transfer at the Fiber/Matrix Interface.* 1972, NASA.

160. Tuttle, M., T. Shifman, and B. Boursier, *Simplifying Certification of Discontinuous Composite Material Forms for Primary Aircraft Structures*, in *SAMPE 2010.* 2010: Seattle, WA p. 11.

161. Hexcel Corporation, *HexMC / C / 2000 / R1A Product Data.* 2008.

162. Fudge, J. *HexMC Public Information.* 2004.

163. Marissen, R. and J. Linsen, *Variability of the flexural strength of sheet moulding compounds.* Composites Science and Technology, 1999. **59**(14): p. 2093-2100.

164. European Council for Automotive R&D (EUCAR), *The Automotive Industry on future R&D Challenges.* 2009.

165. Endruweit, A. and A.C. Long. *Analytical permeability modelling for 3D woven reinforcements.* in *ICCM17.* 2009. Edinburgh.

166. Williams, C.D., S.M. Grove, and J. Summerscales, *The compression response of fibre-reinforced plastic plates during manufacture by the resin infusion under flexible tooling method.* Composites Part A: Applied Science and Manufacturing, 1998. **29**(1–2): p. 111-114.